The Molecular Pathogenesis of Feline Calicivirus Infection

Thesis submitted in accordance with the requirements the University of Liverpool for the degree of Doctor in Philosophy

Emma Louise Newsham

Infection Biology

School of Veterinary Science

University of Liverpool

July 2011

Memorandum

Apart from help and advice acknowledged, this thesis represents the unaided work of the author

---

Emma Louise Newsham

Table of Contents

Memorandum……i

Table of Contents……...……..ii

Acknowledgements……..x

Abstract……xi

List of Abbreviations……..xii

1 Chapter one 1

1.1 *Caliciviridae* family 1

1.1.1 Sapovirus and norovirus genera 2

1.1.2 Nebovirus genera 3

1.1.3 Lagovirus genera 4

1.1.4 Vesivirus genera 4

1.2 Feline Calicivirus 6

1.2.1 FCV genome 6

1.2.2 Proteins encoded by the FCV genome 7

1.2.3 FCV strain variability 10

1.2.4 Clinical signs 11

1.2.5 Epidemiology 16

1.2.6 Host-pathogen interaction 17

1.3 Post-genomic technologies for investigation of host-pathogen interactions. 20

1.3.1 Viral proteomics 20

1.3.2 Viral transcriptomics 23

1.4 Aims 28

2 Chapter two 29

2.1 Introduction 29

2.2 Materials and methods 31
2.2.1 Cells and viruses 31
2.2.2 Sequencing 34
2.2.3 Growth curve 35
2.2.4 Immunofluorescence Assay 36
2.2.5 2D-DIGE 37
2.2.6 Mass spectrometry 43
2.2.7 Protein identification from the predicted cat proteins 45
2.2.8 Functional categorisation of identified proteins 45
2.3 Results 46
2.3.1 Plaque purification of FCV-F9 strains 46
2.3.2 Growth curve 47
2.3.3 Immunofluorescence assay 48
2.3.4 2D-DIGE analysis 49
2.3.5 Gene Ontology 53
2.3.6 Cytoskeletal proteins 54
2.4 Discussion 55
3 Chapter three 59
3.1 Introduction 59
3.1.1 FCV strain variability 59
3.1.2 Diversity of FCV clinical signs 59
3.1.3 Genotypic and phenotypic strain markers 60
3.1.4 Aims 61
3.2 Materials and methods 62
3.2.1 Viral strains 62
3.2.2 Genetic diversity 62
3.2.3 Growth in cell culture 63

3.2.4 2D-DIGE analysis of the effects of four strains of FCV upon the host cell proteome 65
3.3 Results 68
3.3.1 Viral growth curves 68
3.3.2 2D-DIGE analysis of the effects of four strains of FCV upon the host cell proteome 70
3.4 Discussion 80
4 Chapter Four 84
4.1 Introduction 84
4.2 Materials and methods 86
4.2.1 Viral infection 86
4.2.2 Fixation and staining 86
4.2.3 Image analysis with ImageJ software 88
4.3 Results 89
4.3.1 Actin staining 89
4.3.2 Tubulin staining 89
4.3.3 Vimentin staining 100
4.4 Discussion 108
5 Chapter five 112
5.1 Introduction 112
5.2 Materials and methods 114
5.2.1 Viral infection 114
5.2.2 RNA isolation 114
5.2.3 rRNA depletion 115
5.2.4 Creation of cDNA library for SOLiD sequencing 116
5.2.5 Emulsion PCR 119
5.2.6 SOLiD sequencing 120

5.2.7 Read mapping 120
5.2.8 DESeq 120
5.2.9 Gene Ontology 121
5.2.10 Pathway Studio 121
5.3 Results 122
5.3.1 DESeq analysis 122
5.3.2 Gene Ontology 126
5.3.3 Pathway analysis 132
5.4 Discussion 135
5.4.1 DESeq 135
5.4.2 Pathway analysis 137
5.4.3 Comparing RNA-seq and proteomic results 138
6 Chapter six 140
6.1 Introduction 140
6.2 Materials and methods 144
6.2.1 Virus strains 144
6.2.2 RT-PCR of capsid gene and sequencing 144
6.2.3 Sequence analysis 145
6.2.4 RT-PCR of polymerase gene to capsid gene and sequencing 145
6.2.5 Sequence analysis 146
6.2.6 Sequencing the outbreak strain UKOS-A 146
6.2.7 RT-PCR and sequencing 147
6.3 Results 148
6.3.1 Analysis of outbreak shelter strains. 148
6.3.2 Sequencing of the outbreak strain UKOS-A 153
6.4 Discussion 159
7 Chapter seven 163

References.....169

Appendices.....187

Appendix I - Mascot identifications of differentially expressed FEA cell proteins from 2D-DIGE analysis of FCV-F9 infection 188

Appendix II - Mascot identifications of differentially expressed FEA cell proteins from 2D-DIGE analysis of FCV-F9, LS015, R591 and UKOS-A infection 192

Appendix III - Average greyscale values of FCV capsid stain and tubulin stain in infected and mock infected FEA cells 204

Appendix IV - Average greyscale values of FCV capsid stain and vimentin stain in infected and mock infected FEA cells 207

Appendix V - Mann Whitney U test results comparing tubulin and vimentin expression between infected and uninfected FEA cells 210

Appendix VIII - Pathway analysis of differentially transcribed genes in FEA cells in response to FCV-F9 infection including full gene identification key.....213

Acknowledgements

The first group of people I would like to thank in helping me complete this thesis are my supervisors, Professor Jonathan Wastling, Dr Alan Radford, Dr Susan Dawson and Professor Ros Gaskell. Without your constant encouragement, guidance and understanding words when things were not going so well this thesis my never have come to fruition.

I am also indebted to the many, many people who have taught me new techniques, given me advice when things were failing and generally given me a hand in completing the work found in this thesis. With all things cell culture related Ruth Ryvar and Cathy Glover offered invaluable advice and experience, Dr Dave Spiller in the Centre for Cell Imaging was instrumental in ensuring that the confocal microscopy went smoothly and Dr Kevin Ashelford and Suzanne Kay from the Centre for Genomic research were both a massive help in completing the RNA-seq work and getting it analysed. A big thank you is owed to Dr Karen Coyne for all her help with the Sadpal's shelter FCV work and also for some last minute stats advice!

To everyone who has been a part of the two groups I have had the privilege of being a member of; the small animal infectious disease group at Leahurst and the infection biology group at Liverpool, thank you for giving me such a friendly welcome into the groups and making working in the labs such an enjoyable experience. I have also been lucky in being able to share an office with some wonderful people both in Liverpool and at Leahurst. To everyone who has shared G17 with me, thank you for sharing so many good experiences and laughs especially Anne Salisbury, Rachael Hollins and my Everton buddy Bryony Parsons (we will win a trophy soon!). To all those who have been in the Hughes Room past and present, thanks for giving me some of the funniest moments of the past four years especially Hos Weerapol, my partner-in-crime Jenna Kenyani and Sarah Vermont, who is the world's best sport!

Last but definitely not least, I would like to thank my family and friends for sticking with me over the past four years and always being on hand with words of support or a glass of something stronger when necessary! To my mam and dad, who have been there by my side through thick and thin and have always believed in me, even when I have doubted myself. And finally to my wonderful boyfriend Roman, whose love, patience and support have made all this possible, thank you...I promise I'll get a proper job soon!

Abstract

Feline calicivirus (FCV) is an important veterinary pathogen of domestic cats. It is highly variable and rapidly evolving such that many different strains of varying pathogenicity exist from avirulent, to mildly virulent and hypervirulent. FCV is one of only a small number of viruses within the *Caliciviridae* to propagate readily *in vitro*. This property has made FCV a model for the study of the viruses of the calicivirus family. However, relatively little remains known about the way in which these viruses affect host cellular mechanisms. Despite the increasing use of post-genomic technologies in other areas of science, what is known about the effects of calicivirus replication upon host cells has generally relied on relatively conventional technologies to target known defined pathways.

In order to investigate FCV modulation of the host cell proteome a 2D-DIGE experiment was performed upon a single viral strain (FCV-F9) with four time points analysed. The results of this analysis showed that 30 host proteins were differentially expressed in the cells infected with FCV-F9 and of these 30 proteins, 14 were successfully identified using mass spectrometry and 11 of these had cytoskeletal proteins within their identifications.

To further evaluate these host proteome changes and to explore whether variations in strain pathogenicity were associated with varying affects in the host proteome, a second 2D-DIGE experiment was performed upon four strains of FCV isolated from cats exhibiting a range of clinical signs. As in the first experiment, host cytoskeletal proteins appeared to be targeted for modulation during infection. Overall, this experiment uncovered 131 modulated host proteins with 61 proteins successfully identified by mass spectrometry and 16 of these had cytoskeletal proteins within their identifications. Also found within this experiment was evidence of the putative virulent FCV strain UKOS-A having a different affect upon 14 of the differentially expressed proteins to the other three FCV strains tested. UKOS-A was found to down-regulate these proteins whereas the other strains had an up-regulatory effect, these proteins could be a potential marker of hypervirulence but would need further study to confirm their validity.

To follow the modulation of the identified host cytoskeletal proteins, immunofluorescent staining coupled with confocal microscopy was used to track FCV capsid protein and two cytoskeletal proteins vimentin and tubulin. Results showed that during infection with the four FCV strains tested both vimentin and tubulin were both significantly altered during infection with the intensity of fluorescent staining increasing in all cases.

To complement the proteomic analyses, an experiment designed to discover differentially expressed gene transcripts was conducted using RNA-seq technology. Overall, there were 354 genes found to be differentially transcribed within the infected cells at both four and seven hrs post infection (p.i.) with the majority of modulated genes experiencing down-regulation at four hrs p.i. and up-regulation at seven hrs p.i.. Once again, genes within the cytoskeletal regulation pathway were up-regulated alongside genes from the apoptosis regulatory pathway and immune system response pathways.

To further characterise the putative virulent strain used in earlier studies, attempts were made to sequence the rest of this virus using polymerase chain reaction and conventional Sanger sequencing technologies. Although almost 50% of the UKOS-A strain was sequenced, the sequence obtained was no more similar or different to other virulent systemic disease (VSD) causing strains.

Overall, the most marked effects of FCV infection upon the host were found amongst the cytoskeletal genes and proteins which have been demonstrated to undergo extensive modification. This is a completely novel finding in this family of viruses. Further studies will be needed to identify the consequences of the identified cytoskeletal changes to both the host and the virus.

List of Abbreviations

2D-DIGE	Two-dimensional in gel electrophoresis
Ambic	Ammonium bicarbonate
ANOVA	Analysis of variance
APS	Ammonium persulphate
BLAST	Basic Local Alignment Search Tool
BLASTn	Nucleotide-nucleotide BLAST search
BSA	Bovine serum albumin
BVA	Biological Variation Analysis
DAPI	4',6-diamidino-2-phenylindole nucleic acid stain
DIA	Differential In-gel Analysis
ddH_2O	Double distilled water
DMF	Dimethylformamide
DTT	Dithiothreitol
EDTA	Ethylenediaminetetraacetic acid
ePCR	Emulsion PCR
ESI	Electrospray Ionisation
FA	Formic Acid
F-actin	Filamentous actin
FCS	Fetal calf serum
FCV	Feline Calicivirus
FEA	Feline embryonic cell line
FITC	Fluorescein isothiocyanate
GM	Growth media
GO	Gene Ontology
IAA	Iodoacetamide

IEF	Isoelectric focussing
IPG	Immobilised pH gradient
LC	Liquid chromatography
MEM	Eagles minimum essential media
MM	Maintenance media
MS/MS	Tandem mass spectrometry
NEAA	Non-essential amino acids
NCBI	National Centre for Biotechnology Information
ORF	Open reading frame
PBS	Phosphate buffer saline
PCR	Polymerase chain reaction
pI	Isoelectric point
p.i.	Post infection
RNA-seq	RNA sequencing using next generation sequencers
SDS	Sodium dodecyl sulphate
SILAC	Stable isotope labelling by amino acids in cell culture
TBE	Tris/Borate/EDTA
$TCID_{50}$	50% Tissue culture infective dose
TEMED	Tetramethylethylenediamine
URTD	Upper respiratory tract disease
VSD	Virulent systemic disease
VS-FCV	Virulent systemic feline calicivirus

1 Chapter one

Introduction

In 1957, Fastier isolated a new virus whilst trying to induce an infection of feline panleukopenia virus in feline kidney cells (Fastier, 1957). The cells infected by this unknown virus were found to appear rounded and became detached from the glass culture surface. In this original article the virus was named 'kidney cell-degenerating virus' in reference to the culture it was isolated in and it was later renamed feline picornavirus and classified within the calicivirus genera of the picornavirus family (Burki, 1965; Fenner, 1976). From the mid 1970s onwards, however, there were studies performed that found evidence for the reclassification of the calicivirus genera into a completely separate family based upon differences in virion size, translated polypeptide size (Burroughs & Brown, 1974) and viral RNA replication strategies (Black *et al.*, 1978; Ehresmann & Schaffer, 1977) which were atypical of picornaviruses.

1.1 *Caliciviridae* family

The family *Caliciviridae* are members of Class IV of the Baltimore scheme (Baltimore, 1971) for virus classification alongside other positive stranded RNA viruses. The family gains its name from the Latin *calyx* meaning cup in reference to the cup-like depressions on the capsid discovered by electron microscopy (Zwillenberg & Burki, 1966). The *Caliciviridae* are further divided into five genera; vesiviruses, lagoviruses, sapoviruses and noroviruses (Fig 1.1) and the newest genus neboviruses (Carstens & Ball, 2009).

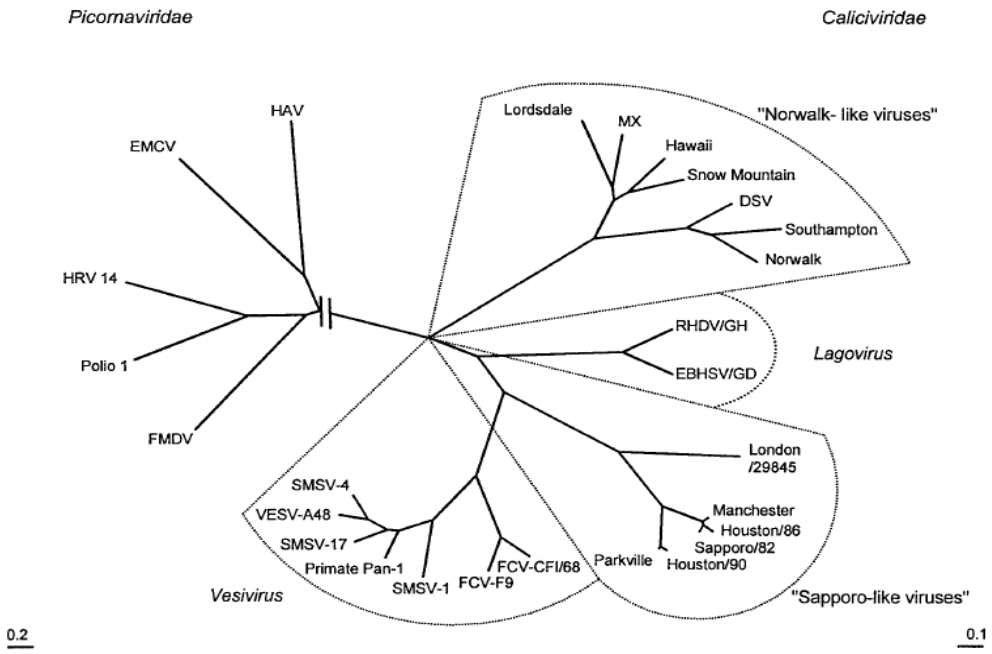

Figure 1.1. Phylogenetic analysis of capsid gene sequence from members of the *Caliciviridae* and *Picornaviridae.* Figure reproduced from Green *et al* (2000).

1.1.1 Sapovirus and norovirus genera

The most common causes of human viral gastroenteritis are sapovirus and norovirus which are both found within the calicivirus family.

Noroviruses gain their name from the first outbreak they were isolated from in humans in Norwalk, Ohio in 1968 (Adler & Zickl, 1969). Human noroviruses are now known to be the leading cause of non-bacterial gastroenteritis (Mead *et al.*, 1999) causing episodes of vomiting and diarrhoea. One major obstacle in the investigation of noroviruses are the lack of *in vitro* cultivation models despite efforts to propagate the virus in a number of cell lines (Duizer *et al.*, 2004) which has lead to feline calicivirus often being used as a surrogate model of infection (Bidawid *et al.*, 2003; Clay *et al.*, 2006; Doultree *et al.*, 1999). There are also a number of animal viruses found within the norovirus genus including Newbury agent II (Oliver *et al.*, 2006; Woode & Bridger, 1978) which cause diarrhoea and enteric disease in cows, a porcine norovirus recovered from pigs with diarrhoea (Bridger, 1980), an enteric canine norovirus (Martella *et al.*, 2008) and a virus recovered from a lion cub which

died from severe haemorrhagic enteritis (Martella *et al.*, 2007). The general significance of these final two viruses to the health of dog and cat populations is currently uncertain. A murine norovirus (MNV) which can be propagated in cell culture has also been discovered (Karst *et al.*, 2003) and this has led to a diversion from using FCV as a surrogate for human norovirus as MNV offers both an *in vitro* model and an *in vivo* model through laboratory mice.

Sapoviruses also gain their name from the area of the first outbreak; in this case it arises from Sapporo, Japan after the virus was isolated from an outbreak of gastroenteritis within an orphanage (Chiba *et al.*, 1980). The sapoviruses are known to cause gastroenteritis in humans (Pang *et al.*, 2009) and pigs (Saif *et al.*, 1980) and a porcine sapovirus has been adapted to grow in cell culture (Flynn & Saif, 1988). However, propagation can be difficult and will only occur in the presence of intestinal content fluid filtrate from gnotobiotic pigs (Chang *et al.*, 2004) which makes it a difficult virus to use as a model for the calicivirus family.

1.1.2 Nebovirus genera

The neboviruses gain their name from the Newbury agent 1 virus recovered from a calf with diarrhoea (Bridger *et al.*, 1984; Woode & Bridger, 1978) and classified as a calicivirus. The decision to include these viruses as part of a new genus arose with the discovery from full genome sequencing that there were only two predicted open reading frames (ORFs) on the genome and phylogenetic analyses showed the viruses clustering in a separate clade to the existing genera (Carstens & Ball, 2009; Oliver *et al.*, 2006).

1.1.3 Lagovirus genera

Rabbit haemorrhagic disease virus (RHDV) is an important veterinary viral pathogen and is found within the lagovirus genera of the calicivirus family. It is believed that RHDV evolved from a non-pathogenic version of a rabbit calicivirus (Moss *et al.*, 2002) circulating within Great Britain and Europe for centuries before developing hypervirulence during an outbreak in rabbits in China in 1984 (Liu *et al.*, 1984). This virulent disease was typified by haemorrhagic lesions forming in the liver and lungs and a very high mortality rate. The causative agent was found to be a calicivirus (Ohlinger *et al.*, 1990) and it was also noted that rabbits under 8 weeks of age were generally less affected by the disease and survived infection (Liu *et al.*, 1984). The non-pathogenic form of the virus still appears to be circulating within the general rabbit populations of Europe, Australia and New Zealand (Le Gall-Recule *et al.*, 2011) and when administered to rabbits, this avirulent virus has been shown to offer protection against the highly virulent form of the disease (Capucci *et al.*, 1996).

European brown hare syndrome virus (EBHSV) is also found within the lagovirus genera and shares some of the same features as the virulent RHDV. It was first discovered to be infecting hares in Sweden in the 1980s and is again characterised by lesions forming in the liver and a high mortality rate (Gavier-Widen & Morner, 1993). Although very similar to RHDV in morphology and clinical effects, EBHSV has been shown to be species-specific with infected rabbits not showing any signs of disease and are also not protected against subsequent infection with RHDV (Chasey *et al.*, 1992).

1.1.4 Vesivirus genera

FCV is found in the genera vesivirus alongside San Miguel sea lion virus (SMSV) and vesicular exanthema of swine virus (VESV).

VESV has been dubbed the prototype of the calicivirus family (Burroughs *et al.*, 1978) and causes vesicular disease in pigs characterised by fever and vesicle formation within the oral mucosa and also on the extremities. SMSV has been shown to produce similar clinical signs within marine mammals (Smith *et al.*, 1973) and when some SMSV isolates are used to infect swine they have been found to induce

disease which is identical to VESV (Smith *et al.*, 1973; Smith *et al.*, 1980). SMSV and VESV have also been shown to be phylogenetically close to each other through sequencing but distinct from FCV (Neill *et al.*, 1995) and as such these viruses have been thought to have evolved together in a marine reservoir and are often termed together as marine caliciviruses (Reid *et al.*, 2007).

Within this thesis feline calicivirus (FCV) will be the virus used to study the effects of infection upon host cells and as such will be discussed in detail in section 1.2. However, it is worth noting at this point that whilst cats are the only known hosts of FCV, there have been incidents where FCV-like viruses have been recovered from dogs (Hashimoto *et al.*, 1999; Martella *et al.*, 2002; Roerink *et al.*, 1999), but the role these viruses play in the epidemiology of FCV is not clear.

1.2 Feline Calicivirus

1.2.1 FCV genome

All members of the *Caliciviridae* have positive stranded RNA genomes. In direct comparisons to DNA viruses, RNA viruses have high mutation rates (Holland *et al.*, 1982), which offers a much quicker rate of genome evolution and as such may offer the virus a greater chance of survival and replication fitness (Domingo *et al.*, 1997). Mutation rates for RNA viruses have been found to be ~ 1 spontaneous mutation per genome per replication (Drake, 1993) and may rise to 1.5 per round of cell infection (Drake & Holland, 1999). This high rate of spontaneous mutation has been attributed to the lack of any proofreading capability within viral polymerases (Steinhauer *et al.*, 1992) which otherwise would be able to find mismatched nucleotides copied from the genome and repair them before translation.

The genome of FCV itself is relatively small, with full genome sequencing putting the length around 7.7 kb in length (Carter *et al.*, 1992; Sosnovtsev & Green, 1995) and is comprised of three open reading frames (ORFs) (Fig 1.2) (Sosnovtsev *et al.*, 2002). As well as the genomic RNA, infected cells also contain a subgenomic RNA (Herbert *et al.*, 1996; Neill & Mengeling, 1988; Neill *et al.*, 1991) 2.4 kb in length (Neill & Mengeling, 1988) corresponding to the 3' end of the full genome from nucleotide base position 5227 (Herbert *et al.*, 1996).

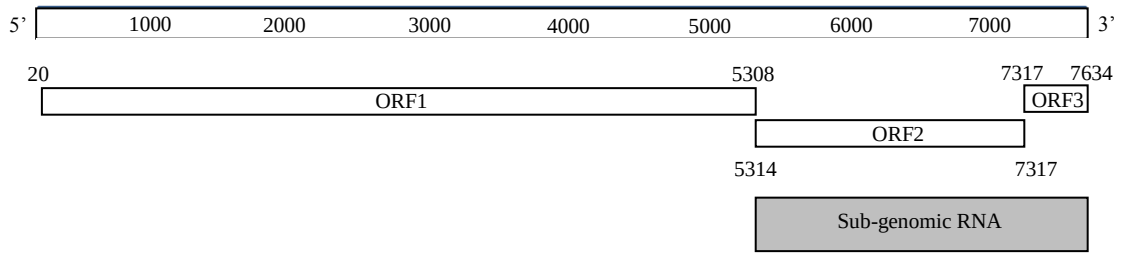

Figure 1.2. Diagram showing the position of the three open reading frames (ORFs) found upon the FCV genome and also the position of the subgenomic RNA relative to FCV-F9 (Genbank accession number m86379). Annotated numbers refer to the nucleotide base positions.

1.2.2 Proteins encoded by the FCV genome

The proteins encoded by the FCV genome can be roughly divided into two categories; structural and non-structural proteins. The non-structural proteins are translated from ORF 1 and the structural proteins are coded for by ORFs 2 and 3.

1.2.2.1 ORF 1

ORF 1 is located between nucleotides 20 and 5308 and when translated encodes for the proteinase polymerase (pro-pol) (Wei *et al.*, 2001), a nucleotide triphosphatase (NTPase) (Sosnovtsev *et al.*, 2002), the VPg (Herbert *et al.*, 1997) and other non-structural proteins (Sosnovtsev *et al.*, 2002). It has been discovered that the polyprotein encoded by ORF1 has five cleavage sites and is processed into six proteins (Sosnovtsev *et al.*, 2002) (Fig 1.3) which includes three proteins of unknown function as well as the pro-pol, VPg and NTPase.

The pro-pol is a precursor protein that is cleaved into the mature viral proteinase and RNA dependent RNA polymerase (RdRp) proteins. It is this proteinase that is responsible for the cleavage of the translated ORF1 polyprotein (Sosnovtseva *et al.*, 1999) and also for the cleavage of the precursor capsid protein into the mature protein (Sosnovtsev *et al.*, 1998). Similar RdRp proteins are found in all positive strand RNA viruses and functions as a catalyst to viral replication (O'Reilly & Kao, 1998). The uncleaved pro-pol protein has also been shown to interact with itself, VPg and the precursor to the capsid protein (Kaiser *et al.*, 2006) and this dimerisation of the polymerase is also known to occur in RHDV (Ng *et al.*, 2002) so may be an important feature of calicivirus replication.

The VPg protein is covalently bound to the 5’ end of the genomic RNA (Herbert *et al.*, 1997). This protein has often been implicated in translation as the addition of proteinase K to remove VPg protein bound to viral RNAs caused a decrease in translation (Herbert *et al.*, 1997) and sequence analysis has been shown to be similar in sequence to eIF1A a host translation initiation factor (Chaudhry *et al.*, 2006). The VPg protein has also been shown to bind directly to translation initiation factor eIF4E during FCV infection and this interaction is necessary for FCV RNA translation (Goodfellow *et al.*, 2005).

1.2.2.2 ORF 2

ORF 2 encodes for the major viral capsid protein (VP1), which has been shown to be translated as a precursor capsid protein with a leader capsid sequence (LC) (Carter, 1989) which is then cleaved to a smaller, mature capsid protein by the viral proteinase (Sosnovtsev *et al.*, 1998). The cleavage points are shown in Figure 1.3.

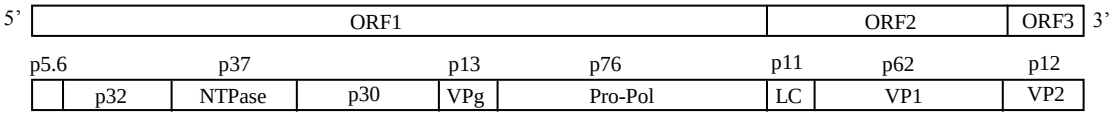

Figure 1.3. Diagrammatic representation of the cleavage map of FCV. The proteins are named when a putative function is available. Where function is not known the proteins are labelled using the protein size. For example p30 is a non-structural protein of 30 kDa in size. Adapted from Sosnovtsev *et al*, 2002.

The capsid protein can be further divided into six regions (A-F) based upon sequence conservation and variability (Neill, 1992; Radford *et al.*, 1999) (Fig 1.4). Region A is the leader capsid protein cleaved by the viral proteinase to create the mature capsid protein (Carter *et al.*, 1989) and this area has shown to be moderately variable although the cleavage site itself is highly conserved (Glenn *et al.*, 1999). Regions B, D and F are the most conserved areas of the capsid protein (Neill, 1992) which suggests that there is a functional importance of these regions. Region B has been shown to contain a putative ATP/GTP binding motif (Seal & Neill, 1995; Seal *et al.*, 1993), and there is homology between this region and the VP3 structural protein of picornaviruses (Neill, 1992; Tohya *et al.*, 1991), suggesting that region B has a similar function and that this function is crucial for viral survival in both caliciviruses and picornaviruses.

Regions C and E are both found to be variable between FCV strains (Glenn *et al.*, 1999; Neill, 1992; Seal, 1994; Seal & Neill, 1995; Seal *et al.*, 1993) (Fig 1.4). Region E is further divided by areas of variability and conservation with 5'- and 3'-hypervariable regions being separated by an area of conservation (Seal *et al.*, 1993). Predictive 3D structuring of the FCV capsid protein has been used to show that these hypervariable regions map to the outer edge of the viral structure (Chen *et al.*, 2006)

and are under positive selection pressure during viral evolution within a colony of cats (Coyne *et al.*, 2007), suggesting they contain the immunodominant antigenic regions of the virus.

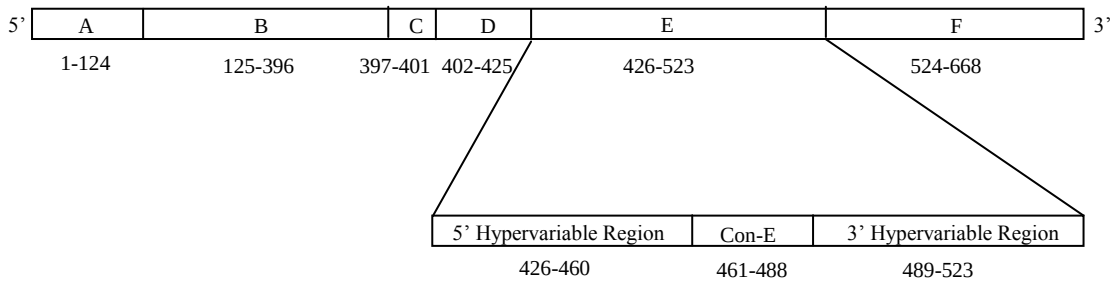

Figure 1.4. Regions A-F of polyprotein translated from ORF2 of FCV genome. Numbers indicate the amino acid position of the region boundaries. Region E is further sub-divided into 5' and 3' hypervariable regions and an area of conservation (Con-E). Amino acid boundaries are marked.

1.2.2.3 ORF 3

ORF 3 has also been found to be translated into a capsid protein as a minor capsid protein (VP2), found as 1-2 copies per virion (Sosnovtsev & Green, 2000). This protein does appear to be essential to the virus as deletion of ORF3 is lethal and mutations within the ORF3 sequence prevent the virus from being infectious (Sosnovtsev *et al.*, 2005). More recently, it has also been demonstrated that the viral capsid does not assemble correctly unless both VP1 and VP2 proteins are expressed (Di Martino & Marsilio, 2010).

1.2.3 FCV strain variability

With the positive strand RNA genome offering FCV a high mutation rate, it can be expected that there are a number of strains in circulation within the cat population. In practice, this assumption holds true both within the general cat population (Sato *et al.*, 2002) and also within populations found in rescue shelters (Bannasch & Foley, 2005; Radford *et al.*, 2001) and private cat colonies (Radford *et al.*, 2003). With colonies and shelters having larger populations of cats within a confined space than private households it has been suggested that they offer optimal conditions for strain evolution. In 2003, a study by Radford *et al*, showed that cat colonies often have their own strains of FCV circulating within them but the variation within these cat colonies in the immunodominant regions of the capsid gene could be as high as 16% (Radford *et al.*, 2003). This diversity is consistent with the virus evolving from a common ancestor within the colony. A longitudinal study of virus diversity within an endemically infected cat colony showed that some cats were persistently infected with their own strains which gradually evolved. However, within the same colonies, other cats seemed to undergo cycles of re-infection such that they became infected and recovered from one strain of FCV before picking up a second strain (Coyne *et al.*, 2007). In addition to evolution by substitution, such high prevalence colonies provide the ideal environment for mixed infections and recombination (Coyne *et al.*, 2006c). At the beginning of the Coyne *et al*, study (2006) the colony was found to be infected with only one strain but later sampling showed a second virus strain had entered the colony. Subsequent sampling showed that a recombinant virus containing the polymerase gene from the first strain and the capsid gene from the second strain was now circulating within the colony. The recombination event was mapped to the region of the ORF1 and ORF2 junction. Such recombination events may offer viruses found within closed populations a quicker method of mutation to avoid host immune responses and will aid viral diversity within a population.

1.2.4 Clinical signs

Since there are a wide range of strains of FCV circulating within the feline population, it is perhaps not surprising that there are also a wide range of clinical signs associated with FCV infection (Radford *et al.*, 2009; Radford *et al.*, 2007).

1.2.4.1 Upper respiratory tract disease

A cat presenting with typical FCV infection will often be suffering from acute upper respiratory tract disease (URTD), symptoms often including ocular and nasal discharge and ulcers on the oral mucosa (Cai *et al.*, 2002; Povey, 1974). The disease is not usually fatal except where the URTD develops into pneumonia and more serious respiratory conditions, although this is usually limited to young kittens (Love & Baker, 1972).

1.2.4.2 Limping syndrome

Feline calicivirus is also known to cause acute temporary arthritis in the joints of cats which cause symptoms often described as limping syndrome. These effects have been reproduced through infecting experimental specific pathogen free (SPF) cats in the laboratory (Dawson *et al.*, 1994; TerWee *et al.*, 1997). The experimentally infected cats in the Dawson *et al* study showed signs of pyrexia, lethargy, anorexia, oral ulceration and URTD in addition to severe lameness and FCV was recovered from the joints of the affected cats.

1.2.4.3 Chronic stomatitis

There is also some evidence of an association between chronic stomatitis, a condition typified by chronic ulcerative lesions in the gingival, fauces and sometimes the cheeks and tongue, and FCV (Healey *et al.*, 2007; Knowles *et al.*, 1989; Poulet *et al.*, 2000; Waters *et al.*, 1993). In the Knowles 1989 study, cats with chronic stomatitis were swabbed alongside a control population and where the control had an FCV prevalence of 0-19%, the chronic stomatitis suffering groups had an FCV prevalence of between 50-92%. Inducing chronic stomatitis experimentally has

proved impossible; however, an accidental infection of FCV in experimental cats previously infected with FIV caused 9/13 to develop chronic gingivitis which may point to co-infections being important in the ultimate development of the condition (Waters *et al.*, 1993).

1.2.4.4 Virulent systemic FCV

More recently, a virulent, systemic form of FCV (VS-FCV) has emerged in outbreaks in the UK (Coyne *et al.*, 2006b), USA (Hurley *et al.*, 2004; Pedersen *et al.*, 2000; Schorr-Evans *et al.*, 2003) and France (Reynolds *et al.*, 2009). High mortality rates have been associated with all the outbreaks and a wider range of clinical symptoms has been observed.

The first outbreak was reported by Pedersen *et al* in 2000 and occurred in a rescue centre and animal clinic in California, USA. In this outbreak a 4 month old kitten from the rescue shelter was found to be suffering from severe URTD and was hospitalised by the animal clinic. Whilst the kitten was hospitalised at the clinic, two other cats visited the clinic and became sick within 4-5 days and had to be re-hospitalised. The clinical signs exhibited by these cats included fever, anorexia, lethargy, depression and ulceration, with oedema of the face and limbs; both cats made a full recovery. Four more cats were affected during this outbreak but these cats were not present in the hospital until they became sick through infection; three were housemates of the two re-hospitalised cats and one was the pet of one of the workers at the veterinary clinic. Of these four cats, two made a full recovery after showing signs of conjunctivitis, fever, oedema, lethargy, nasal congestion and sneezing but the other two cats died or were euthanised. The dead cats both exhibited similar clinical signs to the other infected cats but with more extensive swelling and oedema and deeper lesions which were severely encrusted.

Feline calicivirus was recovered from one of the dead cats (FCV-Ari) and was subsequently used to experimentally infect SPF cats with all three kittens infected showing signs of fever, oedema of the face and limbs, nasal congestion, ocular discharge and anorexia with one of the kittens having to be euthanised. Whilst this experimental infection was being carried out, four other laboratory cats housed two rooms away from the experimentally infected kittens became infected by

contamination, suggesting this virus to be highly infectious even within the confines of an experimental facility. One of these cats was discovered dead within two weeks of the experimental infection commencing with the other three cats showing signs of fever and depression before the decision was made to euthanise them. The authors also performed some genetic analysis upon the FCV-Ari isolate and found that when the capsid gene was sequenced it was a typical FCV strain, with no apparent features to distinguish it from other field and vaccine strains found within the general cat population.

Two further outbreaks have been reported in the USA (Hurley *et al.*, 2004; Schorr-Evans *et al.*, 2003) and in both outbreaks a similar pattern of mortality and clinical signs was observed. In the Schorr-Evans *et al*, 2003 report, 24 cats in a small animal hospital were infected after cats from a neighbouring animal shelter were admitted showing signs of severe URTD. Several other cats hospitalised at the same time were readmitted to the hospital showing signs of fever and anorexia and later developing oedema of the face and limbs, jaundice and oral ulceration. Again in this outbreak a cat belonging to a hospital employee that had never been hospitalised during the outbreak was also found to be infected with the outbreak strain which suggests that the virus can be easily transmitted by fomites. This outbreak had an overall mortality rate of 32% with the virus isolated as the causative agent being designated FCV-Diva. FCV-Diva was sequenced along the hypervariable region of the capsid gene and was found to group separately from both FCV-Ari and FCV-F9 which proves that this outbreak arose from a separate mutation event and not from transmission of the first outbreak strain (FCV-Ari).

In the outbreak described by Hurley *et al*, (2004) the infection was spread across three veterinary practices, a rescue shelter and its associated foster homes, affecting 54 cats in total. Again the clinical signs reported were similar to the first outbreak with fever, oedema of the face and limbs, oral ulcers, nasal discharge, ocular discharge and jaundice all being reported during the outbreak. The overall mortality rate found was 40% and it was also noted during this study that cats older than one year were more likely to get severe disease than kittens. The virus isolated was named FCV-Kaos and again, sequencing of the hypervariable region of the capsid gene showed that FCV-Kaos was a genetically distinct strain, different from both FCV-Ari and FCV-F9.

There have also been outbreaks of virulent systemic disease (VSD) associated with FCV infection in Europe. In France, there was an outbreak of VSD in a veterinary teaching hospital in 2005 with eight cats infected (Coyne *et al.*, 2006b; Reynolds *et al.*, 2009). As with the US cases, the infection appeared to be nosocomial where a cat was admitted to a teaching hospital with depression, hypothermia, oedema of the face and limbs and oral ulceration. The cat was euthanised two days after admission. Over the course of a month, seven more cats were infected with VS-FCV including two cats which were suspected to be infected at home through transmission via their owners who were students studying at the hospital at the time of the outbreak. All cats infected during this outbreak exhibited the clinical signs reported previously and the mortality associated was 63% which is also in keeping with the other outbreaks.

In the UK outbreak of VS-FCV, reported by Coyne *et al* (2006b), three kittens were initially fostered from a local rescue shelter into the home of one of the workers at the shelter. These kittens showed some signs of lethargy but did not display the other clinical signs associated with VS-FCV. Two of the fostered kittens died over the next six days and over the course of two weeks after the fostering occurred three of the four cats already living in this household went on to exhibit signs of infection with VS-FCV. All three of these cats suffered pyrexia and voice loss with two of the three also suffering some form of pain in the leg/lameness. However, only one of the three cats infected in the foster household suffered lethargy, oedema, vomiting and jaundice. A fourth adult cat was also infected during this outbreak from the household next-door to the foster home and this cat showed signs of fever, lethargy, voice loss and jaundice during the course of infection. The mortality rate found in this outbreak was 71% and once again the viruses isolated from the infected cats and sequenced showed that the FCV strains associated with this outbreak were phylogenetically different to the previously reported cases of VS-FCV.

Attempts to identify the origin of these outbreaks by sequencing the capsid gene of VS-FCV strains from outbreaks has shown that each virus was phylogenetically distinct, representing a new strain or sequence type (Coyne *et al.*, 2006b; Hurley *et al.*, 2004; Pedersen *et al.*, 2000; Reynolds *et al.*, 2009; Schorr-Evans *et al.*, 2003). As such it appears that each outbreak is caused by a newly emerged and hypervirulent virus, that rapidly spreads locally, before eventually being eradicated. These apparently conflicting observations suggesting high transmission as well as rapid

extinction have been hypothesised to be associated with behavioural changes in affected cats, such that infected animals become poor transmitters of the hypervirulent viruses (Coyne *et al.*, 2006b).

Several attempts have been made to identify markers of hypervirulent strains that could help explain the pathogenesis of this disorder, as well as act as a diagnostic marker for hypervirulence that could be used to aid disease control (Abd-Eldaim *et al.*, 2005; Foley *et al.*, 2006). Using full genome sequence of two hypervirulent strains, Abd Eldaim *et al* (2005), showed that whole sequence similarity was around 80% for each strain examined. In addition, the authors reported a consistent motif within the amino acid sequence of the VS-FCV strains at position 443 of the capsid protein with asparagine being replaced by serine. This mutation was predicted to create an extra glycosylation site. In a similar study, sequence analysis of VS-FCV strains also predicted the generation of a conserved additional glycosylation site in hypervirulent strains (Foley *et al.*, 2006) and led the authors to speculate that novel receptors or other host-virus interactions could occur as a result of mutated capsid protein structure, allowing VS-FCV strains to target epithelial or endothelial sites. Unfortunately, the two motifs identified within these studies are not consistent and as such may just be a reflection of the variability of the FCV genome, especially within the FCV capsid (Radford *et al.*, 2007).

More recently, studies on the kinetics of growth of FCV in cell culture have led to the suggestion that VS-FCV strains may grow more efficiently *in vitro* under multiple growth cycle conditions than non-VS isolates and this may be a phenotypic characteristic common to all VSD strains (Ossiboff *et al.*, 2007).

1.2.5 Epidemiology

Within the general cat population FCV has a relatively high prevalence of 10-25% of vet visiting cats (Harbour *et al.*, 1991; Porter *et al.*, 2008; Wardley *et al.*, 1974) with prevalence generally increasing within multi-cat households, colonies and shelters up to 70-90% (Bannasch & Foley, 2005; Coyne *et al.*, 2006a; Coyne *et al.*, 2007). This higher prevalence within the multi-cat environments is thought to arise from there being a mixture of acutely infected cats, progressive evolution of the virus within cats undergoing long-term infections and subsequent re-infection of recovered cats with newly evolved viruses (Coyne *et al.*, 2007). The virus has also been found to recombine within these closed environments (Coyne *et al.*, 2006c) which again allows the opportunity of re-infection of cats which have previously recovered from FCV infection within the colony. The virus has also been shown to persist outside of the cat on fomites for up to three days (Clay *et al.*, 2006) which allows the virus an advantage for finding a host and this trait has also been reported in being key in the outbreaks of VS-FCV (Coyne *et al.*, 2006b; Hurley *et al.*, 2004; Pedersen *et al.*, 2000; Reynolds *et al.*, 2009; Schorr-Evans *et al.*, 2003).

These relatively high infection rates and prevalences are despite FCV vaccination being included annually for cats. Traditionally these vaccinations are based upon a single strain such as FCV-F9 (Bittle & Rubic, 1976; Bittle, 1960) or FCV-255, however, there have now been two vaccines developed that includes two FCV strains (Huang *et al.*, 2010; Poulet *et al.*, 2005), and another vaccine developed in Japan containing three strains of FCV (Masubuchi *et al.*, 2010) which may offer increased protection against a greater number of FCV strains (Addie *et al.*, 2008). One reason that the prevalence of FCV may have remained high despite vaccination is due to the fact that although vaccination reduces the severity of FCV associated clinical signs; it does not reduce infection (Binns *et al.*, 2000; Dawson *et al.*, 1991; Gaskell *et al.*, 1982).

1.2.6 Host-pathogen interaction

As FCV has been used as a model of norovirus infection in humans for many years it may be expected that the mode of action of the virus within the cell has been well documented. However, as FCV only grows in feline cell lines the use of this non-model organism has hampered these kinds of studies.

In 2003, two separate studies into the role of FCV infection in cell death were performed and both showed that FCV-infected cells showed signs characteristic of apoptosis (Roberts *et al.*, 2003; Sosnovtsev *et al.*, 2003). Sosnovtsev *et al*, showed that during infection with FCV-Urbana, Crandell-Rees feline kidney (CRFK) cells displayed typical signs of cellular apoptosis. Staining of infected cells with 4', 6-diamidino-2-phenylindole (DAPI) showed chromatin condensation from 5hrs post infection (p.i.) and DNA fragmentation was shown from 8-10hrs p.i.. The authors also showed that caspases were activated during infection with FCV and that although three cellular caspases were found to be activated, caspase-3 activity was found to be at a much higher level than caspase-8 and -9.

Roberts *et al*, also found very similar results in their study with chromatin condensation being visualised and caspase-3 activation being confirmed by Western blotting. Further investigation of the role of these caspases and their importance in FCV infection by Al-Molawi *et al* (2003) demonstrated that caspases were important in the processing of the viral capsid protein. They showed that when the caspases were inhibited viral capsid processing was not observed and that viral capsid cleavage occurred concurrently with caspase activation.

Further investigation has now shown that the apoptotic pathway being triggered in response to FCV infection is the mitochondrial pathway (Natoni *et al.*, 2006) which again suggests that the signal to begin this process during infection is intrinsic within the cell. Many of the hypotheses regarding apoptosis within the *Caliciviridae* have been developed following the discovery that RHDV induces apoptosis especially within hepatocytes (Alonso *et al.*, 1998; Jung *et al.*, 2000). There are also parallels to be drawn with MNV infection as this norovirus has also been shown to induce apoptosis (Furman *et al.*, 2009) and to down-regulate proteins known to inhibit the onset of apoptosis within the cell (Bok *et al.*, 2009).

Other studies into the relationship between the host and FCV have shown that during infection host-cell protein synthesis is inhibited by cleaving of translation initiation factors (Willcocks *et al.*, 2004). Levels of host-protein synthesis were measured using pulse labelling of amino acids and it was found that there was a 50% reduction of host protein synthesis by 5 hrs p.i.. A hypothesis was developed that FCV may act in a similar manner to picornaviruses and have an effect upon two translation initiation factors eIF4GI and eIF4GII (Krausslich *et al.*, 1987), and these proteins were shown to be cleaved during FCV infection. The authors also tested whether this cleavage was as result of caspase activation. When caspases were inhibited, the cleavage of the initiation factors was delayed but not completely inhibited although the cleavage products produced were different to those from FCV infected cells. This led the authors to conclude that the cleavage of the translation initiation factors observed during infection is not a result of caspase activation but as a direct consequence of FCV infection.

One of the most exciting developments in understanding the mechanisms of FCV infection has been the discovery of a possible receptor used during viral entry; feline junctional adhesion molecule (fJAM-1) (Makino *et al.*, 2006). Previous studies had only been able to elucidate that FCV binds to feline cells more efficiently than other non-FCV permissive cells (Kreutz *et al.*, 1994) but no receptor had been identified until Makino *et al* used an expression cloning method to identify surface molecules that interact with FCV. They identified fJAM-A as a binding receptor for FCV and tested this finding by binding the fJAM-A receptor with antibodies which decreased FCV infectivity. They also introduced JAM-A receptors to non-FCV permissive cell lines and found that these altered cell lines then became permissive to FCV infection. This receptor discovery has opened the way for further investigations into how the virus interacts with these glycoproteins in viral entry. The fJAM-A domains required for FCV entry into cells have been mapped (Ossiboff & Parker, 2007) along with the way it interacts with the viral capsid protein (Bhella *et al.*, 2008; Ossiboff *et al.*, 2010). Analysis of fJAM-A distribution within feline cells has also lead to the development of hypotheses regarding the nature of vesicle formation during FCV infection; confocal microscopy has shown that where fJAM-A is normally found to be localised at cell-cell junctions during infection with FCV fJAM-A becomes

redistributed into the cytosol which may contribute to the breakdown of intercellular junctions (Pesavento *et al.*, 2010).

More recently, a further potential receptor for FCV has been described by Stuart *et al,* in the form of α2,6-linked sialic acid which may help to explain why the fJAM-A antibodies in the Makino *et al* study only reduced infection and did not eradicate it (Stuart & Brown, 2007).

1.3 Post-genomic technologies for investigation of host-pathogen interactions

There are now many more technologies available for exploration of host-pathogen interactions at both the cellular transcription and translation level. At the inception of this PhD, these technologies were not being used to test modifications found in the host as a result of viral infection and as such we wanted to explore whether or not these techniques could be applied to virology. Feline calicivirus was chosen as a model virus as relatively little had been elucidated about the mechanisms used by FCV to infect cells but also as a strong *in vitro* system was already available to study this virus.

1.3.1 Viral proteomics

The proteome is the entire complement of proteins expressed by the genome of a cell or tissue at a particular time under certain conditions. The study of these proteomes has become known as proteomics. Developments in mass spectrometry coupled with an increased availability of full genome sequence have allowed for proteomic analysis to be applied to viruses and viral hosts. These techniques are also useful for examining interactions on a more global scale with many proteins available for analysis within a single proteomics experiment.

Within this thesis, changes in the host cellular proteome in response to infection with FCV will be found using a technique known as two-dimensional difference in gel electrophoresis (2D-DIGE) (see section 1.3.1). 2D-DIGE has been used successfully in examination of host proteome changes during infection of porcine endothelial cells with classical swine fever virus, a positive stranded RNA virus from the *Flaviviridae* (Li *et al.*, 2010). During this analysis 15 proteins were found to be differentially expressed and 8 were successfully identified by mass spectrometry showing that during infection the virus altered the host cell metabolism, proliferation and the cytoskeleton.

2D-DIGE has also been used to attempt to find biomarkers in the blood plasma and urine of patients infected with hepatitis E virus (HEV) (Taneja *et al.*, 2009). Within the Taneja *et al* study, the analysis found 30 proteins that were differentially

expressed in the HEV infected patients when compared to control samples from healthy controls. From these 30 modulated proteins, two were shown to be possible biomarkers for acute HEV infection and as such may be important in future diagnoses.

1.3.1.1 2D-DIGE

Relative quantification of protein changes between samples separated by two-dimensional gel electrophoresis is a difficult process due to the poor reproducibility of the 2D polyacrylamide gels. One solution to this problem has been to label all the proteins in a sample with three fluorescent dyes allowing more than one sample to be run on a single 2D gel, this technique is known as two-dimensional difference in gel electrophoresis (2D-DIGE).

The principal behind 2D-DIGE is the ability to visualise spots from different samples separately upon the same 2D polyacrylamide gel. For this to be possible three CyDye fluors have been developed which fluoresce at separate wavelengths but are also mass and charge matched so that any protein which is labelled with a CyDye migrates to the same position on a 2D gel (Unlu *et al.*, 1997). With the ability to run three samples on one 2D gel comes the opportunity to use one of the three dyes to label an internal standard. The internal standard is a pool of all of the samples to be analysed which means that it contains every protein from every sample and this is included on each gel analysed as part of the experiment. With this internal standard included in every gel run, it allows for each gel to be matched to each other and for inter-gel analysis to be completed. A workflow for a DIGE experiment can be seen in Figure 1.5.

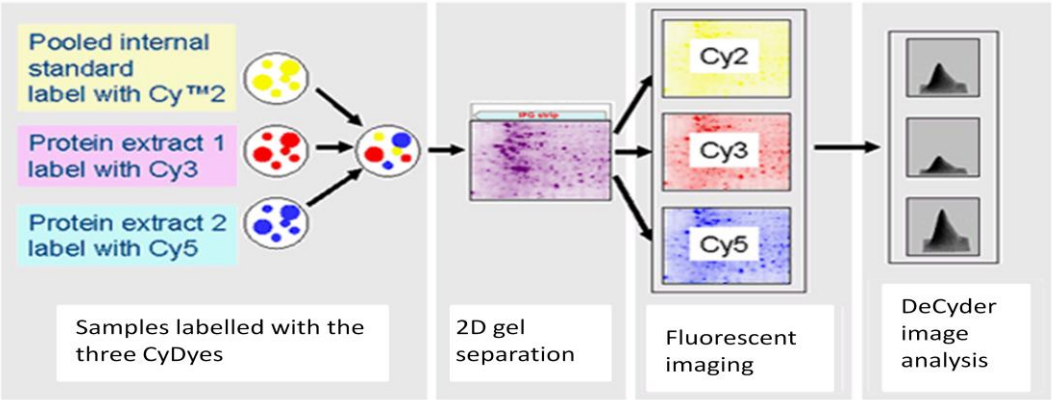

Figure 1.5. Typical workflow for a 2D DIGE experiment (Image taken from GE Healthcare literature).

The internal standard also allows for standardisation across all gels within the experiment as every protein spot can be compared to its counterpart in the standard and a relative abundance calculated automatically using the associated software (DeCyder, GE Healthcare). This process helps to remove inter-gel variation as the abundance of each protein spot is calculated against the standard on that gel so if a spot is missing or enlarged in the sample then it can be referenced back to the standard to ensure that the change is real and not just a result of gel variation (Fig. 1.6).

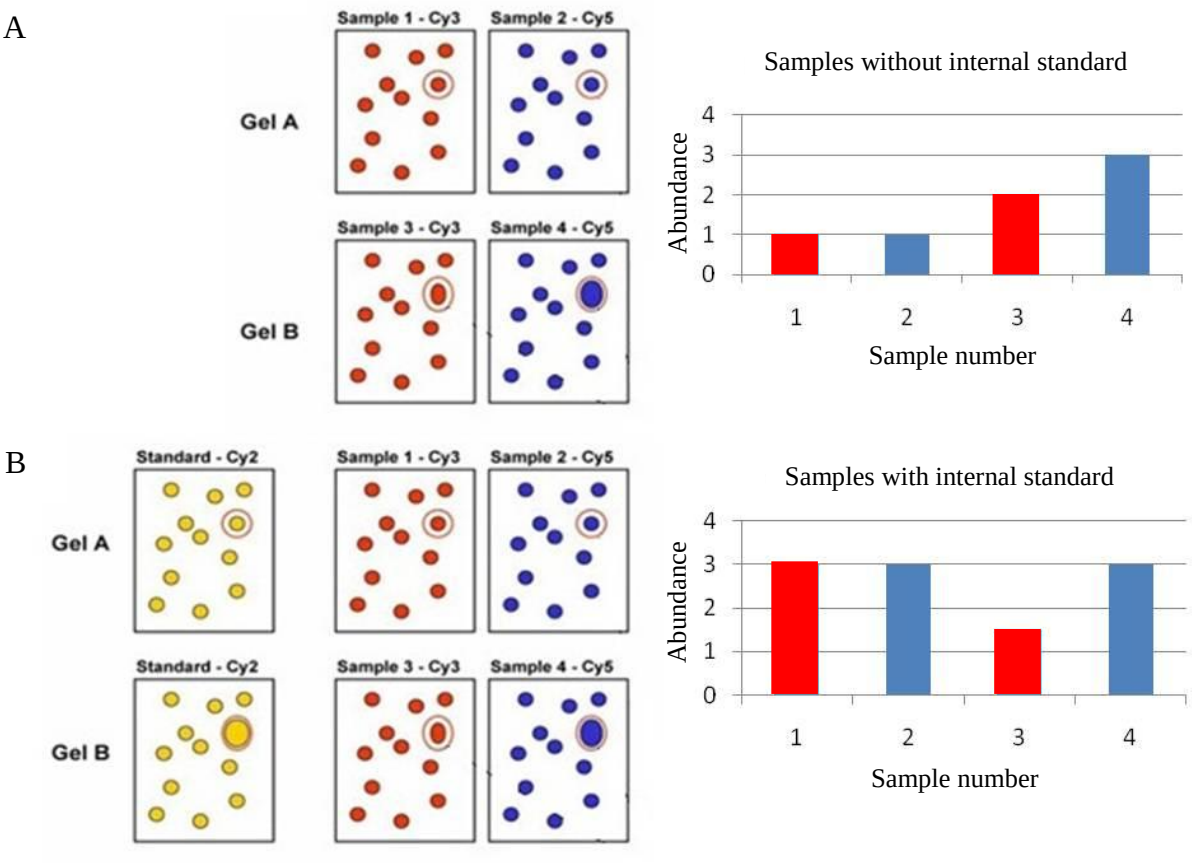

Figure 1.6. Analysis of protein abundance without and with a protein standard present. (A) When analysed without the presence of an internal standard, spots from samples 3 and 4 appear to be up-regulated. (B) When the same samples are analysed with the internal standard present, sample 3 is down-regulated and sample 4 has the same abundance as samples 1 and 2. (Image adapted from GE Healthcare literature)

1.3.2 Viral transcriptomics

Alongside investigations into host proteome changes during infection, changes in host gene transcript levels will be investigated. The traditional method to do this is via microarray analysis or through Sanger sequencing. However, advances in next-generation sequencing technologies have opened up new methodologies for transcriptomic investigations.

1.3.2.1 Microarray

For over a decade, gene transcription has been monitored and assessed by microarray analysis using techniques derived from southern blotting to target genes with specific oligo probes (Ramsay, 1998; Schena *et al.*, 1995). In a typical microarray experiment a chip containing thousands of bound single stranded cDNA or cRNA probes is interrogated with a labelled sample of cDNA/cRNA where complementary genes hybridise with the probes. The hybridisation reaction can either be with many of the probes, with few of the probes or with none of the probes and when the array is excited with a laser the spectra produced can be used to determine the extent of the hybridisation of the sample with the probes. These hybridisation spectra can then be compared to a reference sample and differences in gene expression found and investigated.

There are inherent problems with microarray technologies however, as although many thousands of genes can be interrogated in a single experiment, novel gene transcripts cannot be found using this kind of technology. Microarrays also have the limitation that despite being able to design chips that can detect SNPs and alternative gene splicing they do not allow the user to interrogate the sequence of the transcripts directly. The arrays are also limited in the methods used to quantitate the number of transcripts found in each experiment as they use a relative intensity from the hybridisation reactions to measure abundance and as such do not give an absolute quantification of transcription.

In the analysis of the *Caliciviridae*, microarrays have only been used to interrogate host-pathogen interactions in a norovirus replicon system (Chang, 2009). It was discovered that genes in cholesterol and carbohydrate metabolic pathways were

significantly modulated and when these pathways were disrupted experimentally the levels of replication of the norovirus replicon reduced significantly. Microarrays have also been employed in attempts to detect norovirus isolates in food (Ayodeji *et al.*, 2009) and water sources (Brinkman & Fout, 2009).

1.3.2.2 Serial analysis of gene expression

The first examples of using sequencing technology to interrogate transcriptomes employed techniques based on Sanger method (Sanger *et al.*, 1977) such as serial analysis of gene expression (SAGE) (Velculescu *et al.*, 1995). However, the costs of deep sequencing using technologies developed from this method have proven to be prohibitive.

1.3.2.3 RNA-seq

More efficient and cost-effective sequencing techniques have since been developed and have become more commonly known as "next-generation sequencers" and these have been successfully employed in determining gene transcript levels in a technique called RNA-seq. The most commonly used platforms for this kind of sequencing are the Roche 454, ABI SOLiD, Illumina Genome Analyser and HeliScope with each of these using a different method to sequence samples. These new platforms allow for rapid, in depth sequencing which opens up the possibility of interrogating whole genomes in a very short space of time (Wang *et al.*, 2009).

1.3.2.3.1 Roche 454

The Roche 454 systems works by first generating a single stranded template DNA library, amplifying each template read in the library separately using emulsion PCR and then sequencing the amplified templates through sequencing-by-synthesis (pyrosequencing) (Margulies *et al.*, 2005). This method of sequencing works by adding nucleotides sequentially to the samples across a plate, if this nucleotide stream is complementary to the nucleotide found in the template sequence then the nucleotide is incorporated and a polymerase extends the complementary sequence. This addition of the nucleotide results in a reaction which emits a light signal which

can be recorded and the complementary sequence to the template elucidated. This methodology allows 1,000,000 individual reads to be determined per 10 h sequencing run with individual read lengths of 400-500 bp.

1.3.2.3.2 Illumina

The Illumina Genome Analyser (Bentley *et al.*, 2008) uses a slightly different technique to sequence transcriptome libraries whereby the mRNA or cDNA sample is firstly fragmented, the ends polyadenylated before adaptors are attached to each end. A bridge PCR technique is used to amplify the library with a flow cell surface containing oligo probes being used to ligate to the adaptors attached to each piece of the fragmented library. From these ligations the template library can be cloned to produce an area upon the surface with a large concentration of the template to be sequenced. The reverse strands are cleaved and a cap is placed onto each piece of DNA before sequencing primers are hybridised and sequencing commences. The sequencing occurs base by base along the template, with all four nucleotides added in competition to try to ensure that only the correct complementary base is incorporated into the sequence. Each of the four nucleotides has a different fluorescent label so when it is integrated a different signal is emitted and this can be recorded by the sequencer. The Illumina system gives read lengths of up to 150 bp with up to 6.5 Gb generated in 24 h run with 100 bp read lengths.

1.3.2.3.3 HeliScope

The HeliScope sequencer is the first next generation sequencer not to employ an amplification or cloning phase as part of the sample preparation; rather the sequencer can employ single pieces of DNA or RNA as the template (Harris *et al.*, 2008). Firstly, the entire sample is fragmented and if the sample is double stranded DNA the double-helix is melted into single strands before each strand is polyadenylated. The polyadenylated samples are then hybridised to a flow cell primed with oligo dT which capture each fragment and allows them to be interrogated base by base. Fluorescently labelled nucleotides are added one at a time to the flow cell and if they are complementary to the template they are added to the complementary strand and emit a fluorescent signal which is recorded by the sequencer to build up a sequence

complementary to the template. The HeliScope generates an average read length of 35 bp with 21 to 35 Gb per run.

1.3.2.3.4 SOLiD

Finally, there is also the SOLiD sequencer from ABi available to use in sequencing the whole transcriptome or genome of a sample (Cloonan *et al.*, 2008). SOLiD sequencing works by taking a whole DNA/RNA sample and fragmenting it with an enzyme, before each fragment is hybridised with SOLiD based adaptors. Each fragment is reverse transcribed and size selected to gain reads of the correct size before being amplified by PCR. This library is then placed through a phase of emulsion PCR where the adaptors on the fragmented templates hybridise to beads and an emulsion is created to isolate one bead and one DNA fragment in separate microreactions within the PCR mix. Over 30,000 copies of the templates are made within the microreactions on the bead and these beads are covalently attached to a glass slide for sequencing. SOLiD sequencing is performed by interrogating the templates with fluorescently labelled di-base probes and using multiple rounds of primer ligation. The primers used anneal in a position n-1 of the previous primer used to allow each base of the template to be sequenced more than once which should ensure a high accuracy of sequencing. The SOLiD sequencing process creates reads of 50 bp in length and up to 30 Gb from a 7 day sequencing run.

1.3.2.4 Bioinformatic normalisation of RNA-seq

With all of these sequencing technologies the whole transcriptome can be interrogated very quickly and sequenced transcripts can be mapped back to a reference genome. Very approximately, it could be said that the more transcripts mapping to a gene on the reference genome then the more transcription of that gene is occurring within the cell. In truth, with every system the reads mapping to the reference genome must be normalised either at the mapping stage by using a normalisation such as RPKM values (Reads Per Kilobase of exon model per Million mapped reads) (Mortazavi *et al.*, 2008) or through an analysis package design to deal with the variance within transcription samples such as DeSeq (Anders, 2010). These normalised values can then be compared to other samples and comparisons drawn to

discover whether there is a pattern of differentially transcribed genes between the samples compared.

1.3.2.5 Applications of RNA-seq

With next-generation sequencing technology being so new and RNA-seq still being in its infancy at the time of writing there are only a few hundred studies currently published in which RNA-seq is used in transcriptome analysis. There are even fewer studies published using RNA-seq to examine viruses and at time of writing there is only a single study published that concentrates on the effects the virus has upon the host. Woodhouse *et al* (2010) have published a study which uses RNA-seq, microarrays and proteomics to investigate infection with hepatitis C virus (HCV). This study found that microarray analysis identified the greatest number of non-redundant differentially transcribed genes with almost twice as many as found by RNA-seq. The proteomic analysis identified a smaller number of non-redundant differentially expressed proteins than either of the methods analysing gene transcription levels. Analysis was also undertaken to find any genes/proteins which were identified as modulated by all three of the techniques employed and the authors discovered that there was only a single gene/protein from over 2000 separate gene and protein identifications which was common to all three methods. The results from this study give further evidence to the usefulness of employing more than one technique when studying host-pathogen interactions as the full picture is often missed if only one technique is used.

1.4 Aims

The overall aim of this thesis was to discover the ways in which host cellular proteins and genes are manipulated *in vitro* by feline calicivirus during infection and to use these findings to generate further hypotheses. More specifically the aims were:

- To use proteomic methods in the form of 2D-DIGE to discover changes in the host proteome over a time course of infection with a single FCV strain.
- To use 2D-DIGE to determine whether changes in the host proteome differ during infection with FCV strains of varying virulence.
- To further investigate host protein changes found during the proteomics experiments through immunofluorescent staining and confocal microscopy.
- To use next-generation sequencing technology to determine whether any changes occur at the transcriptional level and whether those changes are consistent with changes observed at the protein level.
- To attempt to gain whole genome sequence for the putative virulent FCV strain obtained from the UK outbreak of virulent systemic disease.

2 Chapter two

Analysis of differentially expressed host cell proteins during infection with FCV-F9

2.1 Introduction

To understand the mechanisms of viral infection and replication, it is very important to consider the effects the virus has upon the host cell machinery which often involves changes both at the gene and protein level. In the past these changes have often had to be elucidated and studied one pathway at a time. In the study of calicivirus infections, hypotheses have often been developed and tested based upon discoveries made in the *Picornaviridae* leading to discoveries such as FCV inhibiting cellular protein synthesis through selective cleavage of eukaryotic initiation factors (Willcocks *et al.*, 2004) and that FCV induces apoptosis to allow cleavage of viral capsid proteins by caspase enzymes (Al-Molawi *et al.*, 2003). Whilst the one pathway at a time approach is useful in discovering whether FCV behaves in a similar way to viruses that have already been extensively studied, it makes it much more difficult to discover any novel pathways being targeted during infection. For these situations it may be beneficial to use a more global approach to find changes induced within the cell as a result of viral infection.

Recent advances in technology have allowed proteomic techniques to be developed that aid discoveries at a whole cell proteome level and allow for large groups of proteins to be analysed in a single experiment. These techniques have been successfully employed in discovering host-pathogen interactions in intracellular parasite invasion (Nelson *et al.*, 2008) uncovering novel protein modulation as well as confirming previous hypotheses of host-pathogen interactions. More recently, these approaches have begun to be employed in virology to elucidate changes in whole cell proteomes induced by infection (Vester *et al.*, 2009; Xiao *et al.*, 2010) and in this chapter these proteomic techniques will be used to interrogate cells infected with FCV-F9.

Through using 2D-DIGE upon FCV-F9 infected cells in this chapter it is hoped that a picture of changes in protein expression in response to infection can be established. It is therefore important to be sure that the strain used is truly FCV-F9 and not a mixture of viral strains, such as is sometimes used in vaccination to offer a wider cross-protection (Huang *et al.*, 2010; Poulet *et al.*, 2005) and also can be found naturally within cats (Coyne *et al.*, 2007). The decision was therefore made that an aliquot of FCV-F9 should be plaque purified and sequenced to ensure only one strain was analysed and that the strain used was truly FCV-F9.

To inform the decision as to the time points to be analysed by 2D-DIGE, a growth curve was performed upon the plaque purified FCV-F9 and from the results four time points were selected. These time points were chosen to allow a full picture of protein changes over a time course of infection to be deduced and then the modulated proteins could be identified using mass spectrometry. These modulated host proteins could then be assessed for functions within the cell and host-pathogen interactions could be inferred.

2.2 Materials and methods

2.2.1 Cells and viruses

2.2.1.1 Cell culture

All cell culture media and reagents were made up according to standard laboratory protocol and are listed in Table 2.1.

A FCV permissive, undifferentiated, diploid cell line called feline embryo cell line A (FEA) (Jarrett *et al.*, 1968) was used through the entire study with passage levels between 43 and 60. FEA cells were chosen as they are an undifferentiated cell line and as such offer the closest *in vitro* equivalent to the whole cat.

The cells were cultured in Eagle's minimum essential medium (Sigma-Aldrich) supplemented with the appropriate amount of fetal calf serum (FCS) (PAA Laboratories Ltd) for growth medium (GM) or maintenance medium (MM) (Table 2.1).

Cells were grown to confluence in either flasks or plates (Corning, Fisher scientific) within an incubator set at 37°C and 5% CO_2. The cells were passaged every three or four days by removing the media and washing twice with PBS before adding 1 ml PBS/EDTA/Trypsin and leaving in the incubator for 1 min to detach the cells from the plastic. The cells could then be used to seed flasks and plates in a split ratio of 1:3. All passaging steps were performed in a sterile hood.

Table 2.1. Stock solution recipes used in cell culture.

Cell culture media stock	Stock concentration	Recipe
PBS	10x	**90 g NaCl 2.25 g KCl 13 g $Na2HPO_4$ 2.25 g KH_2PO_4 Make up to 900 ml with ddH_2O**
PBS	1x	**Add 88 ml 10x PBS to 800 ml ddH_2O**
PBS/EDTA	1x	**Add 0.18 g EDTA to 900 ml 1x PBS**
PBS/EDTA/Trypsin	1x	**Add 1 ml to 50 ml PBS/EDTA**
L-Glutamine (G3126, Sigma Aldrich)	100x 200 mM	**2.92 g in 100 ml ddH_2O**
Penicillin/Streptomycin (P4333, Sigma Aldrich)	100x 10 mg/ml	**As bought**
Amphotericin B (solubilised) (A9528, Sigma Aldrich)	1000x	**Add 100 mg to 50 ml with ddH_2O**
Sodium bicarbonate 7.5% solution (S8761, Sigma Aldrich)	100x	**As bought**
Eagles minimum essential media (MEM) (D2429, Sigma Aldrich)	10x	**As bought**
Non-essential amino acids (NEAA) (M7145, Sigma Aldrich)	100x	**As bought**
Stock media	1x	**100 ml EMEM 10 ml $NaHCO_3$ 10 ml NEAA 10 ml L-glutamine 10 ml Penicillin/Streptomycin 1 ml Amphoterocin B ddH_2O to 1 litre**
Growth media (GM)	7%	**100 ml stock media plus 7 ml fetal calf serum (FCS) (F6178, Sigma Aldrich)**
Maintenance media (MM)	1%	**100 ml stock media plus 1 ml FCS**

2.2.1.2 Plaque Purification

Unless otherwise stated, the strain of virus used throughout the study was FCV-F9 (Bittle & Rubic, 1976; Bittle, 1960) with an unknown high passage number, which was plaque purified using the following method to ensure that there was only one strain being used.

A 10-fold dilution series of FCV-F9 down to 10^{-9} was prepared using maintenance media (MM) (Table 2.1). A confluent monolayer of FEA cells on a 12-well plate was infected with 200 µl of diluted virus or mock infected with 200 µl of MM and then incubated at 37°C for 90 min with gentle agitation. Wells were then overlaid with equal amounts of 2x MM and 2x sterile agarose (2 g in 100 ml dd H_2O) and left at room temperature for 20 min. The plates were then incubated at 37°C for 24 h. After 24 h a plaque plug was picked and transferred to 1 ml MM and a second dilution series prepared. A confluent 12-well plate of FEA cells was infected as before with the dilution series and overlaid as described previously. After a further incubation for 24 h a plaque plug was again picked and underwent one further round of purification. The plaque picked after the third purification was then used to inoculate a 75 cm^2 flask of confluent FEA cells which was incubated at 37°C for 24 h before undergoing three freeze thaw cycles. The cells were then harvested and centrifuged at 2000 × *g* for 10 min before the supernatant was collected and aliquoted for storage at -80°C.

2.2.1.3 Titration

In order to determine how much virus was present in a given sample a viral titration was performed.

A 10-fold dilution series was prepared down to 10^{-9} using MM and confluent FEA cell monolayers in a 96-well plate were inoculated with 50 µl of diluted virus and controls mock infected with MM. The plate was then incubated for 1 h at 37°C before 100 µl of MM was added and the plate left to incubate at 37°C for 4 days. After 4 days the Reed-Munch calculation (Reed, 1938) was used to find the $TCID_{50}$ of the sample virus.

2.2.2 Sequencing

Wherever sequencing has been used throughout this study the following protocol was used unless otherwise stated.

2.2.2.1 RNA extraction

RNA was extracted from the viral samples using QIAamp Viral RNA mini kit (Qiagen), following the manufacturers protocol under RNAse-free conditions.

2.2.2.2 Reverse transcription

Reverse transcription was performed to create cDNA using the following recipe: 1 µl random hexamer oligos (Abgene), 2 µl dNTP mix (Abgene), 5 µl molecular grade H_2O (Sigma Aldrich) and 5 µl RNA prepared as above. The mixture was incubated at 65°C for 5 min and then left on ice for 1 min. The following recipe was then added to the tube: 4 µl 5x first strand buffer (Abgene), 1 µl DTT (Abgene), 1 µl RNAse out (Abgene) and 1 µl Superscript III (Abgene). This mixture was incubated at 25°C for 5 min, 42°C for 60°C min and 70°C for 15 min.

2.2.2.3 Polymerase chain reaction

Polymerase chain reaction (PCR) was used to target a portion of the capsid gene which incorporates the variable region C and the 5' and 3' hypervariable regions of region E. The single stage PCR was performed using the following recipe: 45 µl Reddy Mix (Abgene), 100 ng primer 1, 100 ng primer 2 (primers synthesised by Eurofins MWG Operon), 1 µl molecular grade H_2O and 2 µl cDNA.

Primer 1 (p2 ext): 5'- CCT CAC CTA TAC CAG TGT AAC CAA G-3'
Primer 2 (p1 degenerate): 5'- GAG CGG ATA ACA ATT TCA CAC AGG CCG TTY GTG TTY CAR GCA AAY CG-3'

Thermal cycling condition for PCR consisted of:
95°C for 2 min
95°C for 30 s, 55°C for 30 s and 72°C for 1 min 30 s x40 cycles
72°C for 5 min

2.2.2.4 PCR purification

The PCR product was purified of excess primers and unincorporated single nucleotides using QIAquick PCR purification kit (Qiagen) following the manufacturer's protocol.

2.2.2.5 Sequencing of purified PCR products

Sequencing was performed bidirectionally by Eurofins MWG Operon (http://www.eurofinsdna.com/home.html) according to their instructions to produce a consensus sequence. The primers used in sequencing the products were the forward and reverse primers used in amplifying the PCR products (p2ext and p1 degenerate).

2.2.2.6 Sequence analysis

The forward and reverse sequences obtained from each PCR product were aligned in Chromas Pro (Technelysium Pty Ltd) and a consensus sequence produced for each amplicon.

The consensus sequence was then exported as a FASTA file and the sequence was searched within the NCBI (National Centre for Biotechnology Information) database using the BLASTn tool which searches the nucleotide databases using a nucleotide query. The sequenced amplicons were compared to the whole genome sequence of FCV-F9 (Genbank number m86379) using the megablast algorithm optimised for highly similar sequences.

2.2.3 Growth curve

A viral growth curve was constructed in order to establish the progression of infection over the course of 14 h.

Eight x 25 cm^2 flasks of confluent FEA cells, passage number 43, were infected with FCV-F9 at a multiplicity of infection (m.o.i.) of 10. The flasks were incubated at 37°C for 1h before being washed three times with sterile PBS. A flask was harvested at this point by freezing at -80°C. The remaining flasks were re-fed with 10 ml MM and returned to the incubator. At 2 h post infection (p.i.) another flask was harvested

and intracellular and extracellular virus fractions were stored separately. This process was repeated every 2 h until 14 h p.i.. A mock infected control was also included which was composed of FEA cells treated in exactly the same manner as the infected cells except for mock infection with MM instead of virus and harvested at 14 h p.i.. At each time point the extracellular virus, intracellular virus and virus found in dead cells no longer found adhered to the flask were calculated by titration as described previously (section 2.2.1.3). Extracellular virus was taken directly from the media and virus from non-adherent cells was isolated by pelleting the cells from the media by centrifugation at 2000 × *g*. Intracellular virus was isolated by washing the flask twice with sterile PBS and scraping the adherent cells before pelleting by centrifugation at 2000 × *g*.

2.2.4 Immunofluorescence Assay

To visualise virus in the cells at the time points chosen for use in the 2D-DIGE infections (1 h, 4 h, 7 h and 10 h p.i.) immunofluorescent staining was performed in parallel to the 2D-DIGE infections.

Four x 96-well plates of confluent FEA cells, passage number 43, were infected with 50 µl FCV-F9 at an m.o.i. of 10 whilst control wells were mock infected with 50 µl MM. The plates were incubated at 37°C for 1 h before being washed with sterile PBS. One plate was fixed with 70% ethanol at this point. The remainder were re-fed with 150 µl MM and returned to the incubator. The plates were then fixed at 4 h, 7 h and 10 h p.i. with 70% ethanol. Once fixation was complete the plates were washed three times with sterile PBS and overlaid with 50 µl of primary antibody raised against the capsid protein of FCV-F9 (G784h (Porter, 2004)), diluted 1:20 with PBS. The plates were incubated at 37°C for 1 h and washed in sterile PBS three times before being overlaid with 50 µl of anti-rabbit goat fluorescein isothiocyanate (FITC, Sigma-Aldrich), diluted 1:40 with PBS. The plates were incubated at 37°C for 1 h and washed with PBS before 50% glycerol was added to each well. The plates were viewed under a UV microscope to detect immunofluorescence and pictures were taken using a UV microscope (Zeiss Axiovert 200M with Axiocam hrc camera and Axiovision 3.1 software).

2.2.5 2D-DIGE

2.2.5.1 Viral infection

Cells were virally infected to allow protein to be extracted for proteomic examination.

Eight x 75 cm^2 flasks of confluent FEA cells, passage number 43, were infected with 1 ml of FCV-F9 at an m.o.i. of 10 and eight x 75 cm^2 flasks were mock infected with 1 ml MM. The flasks were incubated at 37°C for 1 h before being washed with sterile PBS. Two infected flasks and two mock infected flasks were harvested and the collected cell pellets frozen at -20°C. The remaining flasks were re-fed with 20 ml MM and incubated at 37°C. Two each of the infected and mock infected flasks were harvested at 4 h, 7 h and 10 h p.i. and the cell pellets frozen at -20°C.

2.2.5.2 Cell lysis

The cell pellets were lysed in 500 µl of lysis buffer (30 mM Tris, 2 M Thiourea, 7 M Urea, 4% CHAPS) plus 10 µl DN/RNases (Roche) and 5 µl of protease inhibitors (complete tablet kit, Roche). The samples then underwent five cycles of freeze-thawing (freezing in liquid nitrogen, thawing at 30°C and vortexing) before centrifuging at 13 000 × *g* for 10 min to remove any remaining cell debris. To remove any salts, detergents, lipids, phenolics and nucleic acids still present in the samples a 2D-clean up kit (GE Healthcare) was used. All clean up steps were carried out on ice unless stated otherwise. 300 µl of precipitant was added to each sample and mix thoroughly by vortexing before being incubated on ice for 15 min. After incubation, 300 µl of co-precipitant was added to each sample mixture and vortexed briefly before centrifugation at 13 000 × *g* for 5 min. The supernatant was discarded and the tubes centrifuged again to ensure that any remaining supernatant was removed. 40 µl of co-precipitant was layered on top of the pellet, carefully so as to avoid disturbing the pellet, and the tubes were incubated on ice for 5 min. The samples were centrifuged again at 13 000 × *g* for 5 min and the wash removed and discarded. 25 µl of ddH_2O was added to each pellet and the tubes vortexed where the pellet was dispersed but not dissolved in the solution. 1 ml of wash buffer (pre-chilled at -20°C for at least 1 h) was added alongside 5 µl of wash additive and the

tubes were incubated at -20°C for at least 30 min with the samples being vortexed for 20-30 s every 10 min. The samples were then centrifuged at 13 000 × *g* for 5 min and the supernatant discarded before the pellet was left to air dry for a maximum of 5 min. The protein pellets were resuspended in 40 µl of 2x sample buffer (2 M Thiourea, 7 M Urea, 2% CHAPS) before determining the protein concentration of each sample by protein assay.

2.2.5.3 Protein assay

For each protein assay used throughout this work the protein concentration of each sample by a Bradford method based protein assay (Biorad Protein Assay) (Bradford 1976). Briefly, bovine serum albumin (BSA) standards were made up which range in concentration from 10 µg/ml to 50 µg/ml and these were placed in duplicate in a 96-well plate along with blanks containing no BSA. The Coomassie plus reagent was diluted down 1 in 4 with ddH_2O to provide the working solution. 100 µl of blank, sample, and standards were added to the appropriate wells and the samples were subjected to a serial dilution series. 200 µl of the working Coomassie solution was added to each well and the protein concentration was read within an hour of the solution being added to the samples. The absorbancies of the plate were read using a Labsystems Multiscan Ascent at 620 nm. A straight-line graph was produced from the blanks and standards and protein concentration of the samples calculated from this graph.

2.2.5.4 2D-DIGE labelling

The optimal protein concentration for 2D-DIGE labelling is 5 mg/ml with a pH between 8 and 9. Both these conditions were tested and the samples were diluted with 2x sample buffer or pH raised with 1 µl of 10 mM NaOH if necessary.

The dry CyDyes first had to be reconstituted with high quality anhydrous dimethylformamide (DMF) (5 µl per 5 nmol CyDye), mixed by vortexing and centrifuged at 12 000 × *g* for 30 s to give a stock solution of 1 mM which could be used immediately or kept at -20°C for 2 months. To make a working solution, one volume of CyDye stock solution was added to 1.5 volumes of high grade DMF to make a 400 pmol/µl solution.

50 µg of each protein sample was labelled with 1 µl of the appropriate CyDye (Table 2.2). An internal standard was created from equal proportions of all 16 samples analysed and 50 µg of the internal standard was labelled with Cy2 for each gel. The mixtures were then mixed and centrifuged briefly before incubating on ice for 30 min in the dark. To stop the reaction 1 µl of 10 mM lysine was added to each reaction and mixed by pipetting and spun briefly in a centrifuge before being incubated on ice for a further 10 min in the dark.

Table 2.2. Experimental design for 2D-DIGE performed on samples infected with FCV-F9 at four time points.

Gel Number	Cy2	Cy3	Cy5
Gel 1 (pick gel)	Internal Standard	1hr p.i. mock infected 1	4hrs p.i. infected 2
Gel 2	Internal Standard	7hrs p.i. mock infected 2	4hrs p.i. mock infected 1
Gel 3	Internal Standard	4hrs p.i. infected 1	7hrs p.i. infected 2
Gel 4	Internal Standard	10hrs p.i. mock infected 1	1hr p.i. infected 1
Gel 5	Internal Standard	1hr p.i. infected 2	7hrs p.i. mock infected 1
Gel 6	Internal Standard	7hrs p.i. infected 1	10hrs p.i. mock infected 2
Gel 7	Internal Standard	4hrs p.i. mock infected 2	10hrs p.i. infected 2
Gel 8	Internal Standard	10hrs p.i. infected 1	1hr p.i. mock infected 2

The labelled samples were combined into eppendorfs according to the gel they would be loaded onto (gel 1 including 300 µg of unlabelled pooled protein to allow spot picking after analysis) and each mixture added to a pH 3-10 IPG strip (GE Healthcare) by cup loading. The IPG strips were rehydrated overnight using 450 µl rehydration buffer (8 M urea, 2% CHAPS, 0.002% bromophenol blue) containing 10 mg/ml DTT and 5 µl/ml IPG buffer containing ampholytes (pH 3-10, GE Healthcare). Once the strips were rehydrated they were each placed onto a ceramic manifold and sample loading cups placed towards the acidic end of the strips. Rehydration buffer was added to each sample mixture up to a maximum volume of 100 µl and these were loaded into the sample cups for isoelectric focussing.

2.2.5.5 2D gel electrophoresis

First dimension separation by isoelectric focussing (IEF) was performed using the Ettan IPGphor II (GE Healthcare) at 30 v for 5 h, 500 v for 1 h, 100 v for 1 h, 8000 v for 2 h and 8000 v for 9 h with current limited to 50 µA/strip. The focussed strips then had to be equilibrated firstly in 10 ml SDS equilibration buffer (2% SDS, 50 mM Tris-HCl pH 8.8, 6 M urea, 30% (v/v) glycerol, 0.002% bromophenol blue) with 10 mg/ml DTT for 15 min to reduce the protein and then for 15 min in 10 ml SDS equilibration buffer with 25 mg/ml iodoacetamide to alkylate the cysteine residues.

The proteins were separated in the second dimension using a manually cast 12.5% acrylamide gel which was stuck to low fluorescence glass plates by pretreating each glass plate with bind silane solution (80% (v/v) ethanol, 18% (v/v) ddH_2O, 2% (v/v) acetic acid, 0.1% (v/v) γ-methacryloxypropyltrimethoxysilane) and allowing to dry completely before casting. Fluorescence reference markers were added to each treated glass plate to allow for references to be picked out when using the automated spot picker (Ettan spot picker, GE Healthcare) and the treated plates were sandwiched with larger untreated plates and placed into a gel casting unit. The 12.5% acrylamide solution was made up (40% (v/v) bis-acrylamide, 25% (v/v) Tris-HCl, pH 8.8, 30% (v/v) ddH_2O, 10% SDS and 0.001% (v/v) TEMED) and left in the fridge for at least 1 h. 0.01% (w/v) ammonium persulphate (APS) was added finally and poured immediately into the casting unit before being overlayed with a 0.1% solution of SDS and leaving to polymerise at room temperature (~20-25°C) overnight. The equilibrated strips were laid on top of the gels and sealed in with an agarose sealing solution (0.5% (w/v) agarose, trace bromophenol blue). The gels were run at 5 W per gel for 30 min and then adjusted to 17 W per gel for 4 h in an Ettan DALTsix electrophoresis unit (GE Healthcare).

2.2.5.6 Ettan DIGE scanner parameters

Once the gels were run they were scanned immediately in an Ettan DIGE imager (GE Healthcare) set at 100 pixels and 0.800 exposure on all three CyDye channels. The pick gel (gel 1) containing an extra 300 mg of unlabelled protein from the pooled samples was then fixed overnight in 40% methanol, 10% acetic acid before staining overnight in Sypro Ruby stain on a rocker. The gel was washed for an hour in 10% methanol, 7% acetic acid then rinsed twice in ddH_2O before scanning in the Ettan DIGE imager under Sypro Ruby conditions at the same exposure as before.

2.2.5.7 DeCyder analysis

DeCyder software is recommended for use with 2D-DIGE gels as it a fully automated image analysis suite which allows for detection, quantitation, matching and analysis of scanned DIGE gel images.

DeCyder software was used for all image analysis of 2D-DIGE gels in this work. The DeCyder software package is made up of four modules; the Image Loader, the Differential In Gel (DIA) module, the Biological Variation Analysis module (BVA) and the Batch Processor.

2.2.5.7.1 Image loader

The image loader module is a tool included in the DeCyder software which allows the user to import the images gained from the Ettan DIGE scanner into separated projects within the DeCyder database with the CyDye chemistry already assigned to the correct image.

2.2.5.7.2 DIA module

The DIA module processes all images from a single gel, allowing parameters to be calculated for dust particle exclusion which can then be filtered against all the other gels analysed. For this experiment dust particles were eliminated from analysis by setting the following parameters; max slope >1.6, max volume <7800.

2.2.5.7.3 Batch Processor

The batch processor is a tool which automates the process of adding the gel images to the DIA and BVA modules as well as allowing the user to include spot exclusion filters which were calculated from analysing one of the gels in the DIA module. The batch processor also enables each gel image to be assigned to a group e.g. standard, infected, and uninfected.

2.2.5.7.4 BVA module

The BVA module is the tool which allows multiple gel images to be matched together and as such allows inter-gel comparisons and relative quantitations to be performed. A master gel is assigned from one of the Cy2 labelled gel images made up of the internal standard and all the remaining gel images are matched to the master first by the software's matching algorithm and then by manual curation through finding common spots across all gels and landmarking them. The BVA module also allows the user to perform statistical analyses on the matched spots such as students t-test and analysis of variance (ANOVA). In this experiment the spots were subjected to student t-test statistical analysis based on variance between infected and uninfected states at each time point and those with a p-value of ≤ 0.05 were selected for spot picking.

2.2.5.8 Spot picking

The selected spots were picked from the pick gel using an Ettan spot picker (GE Healthcare) which is able to automatically calculate the locations of the selected spots based upon the defined reference markers attached to the glass plates during gel casting.

2.2.5.9 Tryptic digestion

The picked spots were then subjected to tryptic digestion to produce peptides suitable for analysis by mass spectrometry. The gel plugs picked were each placed into an eppendorf and 10 µl of 50 mM ammonium bicarbonate (ambic) and 50% acetonitrile (HPLC grade) was added before incubation at 37°C for 10 min. This step was performed to remove any stain on the gel plugs and so the liquid is removed before the steps are repeated again to ensure no stain remains. 10 µl of 100% acetonitrile was then added to each gel spot and incubated at 37°C for a further 15 min. This step dehydrates the gel plug and should turn it white and opaque, if this did not happen then the solvent was discarded and this step was repeated. The solvent was removed from the dehydrated gel plug and the tubes were incubated at 37°C until all traces of the solvent had disappeared (usually about 10 min). Stock solutions of trypsin (100 ng/µl) were diluted 1 in 10 with 25 mM ambic and 10 µl of this was added to each plug and the solution was incubated at 37°C for 1 h. A further 10 µl of 25 mM ambic was added to each spot and incubated overnight 37°C. The digest was either analysed immediately by mass spectrometry or stored at -20°C.

2.2.6 Mass spectrometry

2.2.6.1 LTQ parameters

Samples were analysed using high performance liquid chromatography (HPLC) (UltiMate 3000, Dionex) coupled with tandem mass spectrometry (MS/MS) (Finnegan LTQ, Thermo Scientific). The samples were prepared for analysis by the addition of 2 µl of 2.6 M formic acid to each digested sample followed by centrifugation at 13 000 × *g* for 30 min. In loading the samples onto the machine 10 µl of sample was mixed with 10 µl of 1% formic acid although if more than three samples were being analysed the volume of 1% formic acid added increased by 2 µl every three samples to allow for evaporation.

The samples were first fractionated by the HPLC system (Ultimate 3000, Dionex) on a C18 reverse phase column over a total run time of 50 min per sample. 10 µl of tryptically digested peptides were injected onto the column and eluted over a linear gradient of 0-50% (v/v) acetonitrile/0.1% (v/v) formic acid over 30 min before a

final elution at 80% (v/v) acetonitrile/0.1% formic acid (v/v) for 5 min. The column was then equilibrated in 98.9% water/2% acetonitrile/0.1% (v/v) formic acid for 5 min.

The LTQ was calibrated before and after each run with glufibrinopeptide (500 fmol/µl solution) to ensure that all samples were run under optimal conditions. For analysing samples the LTQ was run in "triple play" mode, where the detector uses information from the data in the experiment to make decisions about the next step automatically. In these experiments a full MS survey was taken (threshold = 400-1500 total ion current) and from this the three most abundant ions were determined. These peptides were then fragmented further in the collision cell with collision energy set at 35% for 30 min. The charge state of each of the fragmented ions was then calculated using the "zoom scan" which uses the presence of ^{13}C atoms to determine the charge state and the ions were finally interrogated with a full MS/MS scan.

The resulting MS/MS data files were merged into a .mgf file which could then be analysed using Mascot searching (www.matrixscience.com).

2.2.6.2 Mascot search parameters

The resulting MS/MS spectra were analysed using a Mascot search database (Matrix Sciences) with the following parameters.

Table 2.3. Parameters used when searching spectra against databases using the Mascot search programme

Parameter	Selected Option
Database	Feline predicted protein database/MSDB and FCV proteins
Enzyme	Trypsin
Missed Cleavage	1
Fixed modification	Carbamidomethylation
Variable modification	Oxidation of methionine

The feline predicted protein database was downloaded from the Ensembl website (http://www.ensembl.org/Felis_catus/Info/Index) and the version used was from the July 2008 genebuild of the March 2006 assembly of the 1.87x coverage genome containing 13 074 projected protein-coding genes. The mass spec database (MSDB) used was locally installed from http://ftp.ncbi.nih.gov/repository/MSDB/msdb.nam, version 20052909.

2.2.6.3 Mascot output

The resulting Mascot output from each spectral search was analysed in the knowledge that it is the ion scores for the individual peptide matches that are statistically significant and that the Mascot programme generates a peptide summary report which groups the peptides matched into protein hits. A protein score is generated from the combined ion scores of the matched peptides and any protein with a score >35 had the protein identification accepted.

2.2.7 Protein identification from the predicted cat proteins

The protein hits identified using the predicted proteins from the cat database required further processing as the cat genome had not been fully annotated at the time of analysis. The full protein sequence from each protein hit was searched against the non-redundant protein sequence NCBI (National Centre for Biotechnology Information) database using the BLASTp tool which searches the protein databases using a protein query. The nucleotide sequence was also obtained from the Ensembl assembly using the location and direction specified within the protein hit ID. The obtained nucleotide sequence was then subjected to BLASTn search against the NCBI nucleotide collection. These steps were then used to assign each protein hit an identification.

2.2.8 Functional categorisation of identified proteins

The Gene Ontology (GO) terms for biological processes were obtained by downloading those available for the annotated genes found on the cat genome from Ensembl using the BioMart tool (Durinck *et al.*, 2005).

2.3 Results

2.3.1 Plaque purification of FCV-F9 strains

To ensure that only one strain of FCV-F9 was being used throughout this study, plaque purification was used upon a lab strain of FCV-F9. Three rounds of plaque purification were performed and from this three plaques were picked and propagated. The resultant viral aliquots were sequenced by RT-PCR to ensure that the virus that had been propagated was FCV-F9. Figure 2.1 shows the PCR products produced from primers designed to amplify the capsid gene.

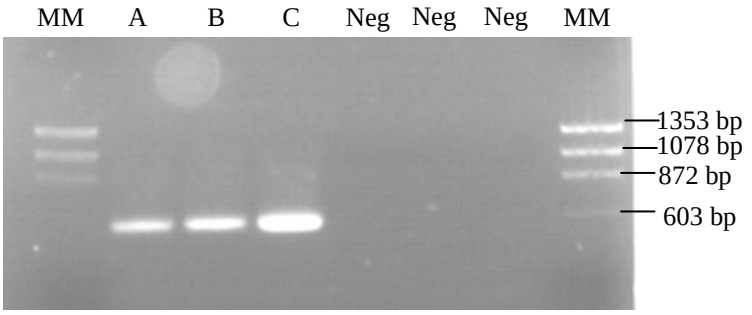

Figure. 2.1. PCR products from amplification with capsid flanking primers. Lanes A-C are amplified from plaque purified FCV-F9. Lanes labelled Neg are negative controls and lanes labelled MM the molecular marker φX174 *HaeIII* digest.

These PCR products were purified and sent for sequencing and once the results returned it showed that each plaque purified FCV-F9 virus had 99% identity across the capsid region with the published FCV-F9 sequence (Genbank accession number m86379) (data not presented).

To discover how much virus was present in each set of plaque purified aliquots a series of viral titrations were performed to produce a 50% tissue culture infective dose figure ($TCID_{50}$). The average titration for plaque A gave a $TCID_{50} = 10^{7.41}/50$ µl, plaque B gave a $TCID_{50} = 10^{8.15}/50$ µl and plaque C gave a $TCID_{50} = 10^{8.47}/50$ µl. Based upon these results it was decided that plaque C should be used in future experiments as it gave the highest titre.

2.3.2 Growth curve

In order to calculate which time points would be most suitable for immunofluorescence and 2D-DIGE analysis a growth curve over 14 h was calculated (Fig. 2.2). The results show that rather than the one-step growth curve expected using an m.o.i. of 10, a two-step growth curve was seen with a second round of viral replication appearing to occur between 10 and 14 h p.i.. It was decided that the best course of action was to investigate the host response to the virus during the initial round of viral replication and proliferation, therefore, the time points selected for immunofluorescence and DIGE investigation were 1, 4, 7 and 10 h p.i..

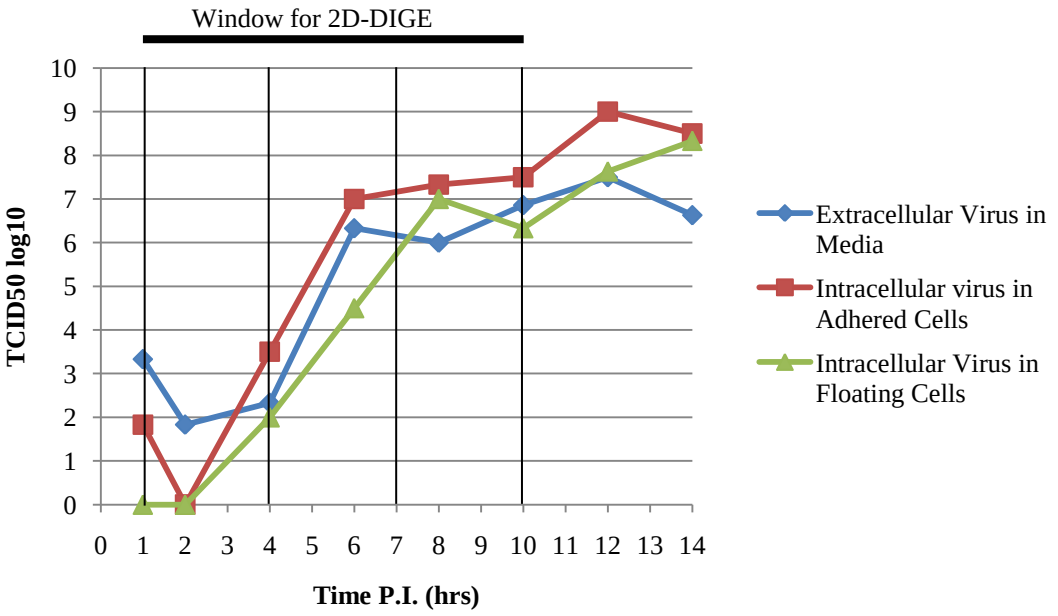

Figure. 2.2. 14 h growth curve of FCV-F9. Three fractions were taken at each time; extracellular virus in media, intracellular virus from cells still adhering to flask surface and intracellular virus from cells which had become detached from the flask surface. Vertical lines show time points selected for further analysis using 2D-DIGE.

2.3.3 Immunofluorescence assay

In order to visualise the amount of virus present at each of the time points selected for 2D-DIGE analysis an immunofluorescence assay was conducted. The results of immunofluorescent staining for FCV-F9 capsid protein (Fig. 2.3) show again that not all of the cells are infected during the first stage of infection. This may have been down to the differences in susceptibility to infection within the cell culture or due to inaccuracies in titration.

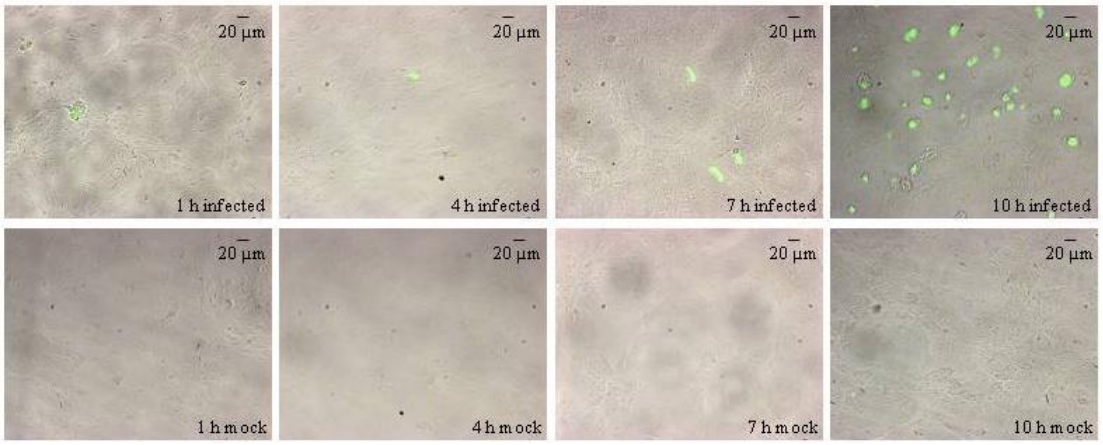

Figure. 2.3. Cells stained with anti-FCV-F9 capsid protein antibody and visualised with FITC conjugated secondary antibody. The FCV capsid protein is stained in green. White light and immunofluorescent channels have been merged in these images.

2.3.4 2D-DIGE analysis

Two biological replicates of infected and mock infected FEA cells at each of the four chosen time points (1, 4, 7 and 10 h p.i.) were analysed by 2D-DIGE. The eight 2D gels produced were fluorescently scanned and the images were uploaded into the DeCyder software for analysis. The gels were processed through the DIA module and matched to each other using the BVA module of the software before statistical testing could be applied. Each of the protein spots from the infected time points was subjected to a student's t-test analysis against the mock infected counterparts and an ANOVA of all the infected protein spots versus mock infected protein spots. From t-test and ANOVA analysis it was found that there were 30 spots which were significantly ($p \leq 0.05$) differentially expressed between infected and mock infected groups. The location of the picked spots can be seen in Figure 2.4.

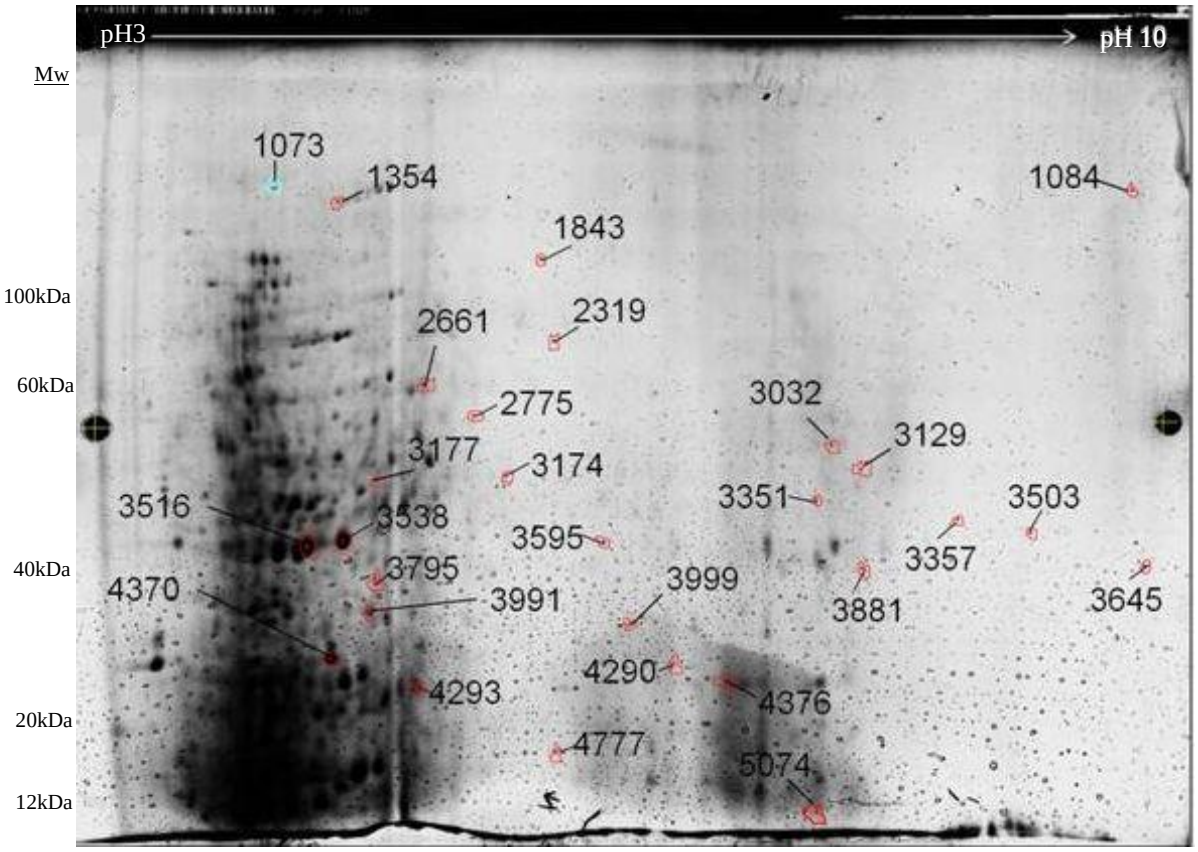

Figure. 2.4. Pick gel showing the positions of the proteins significantly differentially expressed during infection with FCV-F9 and assigned spot number. Proteins were resolved by IEF over a non-linear pH3-10 range and by molecular weight on a 12.5% acrylamide gel. Staining was performed using Sypro Ruby and visualised using an Ettan DIGE imager at an exposure of 0.800.

Of these 30 protein spots, 14 were identified by LTQ analysis and Mascot searching against a cat protein database as described in section 2.2.6.2 (Table 2.4).

Table 2.4. Top Mascot identification for the 14 proteins identified via interrogation of the feline protein database downloaded from Ensembl.

Protein Spot No	Ensembl ID hit	Mascot Score	No of peptide hits	Identification	Gene ID
2319	ENSFCAP00000010586	41	2	Filamin-A	FLNA
3032	Scaffold_101245_108936_112032_-1	92	6	Beta-actin	ACTB
3129	Scaffold_101245_108936_112032_-1	62	4	Beta-actin	ACTB
3351	Scaffold_101245_108936_112032_-1	110	4	Beta-actin	ACTB
3357	GeneScaffold_2254_325966_333780_1	100	5	Thrombospondin, type I, domain containing 4	THSD4
3516	Scaffold_101245_108936_112032_-1	959	34	Beta-actin	ACTB
3538	Scaffold_101245_108936_112032_-1	1447	64	Beta-actin	ACTB
4290	Scaffold_101245_108936_112032_-1	334	8	Beta-actin	ACTB
4293	GeneScaffold_2798_18850_78140_1	151	12	Solute carrier family 22	-
4370	Scaffold_101245_108936_112032_-1	849	27	Beta-actin	ACTB
4376	Scaffold_101245_108936_112032_-1	170	5	Beta-actin	ACTB
4777	ENSFCAP00000008491	45	4	Cyclophilin A	PPIA_FELCA
4797	ENSFCAP00000012591	125	7	Transgelin	TAGLN
5074	ENSFCAP00000004426	84	2	Thioredoxin	TXN

As the cat database is not fully annotated, the spectra were also interrogated with the mass spec database (MSDB) which is a non-identical protein sequence database built from a number of primary source databases and as such contains information from a number of different species of animal. Using this approach gave confirmed identifications for 11 of the 14 protein spots identified from searching against the cat database as well as allowing a further 2 protein spots to be identified. The MSDB

search also offered some alternative identifications for some of the protein spots. For example spots 3516 and 3357 show very strong hits for vimentin from searches against the MSDB. The full table of identifications and Mascot scores can be found in Appendix I.

DeCyder also allows the user to calculate average ratio of the spot intensity between groups, Figure 2.5 shows the results of comparing the infected spots at each time point with their mock infected counterparts.

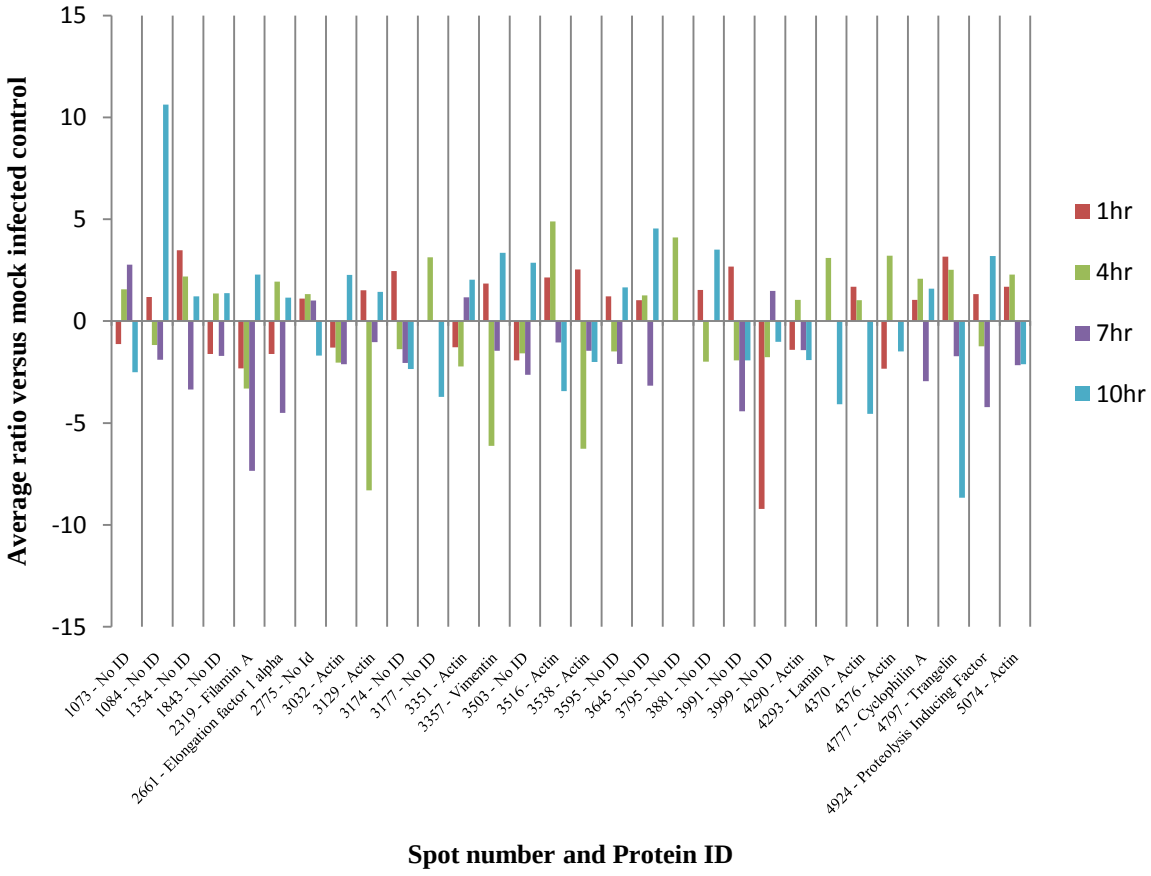

Figure 2.5. Graph showing average ratios of picked spots in infected samples at each time point versus uninfected controls. Protein identifications shown are top Mascot hit for each spot number.

Comparison with the mock infected counterparts show that of the picked spots, none were consistently up- or down-regulated in infected cells across the four time points. There were nine spots that showed changes in the later stages of infection; 2319, 3032, 3351 and 3503 all showed a trend of changing from a down-regulated presence of proteins in infected cells to an up-regulation at 7 or 10 h p.i.. Unfortunately there

were no database hits for spot number 3503 but spot number 2319 was identified as filamin A from MSDB searching and spots 3032 and 3351 were both found to be actin. The up-regulation of actin and filamin A in the latter stages of infection could indicate that the virus needs these proteins in order to aid replication and egress from the cell. Further implications of these finding will be discussed in section 2.4.

Spot numbers 2775, 3174, 3516, 3538, 3991, 4370, 4797 and 5074 all show the opposite trend where the proteins appear to be up-regulated early in infection and then become down-regulated in the latter stages. Of these eight protein spots, three had no identification hits against either database searched and the other five were all found to have multiple identifications. Within these multiple identifications actin was identified within four of the modulated host protein spots, suggesting that this protein and its derivatives undergo extensive remodelling during infection with FCV. This fluctuation in expression can be observed in Figure 2.6, which shows a 3D representation of spot number 3538, a protein spot found to include actin. This graphic representation shows the up-regulation of the protein in infected cells at 1 h p.i. and subsequent down-regulation in the cells at 4-10 h p.i..

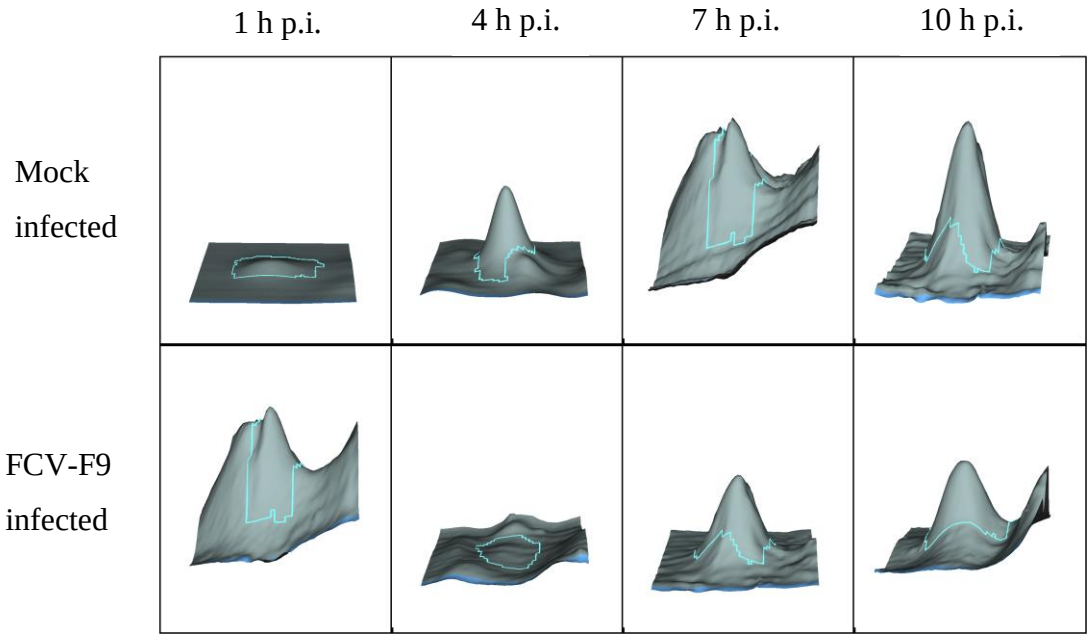

Figure 2.6. 3D modelling of protein expression, calculated within the DeCyder software from intensity of fluorescent protein labels from 2D-DIGE. The output shown has been calculated for spot number 3538, identified as a mixture of actin, roundabout axon guidance receptor and peroxiredoxin-2.

There are also a number of spots in which the amount of protein seems to fluctuate over the course of infection. Spot numbers 1084, 3129, 3357, 3595, 3881 and 4924 all show signs of up-regulation at 1 h and 10 h p.i. but are down-regulated during the middle phases of infection. Again these protein spots are a mixture of those without identification and those with multiple identifications making them difficult to analyse, however, once again actin was found within two of these modulated host protein spots.

2.3.5 Gene Ontology

In order to assign some functional information to the proteins identified from searching against the cat database, the BioMart tool from Ensembl was used to download a full list of biological processes attributed to the proteins by the Gene Ontology (GO) project. Each GO term generated was manually curated into broad definition groupings and a chart constructed (Fig. 2.7).

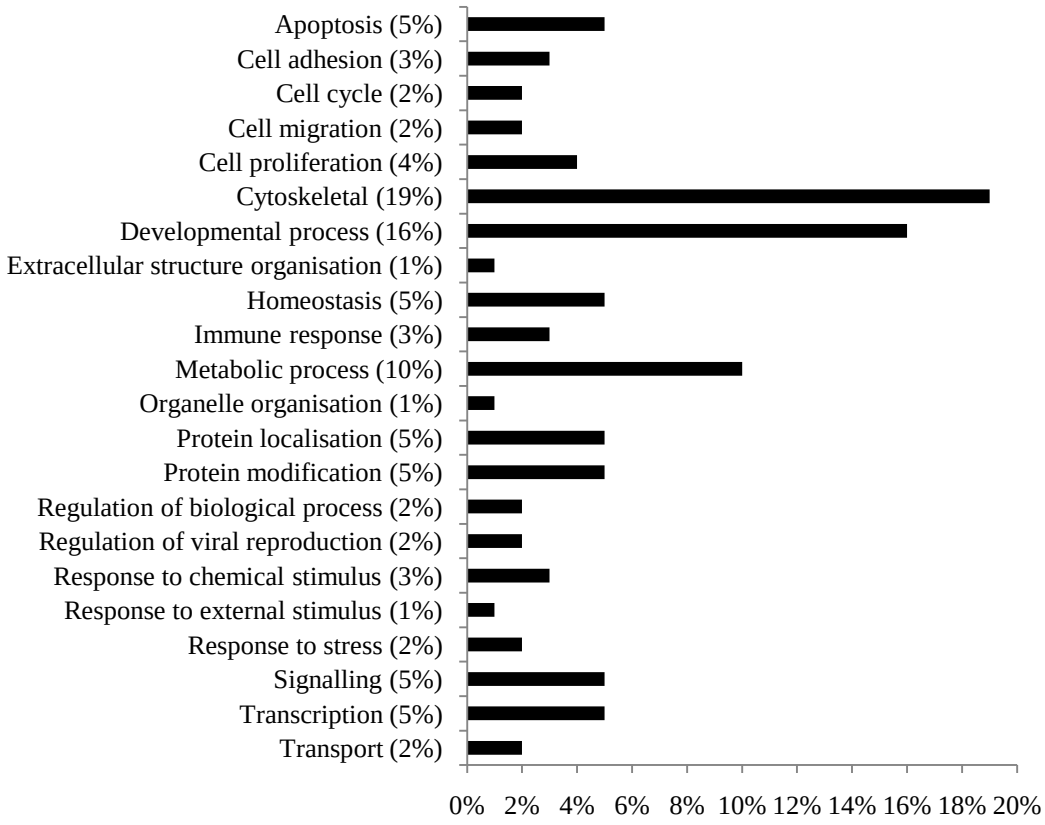

Fig. 2.7. Gene Ontology analysis of the biological processes of the proteins found to be differentially expressed in response to FCV-F9 using 2D-DIGE.

The breakdown of biological process analysis shows that there appears to be a large representation of proteins with a cytoskeletal role within the cell, almost one in five of the functions attributed to this protein set are from the cytoskeletal area. There are also a large amount of functions attributed to developmental processes within the cell and also metabolic mechanisms with these making up over a quarter of the processes found. There are also a number of functions which may be directly related to the viral infection such as those proteins with an immune response function and those which have been found to regulate viral reproduction within the cell.

2.3.6 Cytoskeletal proteins

Throughout the analysis of the differentially expressed proteins found in this 2D-DIGE experiment it has become clear that cells infected with FCV are undergoing profound changes to their cytoskeletal function. Actin appears as an identification in 11 of the 16 modulated proteins and there are also multiple hits for other cytoskeletal proteins such as vimentin, tubulin, desmin and lamin. The implications of modification of these proteins will be investigated further in section 2.4 but it was clear from these results that further examination of the interactions of the virus and these cytoskeletal proteins was needed.

2.4 Discussion

Interrogation of cells infected with FCV-F9 using 2D-DIGE technology suggests that infection causes a number of proteins to be differentially expressed. These changes may be a direct result of the virus manipulating the cell machinery in order to replicate or it may be due to a number of different factors such as a cellular response to infection or cellular degradation.

FCV has been shown in previous studies to induce apoptosis within the cell from 6-8 h p.i. (Natoni *et al.*, 2006) and as such the proteins found to be down-regulated at 7 and 10 h p.i. in the 2D-DIGE experiment may be as a result of programmed cell death. 11 of the 30 protein spots were found to be down-regulated at the latter stages of infection and may be a result of apoptotic degradation; however, there are also 14 protein spots up-regulated at 10 h p.i. which suggests that not all cellular proteins were being broken down at this point.

Within the whole comparison of infected and mock infected cells across the experimental time course the greatest proportion of differentially expressed proteins had cytoskeletal functions. There are three different types of cytoskeletal component; microfilaments, microtubules and intermediate fibres. Microfilaments are mostly made up of actins, microtubules consist of tubulins and intermediate fibres include vimentin and keratin (Sodeik, 2000). Within the identifications obtained from the modulated protein spots in this experiment, there were numerous hits to actin, tubulin and vimentin which suggests that the entire cytoskeletal system is important in FCV infection.

Actin is an important cellular component involved in cellular motility, movement of vesicles and organelles around the cell, cellular division and maintenance of cellular shape. The microfilaments, especially actin, have been found to be essential in infection with a large range of viruses with both human and animal hosts. Vaccinia virus from the pox virus family has been shown to use actin to promote cell-to-cell spread and replication (Cudmore *et al.*, 1995) by stimulating actin tail formation beneath virions to move around the cell and through the formation of actin projections to contact neighbouring cells. Herpesviruses have also been shown to use actin to promote viral spread (Gill *et al.*, 2008) by polymerising actin to produce branches from the plasma membrane to provide a network along which the virions

can move and transmit cell-to-cell. Treatment with actin inhibitors has also been shown to reduce viral replication in cells infected with a virus from the α-herpesvirus family (Kuhn *et al.*, 2005), canine distemper virus (Klauschies *et al.*, 2010) and influenza A (Arcangeletti *et al.*, 2008) which would suggest that the actin network is vital for efficient viral replication in wide range of viruses and hosts.

The microtubules and microfilaments have also been found to have a role to play in cellular movement of virions around the cell. Tubulin has been shown to be necessary for movement of the viral nucleocapsid of hantaviruses through the cell to the golgi region (Ramanathan & Jonsson, 2008) and for hepatitis C entry into the cell (Roohvand *et al.*, 2009). Vimentin is also very important in viral infection and it has been shown in dengue virus infection (Chen *et al.*, 2008) that if the vimentin network is disrupted it significantly affects viral replication whereas disruption of the microtubule network did not. With vaccinia virus infection it has been shown that the manipulation of the microtubule and microfilament networks has an effect on the cell morphology throughout the course of infection (Schepis *et al.*, 2006). In the early phase of infection the cells are seen to become rounded as microtubules retract from the periphery of the cell and vimentin is found to retract around the nucleus. By the latter stages of infection the cells reflatten and become branched at the periphery. This has been shown to be as a result of microtubules re-entering the peripheral regions and extending into protrusions which has been shown to coincide with actin tail formation and viral egress. Calculations show that without the use of a cellular transport system a vaccinia virion would take 5.7 h to move 10 μm by diffusion alone (Sodeik, 2000) and so it would seem that the use of host cytoskeletal networks are vital.

The evidence from these findings would suggest that one hypothesis for the modulation of so many host cytoskeletal proteins in this 2D-DIGE experiment is that FCV requires these proteins for movement around the cell as well as entry and exit.

Cyclophilin A was another protein to be identified in multiple protein spots within this experiment and in cells has a protein folding function which may be useful to FCV during replication. It is also found to associate closely with human immunodeficiency virus type 1 (HIV-1), becoming incorporated into the HIV-1 virions (Franke *et al.*, 1994) and having a role in HIV-1 attachment to target cells (Saphire *et al.*, 2000). This is unlikely to be occurring in FCV infection but it is

useful to remember that the link between host proteins and viruses can be essential in viral replication.

The use of 2D-DIGE as a means to compare proteomes from different infection states gives a good first impression of the differences in protein expression between the cellular proteomes. However, it is not a perfect technique. 2D-DIGE separates the proteins from the lysed cells using 2D gel electrophoresis which is a hydrophilic method of separation which prevents hydrophobic proteins such as membrane proteins from entering the gel and being analysed. There has also been some evidence uncovered that using 2D gels to separate proteins for identification of differentially expressed proteins can lead to similar proteins being found as modulated (Petrak *et al.,* 2008). It is therefore important to ensure that the proteins identified as differentially expressed within a 2D-DIGE experiment are confirmed using alternative methods. Alternative methods for quantitating protein expression without using gels for separation are available such as SILAC (stable isotope labelling by amino acids in cell culture) coupled with off-gel separation (Ong *et al.*, 2002). SILAC uses cell lines grown in media depleted of a key amino acid but supplemented with an isotope labelled form of the missing amino acid ensuring that the proteins found inside the cells are labelled with the isotope. The labelled cells can then be compared to an unlabelled set of cells that have been infected/mock infected as necessary through mass spectrometry by comparing the amount of labelled and unlabelled protein in the samples. This kind of comparison should allow whole cell proteomes to be interrogated without losing proteins during separation. Another method currently in use which allows absolute quantitation of proteins within a sample is QconCAT which is a technique which employs specifically synthesised proteins to absolutely quantitate proteins from samples (Pratt *et al.*, 2006). The QconCAT itself is a concatamer of tryptic peptides from a number of proteins which are labelled with a stable isotope and added to the protein mixture of interest in known quantities. The proteins found within the mixture of interest can then be analysed by mass spectrometry and compared to the labelled QconCAT peptides to discover the amount of protein in the sample.

Another issue confronted during this 2D-DIGE analysis was the difficulties encountered using a non-model genome. As the cat genome is currently only at 1.97x coverage and annotation has been completed through cross-referencing against

six other genomes (Pontius *et al.*, 2007) the protein database used to compare the mass spectrometry outputs does not contain the full set of proteins found in the cat. In this analysis it has lead to 14 out of the 30 modulated host proteins remaining unidentified as the reference database did not contain enough information to provide accurate identification when the mass spectrums were searched against it using Mascot.

The overall results from the 2D-DIGE experiment conducted in this chapter have shown evidence of the modulation of a number of proteins within the host cell proteome as a consequence of infection with FCV-F9. The stand out group of proteins affected by infection appear to be the cytoskeletal proteins and while there is evidence from the literature that this association may be common within viral infections the results of the 2D-DIGE experiment are not conclusive. It was therefore necessary to investigate the association using other methods to confirm the effects, the results of which will be reported in chapter 4.

3 Chapter three

Investigation of *in vitro* pathogenesis of different strains of FCV including a putative virulent strain

3.1 Introduction

In the previous chapter (chapter 2), the *in vitro* pathogenesis of a single strain of FCV was investigated by 2D-DIGE. However, it is difficult to state that this is a definitive analysis for FCV infection. As a plus strand RNA virus, FCV has a genome with a great plasticity and this leads to a wide range of strains being exhibited within populations, therefore using a single strain within an analysis may lead to conclusions being drawn that do not hold true across a number of strains.

3.1.1 FCV strain variability

With the positive strand RNA genome offering FCV a high mutation rate (Drake, 1999), there are a number of strains in circulation within the general cat population (Sato *et al.*, 2002) and also within populations found in rescue shelters (Bannasch & Foley, 2005; Radford *et al.*, 2001) and private cat colonies (Radford *et al.*, 2003). These colonies and rescue shelters also appear to offer optimal conditions for strain evolution with a large population of cats in confined spaces allowing natural strain diversification (Radford *et al.*, 2003). Longitudinal analysis with endemically infected cat colonies has confirmed this (Coyne *et al.*, 2007). In addition, such high prevalence colonies provide the ideal environment for both mixed infections and viral genome recombination (Coyne *et al.*, 2006c).

3.1.2 Diversity of FCV clinical signs

With the large degree of viral diversity found within cat populations, it might be expected that strains act differently within the cat and cause cats to exhibit different clinical signs during infection. This assumption proves to be true, with FCV being associated with a number of patterns of disease including upper respiratory tract

disease, chronic stomatitis, limping syndrome and a virulent systemic disease (Radford *et al.*, 2009; Radford *et al.*, 2007).

Upper respiratory tract disease (URTD) is found to be the most widely reported sign of FCV infection and is usually a relatively mild condition with a low mortality rate. Cats presenting with FCV induced URTD usually show signs of ocular and nasal discharge, pyrexia, anorexia, lethargy and ulceration of the oral mucosa and tongue (Cai *et al.*, 2002; Povey, 1974).

FCV is also associated with acute arthritis which can cause the limping syndrome sometimes observed in infected cats and these limping effects have been recreated experimentally (Dawson *et al.*, 1994; TerWee *et al.*, 1997). A link between FCV and chronic stomatitis, a condition typified by chronic ulcerative lesions in the gingival, fauces and sometimes the cheeks and tongue, has been implied in a number of studies (Healey *et al.*, 2007; Knowles *et al.*, 1989; Poulet *et al.*, 2000; Waters *et al.*, 1993).

Recently, another set of more severe symptoms have been reported with FCV infections in the UK (Coyne *et al.*, 2006c), USA (Hurley *et al.*, 2004; Pedersen *et al.*, 2000; Schorr-Evans *et al.*, 2003), and France (Reynolds *et al.*, 2009). These outbreaks have been termed virulent systemic disease (VSD) due to the systemic nature of the clinical signs associated with these highly virulent strains of FCV (VS-FCV). Cats with VSD present variably with high fever, facial and limb oedema, depression, anorexia, sores on the face, pinnae and feet, pancreatitis and hepatic necrosis. The mortality rate associated with these virulent systemic strains of FCV are also very high, with up to 50% of the cats affected dying or being euthanised.

3.1.3 Genotypic and phenotypic strain markers

Attempts have been made to sub-classify FCV strains, or to find markers associated with the different clinical signs, especially for the hypervirulent VSD strains. Virus neutralisation tests have been developed in an attempt to categorise strain based on antibody neutralisation capabilities (Dawson *et al.*, 1993a; Knowles *et al.*, 1989; Poulet *et al.*, 2000). These studies have shown that while a lot of the virus strains react similarly to the sera and cannot be typed in this way, there are occasions where strains associated with specific clinical signs, especially chronic stomatitis, group

separately according to virus neutralisation tests. This was suggested to be a reflection of the chronic nature of this condition, providing an opportunity for viruses in such cats to evolve away from host immunity (Dawson *et al.*, 1993b; Poulet *et al.*, 2000). Enzyme-linked immune-flow-assays (ELIFA) using monoclonal antibodies have also been used in an attempt to differentiate FCV strain (McArdle *et al.*, 1996). However, whilst strains were able to be differentiated these did not reflect their clinical origins.

There have also been numerous attempts to sequence various regions of the genome to try to identify specific mutations that alter the nature of the strains (Abd-Eldaim *et al.*, 2005; Geissler *et al.*, 1997; Glenn *et al.*, 1999; Ossiboff *et al.*, 2007). They have all found that whilst all the strains are different from one another, the sequences do not phylogenetically cluster according to the disease state they originated from, nor have consistent mutations been identified in hypervirulent strains.

Ossiboff *et al*, 2007, have managed to find one potential marker of hypervirulent strains. They found that when the VSD strains were grown in cell culture at a lower m.o.i. which allows for multiple rounds of viral replication, the VSD strains grew at a significantly quicker rate than the typical FCV strains included in comparison. This finding was consistent for the three VSD strains analysed versus three typical FCV strains including FCV-F9, suggesting that *in vitro* growth rate could act as a diagnostic marker for virulence. Such assays are however, difficult to perform and not easy to standardise between laboratories.

3.1.4 Aims

The aim of this study was to further explore the effects of FCV infection with differing strains of virus upon the host cell proteome in cell culture. By using diverse strains from cats with a range of clinical diseases (a potentially hypervirulent strain, a typical FCV strain, a chronic stomatitis strain and vaccine strain), we aimed to characterise the diversity of the proteomic response to infection and to identify any potential host cell protein markers associated with virulence.

3.2 Materials and methods

3.2.1 Viral strains

Several approaches were used to identify the FCV strains to be used for subsequent proteomic analysis using 2D-DIGE. To capture the range of clinical disease associated with FCV infection, FCV-F9 (Bittle & Rubic, 1976; Bittle, 1960) was included again and also LS015 (Knowles, 1988). FCV-F9 is a vaccine strain often used in yearly boosters given to cats. LS015 is a virus isolated from a cat suffering from chronic gingivostomatitis and has anecdotally been known to always grow to high titre in cell culture. At the time of writing, no known VSD-causing strain was available to the author; therefore, we used a putative hypervirulent strain isolated from a cat with clinical signs and pathology consistent with VSD (Coyne *et al.*, 2006b). However, it is important to note that formal proof that this strain causes VSD in the form of an experimental infection has not been satisfied. In addition to this putative hypervirulent strain, we had access to several other strains available from the same rescue shelter (Coyne, 2005), that were isolated from clinically normal cats (strains R560-R602, Fig. 3.1).

3.2.2 Genetic diversity

It has previously been shown that FCV-F9, LS015 and UKOS-A represent genetically distinct strains (Coyne *et al.*, 2006b; Glenn *et al.*, 1999). We have also shown that R591 is genetically distinct from UKOS-A, whereas R580 and R581 represent variants of the UKOS-A strain having recently shared a common ancestor (Coyne, 2005) and Fig. 3.1.

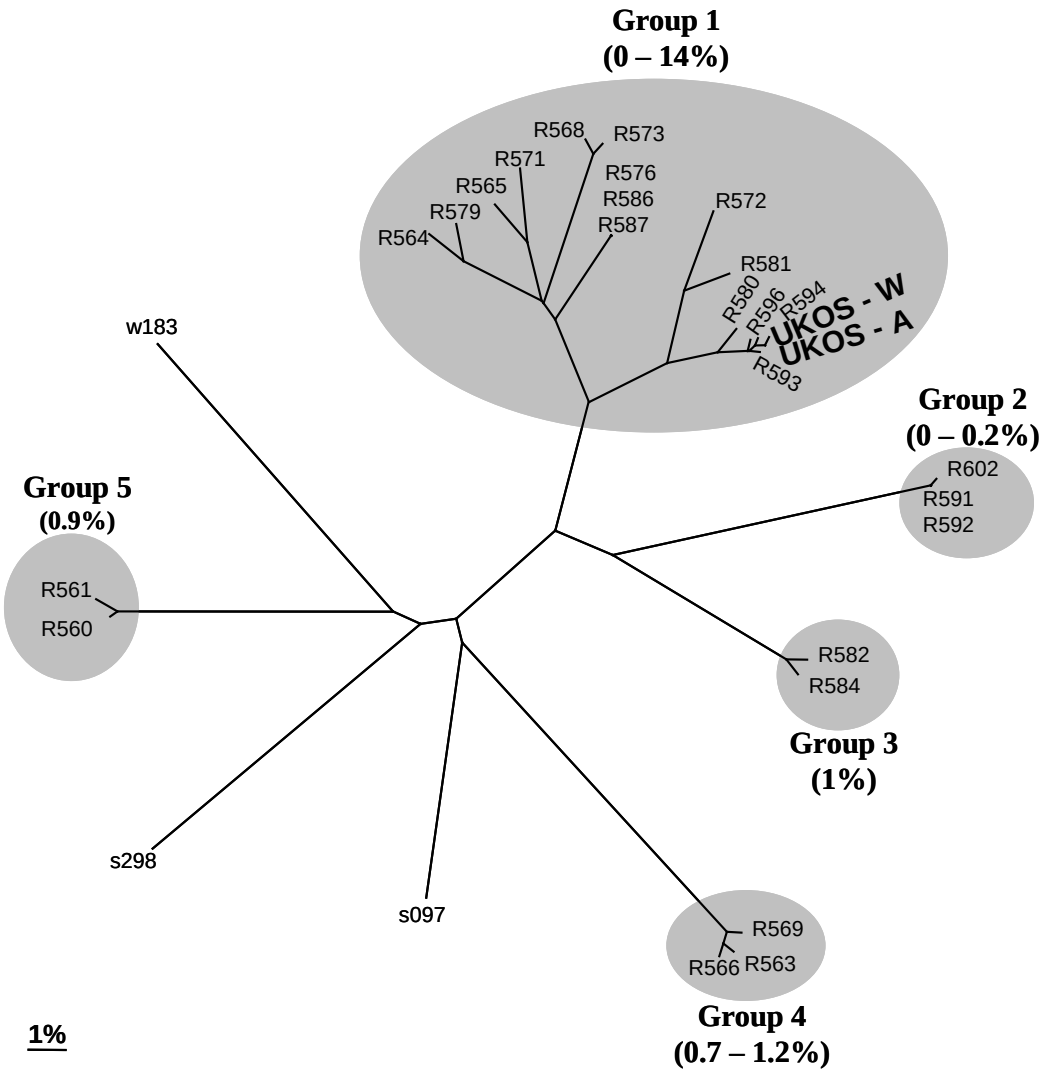

Figure. 3.1. Phylogenetic analysis of FCV polymerase gene sequence obtained from a rescue shelter involved in the suspected outbreak of VSD-FCV in the UK. This figure is reproduced from Coyne (2005). Viruses selected for analysis within this chapter are R581, R580, R591 and UKOS-A.

3.2.3 Growth in cell culture

Previous work (Ossiboff *et al.*, 2007) has shown that there are differences between the virulent systemic strains of FCV and other more typical FCV isolates. Specifically that VSD causing strains of FCV grow more efficiently under multiple-cycle growth conditions and show cytopathic effects earlier than in cells infected with non-VSD strains of FCV. Therefore, in order to further characterise the strains in this study, growth curves were also carried out.

3.2.3.1 Experimental design

The six viral strains selected were used in constructing growth curves over 40 h at two incubation temperatures; 37˚C the temperature typically used to culture FCV and 39˚C, the natural body temperature of a cat, to discover whether temperature had any effect on the growth kinetics.

The six viral strains used were UKOS-A (Coyne *et al.*, 2006b), R591, R581, R580(Coyne, 2005), LS015 (Knowles, 1988) and FCV-F9 (Bittle & Rubic, 1976; Bittle, 1960). Passage numbers for UKOS-A, R591, R581 and R580 were all less than 5 with FCV-F9 and LS015 having unknown, high passage histories.

3.2.3.2 Infection plan

16 x 24-well plates of confluent FEA cells were infected with an m.o.i. of 10 for each viral strain (four wells per strain) with 50 µl being added to each well. Eight plates were then incubated at 37°C and stopped by freezing at -80°C at 4, 8, 12, 16, 20, 24, 32 and 40 h p.i.. A further eight plates were incubated at 39°C and stopped in the same way at 4, 8, 12, 16, 20, 24, 32 and 40 h p.i.. Two more 24-well plates were also mock infected with MM and incubated at 37°C and 39°C to control for possible laboratory contamination.

Each plate was freeze-thawed at -80˚C and the contents of the four wells from each virus were combined for each time point and temperature, centrifuged at 2000 × *g* to pellet the debris and then the homogenate was titrated using methods previously described (section 2.2.1.3) alongside the mock infected controls.

3.2.4 2D-DIGE analysis of the effects of four strains of FCV upon the host cell proteome

As a further study into the effects FCV has upon the host cell proteome a 2D-DIGE comparison was performed upon cells infected using multiple strains of FCV.

3.2.4.1 Viral strains and cell culture

For each viral strain chosen for proteomic analysis two x 75 cm^2 flasks were infected with a 1 ml aliquot of each virus strain and two x 75 cm^2 flasks were mock infected with 1 ml of MM. The flasks were then frozen at -80°C 4 h p.i. and thawed the following day to allow for cell scraping. The scraped cells were collected in a centrifuge tube and pelleted at 2000 × *g* at room temperature for 10mins before the supernatant was discarded and the cell pellet stored at -20°C until lysis.

3.2.4.2 2D-DIGE analysis

The cell pellets were lysed in 500 µl of lysis buffer (30 mM Tris, 2 M Thiourea, 7 M Urea, 4% CHAPS) plus 10 µl DN/RNases and 5 µl of protease inhibitors. The samples were then treated as before (section 2.2.5.2) by freeze-thawing and removal of salts via the 2D-clean up kit (GE Healthcare). The protein pellet was resuspended in 2x sample buffer (2 M Thiourea, 7 M Urea, 2% CHAPS) before determining the protein concentration of each sample by a Bradford method based protein assay (Biorad Protein Assay) (Bradford 1976). The concentration of each sample was adjusted to 5 µg/µl using 2x sample buffer and the pH checked and adjusted to between 8 and 9 if necessary. The samples were CyDye labelled according to the manufacturer's instructions as previously described (section 2.2.5.4) and the labelled samples combined in the following order for isoelectric focussing (IEF) (Table 3.1).

Table 3.1. Experimental design for DIGE performed on samples infected with four strains of FCV.

Gel number	Cy2	Cy3	Cy5
1	Standard	F9_a	R591_b
2	Standard	R591_a	LS015_b
3	Standard	Mock_ a	UKOS-A_b
4	Standard	LS015_a	Mock_b
5	Standard	UKOS-A_a	F9_b
6	Prep Gel		

Once the appropriate samples were combined into 1.5 ml eppendorfs an equivalent volume of rehydration solution (2x sample buffer plus 5 µg/ml pH 3-10 IPG buffer (GE Healthcare) and 10 mg/ml DTT) was added to each and the samples were prepared for rehydration loading by vortexing and leaving on ice for 10 min. More rehydration buffer was added to each eppendorf to make the volume of solution up to 450 µl and this was added to a pH 3-10 24cm IPG strip in a reswelling tray, covered with 3-4 ml of DryStrip cover fluid and left to rehydrate overnight.

IEF was performed using the Ettan IPGphor II (GE Healthcare) at 30 v for 5 h, 500v for 1 h, 100 v for 1 h, 8000 v for 2 h and 8000 v for 9 h with current limited to 50 µA/strip. The focussed strips then had to be equilibrated as described previously (section 2.2.5.5) firstly in 10 ml SDS equilibration buffer (2% SDS, 50 mM Tris-HCl pH8.8, 6 M urea, 30% (v/v) glycerol, 0.002% bromophenol blue) with 10 mg/ml DTT for 15 min to reduce the protein and then for 15 min in 10 ml SDS equilibration buffer with 25 mg/ml iodoacetamide to alkylate the cysteine residues.

The second dimension was carried out using a manually cast 12.5% polyacrylamide gel as previously described (section 2.2.5.5) and the equilibrated strips were laid on top of the gels and sealed in with an agarose sealing solution (0.5% (w/v) agarose, trace bromophenol blue). The gels were at 5 W per gel for 30 mins and then adjusted to 17 W per gel for 4 h in an Ettan DALTsix electrophoresis unit (GE Healthcare).

Once the gels were run they were scanned immediately in an Ettan DIGE imager set at 100 pixels and 0.800 exposure on all 3 CyDye channels. After scanning, the prep

gel was fixed overnight in 40% methanol, 10% acetic acid then stained overnight in Sypro Ruby stain (Invitrogen) with gentle agitation. Before scanning again the gel was washed for an hour in 10% methanol, 7% acetic acid then rinsed twice in ddH_2O before scanning in the Ettan DIGE imager under Sypro Ruby conditions at the same exposure as before.

DeCyder analysis was carried out as described previously (section 2.2.5.7) with the following parameters to eliminate dust particles from inclusion in analysis; max slope >2.81, max area <179, max volume <6949. The spot maps were subject to strain-to-strain student t-test analysis and infected vs. uninfected student t-test analysis. All spots which were found to have a p-value ≤ 0.05 were selected for spot picking.

The spot picking was performed automatically as before (section 2.2.5.8) using the Ettan spot picker and the gel plugs tryptically digested using the same protocol (section 2.2.5.9). The resulting digests were all analysed using HPLC MS/MS under the same conditions as previously described (section 2.2.6.1).

MASCOT searching was performed on the resulting spectra as previously described (section 2.2.6.2).

3.2.4.3 Functional categorisation of identified proteins

The GO terms for biological processes were obtained by downloading those available for the annotated genes found on the cat genome from Ensembl using the BioMart tool as described in section 2.2.8.

3.3 Results

3.3.1 Viral growth curves

In order to discover whether the putative virulent strain isolated during the UK outbreak of virulent systemic FCV disease in the UK shares the same phenotypic growth patterns as other characterised virulent FCV strains (Ossiboff *et al.*, 2007) growth curves were constructed. The resulting growth curves at 37˚C and 39˚C are shown in Figures 3.2 and 3.3. The two temperatures were used as although all cell culture for feline cell lines is performed at 37˚C, the actual body temperature of a cat is 39˚C. Both temperatures were analysed in case the growth characteristics of the stains were different at the two temperatures.

Both of the growth curves show a similar pattern with LS015 growing to the highest titre at 37˚C and 39˚C, while strain R591 appeared to grow to a lower titre than the other FCV strains at most time points and at both high and low temperatures. These growth curves also show two peaks in $TCID_{50}$ indicating that each of the virus strains underwent two rounds of replication over the 40 h of incubation. There does appear to be a difference in the rate of growth of the viruses at the two temperatures. At 37˚C (Fig. 3.2) each of the virus strains reaches the first peak in titre between 16 and 20 h p.i. whereas at 39˚C (Fig. 3.3) this peak is reached much earlier with all strains peaking at 12 h p.i..

The putative hypervirulent strain UKOS-A does not show *in vitro* characteristics which can be characterised separately from the other strains within the growth curve experiment, it does not grow to the highest titre at either 37˚C or 39˚C and does not reach peak titre any quicker than the other FCV strains grown.

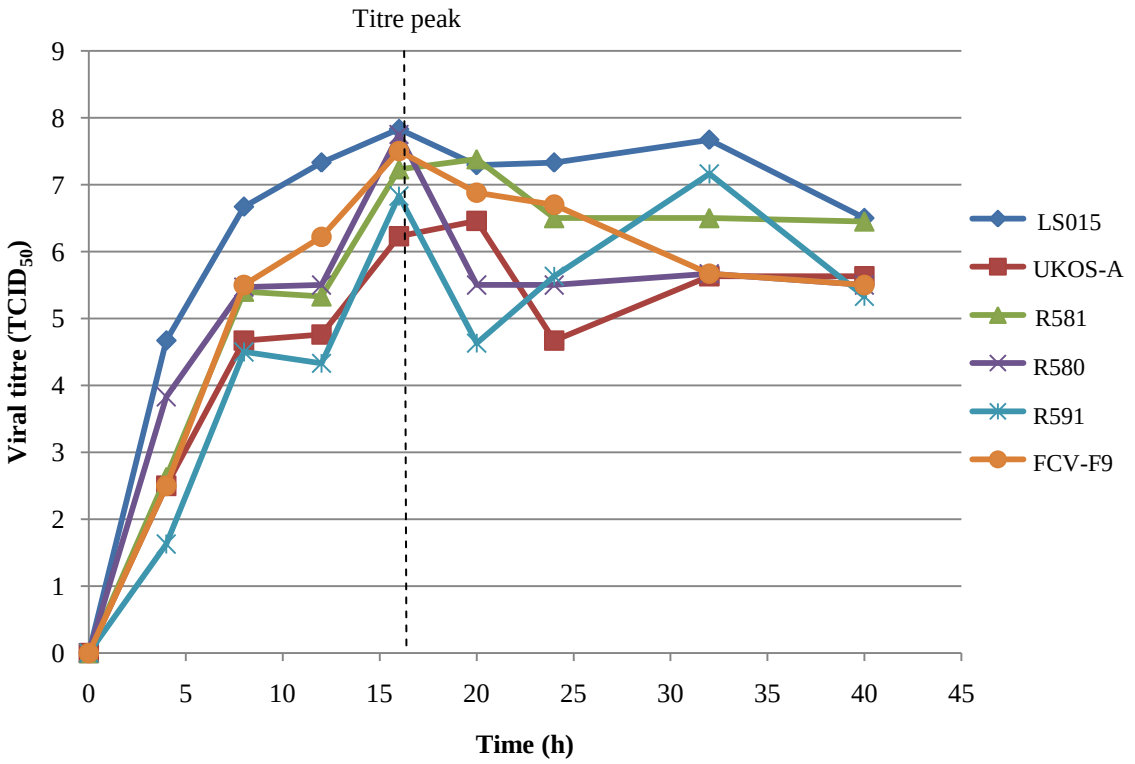

Figure. 3.2. Graph showing growth curves of six strains of FCV growing in FEA cells incubated at 37˚C sampled at 8 time points between 0 and 40 h p.i.

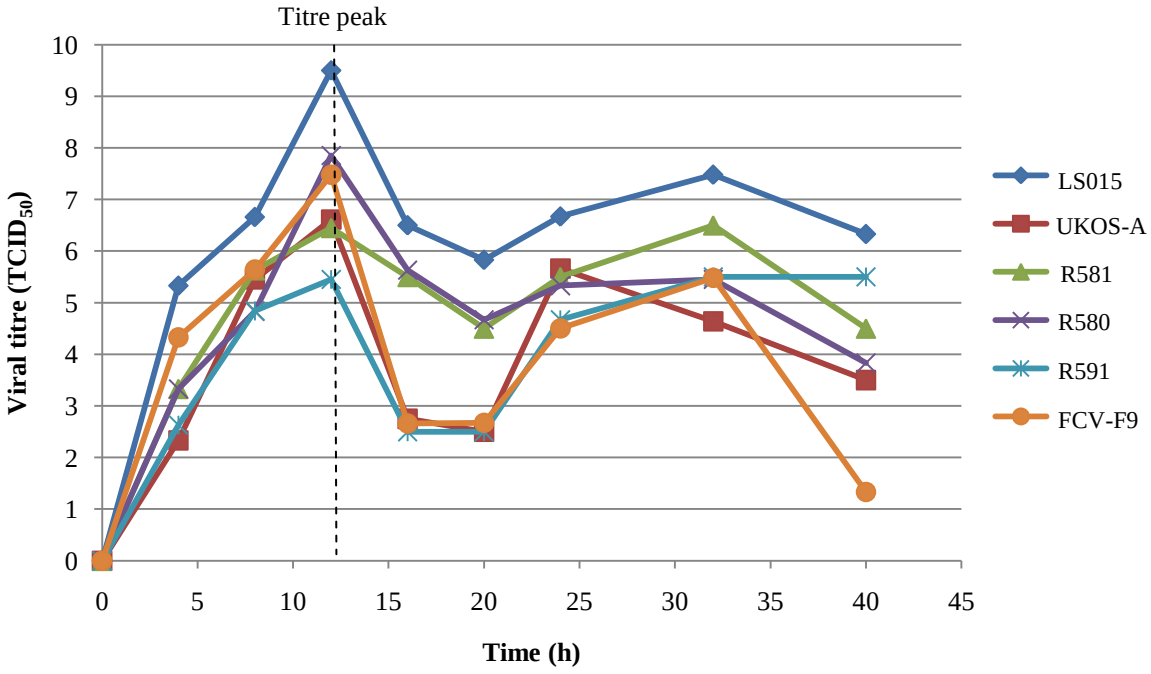

Figure. 3.3. Graph showing growth curves of six strains of FCV growing in FEA cells incubated at 39˚C sampled at 8 time points between 0 and 40 h p.i.

3.3.2 2D-DIGE analysis of the effects of four strains of FCV upon the host cell proteome

As a result of the genetic phylogeny and growth curve analysis, four strains were selected to have their effects upon the host cell proteome analysed by 2D-DIGE at 37°C. Namely FCV-F9 (vaccine strain, lab attenuated), LS015 (isolated from a cat with chronic stomatitis and had the highest titre in the growth curves), UKOS-A (isolated from a possible case of VSD and had intermediate titre on growth curves) and R591 (isolated from the same colony as UKOS-A but from a clinically healthy cat, is genetically distinct to UKOS-A and had low titres in cell culture).

3.3.2.1 Protein identifications

The six gels produced for 2D-DIGE analysis were scanned and uploaded into the DeCyder software for gel to gel matching and analysis. From the protein statistic examinations (t-test and ANOVA) performed in the BVA module of DeCyder 131 host proteins were found to be significantly differentially expressed and were picked and tryptically digested. Of these 131, 61 proteins were successfully identified by HPLC coupled ESI-MS/MS and Mascot ion searches and the positions of the successfully identified protein spots are shown in figure 3.4. The full list of protein identifications can be found in Appendix II.

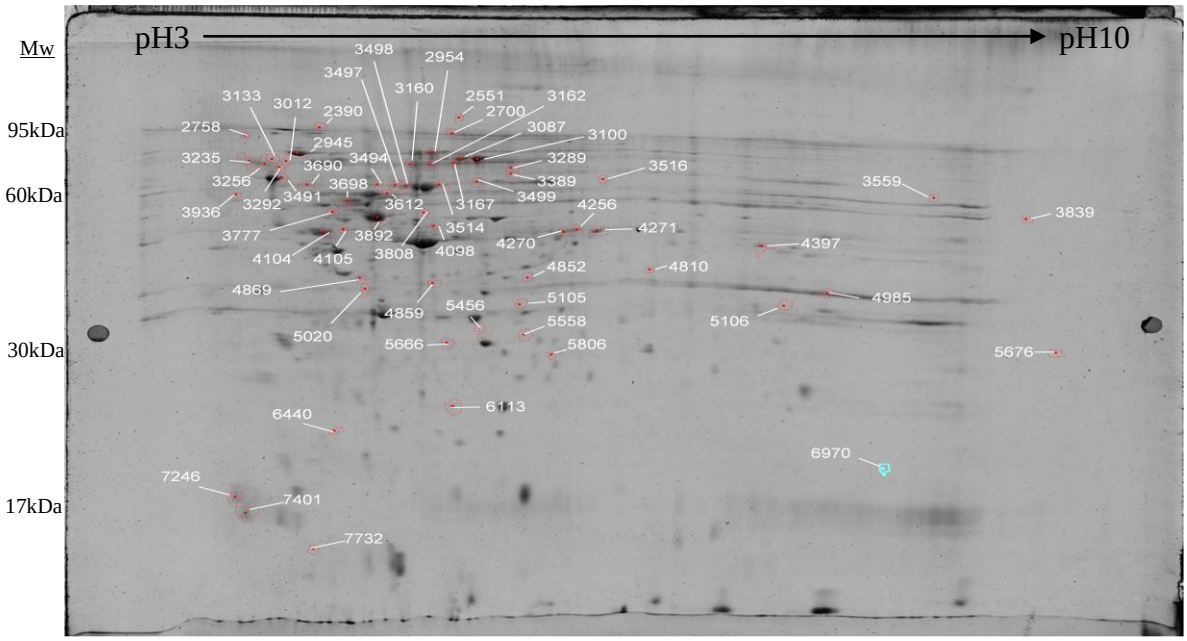

Figure. 3.4. Pick gel showing the positions of the proteins significantly differentially expressed during infection with FCV-F9, LS015, UKOS-A and R591with assigned spot number. Proteins were resolved by IEF over a non-linear pH3-10 range and by molecular weight on a 12.5% acrylamide gel. Staining was performed using Sypro Ruby and visualised using an Ettan DIGE imager at an exposure of 0.800.

The BVA module was also used to calculate average ratios between proteins from cells infected with each of the four strains and the proteins from the mock infected control cells. Within the proteins identified 16 were consistently up-regulated and three consistently down-regulated in the cells infected with each of the different strains of FCV (Fig 3.5 and Table 3.2).

Table 3.2. Identifications of proteins consistently up- or down-regulated in FEA cells infected with all FCV strains. Consistent up-regulation in infected cells is indicated with green highlight/+. Consistent down regulation infected cells is indicated with red highlight/-.

Spot number	Identification(s)	Modulation
2551	elongation factor Tu GTP-binding domain-containing protein 1, ubiquitin-conjugating enzyme E2O	+
2758	protein kinase C substrate 80K-H	-
3235	laminin alpha 1	+
3292	Obscurin, laminin alpha 1, albumin	+
3612	Chaperonin, vimentin, protein tyrosine phosphatase, Heat shock protein 60	+
3839	Obscurin, Cytochrome b, Putative glycine-rich RNA-binding protein 2, Myosin a tail domain interacting protein mtip	+
3892	Actin, eukaryotic translation initiation factor 3, Cytochrome b	+
4104	cathepsin d precursor, sulfate ABC transporter, Lamin-A	+
4985	annexin A2, ATP synthase beta subunit	+
5105	annexin A1, Sodium channel protein type XI alpha, Lipocortin-1	-
5106	voltage-dependent anion channel 2, annexin A2, intestinal cell kinase	+
5456	Obscurin, multiple C2 and transmembrane domain-containing protein 1	+
5806	multiple C2 domains, transmembrane 1, ATP synthase beta subunit	-
6113	multiple C2 domains, transmembrane 1	+
6440	Peptidase, beta-lactoglobulin, sorcin	+
7732	alpha 2 macroglobulin	+

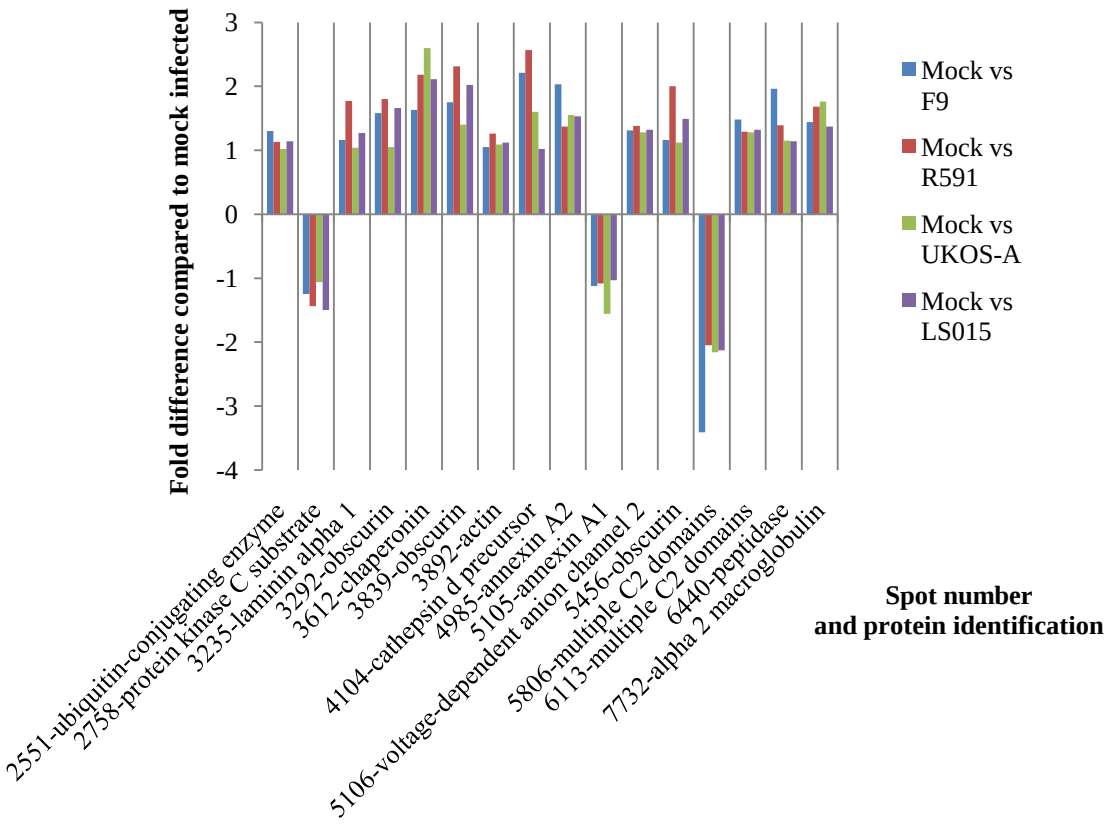

Figure 3.5. Graph showing 16 proteins consistently up- and down-regulated in response to all four FCV strains at 4 h p.i.. Protein identifications shown are top Mascot hit for each spot number.

Figure 3.6 shows an example of the 3D modelling provided by the DeCyder software used to analyse relative protein abundance for spot number 3612. This modelling illustrates the up-regulation in expression of the proteins identified within this spot (chaperonin, vimentin, protein tyrosine phosphatase and heat shock protein 60) in response to infection with each of the FCV strains studied when compared to the mock infected control.

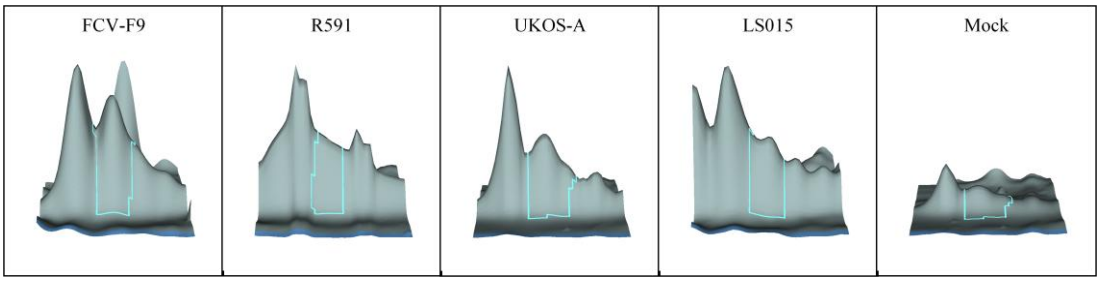

Figure 3.6. 3D modelling of protein expression, calculated within the DeCyder software from intensity of fluorescent protein labels on 2D-DIGE gels. The output show has been calculated for spot number 3612 which was consistently up-regulated in infected cells and was identified as a mixture of chaperonin, vimentin, protein tyrosine phosphatase and heat shock protein 60.

As these host proteins are consistently modulated in the same way by all four FCV strains examined it could be assumed that these proteins are in some way essential to viral replication within the cell. The significance of these proteins in terms of viral propagation will be discussed in section 3.4.2.

There are also possible signs of the putative virulent UKOS-A strain acting in a different way to the other three virus strains examined. For 14 of the 62 proteins identified, infection with UKOS-A causes these proteins to be down-regulated when compared to the mock infected control; whereas the other three viruses cause these proteins to be up-regulated (Table 3.3 and Fig. 3.7).

Table 3.3. Identifications of proteins down-regulated in FEA cells infected with UKOS-A and up-regulated in the remaining three strains when compared to mock infected cells.

Spot number	Identification(s)
2954	Lamin a/c, dihydrolipoamide S-acetyltransferase, calsyntenin 2
3256	Obscurin
3289	Lamin a/c
3389	Lamin a/c
3777	Mitochondrial ATP synthase, vimentin, protein disulphide isomerase associated 6, desmin, cathepsin d, actin
4256	Lamin a/c
4270	Lamin a/c
4271	Peptidase, sortilin-related receptor, lamin a/c, envelope glycoprotein syncytin-B, pleckstrin and Sec 7 domain containing 2
4852	Annexin A1/A2
4859	Annexin A1/A2, acidic ribosomal phosphoprotein P0
4869	ATPase, Annexin A1
5666	Prohibitin, actin
7246	40S ribosomal protein S14
7401	Myosin

Within this group of proteins are some identifications which appear in the list more than once such as lamin a/c and annexin A1/A2. It is possible that the putative virulent strain is modulating these proteins in a different manner to the other 'typical' FCV strains and these could be a marker of virulent systemic disease. The significance of these differences in protein expression will be discussed further in section 3.4.2.

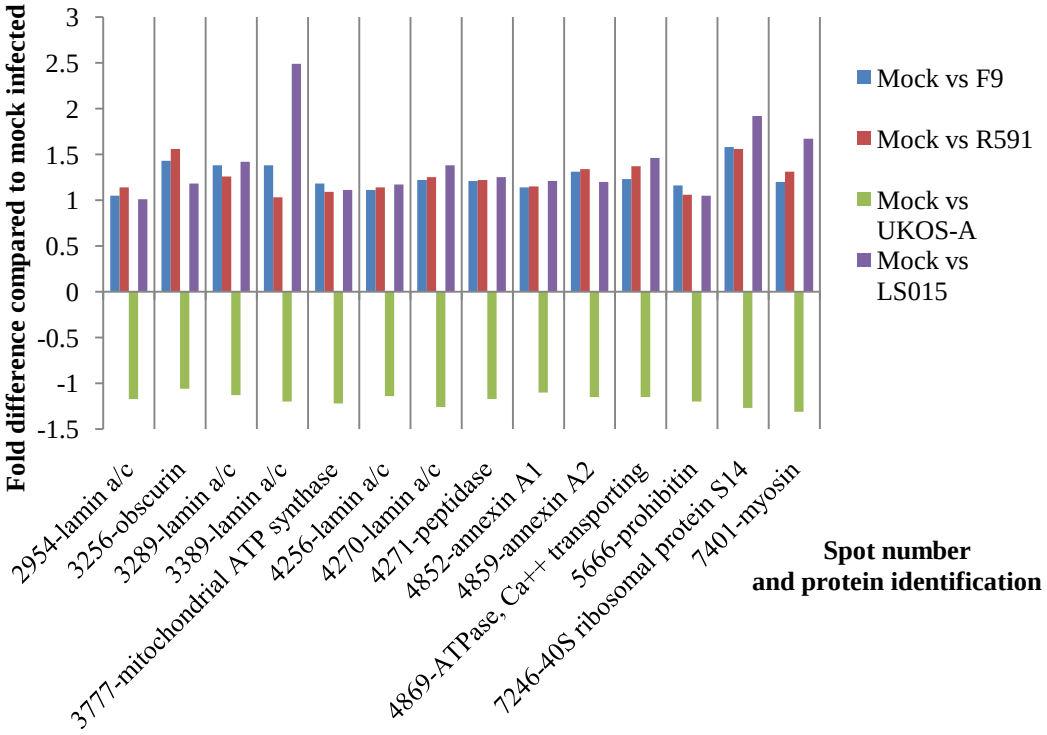

Figure 3.7. Graph showing 14 proteins down-regulated in the FEA host cell in response to UKOS-A infection but up-regulated in the response to the other FCV strains at 4 h p.i.. Protein identifications shown are top Mascot hit for each spot number.

Figure 3.8 shows the average ratio of the remaining 31 modulated host cell proteins in comparison to the mock infected cells and this graph shows that there is a complex pattern of protein expression in response to infection. In the case of spot number 5676, the obscurin protein appears to be greatly down-regulated in response to three of the strains. However, it became up-regulated in response to LS015 which is a marked difference within the modulation of this protein. The 60S ribosomal protein (6970) also showed a marked difference in modulation in the response to infection with the strains examined as it had a large up-regulation during UKOS-A infection but a large down-regulation during the infection with LS015. The implications of these inconsistencies will be discussed in section 3.4.

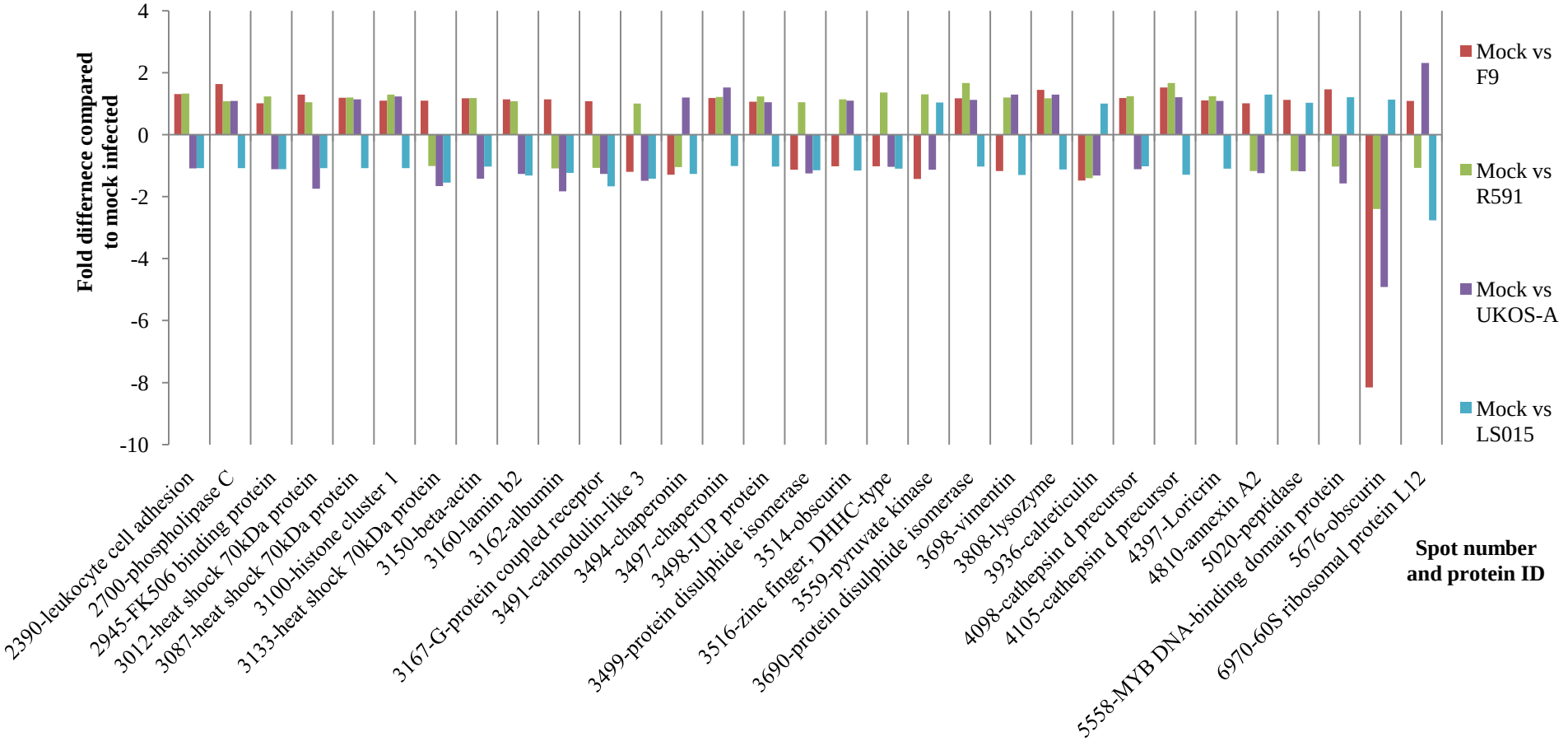

Figure 3.8. Graph showing expression for the remaining 31 identified proteins relative to the mock infected control at 4 h p.i.. Protein identifications shown are top Mascot hit from searching the feline database for each spot number.

3.3.2.2 Gene Ontology analysis

The biological processes assigned from the Gene Ontology (GO) project to each of the annotated genes on the cat genome were downloaded from the Ensembl website and the identified protein set was interrogated against it. Each GO term found was manually curated into broad definition terms and a chart was constructed (Fig. 3.9).

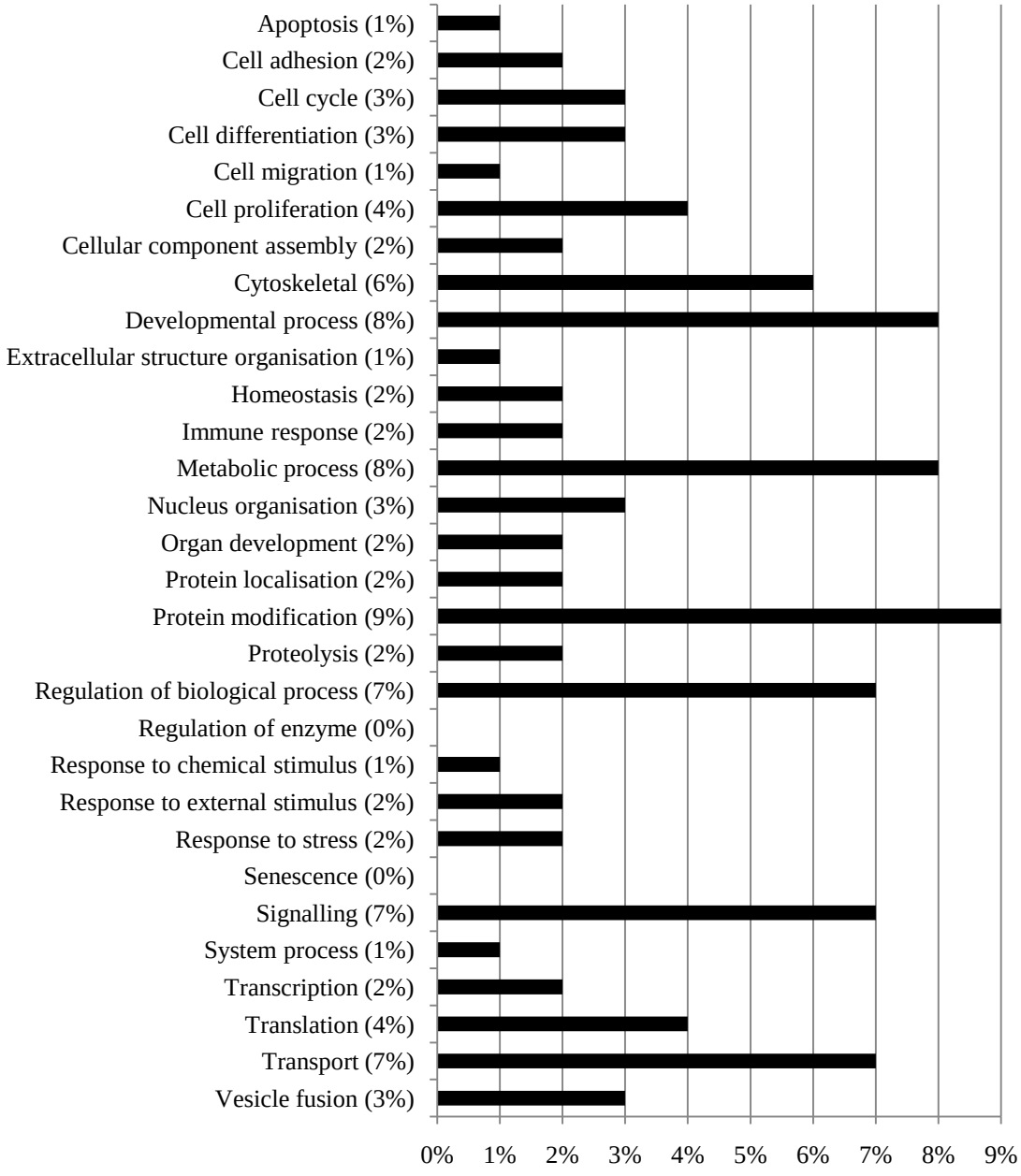

Figure 3.9. Gene Ontology analysis of the biological processes of all 61 proteins found to be differentially expressed in response to infection with FCV-F9, UKOS-A, R591 and LS015 using 2D-DIGE.

This breakdown of the biological processes of the proteins identified shows a similar pattern to that constructed from the 2D-DIGE analysis of a time course of infection (chapter 2). There are a large proportion of proteins which have a function in metabolism, developmental processes and regulation within the cell. There are also a number of proteins which have a cytoskeletal role present again in the list. Although these are less abundant than in the previous 2D-DIGE analysis, there are enough present in the identifications and functional categorisation to suggest that further examination of the effect of viral infections upon the cellular cytoskeleton is needed.

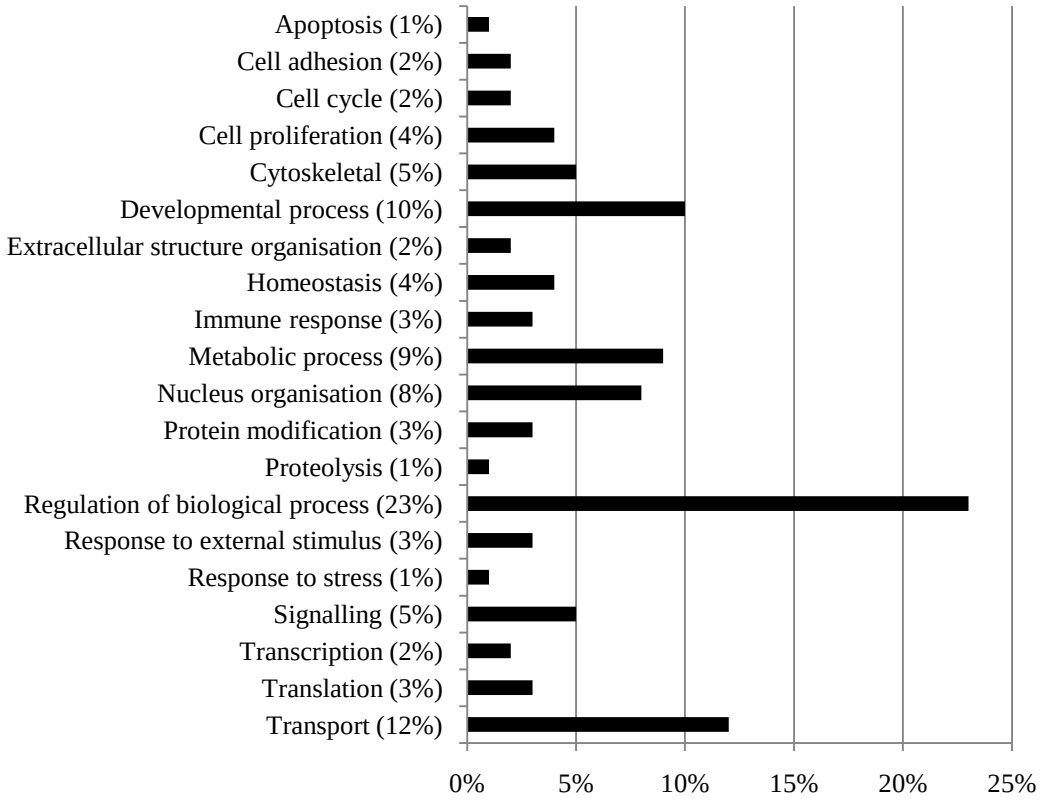

Figure 3.10. Gene Ontology analysis of the biological processes of the 14 proteins found to be down-regulated in response to UKOS-A infection but up-regulated in response to infection with the other three FCV strains analysed.

A further breakdown of biological processes was performed for those proteins found to be modulated differently in response to infection with the UKOS-A strain compared to the other three viral strains (Fig 3.10). The chart shows that the majority of these proteins have regulatory functions such as involvement with metabolism, transport and biological processes. Within this subset of proteins there is also a larger proportion involved in organisation of the nucleus with the percentage involved rising to 8% from 3% in the functional analysis of all modulated proteins (Fig 3.9). This may be expected as 6 of the 14 proteins found within this grouping have been identified as lamins, which are known to be a key component in the structure of the nucleus and as such will be involved in nuclear organisation.

3.4 Discussion

The results from the viral growth curves showed that under both temperature conditions the UKOS-A strain of FCV does not grow to a higher titre or significantly quicker than the other FCV strains grown in parallel as a comparison. This is a different finding to that of Ossiboff *et al,* 2007, whose experiments showed that when using a high m.o.i., 4/6 VSD strains of FCV grew to a higher titre than the comparison strains and at the low m.o.i., they found that all three of the VSD strains tested grew at a significantly quicker rate than the comparison strains. This suggests that either UKOS-A is not a VSD causing strain of FCV or that the ability to grow quickly and to a higher titre in cell culture is not characteristic of all VS-FCV strains.

In the analysis of the growth curves produced at both 37˚C and 39˚C, the results showed that the pattern of infection produced at both temperatures were very similar. The main differences found between the two growth curves were a higher and faster titre peak which can be explained simply by the increase in incubation temperature as most reactions will occur quicker at a higher temperature. There were also no strain specific differences found during the incubation at 39˚C which shows that incubation temperature has no significant effect upon any of the strains examined and further incubations can be carried out at 37˚C without affecting *in vitro* growth kinetics.

The results of the 2D-DIGE analysis showed that there were 16 proteins that were up- or down-regulated consistently across all of the strains which indicate that these proteins are important to the virus. Within these protein identifications actin and vimentin were found to be up-regulated again in all viral samples which is consistent with the results in chapter 2. This again shows that these two proteins appear to be important in viral replication. Other proteins identified to be consistently up-regulated included elongation factor Tu GTP-binding domain-containing protein 1. This protein is of particular interest as x-ray crystallography has shown that Norovirus, another member of the *Caliciviridae*, has a domain upon the capsid protein that is very similar to translation elongation factor-Tu (EF-Tu) (Prasad *et al.*, 1999) and this domain was hypothesised to have a similar function to EF-Tu. Whether this domain is conserved within the FCV capsid protein is unknown but in the cell EF-Tu is a GTP binding protein involved in bringing aminoacyl-tRNAs to

ribosomes during translation thus if the capsid of FCV does not contain a domain similar to this protein it is logical that this protein might be useful in the translation of the viral polypeptide.

Of the other consistently modulated proteins spots only three were down-regulated in all viral samples and protein number 2758 (protein kinase C substrate) was the only one with a single identification. The protein kinase C are a family of enzymes used to control the functions of other proteins through phosphorylation including the nuclear lamins (Gruenbaum *et al.*, 2003). The down-regulation of the protein kinase C substrate could indicate that cellular protein kinases are freed to act upon other proteins within the cell during FCV infection. Lamins were identified within 9 of the modulated protein spots found during 2D-DIGE analysis and as a known substrate of protein kinase C it could be hypothesised that these proteins were modulated through phosphorylation catalysed by protein kinase C. This process has been shown to occur with herpesvirus infection (Leach & Roller, 2010). As herpesvirus capsid proteins are assembled inside the nucleus the virus needs the nuclear lamina to be disrupted to allow the capsid to exit into the cytosol. When the protein kinases were inhibited within the Leach *et al* (2010) study it was found that viral growth was reduced fivefold and capsid proteins were unable to egress from the nucleus. This mode of action may not prove true in the case of FCV as replication is thought to occur in the cytoplasm near the endoplasmic reticulum (Bailey *et al.*, 2010). However, movement of viral proteins into and out of the nucleus may still be necessary in replication and so phosphorylation of nuclear lamins may be an important part of viral infection.

With the other two down-regulated protein spots there are multiple identifications which make it difficult to decipher whether it is one protein responsible for the down-regulation or a combination of all the host proteins identified in the spot. In the case of spot number 5105, annexin is shown as one of the proteins present in the spot and annexin is also found in spot 5106. Looking at the position of these spots on the gel (Fig. 3.2) the molecular weights of the protein spots match and the position of each spot is separated only by isoelectric point resolution which possibly means that the annexin proteins found in both spots may have been modified post-translationally during infection to alter the isoelectric point. Annexin has been shown play a role in hepatitis C virus assembly (Backes *et al.*, 2010) and also in the entry of rabbit vesivirus (RaV) into cells (Gonzalez-Reyes *et al.*, 2009). Annexin A2 was shown to

be bound to RaV virions in the membrane fraction of infected cells and when infecting annexin A2 knock out cells with RaV the titre recovered was significantly lowered. As this study was performed in another member of the *Caliciviridae* it may be that FCV acts in a very similar manner and that annexin or a post-translationally modified form of annexin is important in FCV entry into the cell.

As well as finding proteins which are modulated consistently in response to infection with a number of different FCV strains, a further aim of this study was to try to identify potential markers of virulence using a putative VSD strain of FCV, UKOS-A. The 2D-DIGE results show that there were 14 proteins that were expressed differently in cells infected with the UKOS-A strain compared to the response to the other FCV strain used to infect cells. All of these proteins were down-regulated in the UKOS-A infected samples which may imply that the UKOS-A strain is acting in an independent manner to more typical FCV strains. This different mode of action within the cell may be able to explain why this virus strain was recovered from a cat that showed a number of clinical signs associated with VSD-FCV strains and eventually died. Of the 14 proteins found in Table 3.3, actin and vimentin were again present although as they were down-regulated in the UKOS infected cells, it is possible that the virus is not using them to move around the cell in the same fashion as the non-virulent strains but only further individual analysis of these proteins will elucidate the true action of virus. The proportion of proteins found to be differently expressed in response to infection with the UKOS-A strain was greater than with the other viruses examined within this 2D-DIGE experiment which also suggests that the UKOS-A strain is acting in a different manner within the cell.

The overall results from this chapter have shown that while *in vitro* growth characteristics have not been found to be a marker of virulence for the UKOS-A strain there are differences to be found in the effects of the UKOS virus upon the host cell proteome. There were certain proteins identified that were consistently modulated in response to all of the infections with different FCV strains, however, the vast majority of proteins identified within this study appeared to be affected differently depending on the strain used for infection. This shows that infection with strains isolated from cats exhibiting varied clinical signs produces a very varied proteomic response from infected cells and as such leaves a complex picture of infection.

As only one time point (4 h p.i.) was examined in this 2D-DIGE experiment, there may also be a timing effect being seen within this study. It is impossible to determine whether any of the proteins which are not consistently modulated by all strains are merely exhibiting a time delay and at latter stages of infection there may be more proteins found to be consistently changed between all the viruses tested.

There are however, proteins found within this 2D-DIGE analysis which echo the findings of the previous 2D-DIGE experiment performed upon a single FCV strain (FCV-F9) (chapter 2). Cytoskeletal protein modulation was found once again to be important within this analysis with the proteins actin and vimentin becoming differentially expressed in response to infection. These findings reaffirm the conclusion that cytoskeletal remodelling is important in FCV infection and as such these proteins should be examined on an individual basis to try to discover the mechanisms of host-pathogen interaction involving them.

4 Chapter Four

Investigation of host cell cytoskeletal rearrangement during infection with four strains of FCV using confocal microscopy

4.1 Introduction

Experimental analysis with 2D-DIGE (chapters 2 and 3) has shown that during infection with FCV host cell cytoskeletal proteins are modulated. The cytoskeleton is comprised of three kinds of filaments, categorised into microfilaments, microtubules and intermediate filaments and in this chapter, attempts will be made to visualise and calculate the extent to which one protein from each of these categories is rearranged. The three proteins chosen for further analysis were actin, vimentin and tubulin.

Actin is one of the most abundant host cell proteins and as such is a very important protein for the survival of the cell. Actin is found in the cell as both a monomer and polymerised as filaments with the polymerised filaments able to provide structural rigidity to the cell by forming a cross-linked network (Pollard & Cooper, 2009). The polymerisation process is directionally driven (Wegner, 1976) which allows the cell to "crawl" and also internalise vesicles within the cell. There is also a close relationship found between actin and myosin which allows force to be generated to produce contractions which can move organelles and cellular components short distances along these actin filaments (Pollard & Cooper, 2009). As discussed in previous chapters (chapters 2 and 3), these functions have been shown to be very useful in enabling viruses to move both with the cell and also from cell-to-cell. It has been established a number of years ago that vaccinia virus needs an intact actin cytoskeleton in order to exit the cell (Payne & Kristensson, 1982) and subsequent studies have shown that actin tails are formed below the virion to allow movement around the cell and also actin based protrusions are used by the virus in egress (Cudmore *et al.*, 1995).

The second protein chosen for further investigation is a member of the intermediate filaments called vimentin. Again the main function of the intermediate filaments within cells is to provide cellular structure and integrity although they are also credited with involvement in cell migration and signal modulation (Coulombe &

Wong, 2004). Vimentin specifically has also been implicated with interaction with organelles such as the endo-lysosome complex (Styers *et al.*, 2004) and the golgi body (Gao & Sztul, 2001) giving the impression that this is another important group of proteins within the cell and disruption to this network would be detrimental to the cell in most cases. In virology, vimentin has been specifically linked with dengue virus infection (Kanlaya *et al.*, 2010) and also bluetongue virus infection (Bhattacharya *et al.*, 2007), with viral proteins in both cases associating closely with vimentin proteins in cell culture and aiding the virion in egress from the cell.

Tubulin is the main protein making up the microtubule component of the cytoskeleton and so was chosen to be included in the analysis in this chapter. Within the cell, tubulin is found as monomers of α- and β-tubulin which can polymerise to form microtubules. Initiation of microtubule polymerisation occurs when γ-tubulin forms a ring and acts as a scaffold for the growth of new microtubules (Tassin & Bornens, 1999). This also gives the microtubule polarity with growth heading from the centrosome where the γ-tubulin is found into the cytosol. These polymerised microtubules function as pathways for movement of organelles and cellular components around the cell (Howard & Hyman, 2003) and as such are also a target for viruses to use as a means of movement within a host. There are a number of viruses that have been proven to use microtubules to their advantage to increase their infectivity and chances of replication. Human immunodeficiency virus 1 (HIV-1) uses the microtubule network to move the virus and its genome from the membrane site of entry into the nucleus for reverse transcription (McDonald *et al.*, 2002) and alphaherpesvirus has been shown to remodel the cytoskeleton in a similar manner to vaccinia virus to form cellular projections made up of tubulin and actin in order to contact neighbouring cells and promote viral spread (Favoreel *et al.*, 2005).

Each of the proteins chosen for further analysis has been shown not only to be important to the host cell but also vital in pathogenesis for a number of other viruses. In order to examine these changes closer in this chapter, confocal microscopy was used alongside immunofluorescent staining to visualise viral proteins and host cytoskeletal proteins. Using these techniques will allow any rearrangements of these proteins to be discovered and visualised and for their effects to be traced back to viral infection.

4.2 Materials and methods

4.2.1 Viral infection

Eight chamber slides (Nunc, Lab-Tek II CC2 chamber slide system, Sigma Aldrich) were seeded with FEA cells, passage number 42, and left to become confluent for four days. Once confluent the cells were either infected with previously plaque purified FCV-F9 (vaccine strain) (Bittle & Rubic, 1976; Bittle, 1960), LS015 (from a cat with chronic gingivostomatitis) (Knowles, 1988), UKOS-A (putative VS-FCV strain) (Coyne *et al.*, 2006a) or R591 (typical FCV strain) (Coyne, 2005) at a multiplicity of infection (m.o.i.) 10 or mock infected with supernatant from a freeze-thawed flask of FEA cells. The cells were infected for a period of 7 and 13 h before being stopped by washing three times with PBS and fixing.

4.2.2 Fixation and staining

Cells were fixed using 70% ethanol to fix and permeabilise the cells without interfering with the signal from the conjugated antibody stain. The ethanol was left to incubate at room temperature for two min before being washed three times with PBS. All dilutions were performed using PBS (1x solution, see Table 2.1 for recipe) with 0.5% BSA added as a blocking agent to prevent non-specific binding by the antibodies. The staining was performed as follows:

4.2.2.1 Vimentin

Vimentin proteins were stained using a primary antibody raised against vimentin and a secondary fluorescent antibody raised against the primary antibody. The primary antibody used was a monoclonal anti-vimentin antibody (mouse IgM isotype) (V5255, Sigma-Aldrich) diluted to a 1 in 20 concentration with blocked PBS before 50 µl was added to each well. The chamber slides were left to incubate at 37°C for 1 h before being washed three times in PBS. The secondary fluorescent antibody used was Alexa Fluor 633 (goat anti-mouse IgM) (A21046, Invitrogen) diluted to a 1 in 100 concentration and 50 µl was added to each well. Again the chamber slides were left to incubate at 37°C for 1 h before being washed three times in PBS.

4.2.2.2 Tubulin

Tubulin proteins were stained using a primary and secondary antibody in the same manner as the vimentin staining. The primary antibody used was a monoclonal anti-α-tubulin (mouse IgG isotype) (T5168 Sigma-Aldrich) diluted to a 1 in 50 concentration with blocked PBS with 50 µl being added to each well before being incubated at 37˚C for 1 h and washed three times with PBS. The secondary fluorescent antibody used was Alexa Fluor 633 (goat anti-mouse IgG) (A21050, Invitrogen) diluted to a 1 in 100 concentration and 50 µl was added to each well. Again the chamber slides were left to incubate at 37°C for 1 h before being washed three times in PBS.

4.2.2.3 Actin

The same procedure of using a primary antibody and secondary fluorophore was attempted to stain cellular actin, however, a preliminary investigation using a monoclonal anti-actin antibody (A3853, Sigma Aldrich) showed this staining to be unsuccessful. Therefore, the decision was made to use phalloidin staining. Phalloidin is a toxin derived from the mushroom *Amanita phalloides* which binds to cellular actin and can be conjugated with fluorescent proteins (Faulstich *et al.*, 1988). Phalloidin conjugated with Alexa Fluor 633 (A22284, Invitrogen) was diluted to a concentration of 1 in 50 and 50 µl added to each well before incubating at 37˚C for 1 h and washing three times with PBS.

4.2.2.4 FCV capsid

FCV capsid proteins were stained using an anti-FCV primary antibody previously found to be broadly cross-reactive against many strains of FCV and a fluorescent secondary antibody. The primary anti-FCV capsid antibody G784h (Porter, 2004) was used at a concentration of 1 in 20 and 50 µl added to each well. The chamber slides were then incubated at 37˚C for 1 h before washing three times with PBS. The secondary antibody used was Alexa Fluor 488 (goat anti-rabbit IgG) (A11008, Invitrogen) diluted to a 1 in 100 concentration. 50 µl was added to each well before incubation at 37˚C for 1 h followed by washing with PBS three times.

4.2.2.5 DAPI

All cells were finally stained with DAPI (4',6-diamidino-2-phenylindole) nucleic acid stain, to allow the nucleus of each cell to be visualised, at a concentration of 300 ng/ml.

The chambers were then removed from the slides to allow coverslips to be mounted. Each well was protected with Vectashield (Vector labs) to prevent rapid loss of fluorescence and coverslips were fixed into place with clear nail varnish.

Imaging was performed with the help of Dr Dave Spiller, Centre for Cell Imaging, University of Liverpool. The slides were visualised using a Zeiss Axio Observer Z1 confocal microscope with a x40 lens, pinhole of 272 and an optical slice <3.4 µm.

4.2.3 Image analysis with ImageJ software

To allow comparable analyses to be performed against each sample, images were interrogated with ImageJ software (Abramoff *et al.*, 2004). A line of 20 µm in length was drawn from one DAPI stained nucleus to another. Where the DAPI stained image was unavailable, the line was drawn from the unstained centre of one cell into the centre of the next. In order to make comparison between images possible, data was only recorded when this line terminated at both ends within the area of a nucleus. A plot profile was performed along the line drawn and grey scale values taken for each of the fluorescent channels. This process was repeated 15 times per time point and virus strain to allow average grey scale values to be calculated and plotted against the other fluorescent channels.

Statistical analysis was performed with the assistance of Dr Karen Coyne, Infection Biology, University of Liverpool. Mann Whitney U tests were performed upon the values collected from the grey scale plots with values taken along the line from 0-10 µm being identified as infected cells and values taken from 10.1-20 µm designated as values from uninfected cells. The cut-off was defined as 10 µm as it was the mid-point of the line and defining cell boundaries accurately for each measurement would be difficult, especially as cells have been known to alter morphology during infection with FCV (Knowles, 1988). Statistical significance was set at $p \leq 0.01$.

4.3 Results

During infection with each of the strains of FCV, characteristic cytopathic effects could be seen using light microscopy including the infected cells rounding and becoming refractile by 7 h p.i. (Figs. 4.1 and 4.2) (Knowles, 1988). The mock infected cells did not show any signs of these effects and remained flat and completely adherent to the surface of the slide (Figs. 4.1 and 4.2).

4.3.1 Actin staining

Attempts were made to stain the cells with phalloidin which binds to cellular actin to visualise any actin remodelling as a result of infection with FCV. Unfortunately the conjugated phalloidin used in this study was also not compatible with the feline cells used and the pattern of fluorescence was indistinct (data not presented) and could not be used in this investigation.

4.3.2 Tubulin staining

The fixed, infected and mock infected cells were also stained for host cell tubulin proteins to discover whether the modulation seen during the 2D-DIGE experiment in chapters 2 and 3 could be visualised by confocal microscopy. Figures 4.1-4.5 show examples of cells infected with each of the four viruses studied at 7 and 13 h p.i.. Figures 4.1 and 4.2 also show mock infected cells at 7 and 13 h p.i. stained for FCV capsid proteins and tubulin alongside light microscope images of the same cells.

The pattern of tubulin staining within the mock infected control shows a circular gap within the centre of each of the cells where no staining is shown, this is most probably where the nucleus of each cell is located (Figs. 4.1 and 4.2). Whilst tubulin staining is widespread throughout the cytosol of each cell it is not uniformly distributed, there are areas of high intensity and areas of relatively low intensity. This pattern is typical of tubulin staining as areas of high microtubule distribution will stain with a greater intensity (Armer *et al.*, 2008).

Within each of these images, those cells which show viral capsid protein expression by emitting green fluorescence also appear to show increased intensity of the red

tubulin staining and different distribution. In Figures 4.1, 4.3 and 4.5 there are also signs of cellular modification in the form of blebbing at 7 h p.i., which have been found before during infection with FCV (Fig. 4.6, (Knowles, 1988)). However, these effects disappear at 13 h p.i. and were much less distinct with the cells infected by UKOS-A. There were also differing patterns of viral antigen within the blebs themselves, with strain R591 showing clear staining of FCV capsid within blebs (Fig. 4.5) whereas the blebs found in cells infected with FCV-F9 and LS015 show no signs of viral staining within the blebs (Figs. 4.1 and 4.3).

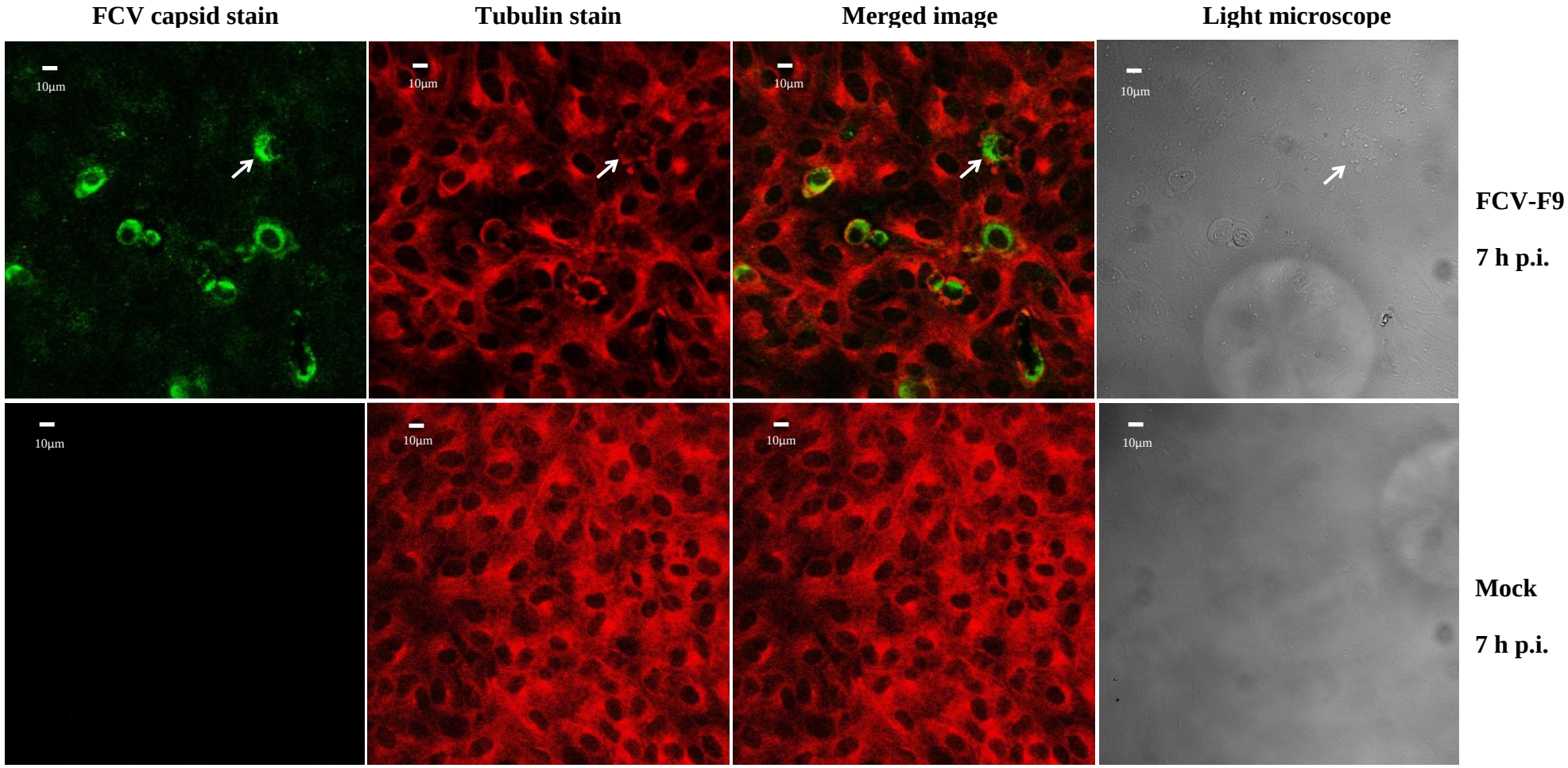

Figure 4.1. Tubulin stained FEA cells infected with FCV-F9 and mock infected at 7 h p.i.. FCV capsid staining was performed using an anti-FCV primary antibody, visualised using an Alexa Fluor 488 conjugated secondary antibody and is coloured green. Tubulin staining was performed using a mouse monoclonal anti-α-tubulin primary antibody, visualised using an Alexa Fluor 633 conjugated secondary anti-mouse IgG antibody and is coloured red. White arrows indicate cells showing signs of blebbing structures.

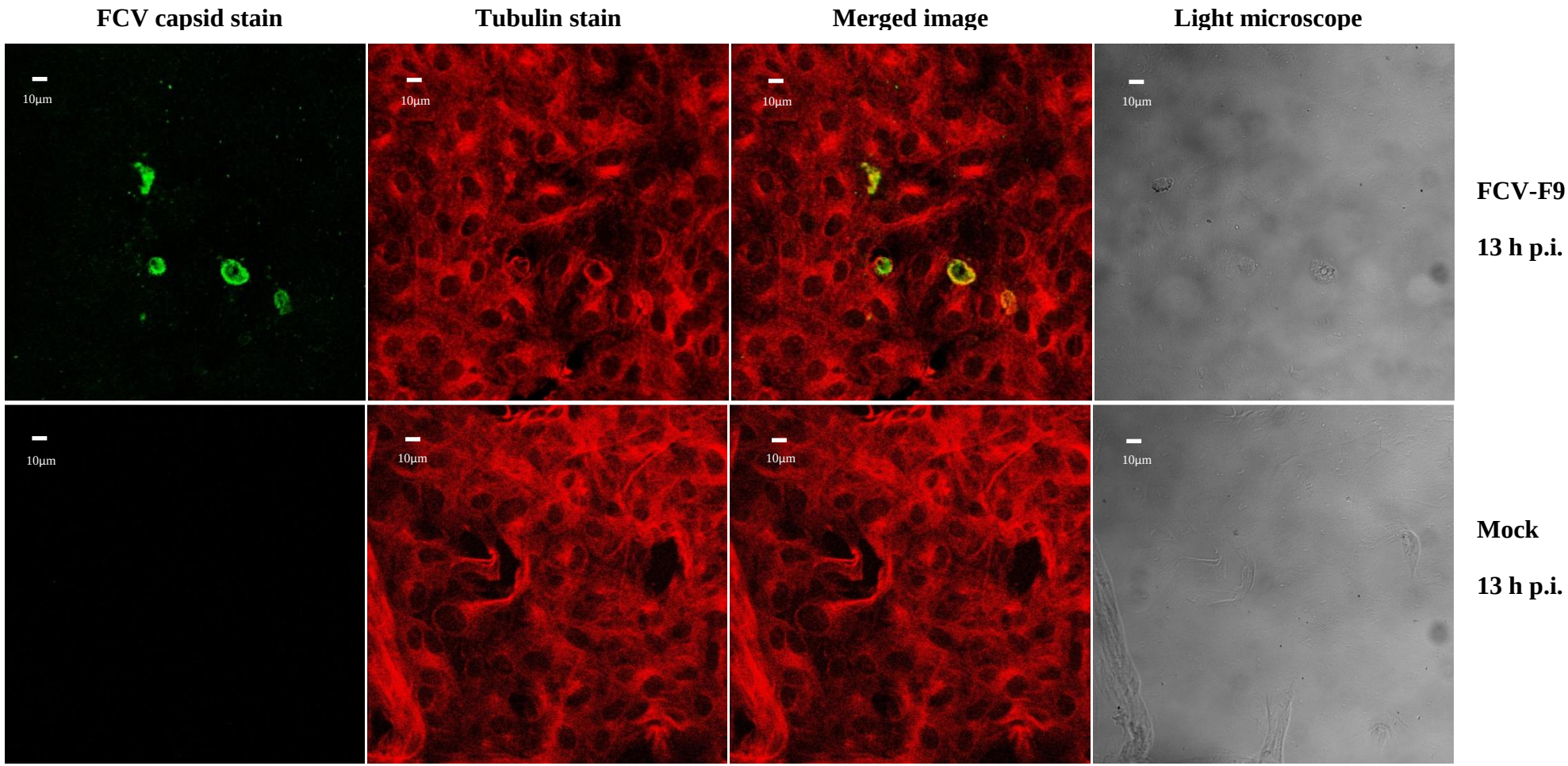

Figure 4.2. Tubulin stained FEA cells infected with FCV-F9 and mock infected at 13 h p.i.. FCV capsid staining was performed using an anti-FCV primary antibody, visualised using an Alexa Fluor 488 conjugated secondary antibody and is coloured green. Tubulin staining was performed using a mouse monoclonal anti-α-tubulin primary antibody, visualised using an Alexa Fluor 633 conjugated secondary anti-mouse IgG antibody and is coloured red.

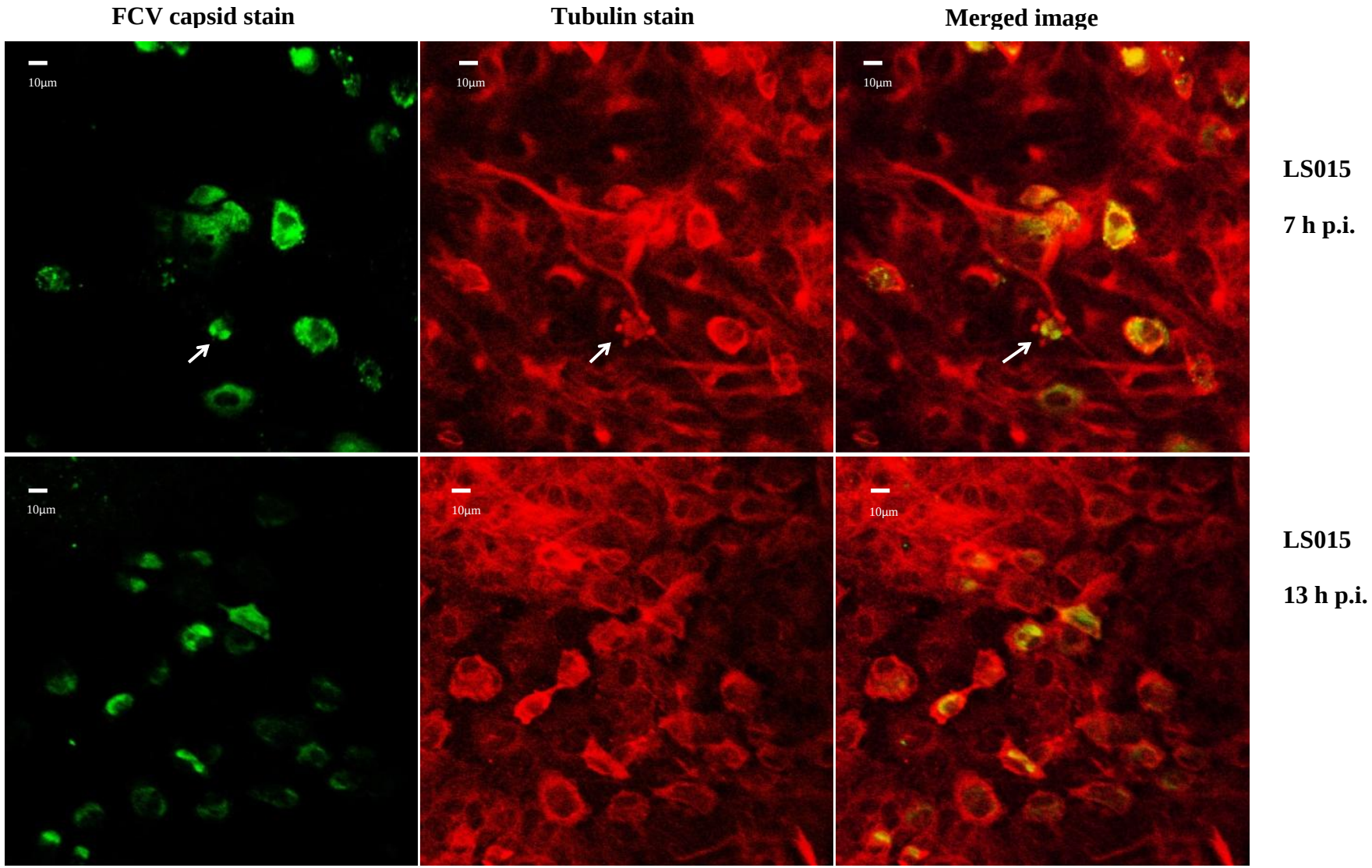

Figure 4.3. Tubulin stained FEA cells infected with LS015 at 7 and 13 h p.i.. FCV capsid staining was performed using an anti-FCV primary antibody, visualised using an Alexa Fluor 488 conjugated secondary antibody and is coloured green. Tubulin staining was performed using a mouse monoclonal anti-α-tubulin primary antibody, visualised using an Alexa Fluor 633 conjugated secondary anti-mouse IgG antibody and is coloured red. White arrows indicate cells showing signs of blebbing structures

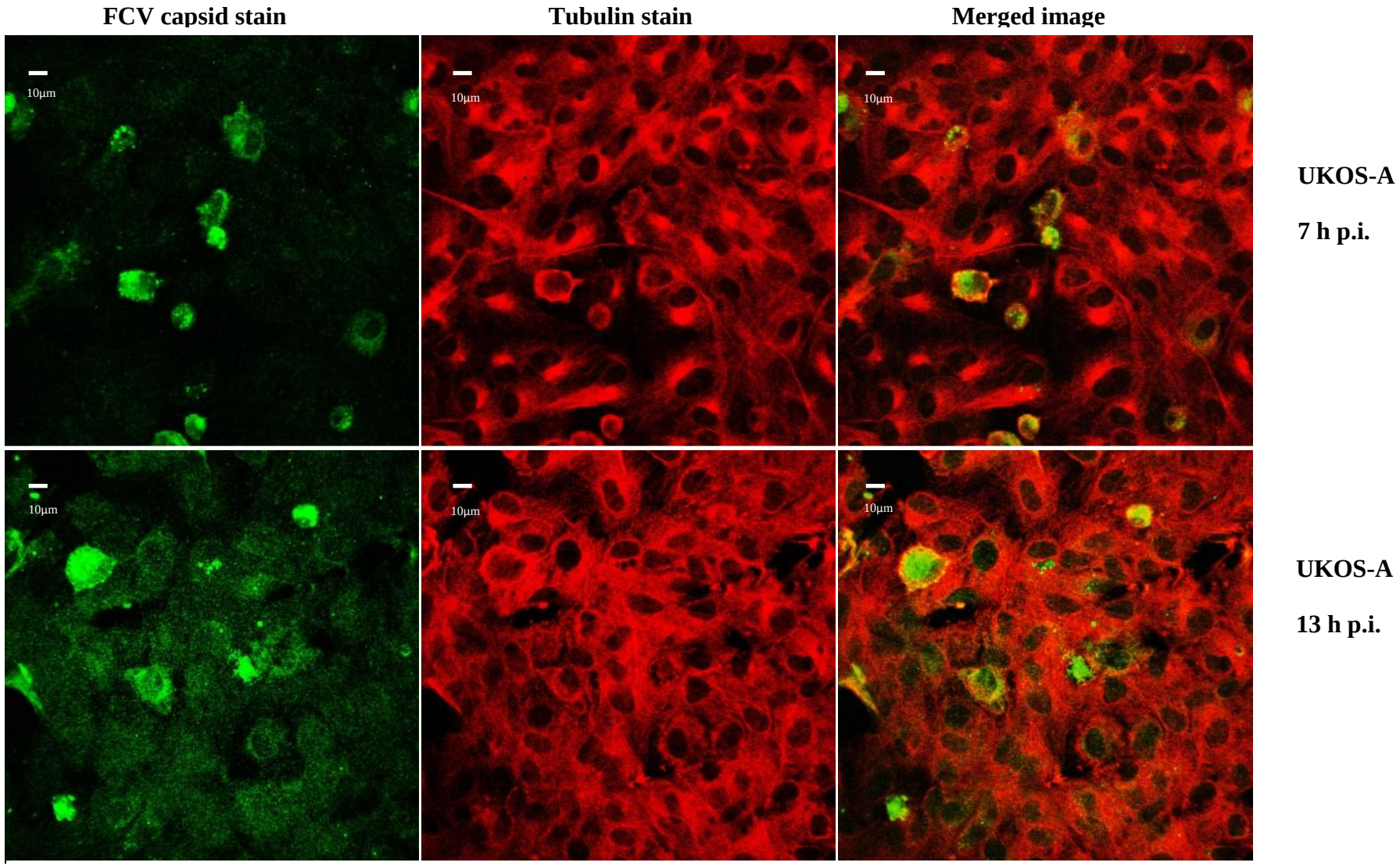

Figure 4.4. Tubulin stained FEA cells infected with UKOS-A at 7 and 13 h p.i.. FCV capsid staining was performed using an anti-FCV primary antibody, visualised using an Alexa Fluor 488 conjugated secondary antibody and is coloured green. Tubulin staining was performed using a mouse monoclonal anti-α-tubulin primary antibody, visualised using an Alexa Fluor 633 conjugated secondary anti-mouse IgG antibody and is coloured red.

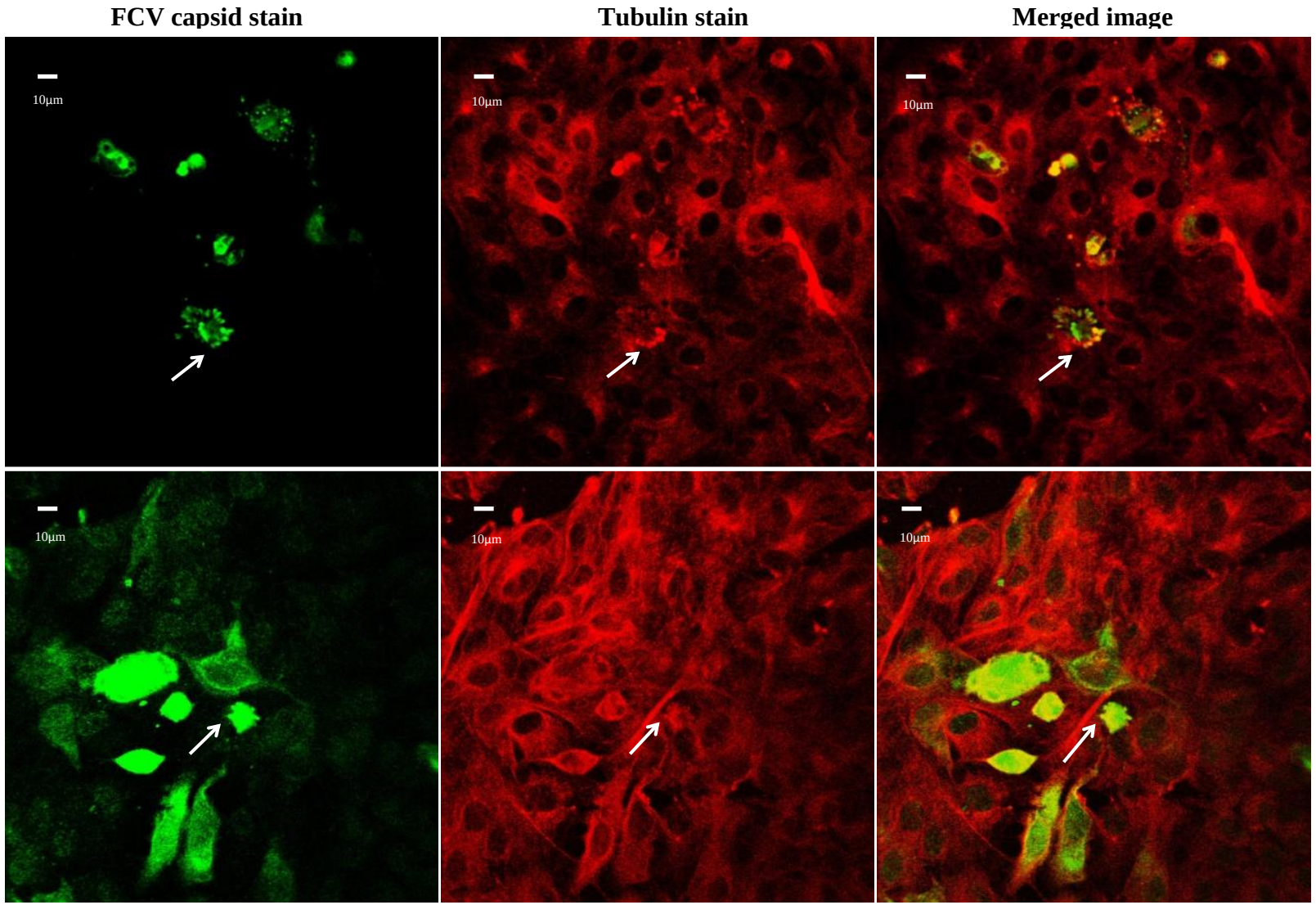

Figure 4.5. Tubulin stained FEA cells infected with R591 at 7 and 13 h p.i.. FCV capsid staining was performed using an anti-FCV primary antibody, visualised using an Alexa Fluor 488 conjugated secondary antibody and is coloured green. Tubulin staining was performed using a mouse monoclonal anti-α-tubulin primary antibody, visualised using an Alexa Fluor 633 conjugated secondary anti-mouse IgG antibody and is coloured red. White arrows indicate cells showing signs of blebbing structures

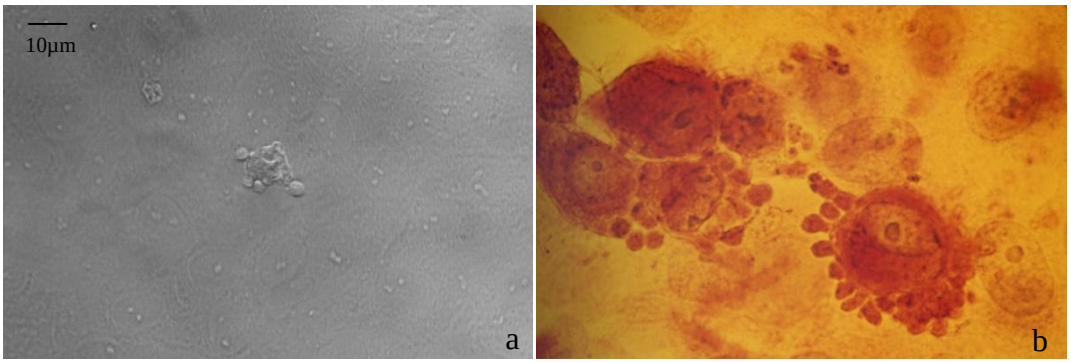

Figure 4.6. Evidence of cellular blebbing during infection with FCV. Image a. is a cell showing FEA cell blebbing as a result of infection with strain R591 taken with light microscope during this thesis. Image b. is taken from Knowles (1988), FEA cells are infected with FCV strain A4 and stained with peroxidise anti-peroxidase (PAP). Magnification is x~7100

To determine whether any of the changes observed in the infected cells are consistent for each infected cell, the intensity of fluorescence along a 20 µm line was calculated (full results Appendix III). Unfortunately in the case of the tubulin stained samples DAPI stained pictures were unobtainable due to technical difficulties so the line was drawn from the centre of an infected cell into the centre of an uninfected cell.

The graphs created from each of the infected samples and a mock infected control can be seen in Figure 4.7. In the mock infected controls (Fig. 4.7i and j) the pattern of fluorescence in both the 7 and 13 h p.i. samples is similar with tubulin fluorescence peaking towards the middle of the line drawn suggesting that tubulin staining was greatest at the cell periphery. In both cases the pattern was symmetrical around this cellular border suggesting as expected, that patterns of tubulin expression were similar in both cells. Within the FCV-F9 infected cells (Fig. 4.7a and b) the tubulin fluorescence peaks are found alongside FCV capsid staining peaks showing that the intensity of tubulin staining increases in the cell expressing FCV-F9 capsid proteins. This pattern is mirrored in the LS015 infected samples (Fig. 4.7c and d) at both 7 and 13 h p.i. with the intensity of tubulin staining being almost twice as high in the cells expressing FCV compared to the uninfected cells. In the UKOS-A infected cells (Fig. 4.7e and f), the pattern is slightly different. At 7 h p.i. (Fig. 4.7e) the tubulin fluorescence intensity once again peaks with FCV capsid protein

expression but at 13 h p.i. the pattern is less defined and the peak tubulin fluorescence intensity actually occurs after the FCV capsid expression has dropped suggesting that any effect the virus was having upon the tubulin proteins within the cell was not being exhibited at 13 h p.i.. In Figure 4.7g and h, R591 appears to act in a similar way to the UKOS-A strain, at 7 h p.i. (Fig. 4.7g) the tubulin staining intensity peaks with viral capsid staining whereas at 13 h p.i. (Fig. 4.7h) the fluorescence pattern of the tubulin staining does not show a peak alongside FCV capsid expression.

To determine whether or not the trends observed within the graphs were statistically significant, Mann-Whitney U tests were performed (Table 4.1). The test specifically looked at the median grey scale value along the line from 0-10 μm (infected cells) vs. the median grey scale value along the line from 10.1-20 μm (uninfected cells). The greyscale values from the mock infected cells were also tested. Full results can be found in Appendix V.

Table 4.1. Table showing p-value results of Mann-Whitney U tests on the median values from tubulin staining of infected and uninfected FEA cells for each strain and time point. Also shown is the percentage increase/decrease of the median value from the infected cells.

Viral strain	Time point (hrs p.i.)	p-value	Change in median expression in infected cells
FCV-F9	7	0.0002	29% increase
FCV-F9	13	<0.0001	48% increase
LS015	7	<0.0001	53% increase
LS015	13	<0.0001	99% increase
UKOS-A	7	<0.0001	27% increase
UKOS-A	13	<0.0001	32% increase
R591	7	<0.0001	48% increase
R591	13	<0.0001	26% increase
Mock	7	0.3911	5% increase
Mock	13	0.0012	17% decrease

Results showed that all viral strains at both time points tested had significantly increased tubulin within the infected cells when compared to the uninfected cells ($p \leq 0.01$). In the Mann-Whitney U tests of the mock infected cells, the comparison made at 7 h p.i. came back as not significant as it had a p-value of 0.39, however, the comparison made at 13 h p.i. did come back as significant at $p=0.0012$. This result may be a reflection of the boundary drawn between the two cells, as there was no DAPI stain available it was difficult to know whether the boundary was a good estimation of the cell-cell junction. This was less of a problem within the infected cells as the disappearance of FCV capsid staining could be used as a guide to the cellular boundaries.

Within the virally infected cell comparisons the largest increase in tubulin staining intensity was found in cells infected with LS015 at 13 h p.i. with the amount of tubulin staining almost doubling within the infected cells. Most of the viruses caused the greatest increase in tubulin staining at 13 h p.i. but strain R591 had the greatest effect on tubulin at 7 h p.i.. Strain R591 also had the least pronounced effect overall at 13 h p.i..

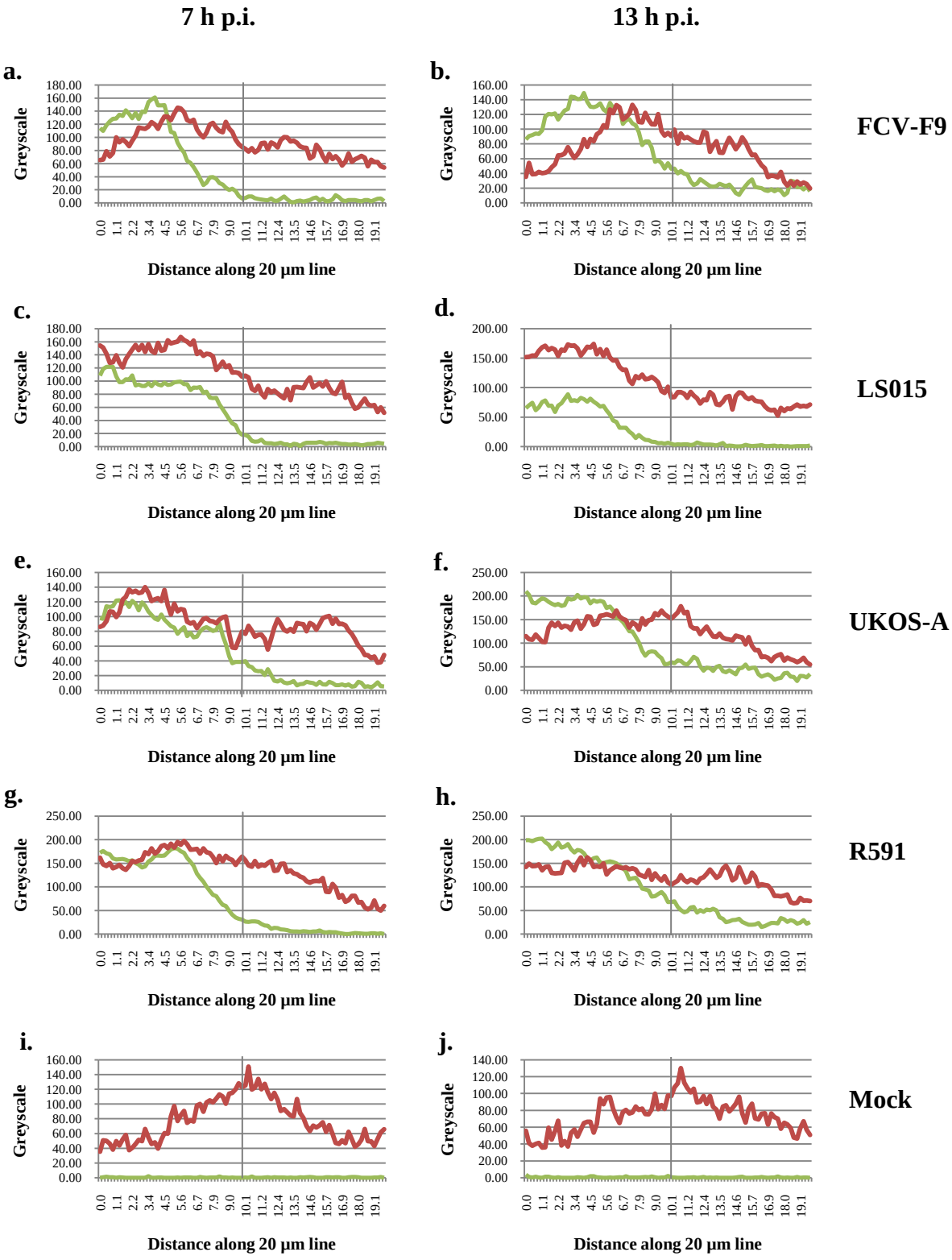

Figure 4.7. Graphs showing average tubulin and FCV capsid protein expression along a 20 µm line drawn from the centre of an infected FEA cell into the centre of an uninfected FEA cell. Tubulin expression is coloured red, FCV capsid protein expression is coloured green. Graphs a, c, e, g and i were all from samples at 7 h p.i. and graphs b, d, f, h and j were from 13 h p.i.. Graphs a and b were infected with FCV-F9, c and d were infected with LS015, graphs e and f were infected with UKOS-A, graphs g and h were infected with R591 and graphs i and j show mock infected samples. The vertical line defines the boundary between two cells.

4.3.3 Vimentin staining

To assess the amount of vimentin remodelling occurring as a result of infection with four different strains of FCV, host cell vimentin proteins were stained and confocal microscope images captured. Figure 4.8 shows vimentin staining in mock infected cells at 7 and 13 h p.i.. The cells show signs of typical vimentin staining (Armer *et al.*, 2008) with vimentin forming a ring around the nucleus and being more disperse in the remainder of the cytosol.

Figures 4.9-4.12 show examples of the images taken of infected cells with FCV capsid protein staining in green, vimentin protein staining in red and DAPI nuclear staining in blue. In each of the images, the cells expressing FCV capsid protein from each of the strains appear to also show an increased fluorescence pattern from the vimentin staining. Again, as observed with some of the infected tubulin stained cells, there are signs of blebbing within the cells infected with strain R591 (Fig. 4.12) except in this case the blebbing appears to have continued to 13 h p.i. with viral antigen appearing stained within the blebs again.

Mock 7 h p.i. **Mock 13 h p.i.**

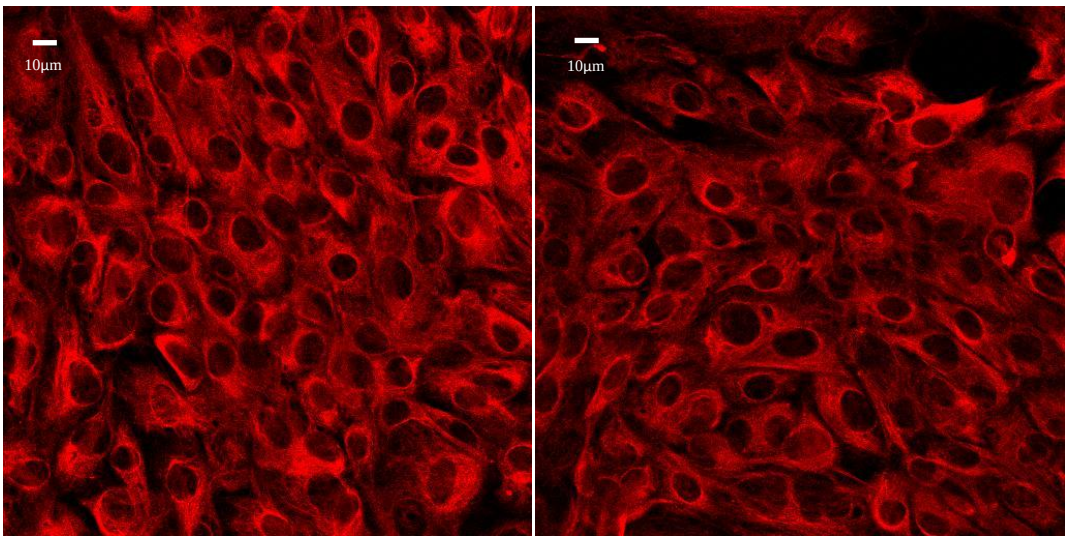

Figure 4.8. Images showing mock infected FEA cells used as controls stained for vimentin using a primary mouse monoclonal anti-vimentin antibody which was visualised using a secondary anti-mouse IgM antibody conjugated with Alexa Fluor 633 at 7 and 13 h p.i.. Vimentin protein staining is coloured red.

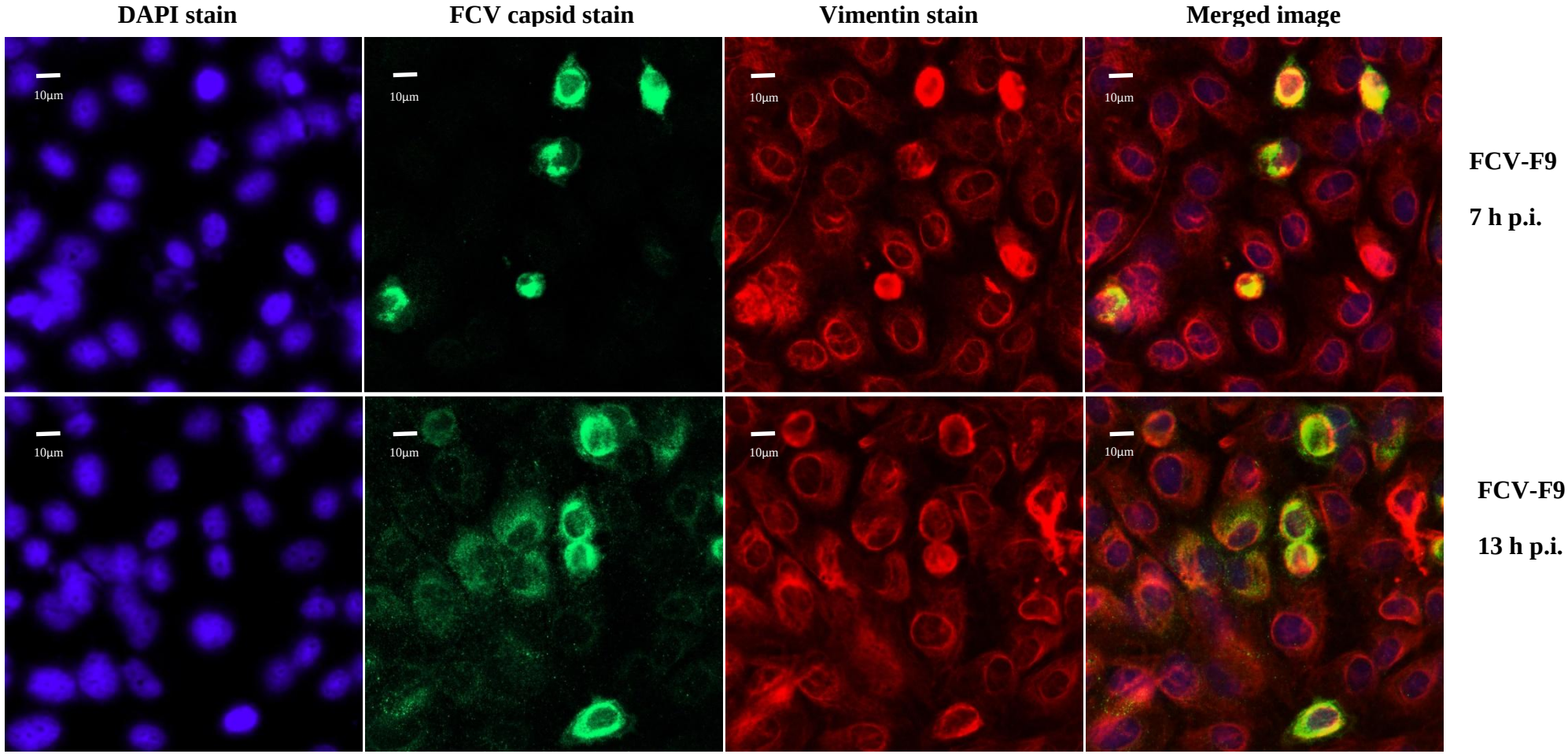

Figure 4.9. Vimentin stained FEA cells infected with FCV-F9 at 7 and 13 h p.i.. FCV capsid staining was performed using an anti-FCV primary antibody, visualised using an Alexa Fluor 488 conjugated secondary antibody and is coloured green. Vimentin staining was performed using a mouse monoclonal anti-vimentin primary antibody, visualised using an Alexa Fluor 633 conjugated secondary anti-mouse IgM antibody and is coloured red. DAPI nuclear stain is coloured blue.

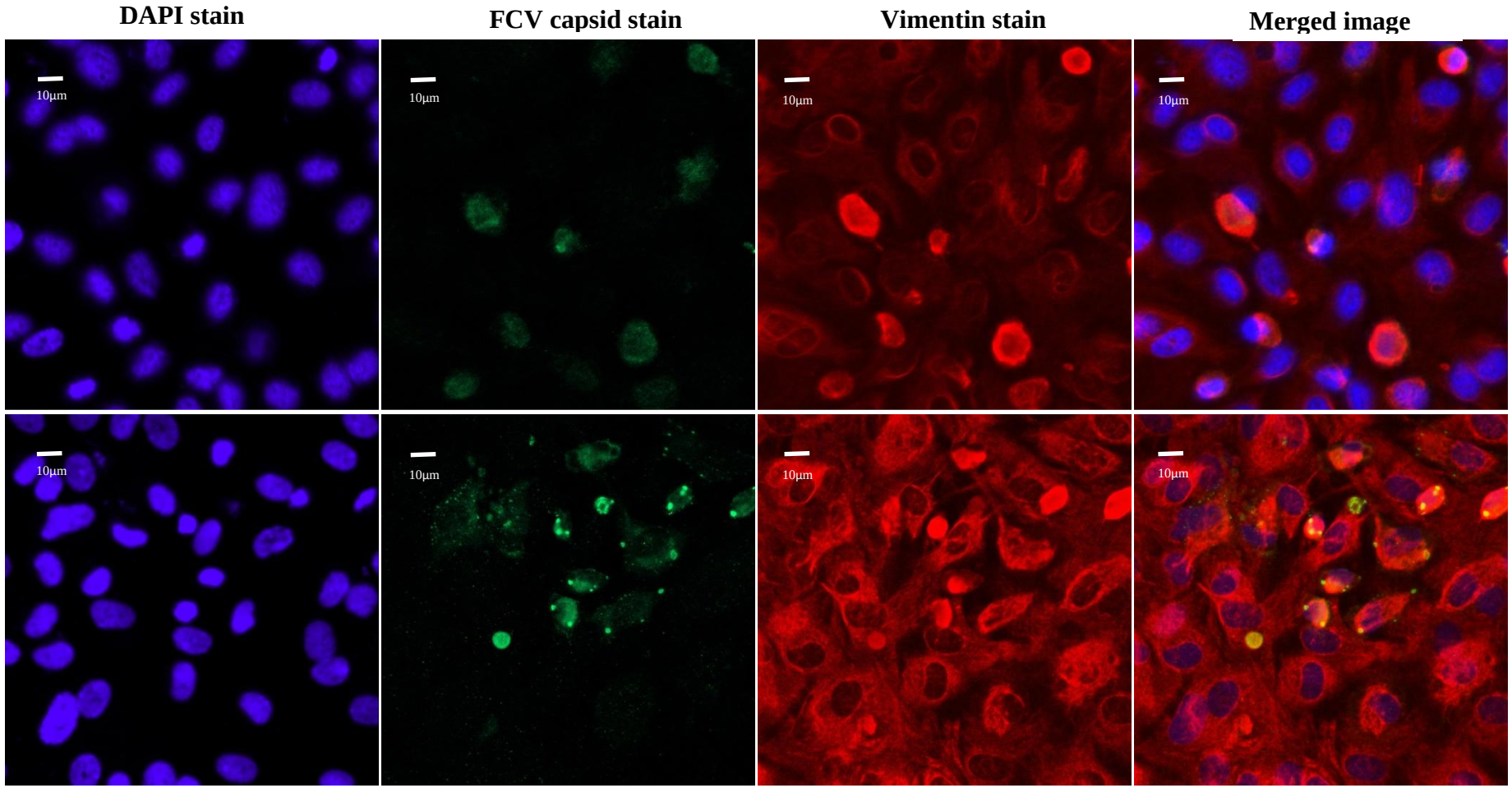

Figure 4.10. Vimentin stained FEA cells infected with LS015 at 7 and 13 h p.i.. FCV capsid staining was performed using an anti-FCV primary antibody, visualised using an Alexa Fluor 488 conjugated secondary antibody and is coloured green. Vimentin staining was performed using a mouse monoclonal anti-vimentin primary antibody, visualised using an Alexa Fluor 633 conjugated secondary anti-mouse IgM antibody and is coloured red. DAPI nuclear stain is coloured blue.

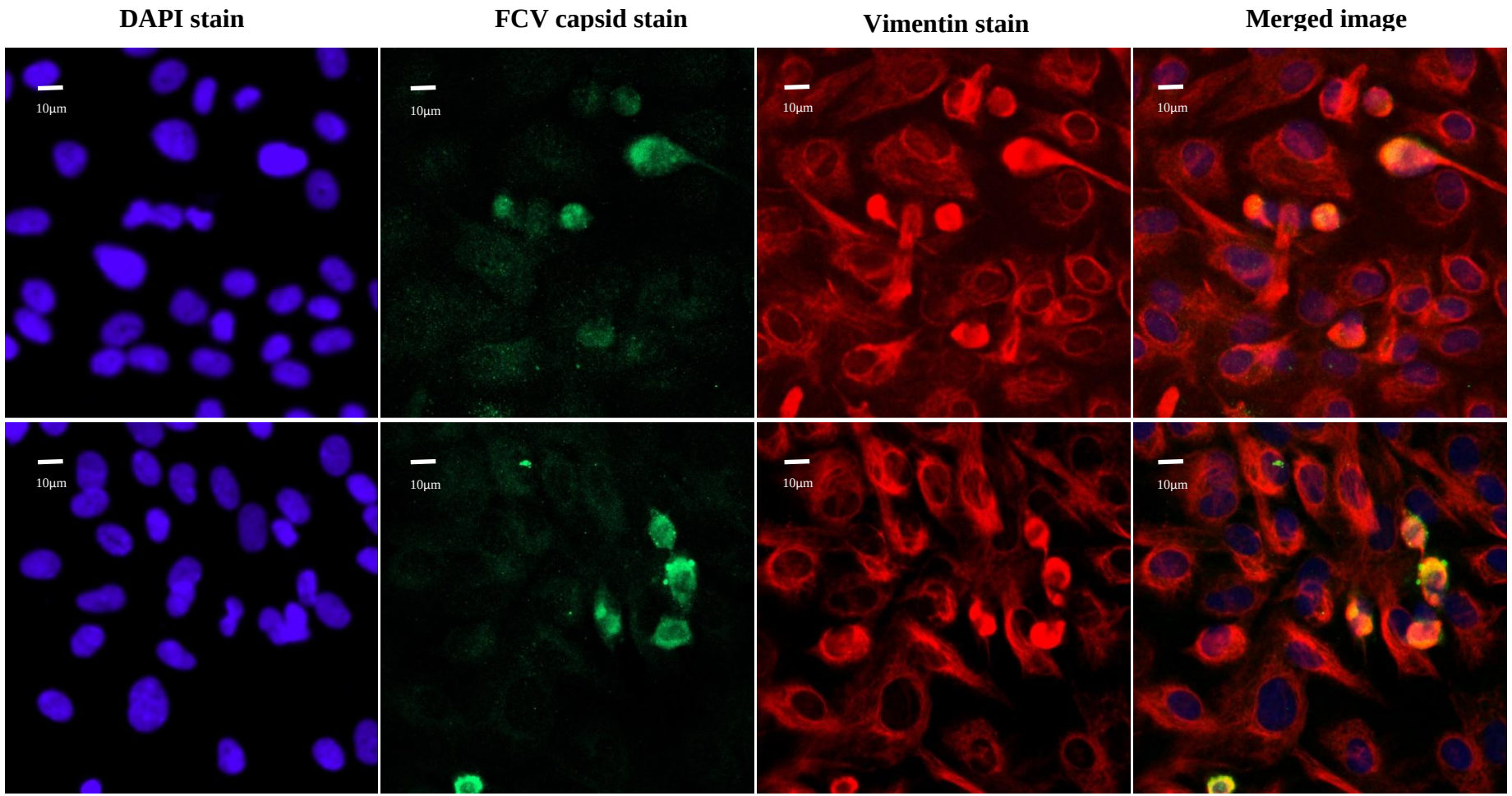

Figure 4.11. Vimentin stained FEA cells infected with UKOS-A at 7 and 13 h p.i.. FCV capsid staining was performed using an anti-FCV primary antibody, visualised using an Alexa Fluor 488 conjugated secondary antibody and is coloured green. Vimentin staining was performed using a mouse monoclonal anti-vimentin primary antibody, visualised using an Alexa Fluor 633 conjugated secondary anti-mouse IgM antibody and is coloured red. DAPI nuclear stain is coloured blue.

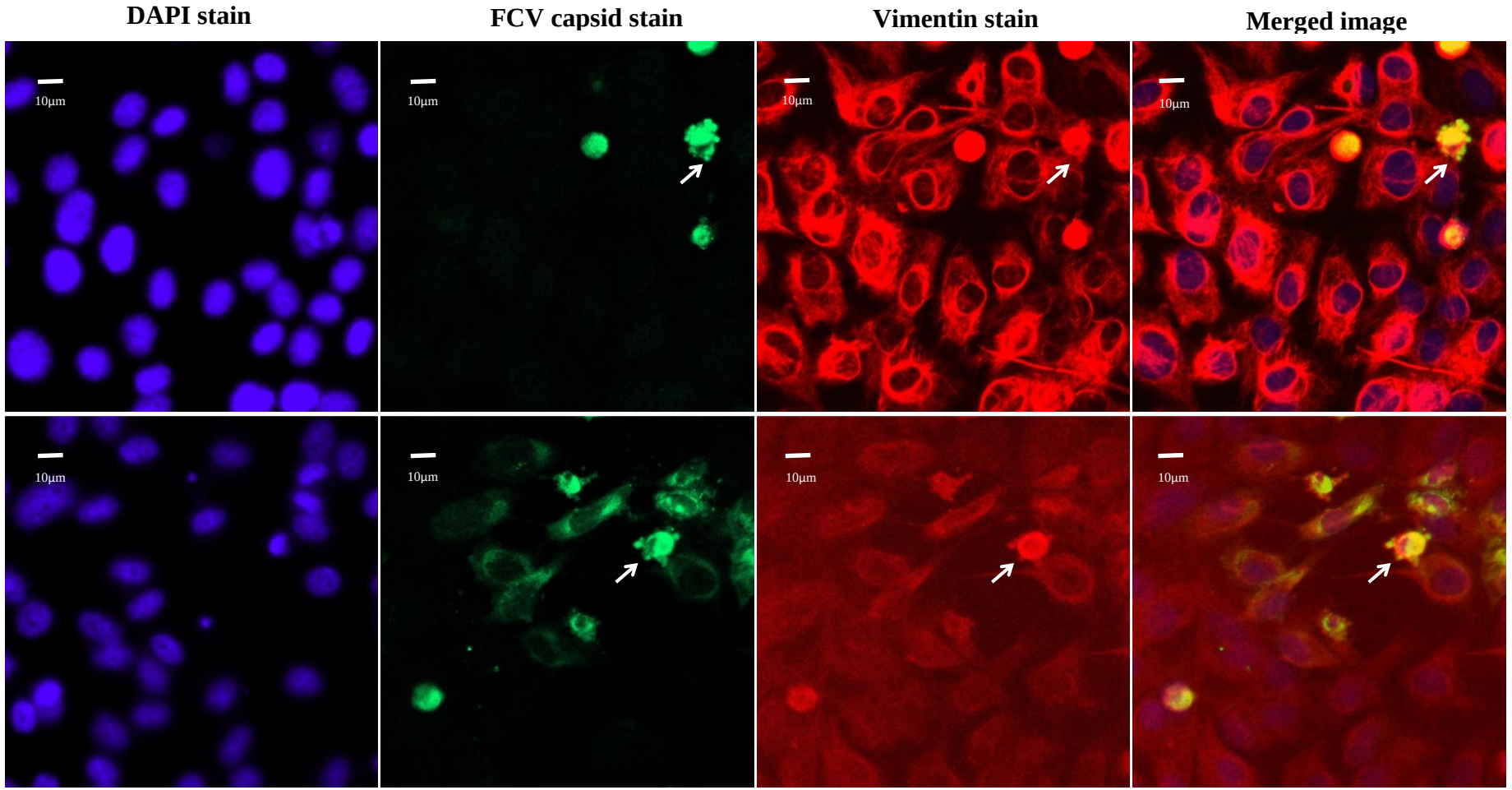

Figure 4.12. Vimentin stained FEA cells infected with FCV-F9 at 7 and 13 h p.i.. FCV capsid staining was performed using an anti-FCV primary antibody, visualised using an Alexa Fluor 488 conjugated secondary antibody and is coloured green. Vimentin staining was performed using a mouse monoclonal anti-vimentin primary antibody, visualised using an Alexa Fluor 633 conjugated secondary anti-mouse IgM antibody and is coloured red. DAPI nuclear stain is coloured blue. White arrows indicate cells showing signs of blebbing structures.

Again, an analysis of fluorescence along a 20 μm line was performed except as DAPI stained images were available the line was drawn from the nucleus of an infected cell to the nucleus of an uninfected cell (full results see Appendix IV). The graphs produced from this analysis are shown in Figure 4.13. The mock infected controls (Fig. 4.13i and j) show a similar pattern of expression for vimentin staining in both the cells fixed at 7 h p.i. and the cells fixed at 13 h p.i., from nucleus to nucleus the expression is constant except for a small peak in the area between the nuclei towards the cell periphery at 7 h p.i. (Fig. 4.13i). In the FCV-F9 infected cells (Fig. 4.13a and b), the pattern of the intensity of vimentin staining peaks in the infected cells at both time points examined although the peak intensity in the cells fixed at 13 h p.i. is much lower than at 7 h p.i.. The pattern is similar in the cells infected with strain R591 (Fig. 4.13g and h) with a larger difference in peak intensity being visible at 7 h p.i. compared to 13 h p.i.. The LS015 and UKOS-A infections gave the most consistent peak intensities for vimentin staining at 7 and 13 h p.i. (Fig. 4.13c-f) with the peak intensities in the cells expressing FCV capsid protein roughly double that of the cells not expressing capsid.

Again, Mann-Whitney U statistical analysis was performed upon the grey scale values from the vimentin staining in infected cells (values from 0-10 μm) compared to the uninfected cells (values from 10.1-20 μm) (Table 4.2). Full results can be found in Appendix V.

Table 4.2. Table showing p-value results of Mann-Whitney U tests on the median values from the vimentin staining in infected and uninfected FEA cells for each strain and time point. Also shown is the percentage increase/decrease of the median value from the infected cells.

Viral strain	Time point (hrs p.i.)	p-value	Change in median expression in infected cells
FCV-F9	7	<0.0001	38% increase
FCV-F9	13	<0.0001	28% increase
LS015	7	<0.0001	93% increase
LS015	13	<0.0001	26% increase
UKOS-A	7	<0.0001	52% increase
UKOS-A	13	<0.0001	102% increase
R591	7	<0.0001	56% increase
R591	13	<0.0001	73% increase
Mock	7	>0.05	1% decrease
Mock	13	0.2599	1% increase

The results showed that for each strain and for both time points the results showed that vimentin was significantly altered within the infected cells when compared to the uninfected cells. The most pronounced alteration is vimentin staining is found in response to infection with the UKOS-A strain at 13 h p.i. with the intensity of staining doubling within infected cells. Response to infection with LS015 produced the smallest increase in vimentin staining at 13 h p.i., showing only a 26% increase.

Within the mock infected samples, there was no significance observed at either time point ($p>0.05$) and the levels of vimentin staining were within 1% of each other. This suggests that the cut-off for the cell boundary was correctly defined within this experiment and the trends observed with the DAPI staining reaffirm this (Fig. 4.13).

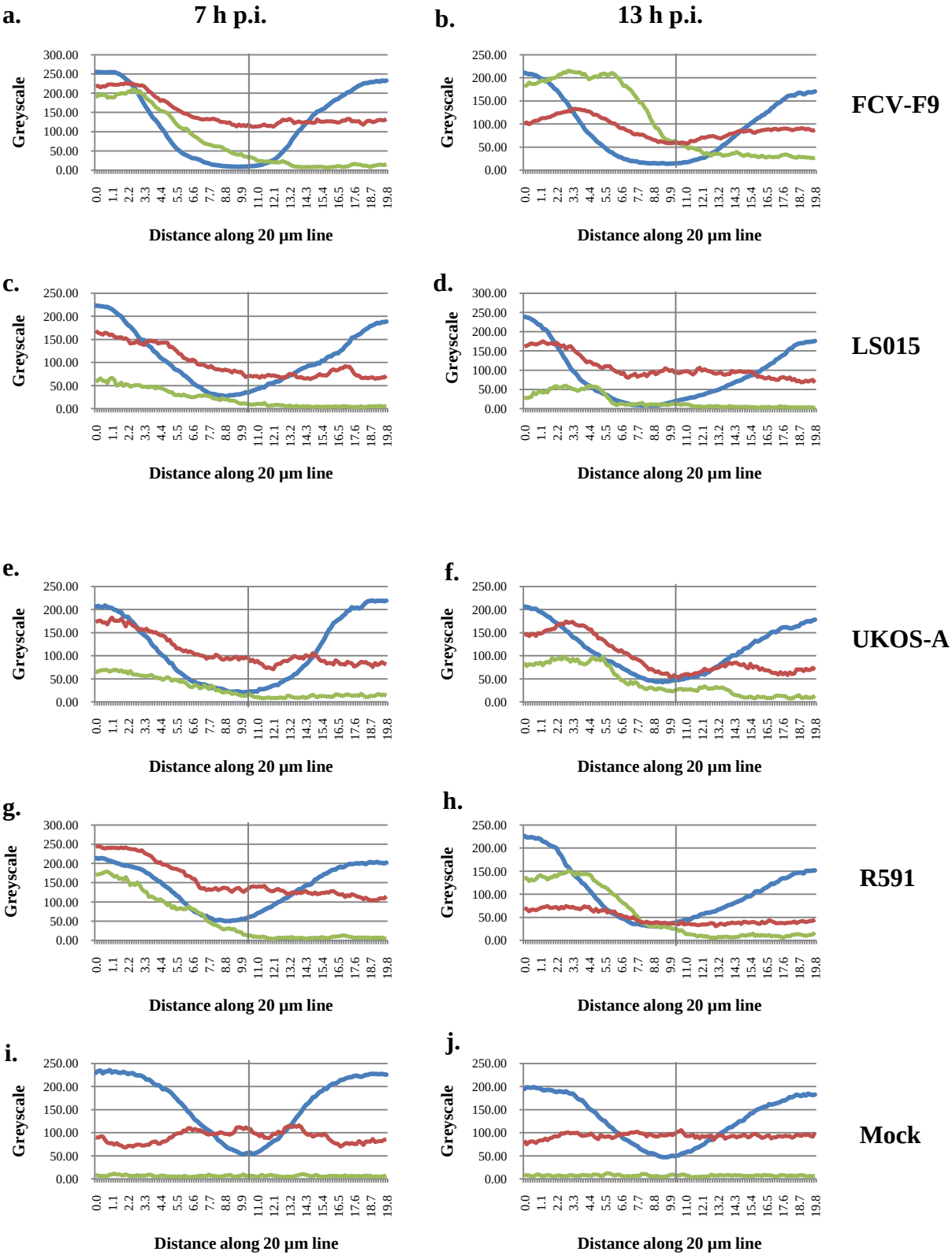

Figure 4.13. Graphs showing average vimentin, FCV capsid protein and DAPI expression along a 20 µm line drawn from the centre of an infected FEA cell into the centre of an uninfected FEA cell. Vimentin expression is coloured red, FCV capsid protein expression is coloured green and DAPI strain is coloured blue. Graphs a, c, e, g and i were all from samples at 7 h p.i. and graphs b, d, f, h and j were from 13 h p.i.. Graphs a and b were infected with FCV-F9, c and d were infected with LS015, graphs e and f were infected with UKOS-A, graphs g and h were infected with R591 and graphs i and j show mock infected samples. The vertical line defines the boundary between two cells.

4.4 Discussion

The aim of this chapter was to discover whether the modulation of cytoskeletal proteins found within the 2D-DIGE experiments could be visualised and confirmed at the cellular level within individual FCV-infected cells.

Within infected cells, increases in vimentin and tubulin staining were seen in cells infected with each strain of FCV (Figs. 4.1-4.5 and 4.9-4.12). The use of microtubules and intermediate filaments in viral movement around the cell has been documented for a number of viruses such as hepatitis C virus (Roohvand *et al.*, 2009) and dengue virus (Chen *et al.*, 2008).

Not all viruses use these proteins in the same manner and differences have even been observed within viral families. Within the *Picornaviridae*, foot-and-mouth disease virus (FMDV) and bovine enteric virus (BEV) have been shown to use microtubules and intermediate filaments in opposing manners (Armer *et al.*, 2008). FMDV disrupts the tethering of microtubules, made up from the polymerisation of tubulin, to the microtubule organising centre but BEV does not. There were also differences found in the alteration of vimentin expression within the cell, FMDV was shown to draw vimentin around the site of viral replication whereas BEV proteins co-localise with vimentin at the site of replication. There were some differences observed in the degree of vimentin and tubulin increase in response to the different FCV strains. Strain R591 was the only viral strain not to cause the greatest increase in tubulin staining in the latter stages of infection (Table 4.1) and this may be indicative of a different mode of viral egress for this strain which is not as dependent on wholesale changes in tubulin expression in the latter stages of infection. The pattern of vimentin staining is even more varied in response to infection with each of the four strains with both LS015 and UKOS-A having the greatest effect upon expression but at different time points. LS015 appears to induce a large increase in vimentin expression relatively early in infection (7 h p.i.) whereas the cells infected with the UKOS-A strain express large amounts of vimentin towards the end of infection which may mean that UKOS-A needs vimentin to aid viral exit.

Also of interest from this study are the blebbing structures observed in Figures 4.1, 4.3, 4.5, 4.6 and 4.11. Blebbing is often taken to be indicative of apoptosis (Bovellan *et al.*, 2010) and may therefore perhaps be used to support the findings of others that

suggest FCV itself induces apoptosis (Al-Molawi *et al.*, 2003; Natoni *et al.*, 2006). No evidence of apoptotic proteins were found during the 2D-DIGE studies but there were modulations found at the transcriptional level and these will be demonstrated in chapter 5.

It is not certain that the blebs observed in this experiment are definitely a consequence of apoptosis as apoptotic blebs are often only present for minutes at a time which would make capturing them using fixed cells difficult and they are characterised by a lack of cytoskeletal protein involvement (Charras, 2008) whereas in the images captured in this experiment tubulin and vimentin are often present within the blebs. Also present within the blebs themselves during infection with R591 are viral capsid proteins which may prove that rather than being a by-product of apoptosis, the blebs are protrusions used by this strain of FCV to aid viral egress and promote cell-to-cell transmission in a similar manner to vaccinia virus infection (Carter *et al.*, 2003; Cudmore *et al.*, 1995).

Neither of these hypotheses can be confirmed or discarded using the data obtained in this chapter. Further analysis upon FCV infected cells will have to be performed. Ideally this would be carried out using live cell imaging to fully track the virus within the cell and analyse viral-host protein interactions within a series of images from the same live cells. To make this possible there is now an infectious clone of FCV available that expresses fluorescent proteins, thereby allowing the virus to be visualised during live cell imaging (Abente *et al.*, 2010). If this clone could be combined with a cell line which expresses fluorescent proteins then studies could be performed which are similar to experiments already carried out with vaccinia virus (Mercer & Helenius, 2008) allowing closer inspection of the interactions between the virus and the host cytoskeletal proteins. However, the availability of a cell line that is able to express fluorescently labelled proteins and is able to be infected by the FCV clone may be a problem for the foreseeable future as currently FCV strains are only culturable in feline cell lines and most fluorescent proteins have only been expressed in human and mouse models.

An experiment that may be able to be performed with more ease and deliver results quicker is one that utilises flow cytometry to examine whether host cytoskeletal changes occur before or after the start of apoptosis. Flow cytometry has already been used to investigate caspase-3 activation and induction of apoptosis during FCV

infection (Natoni *et al.*, 2006) and if the changes seen in the cytoskeletal proteins during infection could be quantified by flow cytometry then the effects of infection on both these sets of proteins could be examined simultaneously.

All of the cells infected with all strains used in this experiment showed increases in the expression of both cytoskeletal proteins examined which indicates that these cytoskeletal changes are important for every strain of FCV examined. However, UKOS-A was the only strain not to show any signs of inducing blebbing within these cells. This difference found in the UKOS-A infected cells may simply be an artefact of timing, if the blebs are transient then the cells may have been fixed at the wrong time, or it may be indicative of a different mode of action for this putative hypervirulent strain. This difference also mirrors the results of the 2D-DIGE analysis (chapter 3) upon these four strains of FCV with cells infected by UKOS-A being found to have a number of proteins modulated in a different manner to cells infected with the other three virus strains. Both of these experiments have shown that closer examination of the UKOS-A strain is warranted, ideally alongside a hypervirulent strain of FCV that has been used to recreate VSD experimentally to discover whether any of these differences are consistent for hypervirulent strains of FCV.

Unfortunately images could only be satisfactorily obtained for two of the three proteins targeted; the staining of FEA cells with phalloidin to visualised cellular actin was unsuccessful. Phalloidin was used as a toxin which binds preferentially to F-actin within the cell and in this case was conjugated to a fluorescent stain, however, the staining observed in this experiment was not specific and one reason for this may be due to the use of a feline cell line. Although actin is generally considered to be a conserved protein within eukaryotes there may have been differences in the phalloidin binding site present in the cell line used and so specific staining could not be performed. To circumvent this problem in future studies, other types of staining will have to be considered such as using other brands of phalloidin or using a specific anti-actin primary antibody that has been raised against the actin proteins found in the cell cultures studied. Secondary staining with a fluorescent antibody could then be performed in the same manner as with the tubulin and vimentin staining in this experiment.

Overall, the data collected within this chapter has shown that the modulations of the cytoskeletal proteins found within the two 2D-DIGE experiments were confirmed at

the cellular level by direct cell imaging using immunofluorescent confocal microscopy. Both vimentin and tubulin expression were significantly increased in cells infected with all strains of FCV although there were no real differences found between each FCV strain examined which may prove that the alteration of the host cytoskeleton is an essential part of FCV virion replication.

5 Chapter five

Investigation of host gene transcript changes as a result of infection with FCV-F9 using RNA-seq

5.1 Introduction

In the previous chapters, changes in the cellular proteome in response to infection with FCV have been studied whereas in this chapter the focus will be upon the changes in gene transcription levels.

At time of writing there have been no attempts made to discover the effects of FCV infection upon global cellular transcription; however, one study has been successful in examining cells infected with a norovirus replicon system with a microarray (Chang, 2009). It was discovered that genes in cholesterol and carbohydrate metabolic pathways were significantly modulated and when these pathways were disrupted experimentally the levels of replication of the norovirus replicon reduced significantly. As discussed previously (chapter 1) there are limitations with using a microarray system especially as the probes used to interrogate transcripts are user defined and with using a non-model system such as the feline genome, designing these probes may be problematic and novel genes would be overlooked completely.

Real-time PCR has also been employed to target the host cytokine response to infection with VS-FCV (Foley *et al.*, 2006). They used the skin lesions formed during infection with VS-FCV and targeted 9 host cytokines and found that on average, 3.8 were significantly elevated in the tissue infected with VS-FCV. Again, this is a limited method of investigation as only a few gene transcripts can be targeted at a time during each experiment and novel genes will be overlooked.

To overcome these limitations with microarray and real-time PCR analysis the decision was made to employ next-generation sequencing technologies to investigate gene transcript changes as a result of infection with FCV. These next-generation sequencers are still a very new technology and as such there are only a few studies in which they have been used to interrogate the whole transcriptome and only one example of this technology being used to investigate the transcriptional changes as a

result of viral infection (Woodhouse *et al.*, 2010). Other viral studies using next-generation technologies have focussed upon the virus itself and have used the sequences obtained to reveal viral transcript boundaries and novel transcripts (Legendre *et al.*, 2010) and also to find novel splice sites (Lin *et al.*, 2010).

In this chapter, next generation sequencers were employed to interrogate the transcriptome of samples in a technique known as RNA-seq. The transcriptome of FEA cells infected with FCV-F9 was sequenced by SOLiD sequencing at 4 and 7 h p.i. along with mock infected counterparts. By sequencing the transcriptome of infected and mock infected cells, comparisons can be made between the samples and genes which are differentially transcribed as a result of infection with FCV. The experimental design included two biological replicates of each condition to allow for natural variance between samples to be normalised, however, the decision was made not to include any technical replicates within the experiment as there have been previous studies performed showing that the techniques used in RNA-seq are highly reproducible and that technical replicates are largely unnecessary (Marioni *et al.*, 2008). The results obtained from RNA-seq were then compared to the modulated proteins identified from the 2D-DIGE experiment performed upon FCV-F9 in chapter 2. This was performed to discover whether any correlation between the two data sets existed or whether this experiment would follow the pattern of others performed using microarrays and proteomics and show poor correlation between the differentially transcribed genes and proteins (Barros *et al.*, 2010).

5.2 Materials and methods

5.2.1 Viral infection

FEA cells (passage 45) were infected with FCV-F9 (Bittle & Rubic, 1976; Bittle, 1960) at an m.o.i. 10. The virus was added in a 1 ml solution of MM and incubated at 37°C for 1 h. The flasks were then washed three times with PBS and re-fed with 20 ml MM. The infections were then stopped either 4 or 7 hours post infection by freezing at -80°C. Mock infected flasks were created by seeding with 1 ml MM instead of virus solution and treated in the same way as their infected counterparts.

Cell pellets were created by scraping the monolayer and spinning the supernatant at 2000 × *g* for 10 min.

5.2.2 RNA isolation

RNA was isolated from the infected and mock infected cell pellets using a Purelink RNA mini kit (Invitrogen 12183018A) following the manufacturers protocol.

This involved preparing fresh lysis buffer by adding 20 µl of 2 M DTT per ml of the lysis buffer included in the kit. 0.6 ml of the freshly prepared lysis buffer was added to each cell pellet and vortexed at high speed until the cell pellet is completely dispersed. The cells were then homogenised at room temperature using a pellet pestle to ensure that the cells were completely lysed. 0.6 ml of 70% ethanol was then added to each cell lysate and vortexed at high speed to disperse any precipitate that forms as a result of the ethanol addition. Up to 700 µl of sample at a time is added to the spin cartridge included in the kit and is then centrifuged at 12 000 × *g* for 15 s with the flow through being discarded. This is repeated until all of the lysate has been passed over the spin column. 700 µl of wash buffer I is then added to each spin cartridge and centrifuged at 12 000 × *g* for 15 s. The flow through is once again discarded and the spin column placed into a clean collection tube for the next step. Wash buffer II has 96-100% ethanol added at first use and 500 µl of this is passed through the spin column by centrifuging at 12 000 × *g* for 15 s discarding the flow through once centrifugation is completed and repeating the second wash once more. The membrane with the attached RNA is then dried thoroughly by centrifuging the

spin column at 12 000 × *g* for 2 min before the collection tube is discarded and the column is inserted into a clean recovery tube. 30 µl of RNase-free water was then added to the centre of the spin cartridge and incubated at room temperature for 1 min. The spin cartridge is then spun at 15 000 × *g* for 2 min to elute the RNA from the membrane into the recovery tube. At this stage the extracted RNA is either kept on ice to be used immediately or stored at -80˚C for longer term storage.

5.2.3 rRNA depletion

As the most abundant RNA in the cell is ribosomal RNA this must be depleted to allow other RNA to be found and analysed by RNA-seq. The rRNA was depleted in this experiment using the Ribominus Eukaryote Kit for RNA-seq (Invitrogen A10837-08).

2-10 µg of extracted RNA in a volume of less than 20 µl was combined with 10 µl of Ribominus probe and 300 µl of hybridisation buffer in a sterile, RNase-free 1.5 ml tube. The samples were then incubated at 75˚C for 5 min to denature the RNA and then cooled slowly over 30 min to a temperature of 37˚C to promote sequence specific hybridisation. Magnetic beads were prepared by washing them several times before resuspending in hybridisation buffer. The cooled samples are then added to the prepared beads and incubated at 37˚C for 15 min. The tubes were then placed on a magnetic separator to pellet the rRNA-probe complex attached to the magnetic beads. The supernatant is collected and added to another batch of prepared beads and the process repeated. This ensures that the supernatant is totally depleted of rRNA.

5.2.4 Creation of cDNA library for SOLiD sequencing

In order to create a library of cDNA suitable for sequencing with the SOLiD high throughput sequencer the rRNA depleted samples must be fragmented, reverse transcribed, size selected and then amplified.

5.2.4.1 Fragmenting the RNA

The RNA is fragmented using RNase III (Applied Biosystems AM2290) to produce fragments of a size suitable for SOLiD sequencing (50-100 bp).

0.5 µg-1 µg of each rRNA depleted sample was made up to 8 µl with nuclease free water and added to 1 µl of RNase III and 1 µl of 10x RNase III reaction buffer on ice. The mixture was mixed thoroughly and incubated in a thermocycler set to 37˚C for 10 min. Immediately after incubation 90 µl of nuclease-free water was added and the resulting fragmented RNA mix is immediately cleaned up using parts from the Ribominus Concentration Module (Invitrogen K1550-05). 100µl of binding buffer (L3) and 250 µl of 100% ethanol is added to the digested RNA mix and then loaded onto a spin column and centrifuged at 12 000 × *g* for 1 min. The flowthrough is discarded and 500 µl of the wash buffer (W5) is added to the spin column. The column is spun at 12 000 × *g* for 1 min and the flowthrough is discarded before the spin column is placed into a clean wash tube and spun again at maximum speed for 2 min. To elute the RNA from the spin column 20 µl of RNase-free water was added to the centre of the spin column and incubated at room temperature for 1min before centrifuging at maximum speed for 1 min. The fragmented RNA was collected from the flowthrough and the yield assessed by running 1 µl on a Nanodrop Spectrophotometer (Thermo Scientific).

5.2.4.2 Hybridisation and ligation of the RNA

The fragmented RNA was then hybridised and ligated with an adaptor mix included in the SOLiD Small RNA Expression Kit (Ambion 4397682). Inside the adaptor mix is a set of oligonucleotides with a single-stranded degenerate sequence at one end and a defined sequence required for the SOLiD system sequencing at the other end.

3 µl of fragmented RNA sample (equivalent to 50-100ng of RNA) was mixed with 2 µl of adaptor mix A and 3 µl of hybridisation solution on ice. The mix was then incubated in a thermocycler at 65˚C for 10 min and 16˚C for 5 min. Once the incubation was completed 10 µl of 2x ligation buffer was added followed by 2 µl of ligation enzyme mix. Once mixed the ligation reaction was placed in a thermocycler set to 16˚C for a 16 hr incubation.

5.2.4.3 Reverse transcription of RNA

A reverse transcription master mix was made up for each sample using components from the SOLiD Small RNA Expression Kit. This mix consisted of 13 µl of nuclease-free water, 4 µl of 10x reverse transcription buffer, 2 µl of 2.5 mM dNTP mix and 1 µl of ArrayScript Reverse Transcriptase. Once the master mix was added to the RNA ligation reaction and mixed it was incubated in a thermocycler at 42˚C for 30 min. The cDNA was then purified using components from the MinElute PCR Purification Kit (Qiagen 28004). 60 µl of nuclease-free water and 500 µl of buffer PB/PBI was added to all of the cDNA created in the reverse transcription stage. This mix was then loaded onto the MinElute column and spun at 13 000 × *g* for 1 min and the flowthrough discarded. To wash the sample adhered to the MinElute column, 750 µl of buffer PE was added to the column and spun at 13 000 × *g* for 1 min before discarding the flowthrough, returning the column to a new tube and spinning again at 13 000 × *g* for 1 min. The cDNA was eluted from the column by adding 10 µl of buffer EB to the centre of the MinElute column and spinning at 13 00 × *g* for 1 min.

5.2.4.4 Size selection of cDNA.

In order to amplify cDNA of the correct size the samples must be run on a gel and bands of the correct size for SOLiD sequencing excised. This was performed using the precast Novex 6% TBE-Urea Gels, 1.0 mM, 10-well (Invitrogen EC6865BOX), Novex TBE running buffer 5x (Invitrogen LC6675) and Novex TBE-Urea sample buffer 2x (Invitrogen LC6876). The TBE-Urea gels were placed into a tank filled with 1x TBE running buffer and the cDNA and DNA ladders were prepared. 5 µl of the cDNA samples/50 bp DNA ladder and 5 µl of 2x TBE-Urea sample buffer were mixed together and heated at 95°C for 3 min before snap cooling on ice. Before

loading the samples, the wells of the gel were flushed through with 1x TBE running buffer to ensure that there was no urea left in with the samples and to obtain sharp bands. The samples and ladder were loaded onto the gel and it was run at 180 V for ~17 min. The gel was then stained with Sybr Gold nucleic acid stain (Invitrogen S11494) for 40 min before illumination with a UV transilluminator. The 100-200 nt material was then excised from the gel using a clean scalpel and split vertically into 4 pieces and placed in separate 1.5 ml microcentrifuge tubes.

5.2.4.5 Amplifying the cDNA

The cDNA was amplified to ensure there was sufficient available for SOLiD sequencing. This used components from the SOLiD Small RNA Expression Kit (Ambion 4397682). To prepare sufficient cDNA for the emulsion PCR step of SOLiD sequencing two PCR reactions were performed for each sample each using one of the gel pieces excised during size selection. Each PCR reaction required 100 µl of PCR master mix made up of the following; 78 µl nuclease-free water, 10 µl 10x PCR buffer I, 2 µl SOLiD PCR primers 1-10, 8 µl 2.5 mM dNTP Mix and 2 µl AmpliTaq DNA Polymerase. The PCR reaction was then run under the following conditions (Table 5.1).

Table 5.1. PCR conditions for SOLiD library amplification of cDNA obtained from FEA cells infected with FCV-F9 and mock infected at 4 and 7 h p.i..

Stage	Temperature (°C)	Time
Hold	95	5min
Cycle (15 cycles)	95	30sec
	62	30sec
	72	30sec
Hold	72	7min

The amplified cDNA was then purified using components from the Purelink PCR micro kit (Invitrogen K310050) to remove unincorporated primers which may have affected the final quantitation and emulsion PCR. The two 100 µl PCR reactions were combined and 800 µl of binding buffer (B2) was added to the tube and mixed. 500 µl of this mixture was then added to the Purelink Micro Kit column and centrifuged at 10 000 × *g* for 1 min. the flowthrough was discarded and the process repeated with the remaining sample. The column was then washed with 600 µl of wash buffer (W1) and spun at 10 000 × *g* for 1 min before discarding the flowthrough, returning the column to the collection tube and spinning again at 14 000 × *g* for 1 min. the bound DNA was eluted by adding 10 µl of elution buffer to the centre of the column membrane, incubating for 1min and centrifuging at 14 000 × *g* for 1 min. This process is repeated to ensure that all of the cDNA is recovered from the column.

5.2.5 Emulsion PCR

Emulsion PCR (ePCR) and SOLiD sequencing was performed by Miss Suzanne Kay at the Centre for Genomic Research, School of Life Sciences, University of Liverpool. Briefly, this involved amplifying the short DNA fragments onto SOLiD P1 DNA beads using ePCR. Oil is used to create droplets of solution which aim to contain a single DNA bead and a single DNA fragment template. The emulsion was then placed on a thermal cycler and a standard PCR conditions run according to manufacturer instructions and during this amplification >30 000 copies of each template were amplified onto each SOLiD P1 DNA bead. Once amplification was complete the emulsion was broken with 2-butanol and the beads washed to clear away the remaining oil and emulsifiers. There then has to be an enrichment step to isolate template beads from non-amplified or poorly amplified DNA beads. To do this polystyrene beads with an adaptor attached were used to capture template beads before the mixture was centrifuged on a 60% glycerol cushion. This step resulted in separation of the enrichment beads along with attached DNA beads at the top of the mixture and the non-amplified beads in a layer at the bottom. The enriched beads were then extracted and denatured using a denaturing buffer to remove the enrichment beads from the solution. The enriched DNA beads are then prepared for the SOLiD sequencer by covalent bonding to a glass slide.

5.2.6 SOLiD sequencing

Primers hybridise to the P1 adaptor sequence added during the ePCR stage and a set of four fluorescently labelled di-base probes are added. Once the correct di-base probe has ligated to the primer the fluorescent tag attached is cleaved and the colour emitted is recorded. The process is then repeated through multiple cycles to extend the sequence. This extended sequence is then removed from the template and a new primer is added to the adaptor but in a position n-1 of the first primer. The di-base probes are again added and the ligation – fluorescence – cleavage cycles repeated. Once the sequence has been extended it is again removed from the template and the whole process is repeated with another three primers (positioned at n-2, n-3 and n-4 from the original primer position). This method ensures that each base of the template is interrogated twice and so sequencing errors should be minimised.

5.2.7 Read mapping

Once the reads had been generated by the SOLiD sequencer they then had to be mapped onto the cat genome. This process was performed by Dr Kevin Ashelford at the Centre for Genomic Research, School of Life Sciences, University of Liverpool. The cat genome was downloaded from Ensembl (Assembly CAT, Mar 2006. Database version 58.1g) and was artificially divided into 16 chromosomes as the current assembly consists of scaffolds which were unsuitable for processing. The artificial chromosomes were subdivided into eight chromosomes which contained all of the annotated genes from the genome whilst the other eight chromosomes contained those scaffolds without annotated genes. The Bioscope pipeline was used to map the SOLiD reads onto the cat genome chromosomes and this pipeline allows up to 10 mismatches against the reference genome per 50 bp read.

5.2.8 DESeq

Those reads that mapped to the annotated genes found on the cat genome were analysed for differential expression using DESeq which is an R package that is able to analyse gene expression based on the negative binomial distribution (Anders 2010). Genes with an adjusted p-value of ≤ 0.01 were deemed to be significantly

differentially transcribed. The adjusted p-value is calculated by the Benjamini-Hochberg procedure which controls with false discovery rate of the differentially transcribed genes (Benjamini and Hochberg 1995).

5.2.9 Gene Ontology

Those genes that were found to have an adjusted p-value ≤0.01 with an up or down regulation were selected for further analysis on the basis that using the adjusted p-value means that there is a lesser likelihood of the selected genes containing false positives and the low p-value cut off means it is unlikely that any genes appear within the list by chance. The GO terms for biological processes were obtained by downloading those available for the annotated genes found on the cat genome from Ensembl using the BioMart tool.

5.2.10 Pathway Studio

The significantly differentially expressed genes were also analysed by pathway analysis software, Pathway Studio (Ariadne) (Nikitin *et al.*, 2003). Those genes with recognised gene identifications were uploaded into the software and the genes were mapped onto created pathways in the software.

5.3 Results

5.3.1 DESeq analysis

There were 34 843 genes analysed by DESeq to find the $\log_2$ fold difference and adjusted p-value for each gene comparison between groups (Appendix VI). Comparisons were made between infected and mock infected groups at each time point and also between mock infected group's only and infected groups only. A summary of overall numbers of differentially transcribed genes by $\log_2$ fold difference and by adjusted p-value significance ($p \leq 0.01$) can be found below (Table 5.2); the full list can be found in appendix VII.

To ensure that the genes found to be significantly differentially transcribed between infected and mock infected groups are a result of viral infection and not an artefact of normal cellular processes, closer investigation of the genes found in the mock 4 h vs. mock 7 h comparison was performed. Table 5.3 shows the full list of the significantly differentially transcribed genes in the mock infected comparison and the $\log_2$ fold difference. Also included is the $\log_2$ fold differences from the other three comparisons provided the gene was found to be significantly differentially expressed by having an adjusted p value ≤ 0.01 for that comparison group. The table shows that of the genes found within the mock infected comparison correlate closely with the infected group's comparison, 61 of the 64 genes found in the uninfected comparison were also significantly differentially expressed in the infected group's comparison. All of these genes were up- or down-regulated in the same patterns in both comparisons which offers the conclusion that these genes were differentially transcribed as a result of normal cellular processes although the effects in the infected comparison were of a greater magnitude in all but one case. Within the mock vs. infected comparisons at both time points, the differentially transcribed genes shared with the mock infected comparison are all down-regulated whereas in the mock infected comparisons they are all up-regulated. These results would indicate that during infection the transcription of these genes is disrupted especially in the early stages of viral replication.

With taking all of these findings into account it shows that the genes found to be differentially transcribed within the mock infected and infected comparisons can be

considered to be an effect of the infection rather than solely a result of cellular processes.

Table 5.2. Table showing summary of overall numbers of differentially transcribed genes analysed by DeSeq by log_2 fold difference and by adjusted p-value significance ($p \leq 0.01$). Genes were found to be significantly transcribed in FEA cells in response to infection with FCV-F9 or mock infection at 4 and 7 h p.i..

Comparison groups	**Genes with a log_2 fold difference**						**Significantly differentially transcribed gene ($p \leq 0.01$)**		
	Total number of up-regulated genes	**Total number of down-regulated genes**	**Genes up-regulated with a ≥1 log_2 fold difference**	**Genes down-regulated with a ≥1 log_2 fold difference**	**Genes up-regulated with a ≥2 log_2 fold difference**	**Genes down-regulated with a ≥2 log_2 fold difference**	**Total genes**	**Up-regulated genes**	**Down-regulated genes**
Mock 4 h vs. Infected 4 h	12 087	11 972	2 651	3 261	769	1 069	172	32	140
Mock 7 h vs. Infected 7 h	12 582	11 786	3 575	3 017	1 223	779	182	174	8
Mock 4 h vs. Mock 7 h	12 482	12 538	2 837	2 076	714	572	64	61	3
Infected 4 h vs. Infected 7	12 546	10 950	4 331	2 835	1 680	737	317	287	30

Table 5.3. Table showing all genes differentially transcribed ($p<0.01$) in FEA cells in the comparison of mock 4 h vs. 7 h and the $\log_2$ fold difference found in all comparisons within the experiment. Genes up-regulated are marked in green, genes down-regulated are marked in red. NA means that those genes were not transcribed significantly differently within that comparison

ID from cat genome	Gene ID	Mock 4 h vs Mock 7 h	Mock 4 h vs Infected 4 h	Mock 7 h vs Infected 7 h	Infected 4 h vs Infected 7 h
ENSFCAG00000019535	U5	3.72	NA	NA	4.52
ENSFCAG00000019870	SNORD70	3.07	-2.79	NA	5.51
ENSFCAG00000019525	SNORA74	2.70	-2.30	NA	4.30
ENSFCAG00000020008	SNORD111	2.67	NA	NA	4.31
ENSFCAG00000020237	SNORD79	2.62	-4.61	NA	5.87
ENSFCAG00000019817	SNORD72	2.68	-5.55	-2.61	5.62
ENSFCAG00000019540	SNORD112	2.21	-3.48	NA	4.37
ENSFCAG00000019860	No ID	2.30	-3.63	NA	4.45
ENSFCAG00000020177	SNORA65	2.36	-3.47	NA	4.61
ENSFCAG00000019548	snoZ40	2.50	-2.39	NA	4.67
ENSFCAG00000020113	SNORD63	4.00	NA	NA	5.76
ENSFCAG00000019967	SNORD113	2.12	-3.59	NA	4.84
ENSFCAG00000019710	SNORA3	2.04	-2.83	NA	3.48
ENSFCAG00000019412	SNORD113	2.11	-3.52	NA	4.59
ENSFCAG00000019852	SNORD96	2.18	-3.88	NA	4.85
ENSFCAG00000020310	No ID	2.08	-3.52	NA	4.63
ENSFCAG00000020468	SNORA35	1.84	-5.44	-1.65	5.62
ENSFCAG00000019857	SNORA11	1.93	-2.50	NA	3.27
ENSFCAG00000019757	SNORA11	2.02	-3.48	NA	3.96
ENSFCAG00000019919	SNORA72	2.46	NA	NA	4.31
ENSFCAG00000017742	U3	2.40	NA	NA	4.52
ENSFCAG00000020135	SNORD15	1.76	NA	NA	2.90
ENSFCAG00000019705	SNORA71	1.95	-2.48	NA	4.15
ENSFCAG00000020121	No ID	1.82	-1.98	NA	3.68
ENSFCAG00000019908	SNORA18	2.06	NA	NA	3.05
ENSFCAG00000019682	SNORA5	2.13	-2.61	NA	3.84
ENSFCAG00000020027	SNORD52	2.09	-2.97	NA	4.68
ENSFCAG00000020119	SNORD113	1.82	-2.95	NA	4.29
ENSFCAG00000019800	SNORD35	1.79	-1.95	NA	3.58
ENSFCAG00000020098	snoU6-53	1.67	-2.37	NA	3.85
ENSFCAG00000013775	CYP1B1	-1.59	NA	NA	-1.67
ENSFCAG00000019570	SNORD18	2.50	NA	NA	4.57
ENSFCAG00000017140	U2	2.86	NA	NA	NA
ENSFCAG00000003645_dup2	TXNRD1	-1.59	NA	NA	-2.23
ENSFCAG00000020281	SNORD71	1.49	-2.09	-1.45	2.13
ENSFCAG00000020040	SNORA21	2.08	-3.07	NA	4.78
ENSFCAG00000020262	SNORA27	1.78	-3.38	NA	5.19
ENSFCAG00000019725	SNORD113	1.55	-2.32	NA	3.06
ENSFCAG00000001125	KIAA1539	2.10	NA	NA	NA
ENSFCAG00000020211	U5	2.48	NA	NA	3.52
ENSFCAG00000019827	SNORA64	1.76	-2.19	NA	3.75
ENSFCAG00000020187	No ID	1.85	NA	NA	3.71
ENSFCAG00000019978	SNORA19	3.57	NA	NA	4.30
ENSFCAG00000019820	U5	1.88	-3.18	NA	5.02
ENSFCAG00000019497	SNORND104	1.70	-2.96	NA	4.47
ENSFCAG00000020172	SNORD43	1.71	NA	NA	3.24
ENSFCAG00000019687	SNORD62	1.79	NA	NA	3.64
ENSFCAG00000019839	SNORD101	1.60	-2.94	NA	3.90
ENSFCAG00000019838	SNORD105	1.47	-1.88	NA	3.77
ENSFCAG00000020198	snoMe28S-Am982	1.76	-3.24	NA	2.79
ENSFCAG00000020194	SNORD49	2.26	-2.94	NA	4.04
ENSFCAG00000019574	SNORD83	1.52	NA	NA	3.57
ENSFCAG00000007466	SLC40A1	-1.76	NA	NA	-3.43
ENSFCAG00000017534	5S_rRNA	1.99	NA	NA	4.91
ENSFCAG00000019713	SNORA29	2.25	NA	NA	4.70
ENSFCAG00000019614	SNORD18	4.09	NA	NA	NA
ENSFCAG00000019795	SNORD18	1.89	-1.17	NA	1.84
ENSFCAG00000020330	SNORA17	1.58	-2.46	NA	4.04
ENSFCAG00000019657	SNORA55	1.57	-2.11	NA	3.30
ENSFCAG00000019419	SNORD99	1.33	-1.65	NA	2.17
ENSFCAG00000020447	SNORA40	1.80	NA	NA	4.81
ENSFCAG00000019994	SNORD25	1.56	-4.10	NA	5.35
ENSFCAG00000019961	SNORA46	1.33	-3.11	-1.61	2.83
ENSFCAG00000019465	SNORD75	1.49	-1.69	NA	2.49

5.3.2 Gene Ontology

Those genes that were found to have an adjusted p-value ≤0.01 were selected for further analysis by discovering the biological processes associated with each gene set. Not all of the differentially transcribed genes had this information available and so they had to be excluded from the functional analysis; a summary of these genes included can be found in Table 5.4. Each comparison group was interrogated for biological process functions and grouped according to the Gene Ontology (GO) definition. From these groupings, pie charts were constructed for all genes found within that comparison (Figs. 5.1 and 5.2). The overall pie charts show a large difference between the comparisons made at 4 h (Fig. 5.1) and 7 h p.i. (Fig. 5.2). In the comparison between the infected and mock infected groups at 4 h p.i. over 50% of the genes that had functional information available were found to be small nucleolar RNAs whereas this proportion drops dramatically in the comparison made between the infection states at 7 h p.i. where only 1% of the differentially transcribed genes were found to be small nucleolar RNAs. One the comparison is broken down further into up- and down-regulated transcripts (Figs. 5.3-5.6) then the picture becomes a little clearer. The vast majority of small nucleolar RNAs seen in the comparisons between infected and mock infected groups are down-regulated (Figs. 5.4 and 5.6) which suggests that these RNAs are less useful to the virus during replication.

Taking a closer look at the up-regulated genes from each infected vs. mock infected comparison it is clear that there are a vast range of genes undergoing transcriptional changes as a result of infection with FCV-F9. At 4 h p.i. the majority of the genes undergoing an increase in transcription were those involved in cellular signalling (11%), developmental processes (7%) and organ development (10%) whereas by 7 h p.i. the proportions of genes involved in these functions had dropped to 7% for signalling, 5% for developmental process and 5% for organ development. The majority of differentially transcribed genes at 7 h p.i. were genes involved in immune response (12%) and genes used in transcription (10%), the proportions of each of these gene functions were increased from the comparison made at 4 h p.i..

Table 5.4. Table showing summary of genes differentially transcribed (adjusted p value ≤ 0.01 from DeSeq analysis) in FEA cells in response to infection with FCV-F9 at 4 and 7 h p.i.. Only genes with functional information available from GO were included in further analyses.

Comparison groups	All genes		Up-regulated genes		Down-regulated genes	
	With functional information	Without functional information	With functional information	Without functional information	With functional information	Without functional information
Mock 4 h vs. Infected 4 h	149	23	22	10	127	13
Mock 7 h vs. Infected 7 h	132	50	124	50	8	0

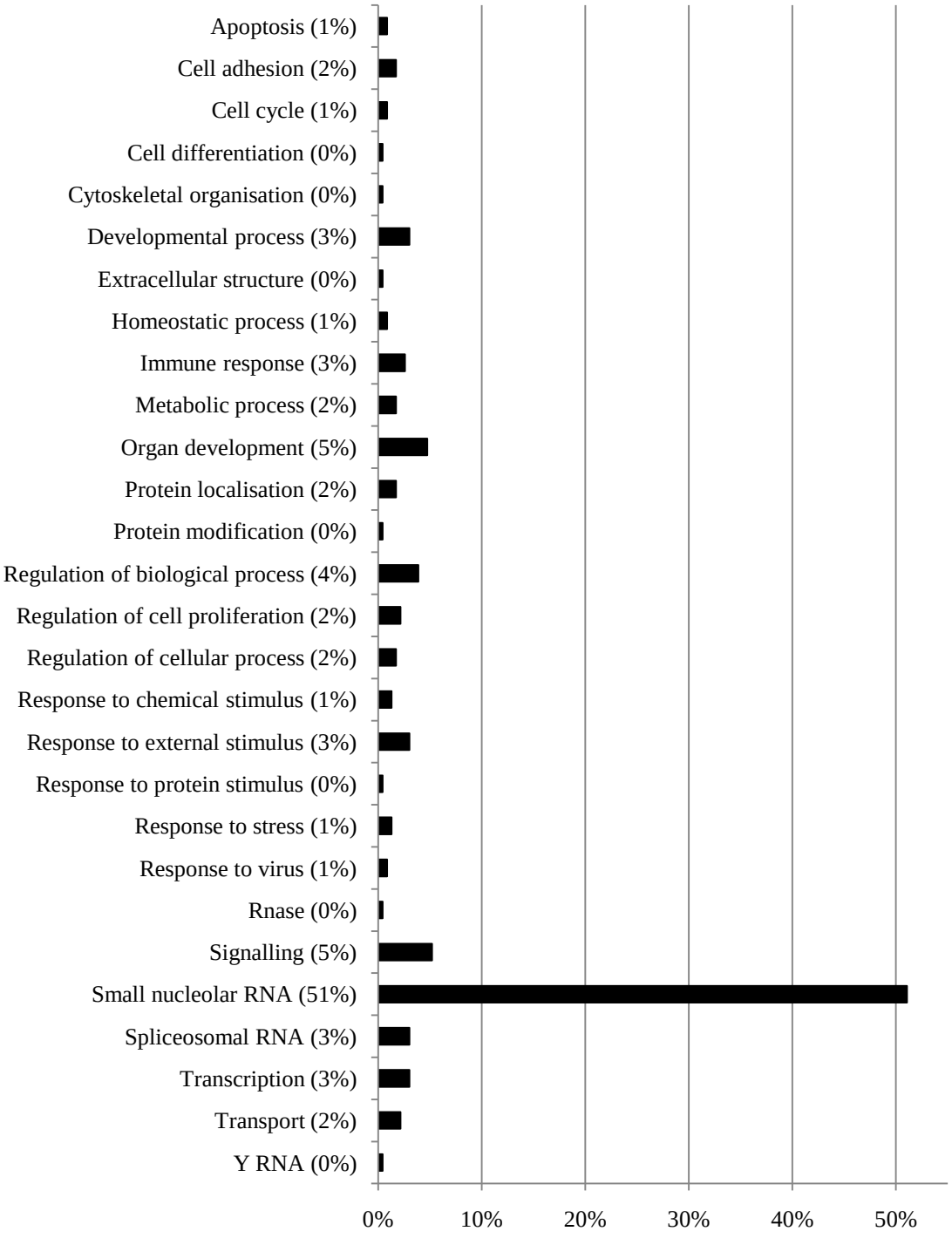

Figure 5.1. Gene Ontology analysis of the biological processes of the genes significantly differentially transcribed in FEA cells in response to infection with FCV-F9 at 4 h p.i..

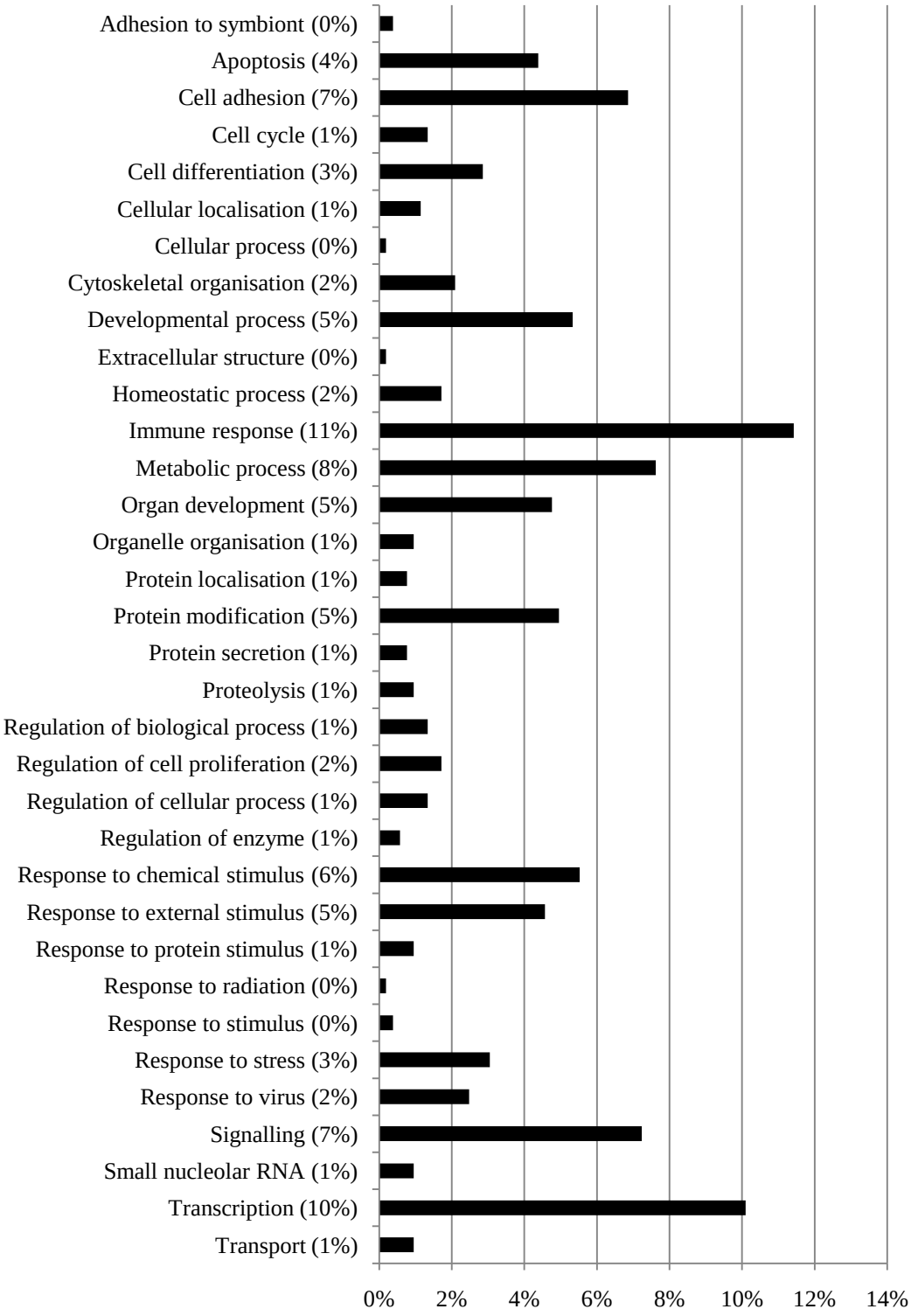

Figure 5.2. Gene Ontology analysis of the biological processes of the genes significantly differentially transcribed in FEA cells in response to infection with FCV-F9 at 7 h p.i..

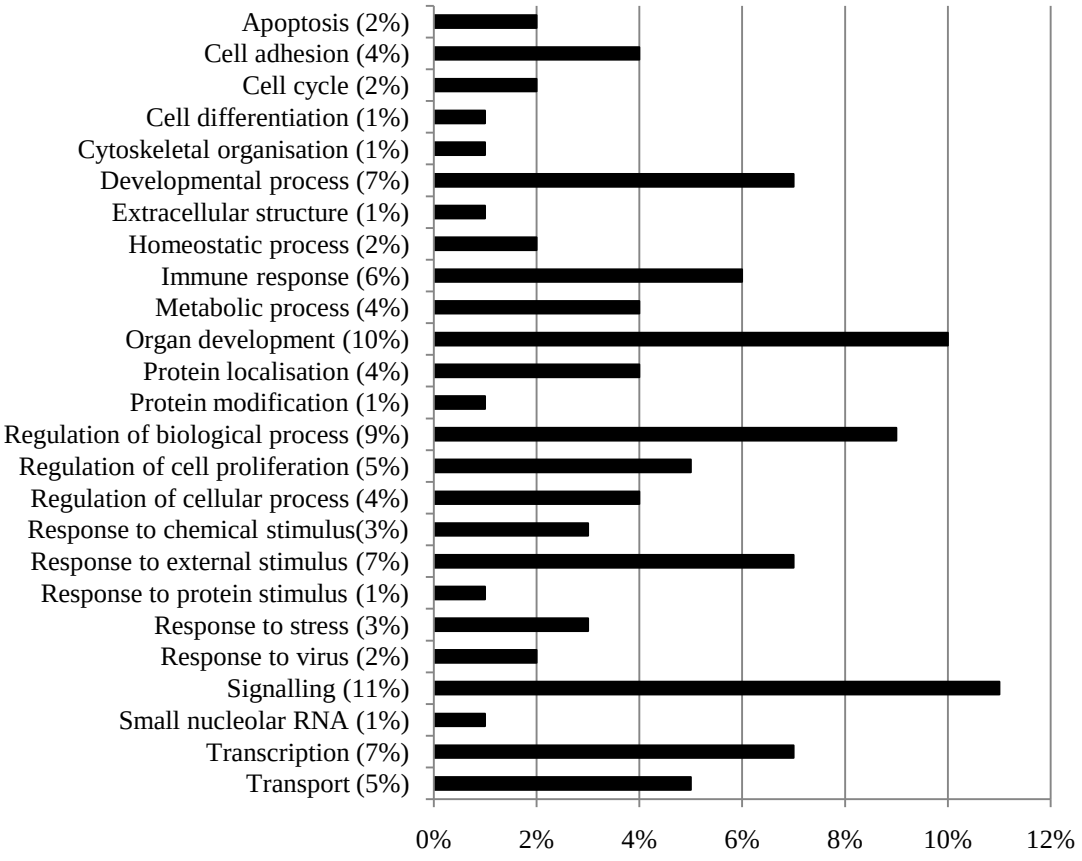

Figure 5.3. Gene Ontology analysis of the biological processes of the genes significantly up-regulated in FEA cells in response to infection with FCV-F9 at 4 h p.i..

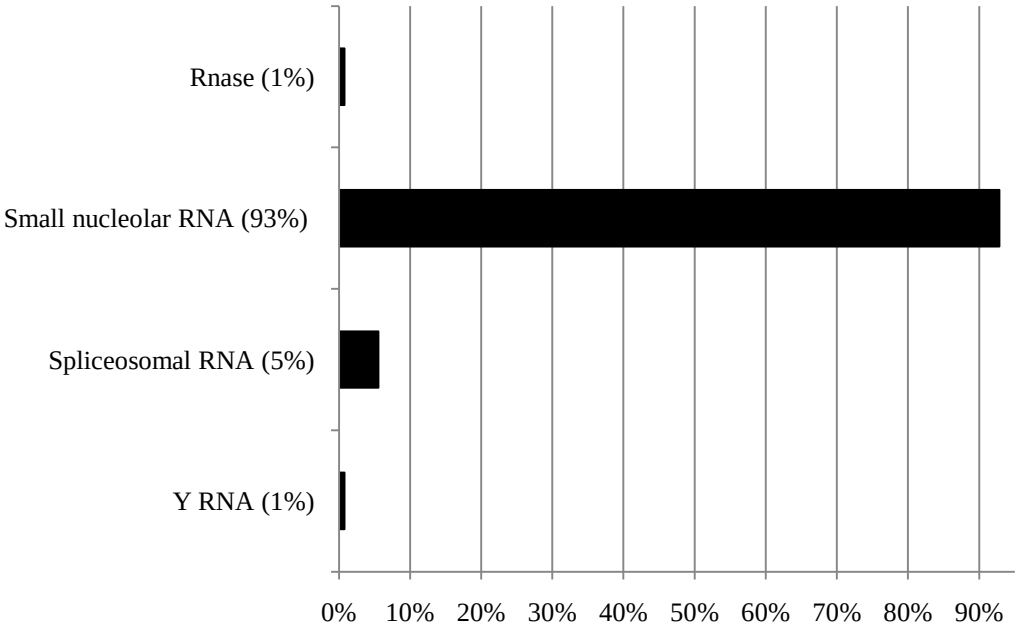

Figure 5.4. Gene Ontology analysis of the biological processes of the genes significantly down-regulated in FEA cells in response to infection with FCV-F9 at 4 h p.i..

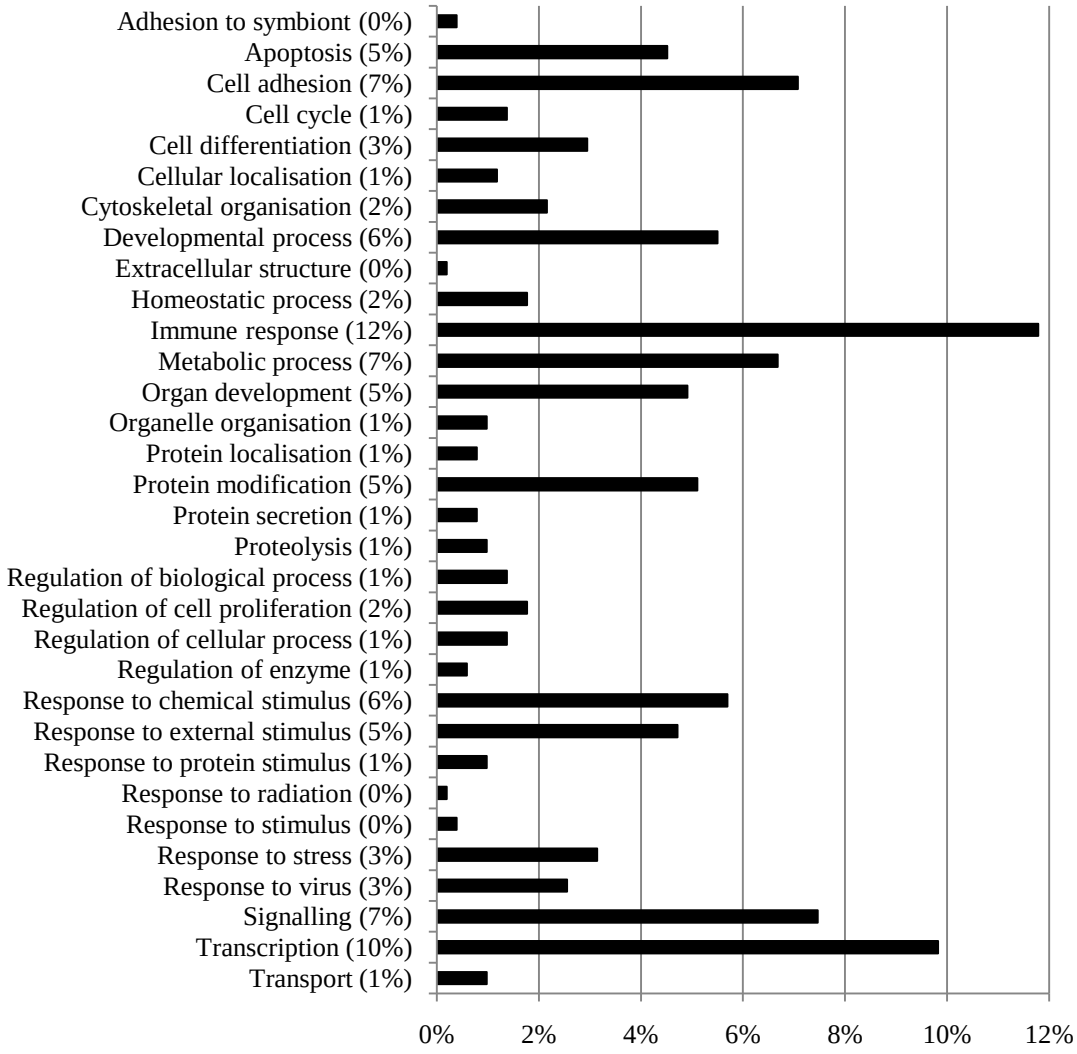

Figure 5.5. Gene Ontology analysis of the biological processes of the genes significantly up-regulated in FEA cells in response to infection with FCV-F9 at 7 h p.i..

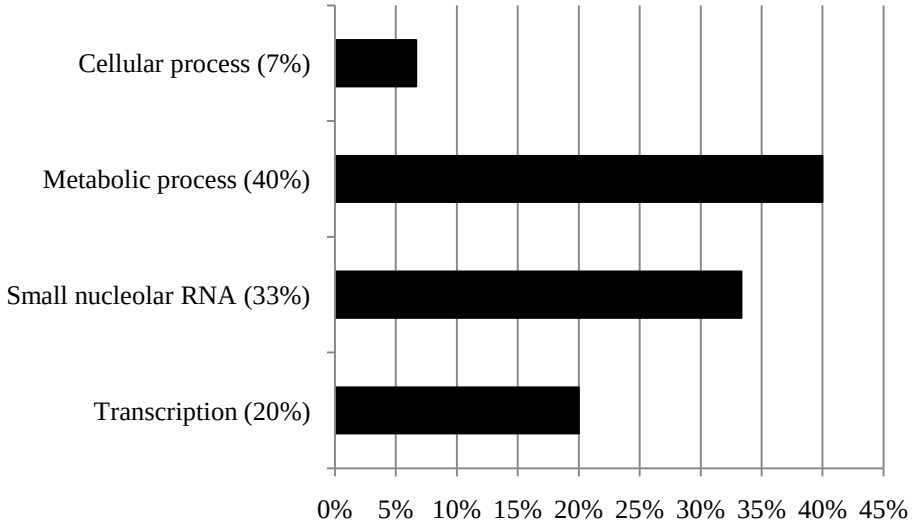

Figure 5.6. Gene Ontology analysis of the biological processes of the genes significantly down-regulated in FEA cells in response to infection with FCV-F9 at 7 h p.i..

5.3.3 Pathway analysis

Significantly up-regulated and down-regulated genes were entered into the pathway analysis software, Pathway Studio (Ariadne) (Nikitin *et al.*, 2003). The software has pre-constructed mammalian pathways available and once a gene list has been uploaded, the software automatically maps these genes onto the pathways and shows whether these genes have been up- or down-regulated. All of the significantly differentially transcribed genes from the comparisons mock vs. infected at 4 h, mock vs. infected at 7 h and also mock infected 4 h vs. mock infected 7 h were entered into the software.

The results of the analysis showed that there were a number of pathways targeted during infection. Those pathways which had a number of genes which were transcriptionally up-regulated included actin cytoskeletal regulation (Figs. 5.7 and 5.8), apoptosis regulation, B cell activation, natural killer cell activation and translation control (Appendix VIII). In each case the amount of genes up-regulated in a pathway as a result of infection increases with time. This could have been attributed to normal cellular processes becoming activated over time but the genes differentially transcribed in the mock infected group comparison were also inputted into the pathway analysis software and in each case none of the genes within these pathways were up- or down-regulated. These findings show that the up-regulation shown in the pathways is due to infection of the cell with FCV-F9 and as such it can be inferred that these pathways are important in viral replication and transmission but to what extent is unknown. The pathways found in this analysis match pathways found in the previous DIGE analyses (chapters 2 and 3) and also pathways identified by other studies.

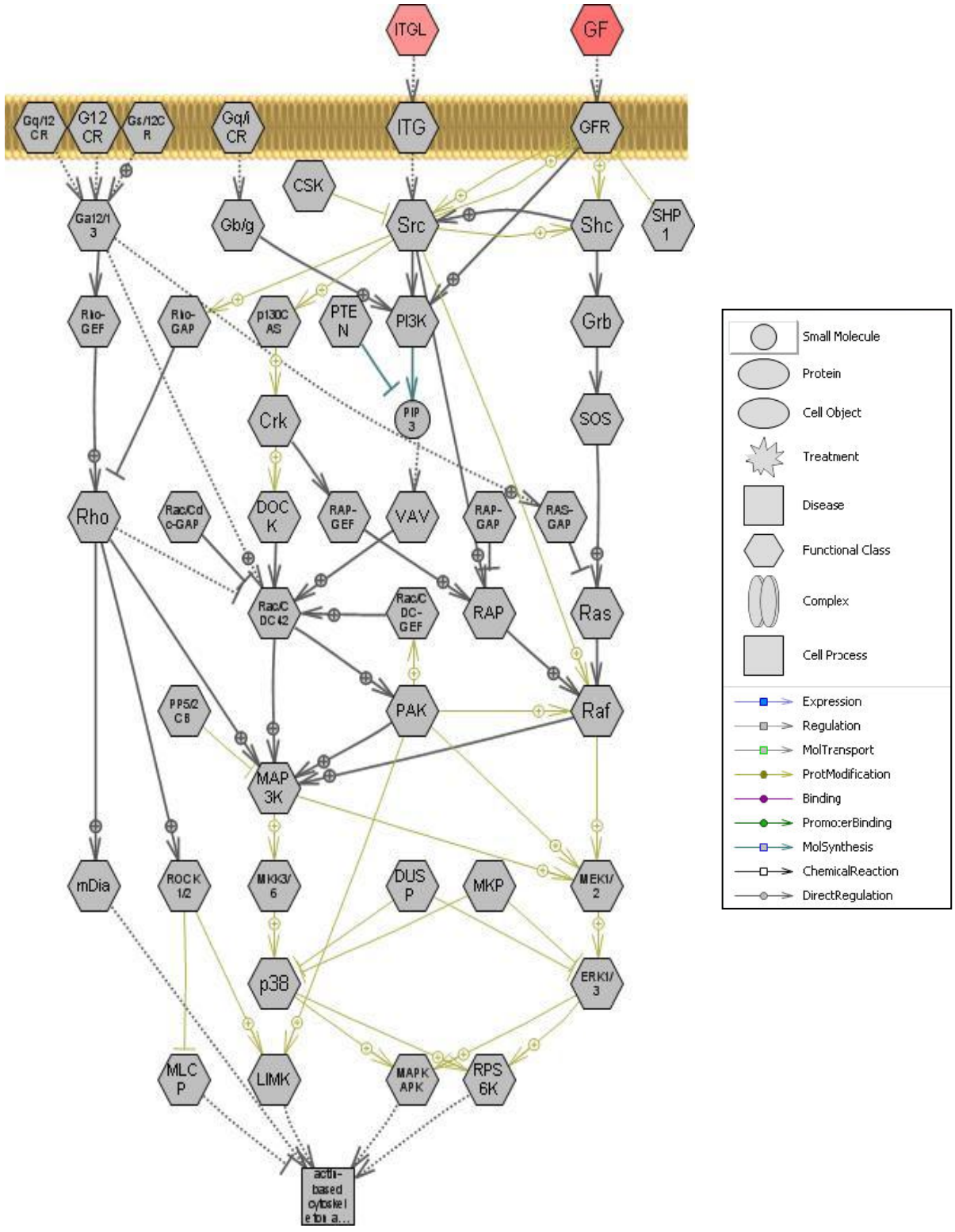

Figure 5.7. Actin cytoskeletal regulation pathway. Pathway shows genes with up-regulated transcription in FEA cells during infection with FCV-F9 at 4 h p.i.. Those genes highlighted in red have up-regulated transcription in the infected samples, the brighter the colouration, the greater the up-regulation in transcription. A full key of gene identification can be found in the appendix (Table A8.1).

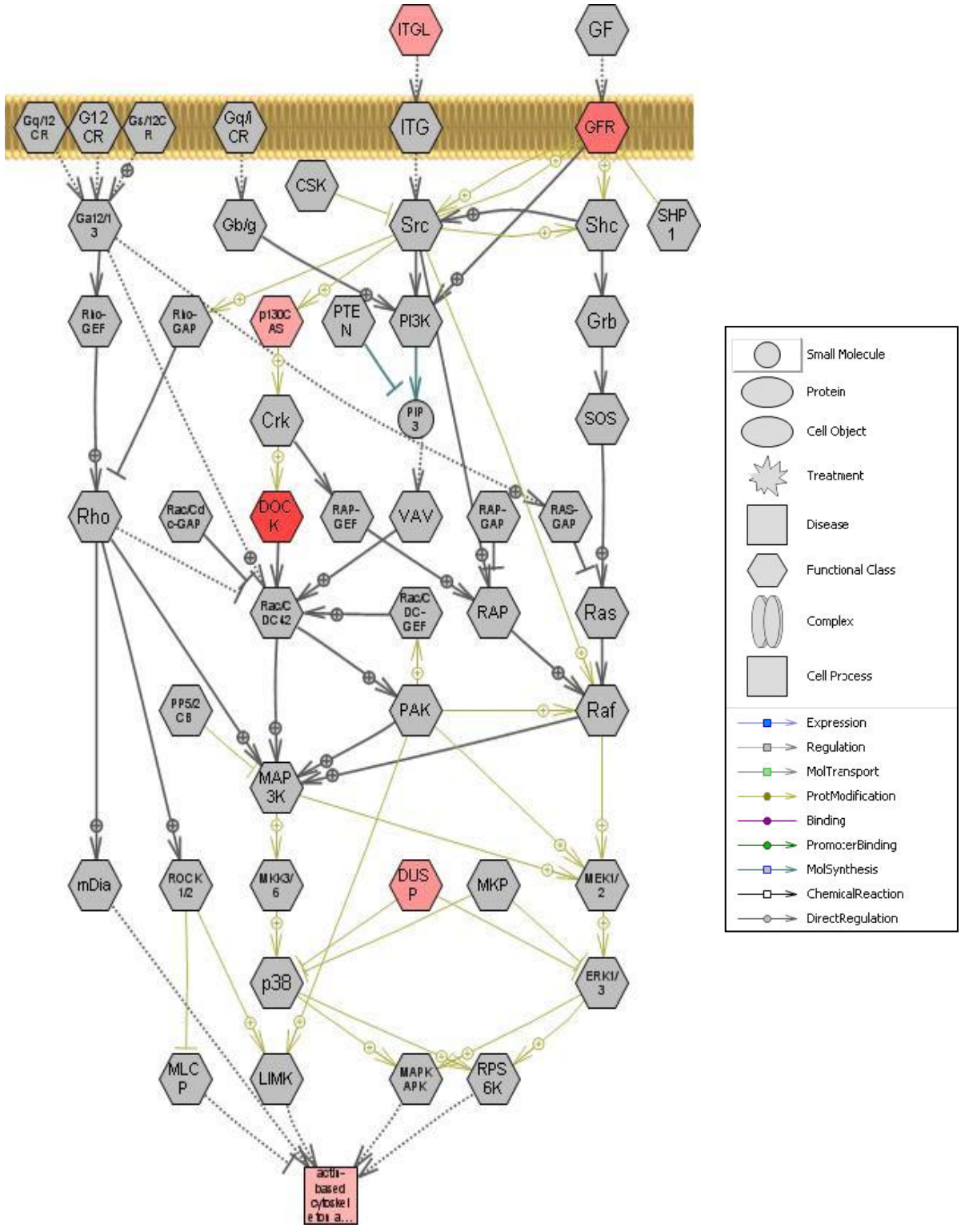

Figure 5.8. Actin cytoskeletal regulation pathway. Pathway shows genes with up-regulated transcription in FEA cells during infection with FCV-F9 at 7 h p.i.. Those genes highlighted in red have up-regulated transcription in the infected samples, the brighter the colouration, the greater the up-regulation in transcription. A full key of gene identification can be found in the appendix (Table A8.1).

5.4 Discussion

This chapter describes the use of next-generation sequencing technology to relatively quantify transcripts from FEA cells infected with FCV-F9 at two time points post infection. By using SOLiD sequencing to rapidly sequence the RNA transcripts, a number of genes have been found to be differentially transcribed in response to infection and an accurate count of relative expression of these genes has been obtained.

The genes analysed in this experiment were solely based upon those reads which mapped to existing genes on the current cat genome annotation although there were reads mapping to other unannotated areas found on the genome. In this current study there was not time to investigate these areas of mapping but these reads may be investigated in the future to aid further annotations of the cat genome through definition of gene exon boundaries and splice sites. There were also instances of reads from the SOLiD sequencing which did not map to the cat genome at all, again these reads will have to be revisited at a future date but they may be a useful tool in the development of a *de novo* method of SOLiD read assembly where a reference genome is not available or is not completed to a high enough standard for high quality mapping of reads.

It has also been necessary to exclude the reads which have mapped to the FCV-F9 genome in this analysis as the amount of reads mapping has given an average coverage of ~50 000x coverage of the viral genome. This coverage is too high for the details of the viral transcriptome to be elucidated and as such these reads will have to be bioinformatically processed much further before any discoveries about the way in which the viral genome is replicated can be found. However, this level of coverage does suggest that next-generation sequencing might now provide a cost-effective way of sequencing such variable genomes in a sequence independent manner, avoiding the difficulties of designing PCR primers (see chapter 6).

5.4.1 DESeq

Those genes which mapped to the genes already annotated on the current cat genome release were analysed using the DESeq statistical package (Anders, 2010) which

uses a negative binomial distribution based model to discover genes which are significantly up- or down-regulated within a sample with regard to a reference sample. The DESeq package is also able to calculate an adjusted p-value which takes into account the number of likely false discovery rate (Benjamini & Hochberg, 1995) and adjusts the p-value accordingly. Those genes with an adjusted p-value of <0.01 were deemed to be truly differentially expressed and not just found as a result of chance. At present there is only one other study which has employed RNA-seq to compare the transcription levels in response to infection with a virus where RNA-seq was used in tandem with microarray and proteomic techniques to find differences in cells infected with hepatitis C virus (HCV) (Woodhouse *et al.*, 2010). The results of their RNA-seq analysis found that 753 genes were differentially expressed in response to HCV infection whereas in this study we have found that 354 genes are up- and down-regulated in infected cells when compared to their uninfected counterparts. This would appear to show that HCV has a much greater effect on the transcription of genes within a cell than FCV. However, HCV was only sampled at one time point when ≥90% of cells were infected whereas in this study although a high m.o.i. was used it has been found that not all cells are infected at the same time which may have had an effect on the number of genes found to be differentially transcribed. The method used in the HCV study to assign differentially expressed status to genes was also different to the method described in our FCV experiment. They used the fold-difference coupled with the number of counts mapping to that gene as an arbitrary cut-off for differential expression rather than using a statistical package and this may have lead to an over estimation of differentially expressed genes in the HCV study. Finally, the HCV study was performed on infected human cells and so the transcript reads obtained in this study were matched to a genome that has much greater annotation than the feline genome. This should ensure that the majority of reads sequenced could be mapped to the genome and may be another factor in the apparent large discrepancy in identified gene numbers between this study and our FCV transcriptome study. Until more papers are published which use RNA-seq to establish gene transcription changes in cells infected with viruses it is difficult to know whether the results we have found during infection with FCV-F9 are typical of a viral transcriptome experiment.

5.4.2 Pathway analysis

Pathway analysis software (Pathway studio, Ariadne) (Nikitin *et al.*, 2003) was used to group the differentially transcribed genes within known biological pathways. One pathway of interest which appears to contain a number of differentially expressed genes is the apoptosis regulation pathway which does correlate with previous research into FCV infection (Al-Molawi *et al.*, 2003; Natoni *et al.*, 2006; Roberts *et al.*, 2003; Sosnovtsev *et al.*, 2003). Studies have also shown that rather than just being a cellular response to combat viral infection, apoptosis is actually necessary for viral polypeptide processing through use of cellular caspase activity (Al-Molawi *et al.*, 2003). There were very few examples of apoptotic proteins being identified within the two 2D-DIGE experiments (chapters 2 and 3), which suggests that these two techniques do not correlate with each other fully.

Actin was found to be differentially expressed in both 2D-DIGE analyses (chapters 2 and 3) and Figure 5.7 shows up-regulation of genes within the actin regulatory pathway which again suggests an importance in viral infection. As discussed in previous chapters (chapters 2, 3 and 4), the host cytoskeleton plays a large role in the movement of virions around an infected cell and also has a role in promoting cell-cell spread (Cudmore *et al.*, 1995; Sodeik, 2000). Further work is needed to ascertain exactly how FCV uses these proteins but these are the most consistently modulated genes and proteins found within all of the comparisons and so it clear that they have a role to play in FCV infection within the cell.

The remaining three pathways, whilst not confirmed by the literature or the proteomic analyses, appear to be consistent with viral infection. Whilst the cells used in this experiment were neither B cells nor natural killer cells the genes necessary to activate these cells have been shown to be up-regulated within the infected cells. This may be part of the adaptive immune response to viral infection and as such may be a response that the virus elicits within the cell which is detrimental to its survival.

The up-regulation of the translation control pathway is also, perhaps an expected consequence of viral infection. The virus, once it enters the cell has an aim to replicate as many times as possible, and for this to happen a large amount of translation of the viral genome would have to occur. Therefore, it would be advantageous to increase the amount of the control proteins available within the cell.

There are also genes present within this analysis which have an effect upon more than one pathway (Appendix VIII). For example, DUSP is present in four of the five pathways modulated during infection. DUSP is a dual specificity phosphatase which inactivates many proteins within the cell through dephosphorylation and so appears in many pathways of regulation and control (Patterson *et al.*, 2009). With DUSP being so ubiquitous within many pathways, it is difficult to know whether all pathways are being affected by the up-regulation in transcription in this gene, or if perhaps the effects are more targeted through the modulation of surrounding genes and proteins. Until more specific assays are used to quantify the changes in these types of genes and of their target genes and proteins either by real-time PCR or quantitative proteomics (e.g. QconCAT (Pratt *et al.*, 2006)) the ultimate effect of their up-regulation cannot be determined.

5.4.3 Comparing RNA-seq and proteomic results

With the RNA-seq experiment performed in this chapter mirroring the FCV strain and time points used in the proteomic experiments, a comparison of differentially expressed genes and proteins should be possible.

Looking at all of the identifications of the differentially expressed proteins of the two 2D-DIGE experiments (chapters 2 and 3, Appendix I and II) and the differentially transcribed genes in the RNA-seq study (Appendix VII) it would appear that there is very little correlation between the genes identified and the proteins expressed. There are also no significant matches in the GO analyses with the DIGE experiments proving to have a much larger proportion of cytoskeletal proteins than any of the RNA-seq comparisons. The pathway analysis of the RNA-seq genes, however, shows that there are some significant genes up-regulated within the actin cytoskeletal regulation pathway. This does correlate with the findings of the previous 2D-DIGE experiments and fits with the hypothesis that the virus is acting upon the host cytoskeleton in order to aid replication and spread.

This poor correlation between transcription levels and protein expression is not uncommon amongst studies where transcriptomics and proteomics are run in parallel (Barros *et al.*, 2010). Rogers *et al*, (2008) suggest that the relationship between transcription and translation diverges with evolution as organisms such as bacteria

and yeast often show good correlation whereas in mammalian samples the correlation becomes much weaker. The authors hypothesise that the transcriptional and translational networks have evolved independently within the cell and so they are not directly linked which may explain the often seen discrepancies between transcriptomes and proteomes. Another analysis performed by Wang *et al*, (2010) gave a hypothesis that transcription and translation contained a time-delayed component and once this is taken into account then the correlation is much greater.

The overall results from this study show that there are a large number of genes whose transcription is significantly altered as a result of FCV-F9 infection and although this investigation was only possible upon genes previously annotated upon the feline genome there was still a vast amount of data generated. Future interrogation of the data will rely heavily upon bioinformatics methods but now the data has been generated it may be useful in driving forward the annotation of the cat genome.

6 Chapter six

Sequence analysis of a UK outbreak of virulent systemic FCV

6.1 Introduction

Infection with FCV has been shown to be associated with a wide range of clinical signs although until recently these clinical signs have generally been found to be self limiting with a low mortality rate. In recent times outbreaks of new, highly virulent strains of FCV have been reported in the USA and Europe which show much greater mortality rates and clinical signs.

The first three outbreaks were reported in the USA (Hurley *et al.*, 2004; Pedersen *et al.*, 2000; Schorr-Evans *et al.*, 2003) and followed similar patterns. Cats infected during the outbreaks showed clinical signs such as fever, anorexia, oedema of face and limbs, oral ulceration, ocular and nasal discharge, jaundice and a very high mortality rate of up to 50%. There have also been two similar outbreaks in Europe; one in the UK (Coyne *et al.*, 2006b) and one in France (Reynolds *et al.*, 2009). In France the outbreak occurred at a veterinary teaching hospital in 2005 and the clinical signs observed were similar to those from the US outbreaks. The overall mortality rate was even higher than the previous outbreaks reported with 63% of cats dying or being euthanised.

The viruses used in this chapter have been isolated from the UK outbreak of VS-FCV, reported by Coyne *et al* in 2006. The UK outbreak was traced back to three kittens being initially fostered from a local rescue shelter into the home of one of the workers at the shelter. During the fortnight following the fostering two of the kittens died. Subsequently, three of the four cats already living in this foster household went on to exhibit signs of infection with VS-FCV. All three of these cats suffered pyrexia and voice loss with two of the three also suffering some form of leg pain/lameness. Only one of the three cats infected in the foster household suffered lethargy, oedema, vomiting and jaundice. A fourth cat was also infected during this outbreak but this cat lived in the household next-door to the foster home. This cat experienced fever, lethargy, voice loss and jaundice during the course of infection and was eventually euthanised. In this outbreak five of the affected kittens and cats died or were

euthanised giving an overall mortality rate of 71% which again is in keeping with the previous reports. VS-FCV was isolated from the three dead adult cats and given the nomenclature UKOS-A, UKOS-B and UKOS-W. Capsid sequencing was performed upon these three isolates and the results were compared to the other outbreak strains, other published genomes and some unpublished lab strains using phylogenetic analysis (Fig. 6.1, reproduced from Coyne *et al* (2006b)).

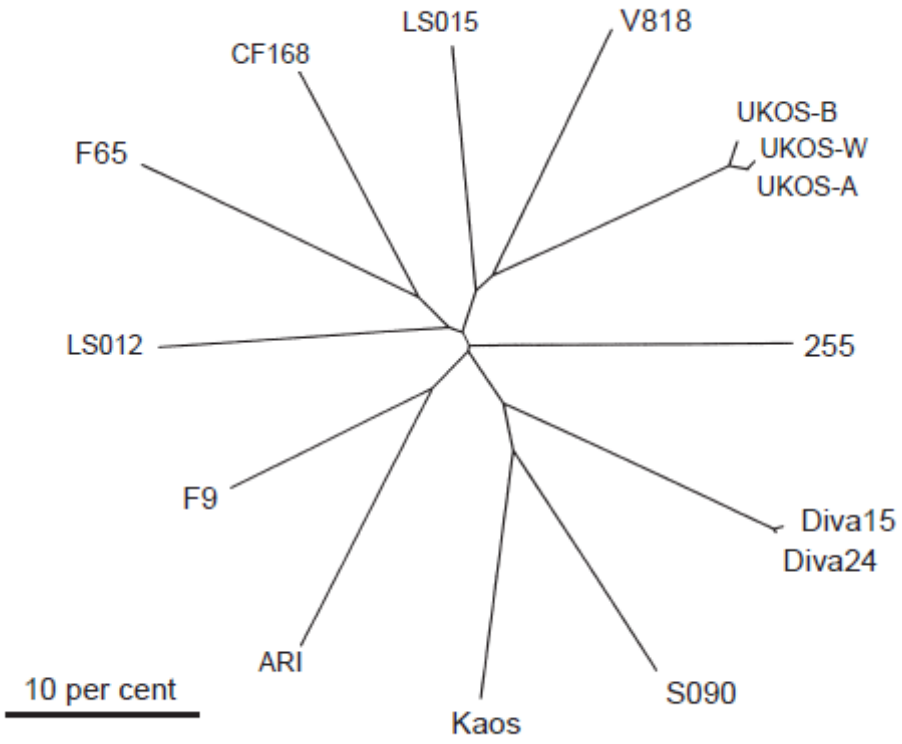

Figure 6.1. Phylogenetic tree based upon capsid sequence. Included in this analysis are the three UKOS strains; FCV-Ari (Pedersen *et al.*, 2000), FCV-Kaos (Hurley *et al.*, 2004), FCV-Diva (Schorr-Evans *et al.*, 2003). Also included are FCV-F9 (Genbank M86379), LS012 (Genbank AF109467), LS015 (Genbank AF109464), F65 (Genbank AF109465), CF168 (Genbank U13992), 255(Genbank U07131) and unpublished field viruses (S090 and V818) (Coyne *et al.*, 2006b).

Also as part of the Coyne *et al* study into this outbreak, FCV isolates were collected 58 days after the outbreak began from 28 of 42 cats housed in the local rescue shelter where the 3 kittens were fostered from. These types of shelters have previously been shown to have higher prevalences of FCV than private cat homes and that there are often a number of strains found circulating within them (Radford *et al.*, 2001) (Bannasch & Foley, 2005). As such there are also more chances of recombination

events occurring within these shelters and colonies which can aid rapid evolution of FCV strains (Coyne *et al.*, 2006c). It has been hypothesised that such environments provide the ideal environment for the evolution of the hypervirulent phenotype (Coyne *et al.*, 2006b). Selection pressures within the colony favour the selection of rapid high titre replication as such viruses are likely to have a high transmission advantage. Within the confines of the colony, cats in the shelters acquire and evolve immunity in a progressive, step-wise fashion, in parallel with this viral evolution, allowing the replication of these viruses to be controlled within relatively low limits, preventing manifestation of VS-FCV symptoms. However, when these virus strains are introduced to naïve populations, these newly infected cats have no strain-matched acquired immunity and so are unable to fight off the infection in the same manner, such that the shelter viruses are able to fulfil their high titre/fast replication rate phenotype leading to the development of the severe clinical signs associated with VS-FCV. Such a mechanism would allow each outbreak of VS-FCV disease to be associated with a new strain of FCV.

The collection of isolates from the UK outbreak has for the first time, allowed some analysis to be made on the relatedness of the UKOS strains to those found within the rescue shelter from where the putative index case kittens originated. This has already been done using sequence analysis of a small region of the polymerase gene (Coyne, 2005), showing that the rescue shelter contained at least five strains of FCV. The most frequently recognised strain in the rescue shelter was FCV-UKOS, confirming the shelter as the likely source of this outbreak, despite the fact that the cats in the shelter were generally healthy. Within the shelter, viruses belonging to this strain were highly diverse, with some viruses being extremely similar to this found in the dead cats, whilst others were less similar.

The aim of this chapter was two-fold. Firstly, further sequence analysis of the genome of one of the strains isolated from a cat which died during the outbreak (UKOS-A) was attempted to discover whether there are any characteristics found at the sequence level that are similar to other outbreak strains which have previously been sequenced and published. If there are areas of sequence which are very similar in strains isolated from VS-FCV outbreaks then it could be hypothesised that these areas are important in the increased virulence and mortality associated with these virus strains.

Secondly, we wish to capitalise on the unparalleled availability of viral strain variants of FCV-UKOS in the rescue shelter, to further characterise the diversity and evolution of FCV in this environment. In particular, by analysing sequence of the capsid gene (complimenting the already available polymerase sequence), it was hoped to discover how much strain variation was present in the shelter and whether there were any recombination events occurring that may have aided evolution of a hypervirulent strain.

6.2 Materials and methods

6.2.1 Virus strains

Virus strains used were recovered from a rescue shelter involved with an outbreak of virulent systemic FCV (Coyne, 2005).

Partial polymerase gene sequences equivalent to 486 bp from position 4766-5251 of the genome, are already available for 27 viruses from this shelter. This suggested this colony contained only five strains. Using these viruses R564, R573, R572, R581, R580, R593, R591 and R584 were selected to have capsid gene sequence obtained as they represented a broad selection of viruses, including at least one of each of the strains found within the colony.

6.2.2 RT-PCR of capsid gene and sequencing

RNA extraction, reverse transcription and subsequent PCR were all performed as previously described (section 2.2.2). The primers used to amplify the hypervariable regions C and E of the capsid gene were also described previously (section 2.2.2.3) (Table 6.1). The PCR products were purified using the QIAquick PCR purification kit (Qiagen) and sequencing was performed by Eurofins MWG Operon (section 2.2.2.5).

Table 6.1. Sequences of primers used to amplify the hypervariable regions C and E of the capsid gene of virus strains R564, R573, R572, R581, R580, R593, R591 and R584.

Primer name	Sequence (5' – 3')	Binding site relative to F9 (nt)
P1_degen (forward)	GAG CGG ATA ACA ATT TCA CAC AGG CCG TTY GTG TTY CAR GCA AAY CG	6381-6428
P2_ext (reverse)	CCT CAC CTA TAC CAG TGT AAC CAA G	6910-6935

6.2.3 Sequence analysis

The forward and reverse sequences obtained from each PCR product were aligned in Chromas Pro (Technelysium Pty Ltd) and a consensus sequence produced for each amplicon as previously described (section 2.2.2.6).

Separate alignments of polymerase gene sequences and capsid gene sequences were then produced using Clustal as implemented in Mega 4 (Tamura *et al.*, 2007). The phylogenetic trees were drawn using neighbour joining with the Kimura 2 parameter substitution model with the significance of the observed phylogeny assessed using 1000 bootstraps.

6.2.4 RT-PCR of polymerase gene to capsid gene and sequencing

In order to further characterised viruses in this shelter, attempts were made to bridge the gap from the partial sequence of the polymerase gene to the partial sequence of the capsid gene for those viruses where available. Primers were designed based on the previously obtained (this study and Coyne (2005)) partial capsid and polymerase sequences. This PCR was successful for four virus strains; R580, R581, R591 and UKOS-A. The primers that allowed successful amplification are detailed in Table 6.2.

Table 6.2. Primers used to amplify the region of the FCV genome from the polymerase gene to the capsid gene.

Virus amplified	Primer name	Sequence (5' – 3')	Binding site relative to F9 (nt)
R580	w580_for	CGG CTT GAA ACC CAC ACG AGT AG	4858-4880
	w580_rev	CGA TGT AAT CTG TTG CGA TCC C	6550-6529
R581	w581_for	GGC TGT TGA ATG TGA GGG ATT G	5169-5190
	w581_rev	CAG GAA CAA TGG AAT CAG TGG C	6553-6532
R591	w591_for	GGC AGA AAG AGC TGT GGA ATA CG	5146-5168
	w591_rev	TCA GTT GCT ATT CCG GTG CC	6542-6523
UKOS-A	w494_for	CGC CAG TCA ACA TGG TGT TG	5099-5118
	w494_rev	GCC AGG AAC AAT AGA ATC AGT GGC	6558-6535

PCR was performed as previously described (section 2.2.2.4) and PCR products were purified using the QIAquick PCR purification kit. Where more than one band appeared on an agarose gel, the band of the correct size was excised from the gel and purified using QIAquick gel extraction kit (Qiagen).

Sequencing was performed bidirectionally by MWG Eurofins according to their recommended protocols (section 2.2.2.5).

6.2.5 Sequence analysis

The forward and reverse sequences obtained from each PCR product were aligned in Chromas Pro (Technelysium Pty Ltd) and a consensus sequence produced as previously described (section 2.2.2.6).

Each polymerase - capsid gene sequence was then aligned to each other in Mega 4 (Tamura *et al.*, 2007) and analysed using Simplot (Lole *et al.*, 1999). Simplot creates similarity plots in comparison to one query sequence. In this experiment, each strain was compared to UKOS-A, the UK outbreak strain to discover how different or similar the different strains from the same shelter were. Simplot is also a useful tool in discovering whether any of the strains analysed could potentially be a recombinant strain.

6.2.6 Sequencing the outbreak strain UKOS-A

At the time of starting this project full genome sequence was only available publicly for two other strains of FCV associated with outbreaks around the world (Abd-Eldaim *et al.*, 2005). Therefore, we aimed to sequence the full genome of the UKOS-A strain. Primer pairs were designed based upon consensus sequence of other viruses to produce PCR products that would span the whole genome and could be sequenced bidirectionally to give the full genome sequence. The primer pairs used and binding sites relative to FCV-F9 are given in Table 6.3.

Table 6.3. Primers pairs used in the sequencing of the UKOS-A strain of FCV along with binding sites relative to FCV-F9

Part name	Primer name	Sequence (5' – 3')	Binding site relative to F9 (nt)
Part A	vpol1_for	GGACAACAGCTCTGGAATGCATG	5078-5100
	vRegionE2_rev	TCACTGGGGATTGTTGTGTCTGG	6572-6594
Part B	vPart1_for	CCAGTTTGTTACATTCTTACCGGCCC	1448-1473
	vMid1_rev	AGCCCAGGCCAAATCAAACACCG	2457-2479
Part H	pcrH_for	GGCTTGCCTCAAACATTAGGAGTG	7289-7312
	vPart3_rev	CCCTGGGGTTAGGCGCAAGTGCG	7668-7690
Part J	J_for	TCAAACTCTGAGCTTCGTGCT	25-45
	J_rev	ACAAACCTCATTGCCTGTGT	1575-1595
Part K	A-H_for	TCCTAGGTAATCGCCCAATCA	6358-6379
	A-H_rev	AGCCCGAAGGGATACATGA	7647-7665

6.2.7 RT-PCR and sequencing

RNA extraction, reverse transcription and PCR were all performed as previously described (section 2.2.2.1).

Purification of the PCR products was performed as before using the QIAquick PCR purification kit (Qiagen) if a single band was present after agarose gel electrophoresis or where multiple bands were produced, the band of the correct size was excised from the gel and purified using QIAquick gel extraction kit (Qiagen).
Sequence analysis was performed as previously described to produce consensus sequence and each sequence part was then compared to F9 (Genbank accession m86379).

6.3 Results

6.3.1 Analysis of outbreak shelter strains.

To try to understand the evolution of the strains involved in the VS-FCV outbreak in the UK isolates were obtained from the rescue shelter involved in the outbreak and polymerase sequence was obtained for 25 of the 28 isolates (Coyne, 2005). In this study capsid gene sequences were analysed to discover whether the groupings obtained from the polymerase sequences were consistent along the genome or whether possible recombination events had occurred within the colony. Of the eight strains selected based on the polymerase gene analysis for further capsid sequencing four were successfully amplified by PCR and sequenced bi-directionally. Figure 6.2 shows a phylogenetic tree of the strains from the shelter successfully sequenced for the polymerase gene (work completed by Dr Karen Coyne) and those strains for which capsid gene sequence was obtained. Strains highlighted with asterixes are those obtained during this project; all other strains were obtained previously (Coyne, 2005). From the results of the phylogenetic tree analysis two potential recombinants were identified. Strain R580 clustered in group 1 on the polymerase gene tree but was isolated from group 1 on the capsid gene tree. Strain R593 also clustered within group 1 on the polymerase tree but within group 2 on the capsid tree.

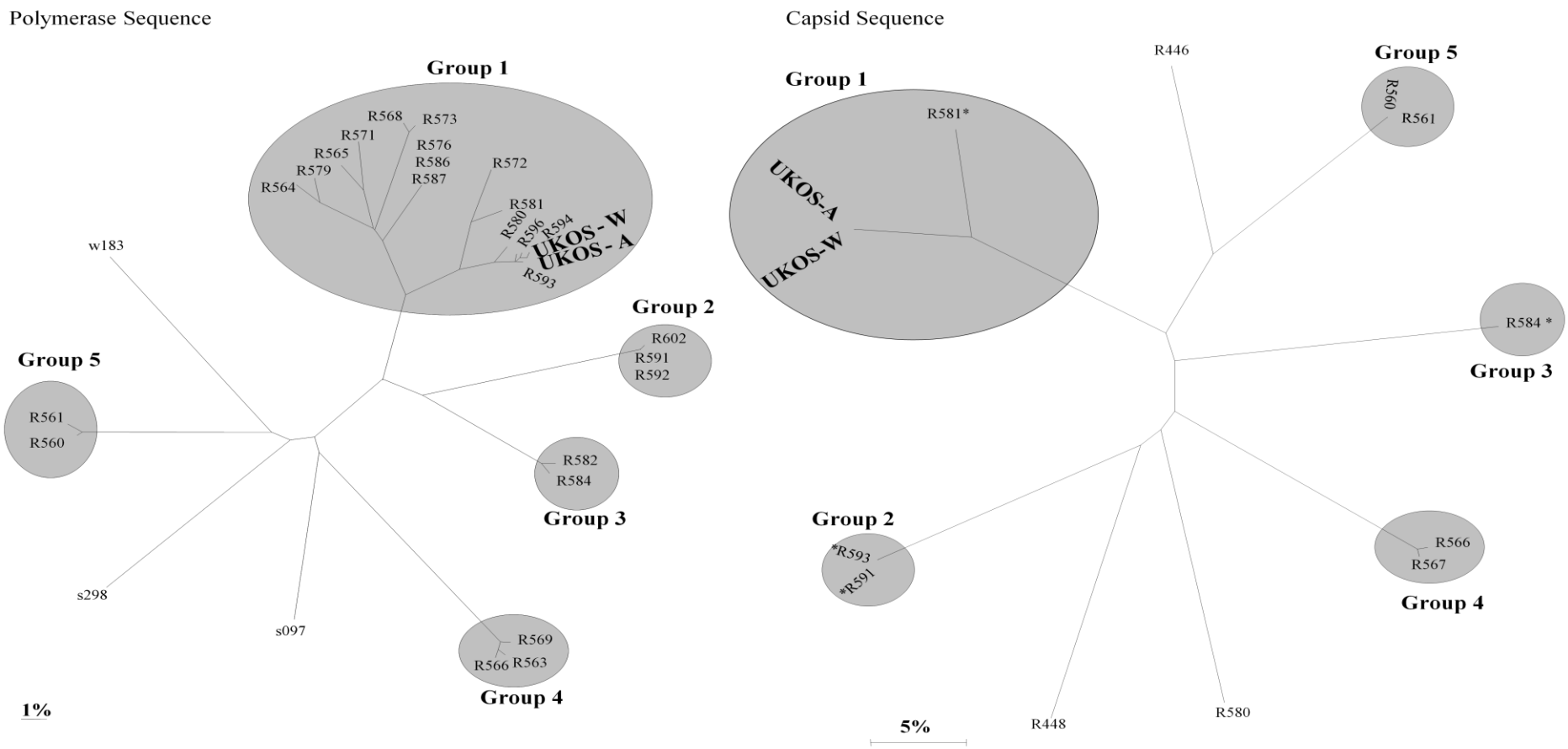

Figure 6.2. Phylogenetic tree analysis of capsid and polymerase gene sequences isolated from cats housed at the rescue shelter involved in the UKOS outbreak produced from Clustal W alignments through neighbour joining with Kimura 2 parameters. UKOS-A is the outbreak strain studied in this chapter, UKOS-W was recovered from one of the other dead cats. Capsid sequences obtained by the author during this study are marked with an asterixes. All other sequences were obtained by Dr Karen Coyne and the polymerase tree is reproduced from Coyne (2005). Scale bar represents percentage divergence.

To test the hypothesis that recombination had occurred within the shelter, primers were designed within the polymerase gene sequence and within the capsid gene sequence for strains which had both present. However; only R591, R581, R580 and UKOS-A were successfully amplified. Good polymerase-capsid bidirectional sequence was obtained for strains R591, R581 and R591 whereas the sequence obtained from R580 suggested this was a mixed infection. Figures 6.3 and 6.4 show the electropherograms of UKOS-A aligned with R580 in both the forward and reverse directions and these show evidence of a mixed infection within R580 which could be a cause of R580 grouping alongside different strains for the two genes sequenced. In Figure 6.3, the two sequences do not align well with each other but when you look at the minor sequence underneath the peaks in sequence from strain R580, the sequences seem to align much better and this may be evidence of two strains being amplified within this PCR. The other electropherogram (Fig. 6.4) shows that the sequences for R580 and UKOS-A align with each other. However, the sequence from strain R580 has much more background noise which again suggests that there are more than one strain being amplified by this PCR.

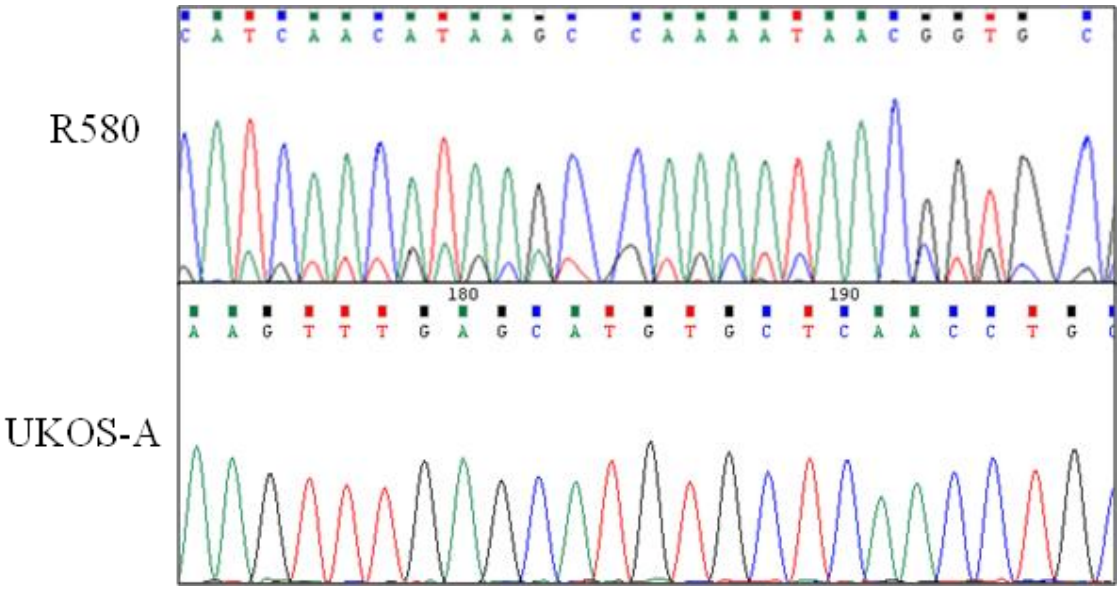

Figure 6.3. Electropherogram screenshot of forward sequence obtained for R580 (top panel) and UKOS-A (bottom panel). Sequence from UKOS-A appears to align with the "minor" sequence observed in the R580 sequence.

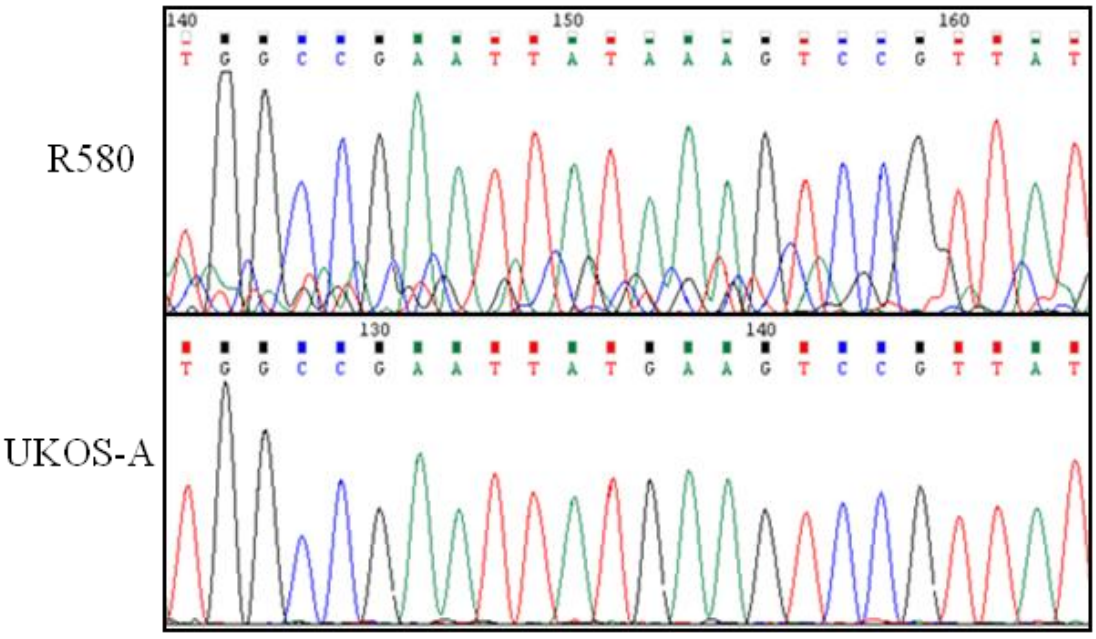

Figure 6.4. Electropherogram screenshot of reverse sequence obtained for R580 (top panel) and UKOS-A (bottom panel). Sequence from R580 contains a large amount of background noise which may indicate difficulties in amplification of a single strain from a mixed infection.

To further scrutinise the sequence of R580 for possible recombination, a SimPlot analysis (Lole *et al.*, 1999) was performed where the polymerase-capsid sequence obtained for R580, R581 and R591 was plotted against UKOS-A to find areas of similarity and differences. Figure 6.5 shows the result of this plot and the trace shows that the sequence obtained for R580 is very similar to the sequence it was compared against; UKOS-A. This provides further evidence that R580 was not a recombinant virus and that the differences found when analysing the phylogeny of the two genes was a result of a mixed infection. The original PCRs performed may have preferentially amplified different strains within the mixed infection for each gene and as a result grouped separately on the two trees. The other two viruses analysed against the UKOS-A strain behaved in the expected manner with R591 being the least related to the UKOS strain which was anticipated from the polymerase and capsid gene phylogenetic tree analysis.

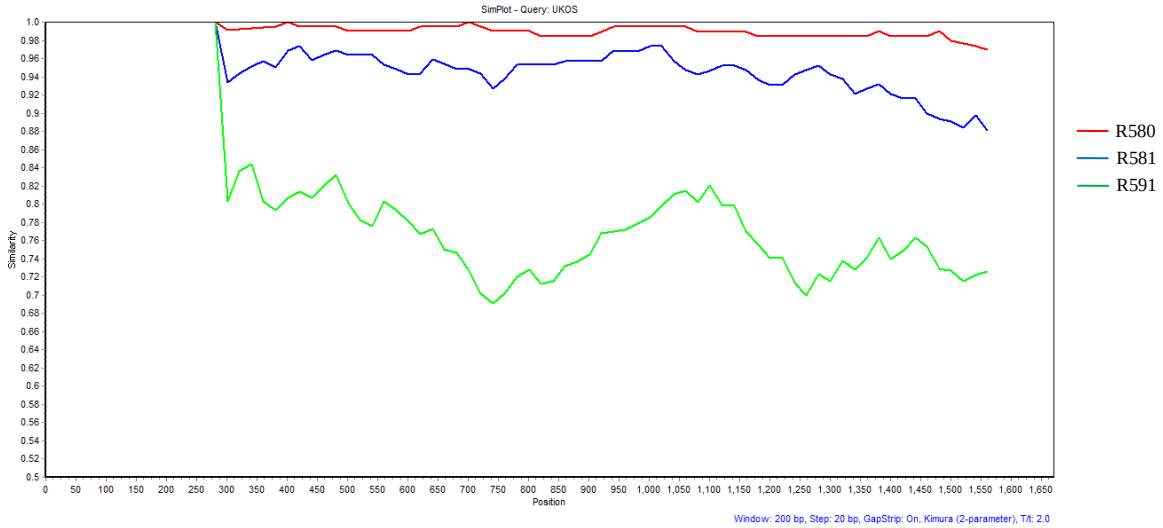

Fig. 6.5. Simplot analysis of the polymerase-capsid sequence of R580, R581 and R591 compared to the UKOS-A strain. The strains which show greatest similarity to the query strain UKOS-A will plot a higher line on the graph.

6.3.2 Sequencing of the outbreak strain UKOS-A

In order to discover whether there are any obvious signs of differences between the putative outbreak strain and other typical strains of FCV an attempt was made to sequence the whole genome of UKOS-A; the strain recovered from a cat which died of virulent systemic FCV. The capsid gene sequence of the UKOS outbreak strains including UKOS-A had previously been found to be unrelated to the capsid gene sequences recovered from the other outbreak strains (Fig. 6.1) or those of other published FCV genomes.

At the beginning of this study 1436 bases of the UKOS-A virus were known. Within this experiment four further amplicons were obtained giving an additional 2087 nucleotides of sequence and a total of 3523 bp of known UKOS-A sequence (Fig. 6.6). Part B gave partial sequence for ORF 1 which encoded for the viral non-structural protein; part A bridges the gap between the polymerase gene in ORF1 and part of the capsid gene encoding for protein VP1 in ORF2; part K also bridges the gap between ORF 2 and ORF3 from the VP1 protein to VP2 and part H includes the remaining sequence for ORF 3 which encodes for the viral protein VP2. For each of the new genome segments sequenced there was no evidence of global rearrangement or insertion/deletion (data not presented).

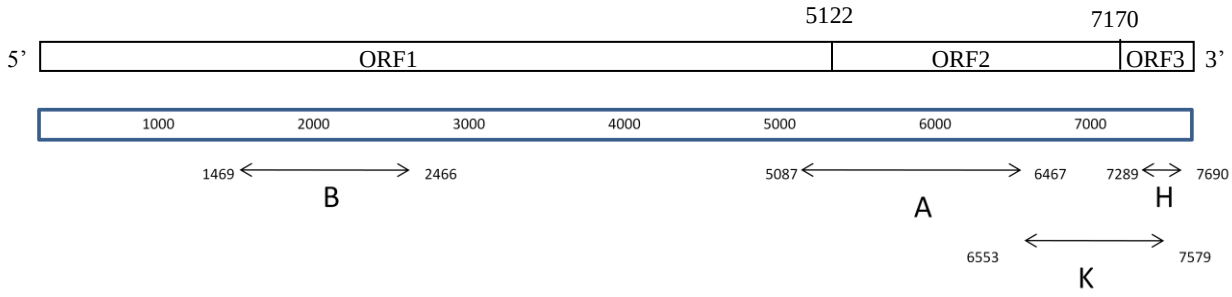

Figure 6.6. Position of sequence parts A, B, H and K as compared to FCV-F9 (Genbank M86379). Numbers at the end of each arrow show the base position start number and end number. Diagram above shows the position of the three open reading frames found upon FCV-F9 including the position of the divisions labelled in nucleotides from 5' to 3'.

Each of the parts obtained for strain UKOS-A were compared to published complete FCV genome sequences and a bootstrapped phylogenetic tree constructed (Figs. 6.7-6.10). The list of genomes used in the alignment and comparison can be found in Table 6.4.

Table 6.4. Whole genome sequences used in alignments with UKOS-A partial sequences and phylogenetic tree construction. Strains UTCVM-H1 and UTCVM H2 are believed to be hypervirulent strains of FCV.

FCV strain name	Genbank Accession Number	Reference
FCV-F9	M86379	(Carter *et al.*, 1992)
FCV USDA	AY560118	(Abd-Eldaim *et al.*, 2005)
FCV 2024	AF479590	(Thumfart & Meyers, 2002)
FCV/DD/2006	DQ424892	Unpublished, submitted by Behm *et al* 2006
FCV F4	D31836	(Oshikamo *et al.*, 1994)
FCV GD	GU214989	Unpublished, submitted by Hua *et al* 2009
FCV F65	AF109465	(Glenn *et al.*, 1999)
FCV CFI/68	U13992	Unpublished, submitted by Neill 1998
FCV Urbana	L40021	(Sosnovtsev & Green, 1995)
FCV UTCVM-NH1	AY560113	(Abd-Eldaim *et al.*, 2005)
FCV UTCVM-NH2	AY560114	(Abd-Eldaim *et al.*, 2005)
FCV UTCVM-NH3	AY560115	(Abd-Eldaim *et al.*, 2005)
FCV UTCVM-H1	AY560116	(Abd-Eldaim *et al.*, 2005)
FCV UTCVM-H2	AY560117	(Abd-Eldaim *et al.*, 2005)

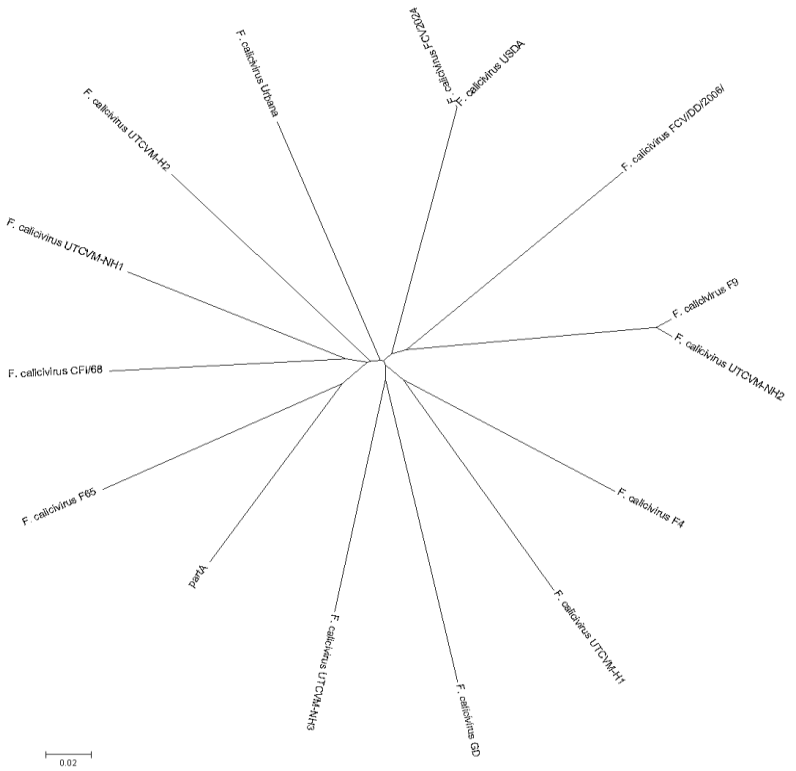

Figure 6.7. Bootstrapped phylogenetic tree based on alignment of whole genome sequences with part A of UKOS-A, polymerase gene to capsid gene sequence. Details of FCV whole genome sequences used in this comparison can be found in Table 6.4 .

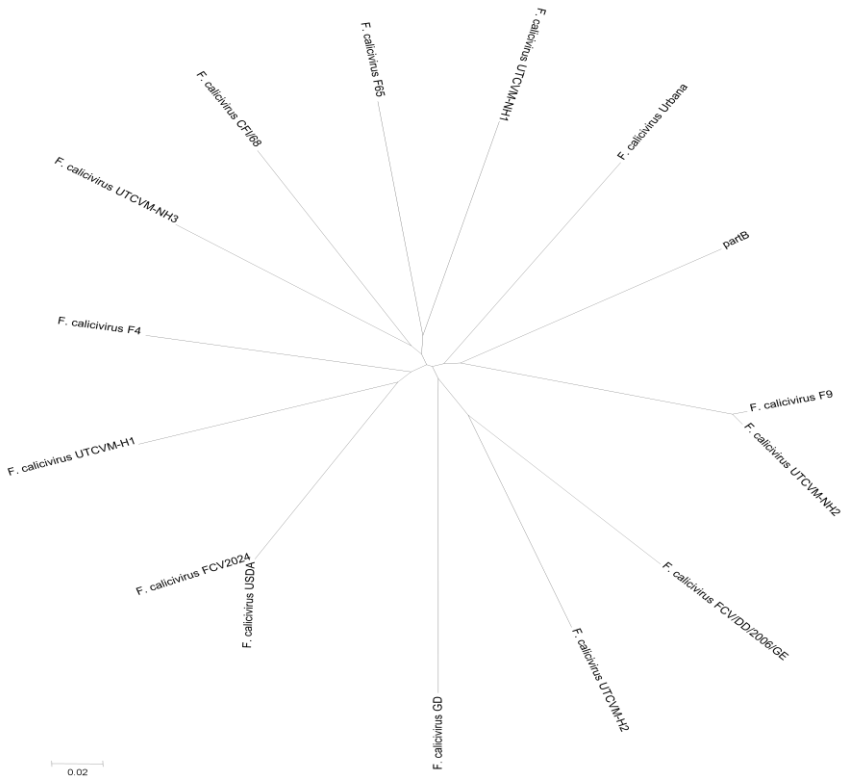

Figure 6.8. Bootstrapped phylogenetic tree based on alignment of whole genome sequences with part B of UKOS-A, partial ORF1 sequence coding for non-structural proteins. Details of FCV whole genome sequences used in this comparison can be found in Table 6.4

Figure 6.9. Bootstrapped phylogenetic tree based on alignment of whole genome sequences with part H of UKOS-A, ORF3 sequence encoding for VP2. Details of FCV whole genome sequences used in this comparison can be found in Table 6.4

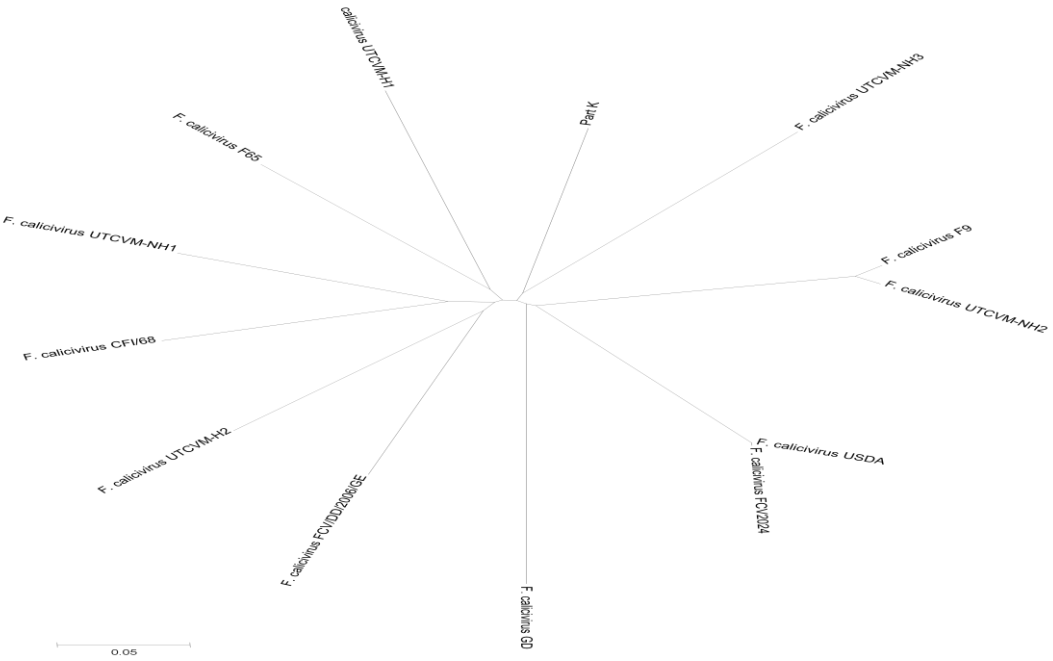

Figure 6.10. Bootstrapped phylogenetic tree based on alignment of whole genome sequences with part K of UKOS-A, ORF2 sequence encoding for viral protein VP1. Details of FCV whole genome sequences used in this comparison can be found in Table 6.4

The results of the phylogenetic tree analysis show that each part of the sequence obtained from UKOS-A is not related to any of the previously published full FCV genomes as it groups separately on every tree produced. Within the group of genomes used in the analysis were two hypervirulent strains isolated in USA in 1999 and 2002 (Abd-Eldaim *et al.*, 2005) designated UTCVM-H1 and UTCVM-H2. With the UKOS-A strain not grouping with either it appears that the strain evolved independently during each outbreak.

The Abd-Eldaim *et al* study also found evidence of motifs (Fig. 6.11) included in the amino acid sequence of the capsid protein VP1 for the hypervirulent strains and so evidence of these motifs being conserved within the UKOS-A strain was examined alongside further possible motifs highlighted in the Foley *et al* study (2006). The result of this investigation can be seen in figure 6.11.

```
        426                                                    480
        |                                                       |
UKOS    -S--T-----S---KN-----S-SD--S--E---T----S-----A---------
F9      PGELIPAGDYAITNGTGNDITTATGYDTADIIKNNTNFRGMYICGSLQRAWGDKK
KAOS    -E--T-------V---.S-IA-K-Q-EA-T--T-----KS---------------
CAT15   -NK-----------QS----Q-KEE-ES-M--S-----KS---------------
ARI     -EK-T-------VD-S------KDK-ES-V-------------------------
H1      ----T-------V-QNNS--A-KQA-ES-TS-E-----KS-------H-------
H2      -TV-T---K----S-NNS--L-RND-EN--V--------S--------------D
            #        #  ***     #   #
```

Figure 6.11. Alignment of the amino acid sequence of five VS-FCV strains (FCV-Kaos Genbank accession number DQ910795.1, Cat 15 Genbank accession number L40021, FCV-Ari Genbank accession number DQ910794, FCV UTCVM-H1 Genbank accession number AY560116 and FCV UTCVM-H2 Genbank accession number AY560117) with FCV-F9 and UKOS-A for the VP1 protein from residue 426 to residue 480. * denotes positions of suspected hypervirulent motifs reported in Abd-Eldaim *et al*, 2005. # denotes positions of suspected hypervirulent motifs reported in Foley *et al*, 2006.

The alignment results in Fig 6.11 show that none of the motifs reported in the previous studies are consistent across all five hypervirulent strains included and UKOS-A. Only two of the substitutions observed within the two previous studies were found to be present in the UKOS-A strain, the first motif from Foley *et al* at amino acid position 430 and the first substitution found within the Abd-Eldaim *et al* study at amino acid position 441. The final substitution found within the Foley *et al* paper (amino acid position 452) is also an interesting potential marker of hypervirulent strains as although it does not appear within the UKOS-A sequence it is consistently changed within the confirmed VS-FCV strains from aspartic acid to glutamic acid.

6.4 Discussion

The emergence of highly virulent strains of FCV has been a worrying development in recent times, with each outbreak of VS-FCV being associated with a high mortality rate and systemic clinical signs. Each reported outbreak has appeared to follow a very similar pattern, with the same symptoms being reported and with similar outcomes in each case. As the outbreaks appear to be so similar it may be most logical to assume that it is the same strain of virus circulating within each epizootic incident. However, each of the viral strains isolated and sequenced grouped separately on phylogenetic trees (Coyne *et al.*, 2006b; Hurley *et al.*, 2004; Pedersen *et al.*, 2000; Reynolds *et al.*, 2009; Schorr-Evans *et al.*, 2003). These findings prove that the viral strains isolated from each outbreak have evolved independently and are not a result of transmission of a single strain.

The origins of these strains and the evolution patterns associated with the outbreaks may be an important characteristic of the VS-FCV outbreaks and analysing them closely could give clues as to why these strains develop. In each of the VS-FCV reports, the outbreak is often anecdotally linked to the introduction of a cat or cats from a shelter into a veterinary hospital or private household. However, to date, this link has never been proven by molecular epidemiology and sequence analysis. In the UK outbreak, this link between the infection within the private households and the rescue shelter has been previously suggested based on partial polymerase gene sequences (Coyne *et al.*, 2006a). In this study we have confirmed this finding by showing that capsid sequences from the outbreak also cluster closely with viruses within the rescue shelter (Fig 6.2).

In previous studies within multi-cat colonies and shelters it has been shown that FCV evolves progressively within a population to allow re-infection of previously infected cats (Coyne *et al.*, 2007) and also that two strains of FCV have the ability to recombine to provide an additional mechanism to rapidly evolve strains with a greater infectivity within a colony. From analyses performed within this chapter and previously (Coyne, 2005) there is evidence that both of these mechanisms may have been employed by the virus within the shelter at the time of the evolution of the UKOS strains. Figure 6.2 shows a large number of strains grouped within group 1 for the polymerase gene which is the group that included the UKOS strains which is

indicative of a gradual evolution towards the outbreak strains. The capsid gene sequence analysis shown in Figure 6.2 also gave evidence that recombination may have been occurring within the FCV strains in the shelter with isolates R580 and R593 grouping differently on the capsid and polymerase genes. Further investigation of these possible recombination events was attempted by sequencing from polymerase gene to capsid gene; however, amplification of isolate R593 was unsuccessful. Analysis of the sequence obtained for isolate R580 suggested that the mismatched grouping between the polymerase and capsid gene was not a result of recombination but was more likely to be a product of a mixed infection. The alternate grouping along the polymerase and capsid trees is therefore most probably due to the PCRs performed for both of these genes preferentially amplifying different strains in the capsid and polymerase region, giving the false impression of a recombination event. A mixed infection may also be the reason R593 was difficult to amplify from polymerase gene to capsid gene. The primers used were designed from the sequences obtained from the capsid gene and polymerase gene amplifications and if these were generated from two separate strains then the primers pairs will have been unlikely to match up. This observation is why recombination events should only be formally defined based on sequencing a single molecule (Coyne *et al.*, 2006c).

Within this chapter an attempt was also made to sequence the entire genome of UKOS-A to try and identify genetic lesions associated with its putative hypervirulent phenotype. Unfortunately whole genome sequence could not be obtained and this may be due to the method used as designing primer pairs for a virus known to have such a variable genome is difficult. As demonstrated in the previous chapter (chapter 5) next-generation sequencing could be the answer to this problem as during the RNA-seq experiment the FCV-F9 genome was sequenced to a coverage of ~50 000x in a relatively short space of time and without the need to design primer pairs based upon variable genomes.

Abd-Eldaim *et al* in 2005 did manage to obtain full genome sequence two VS-FCV strains and compare these to three FCV strains isolated from cats exhibiting clinical signs of more typical FCV infection. The results of the sequence analysis in this 2005 study found that each strain was approximately 80% similar to other FCV strains suggesting that the VS-FCV strains sequenced are no more similar or

different than more typical FCV strains sequenced. These finding are consistent with those found in this chapter. In particular, in each of the four parts of UKOS-A sequenced, the virus was found to be equally distinct from other FCV strains, whether they were obtained from hypervirulent or more typical outbreaks of FCV-related disease.

The UKOS-A strain was also examined to discover whether it contained any of the sequence motifs previously observed to be a marker of hypervirulent strains in the amino acid sequence of the VP1 protein (Abd-Eldaim *et al.*, 2005; Foley *et al.*, 2006) (Fig 6.11). There were no motifs identified that were consistently found in all of the hypervirulent strains studies and the UKOS-A strain. There were two amino acid substitutions found in these previous studies which also appeared within the translated UKOS-A sequence but there was also one motif found that had a consistent amino acid substitution within all of the VS-FCV strains but was absent from the UKOS-A strain. It is worth noting at this point that UKOS-A is a putative hypervirulent strain, it has not been used to recreate VSD experimentally in cats and so this may be a reason it does not share this consistent amino acid substitution with the confirmed VS-FCV strains. There is also evidence that these changes which are consistent within the VS-FCV strains may occur as part of the natural variation found within these regions of the capsid protein as a further brief search using this motif at amino acid position 452 shows that non-virulent strains from Australia (Genbank accession number AAF186244) and the UK (Genbank accession number ABD72469) also show the change from aspartic acid to glutamic acid at this position.

The lack of consistent genetic changes associated with the virulent strains of FCV is not a trait that is unique within the *Caliciviridae*. Rabbit Haemorrhagic Disease Virus (RHDV) has also been found to have pathogenic and non-pathogenic strains of virus and analysis of the genetic diversity of these phenotypically different virus strains has been unable to find a genetic cause of virulence (Moss *et al.*, 2002; White *et al.*, 2004). It may therefore be a characteristic of the calicivirus family that pathogenesis associated with strains may be determined more by host-immune response than the genetic characteristics of the virus strains. However, since the hypervirulent phenotype can be reproduced experimentally for both RHDV and FCV, it suggests that as yet unidentified, subtle and perhaps inconsistent genetic

lesions are responsible for this complex phenotype in each outbreak. Ultimately, it will be necessary to sequence many more virulent viruses in order to identify any such subtle lesions within the complex diversity observed between distinct FCV strains.

In summary, within this chapter we have been able to obtain sequence for 46% of the UKOS-A genome including all of ORF3 and all but 86 bases of ORF2. Analysis of the sequence has shown that there were no large scale genetic mutations identified and no substitution consistently found within VS-FCV strains was found within the UKOS-A strain. This suggests that these mutations may not be necessary for virulence however, UKOS-A is not a proven VSD causing strain and until experimental infections are conducted it is difficult to include this strain alongside the other VS-FCV strains.

7 Chapter seven

General discussion and future perspectives

This thesis aimed to use new post-genomic techniques and technologies to examine the molecular pathogenesis of feline calicivirus (FCV) infection and also the validity of using these techniques within a virological setting.

Previous work has established FCV as a model virus for studying the *Caliciviridae* as it readily replicates in cell culture (Bidawid *et al.*, 2003), has a well defined host and a broad spectrum of virulence and clinical signs exhibited by infected cats (Radford *et al.*, 2007). These characteristics were desirable in this study as it meant that suitable quantities of cellular protein and mRNA could be produced for both infected and mock infected samples and also, a number of different strains could be examined to discover whether there were differences in the way the strains manipulated the host cell at the molecular level.

Using FCV as a model virus in these systems was not without its difficulties, not least being the fact that the cat does not have a completely sequenced or annotated genome. The current release of the feline genome has a 1.9x coverage which means that there is only ~65% of the sequence available with ~20 000 putative genes annotated (Pontius *et al.*, 2007). As a result bioinformatic analyses are not as straightforward as using a host with a fully annotated genome such as mice and humans. However, as genomes are constantly being re-annotated and updated the data collected and archived throughout this thesis can still be re-analysed and re-evaluated as these new updates are released. There are also opportunities for using the data acquired within this thesis in aiding the feline genome project. The data collected from the proteomics and RNA-seq experiments contain information on actual gene transcripts obtained from a feline cell line and as such can be useful in defining exon boundaries and splice sites as has been proven with other mammalian (Liu *et al.*, 2010; Mortazavi *et al.*, 2008) and also pathogen genomes (Xia *et al.*, 2008). Within this thesis it has been shown that proteomic and transcriptomic studies can be used successfully upon virally infected cells in a non-model host and at the time of writing, is the first study to use RNA-seq to examine the effects of viral

infection upon the transcriptome in a host which currently does not have a deeply sequenced genome available.

The most consistent results gained from the proteomic analysis of both a single FCV strain and comparison of four FCV strains is that modulation of proteins involved in maintaining the cellular cytoskeleton occurs during each viral infection. These results, whilst they are the first of their kind found during infection with FCV, are in keeping with findings presented by authors of studies using other viruses. One of the best characterised viral modulators of the host cytoskeleton is vaccinia virus which uses host actin proteins to form tails beneath the virion (Cudmore *et al.*, 1995) and to create cellular projections to facilitate cell-to-cell spread (Sanderson *et al.*, 1998). Vaccinia virus has also be shown to move within the cell using microtubules (Carter *et al.*, 2003; Mallardo *et al.*, 2001) which is consistent with the conclusions drawn by Sodiek in 2000 which stated that viruses moving by diffusion alone within the cytoplasm would take considerably longer than is observed in experimental analysis (Sodeik, 2000).

There are now many other examples of cytoskeletal modulation during viral infections with bluetongue virus having been shown to need vimentin in order to exit the cell (Bhattacharya *et al.*, 2007) and hepatitis E viral proteins having been demonstrated to interact with microtubules (Kannan *et al.*, 2009). Not every virus has been found to interact with these proteins in the same manner and there have also been differences found within viral families and strains regarding the modulation of cytoskeletal proteins. For example, within the *Picornaviridae* foot-and-mouth disease virus (FMDV) has been shown to disrupt the tethering of microtubules to the microtubule organising centre. In contrast, another virus from the same family, bovine enteric virus (BEV), did not show the same effects (Armer *et al.*, 2008). These two viruses also differed in their modulation of vimentin with FMDV drawing vimentin around the replication site whereas BEV proteins and vimentin were both found co-localised within the replication centre. Differences have also been found with different strains of the same virus. Two strains of equine herpesvirus 1 (EHV-1) were used to infect two different cell lines and their effects upon the host cytoskeleton were examined (Turowska *et al.*, 2010). The authors discovered that each of the EHV strains had opposing effects in each of the cell lines examined with the attenuated strain disrupting actin polymerisation with equine cells but the wild-

type strain not having the same effect. Within the second cell line used (Vero cells) the wild-type strain modulate both F-actin and microtubules but the attenuated cells had no discernable effects upon the cytoskeleton. These results tie in with the finding from the 2D-DIGE experiment performed in this thesis upon four FCV strains as the analysis showed that for the majority of modulated host cell proteins the viral strains appear to affect them in different ways and to different extents.

The identification of host cytoskeletal proteins as targets for viral modulation could offer some new avenues for development of antiviral drugs for combating FCV infection. Tubulin binding agents are already used in the therapeutic treatment of tumour cells in cancer to prevent tumour spread by inhibiting the cells motility and its ability to perform mitosis and increase tumour spread (Dumontet & Jordan, 2010). Whilst these therapeutic drugs do prevent tumour spread, they are not selective and also cause damage to non-cancerous cells. If a similar therapy was designed to combat virally infected cells then it would encounter the same problem in that whilst it may have an effect of preventing viral spread, it would also detrimentally affect the non-infected cells in the surrounding area. Cancer therapeutics combat this by carefully balancing these toxic side effects with the minimum dose necessary to inhibit tumour growth and it is possible that a balance could also be found for antiviral therapy. However, the severity of the clinical signs exhibited during the viral infection would have to outweigh the side effects caused by these types of therapeutic drugs.

To examine these changes further, three proteins were chosen from the 2D-DIGE results from the single strain and multiple strain experiments and were tracked using immunofluorescent staining and confocal microscopy. The results of imaging showed that whilst all viral strains changed the fluorescent staining of tubulin and vimentin significantly there were also subtle differences exhibited in strain-to-strain comparisons. The most obvious differences were the presence and absence of cellular blebs and also the presence and absence of viral antigen within these blebs. The UKOS-A strain was the only strain not to produce blebbing on the cell periphery which may be a sign of a different mechanism of infection or may be because the blebs are transient in nature and the cells were simply fixed at the wrong time to capture them. Only strain R591 showed viral antigen co-localising within the blebs during infection at both 7 and 13 h p.i., this could be evidence of this strain of FCV

using the blebs for viral egress in a similar manner to the protrusions observed with vaccinia virus (Cudmore *et al.*, 1995). This blebbing has been observed previously with FCV infection (Knowles, 1988) and is also thought to be a signature of apoptosis (Bovellan *et al.*, 2010) which may confirm previous studies which showed that FCV induces apoptosis for use in viral protein processing (Al-Molawi *et al.*, 2003; Natoni *et al.*, 2006). Further analysis of the confocal images has shown that there are significant changes to the expression of both tubulin and vimentin within cells infected with all strains of FCV examined; however, these images do not show the entire story and so further work would have to be performed. This may be as straightforward as repeating the examination with more time points to discover whether the modulation of the cytoskeletal proteins and blebbing occurs at different times with different strains or developing a live cell imaging assay to follow the effects of infection upon these proteins in real time. A live cell imaging assay would be a powerful tool for investigating host cell responses to infection and has been used successfully with other viruses such as vaccinia virus (Mercer & Helenius, 2008) and vesicular stomatitis virus (Cureton *et al.*, 2010). A molecular clone of FCV has already been shown to be able to replicate in cell culture and express fluorescent reporter proteins (Abente *et al.*, 2010). If a cell line could be found which would express fluorescent proteins as well as being susceptible to infection with the FCV molecular clone then this system could be used with live cell imaging confocal microscopy to target some of the proteins identified as modulated within this thesis.

It is also possible that these subtle differences in the modulation of the host cell proteome found with the different strains of FCV are possible markers of the differential virulence associated with each isolate. At present there are no consistent antigenic or genotypic markers (as examined in chapter 6) and the only phenotypic marker found to date is that VS-FCV strains grow quicker under multiple infection cycle conditions *in vitro*, but this phenotype could not be reproduced in this thesis (Ossiboff *et al.*, 2007). Again, there is not enough information garnered from the 2D-DIGE to confirm that any of the proteins identified could be used as markers for virulence but it has provided a list of potential proteins which could be analysed further to discover whether the differential modulation patterns are consistent across the VS-FCV strains. There has also been the added complication within this thesis of using a putative hypervirulent strain of FCV to attempt to discover protein markers.

In order to confirm whether or not a FCV strain does cause VSD in cats an experimental infection would have to be performed and as such there are very few known VS-FCV strains available which is why a putative hypervirulent strain was used throughout this thesis. If experiments were to be repeated, the inclusion of a known VS-FCV strain alongside the putative UKOS-A strain could offer greater insights into which proteins are suitable markers for virulence which, in future, could be used in place of experimental infections in the confirmation of hypervirulence.

As stated above, the blebbing observed in the confocal images may also be a sign that the infected cells are undergoing apoptosis which has been reported previously during infection with FCV (Natoni *et al.*, 2006; Roberts *et al.*, 2003; Sosnovtsev *et al.*, 2003) and capsases activated during apoptosis have been shown to cleave the viral capsid protein (Al-Molawi *et al.*, 2003). The analysis of the RNA-seq data also offered some correlation with these previous findings as a number of differentially transcribed genes were found to be up-regulated within the apoptosis regulatory pathway again suggesting that the virus is inducing apoptosis rather than inhibiting its onset.

Overall comparison of the differentially expressed genes from the RNA-seq experiment to the differentially expressed proteins identified within the two 2D-DIGE experiments does not appear to show a very strong correlation between the two data sets. This phenomenon is not entirely unexpected as alteration of gene transcript levels and alteration of protein levels, though they are obviously linked, are two very different measurements. It has been suggested that transcriptional and translational networks have evolved independently within the cell and that the relationship between the two diverges with evolution as bacterial transcriptome and proteomes often show good correlation whereas mammalian samples show a much poorer correlation (Rogers *et al.*, 2008). Another hypothesis for these discrepancies in correlation is that there may be a time-delayed component to transcription-translation correlation and if you are able to take that into account then the correlation is greater (Wang *et al.*, 2010). By taking transcriptional data at the same time points as the proteomic data within this thesis the chances of the two data sets correlating may have been diminished. Therefore, in future studies where RNA-seq is to be used alongside proteomics it may be worthwhile to take these time delays into account during experimental design and possibly use different time points for

each analysis. A further complexity when looking at proteomes and transcriptomes is that genes do not act uniformly and the delays observed within a transcriptome-translation comparison may be unique for each modulated gene as well as each transcript and protein having a unique degradation and turnover rate. For these complexities to be taken into account an experiment may have to be designed which can track protein turnover and expression in the face of viral infection such as a labelled pulse chase study which has been successfully employed in other studies examining the effects of viral infection upon host cell proteins (Bruce *et al.*, 2009).

A further outcome of the RNA-seq experiment was that transcripts generated from the FCV-F9 virus were sequenced and the reads could be mapped to the FCV-F9 genome. This gave an average coverage of ~50 000x of the viral genome and demonstrates the possibility of using these next-generation sequence technologies in viral genome sequencing. As the attempt to sequence the whole genome putative virulent strain, UKOS-A, within this thesis was ultimately unsuccessful it may be useful in future to employ next-generation sequencers to guarantee rapid whole genome sequencing. This would eliminate the need for prior amplification through PCR and as such would eliminate the requirement to design primers based on homologous sequences that often fail to recognise their target sequence due to the variability present throughout the FCV genome.

The undifferentiated cell line used within this thesis was chosen as a surrogate for a whole cat system. However, it may also be useful to use these techniques to investigate the effects of FCV infection upon a tissue culture derived from areas in which FCV virions can be isolated such as the upper respiratory tract. *In vivo* modelling would be the ideal environment in which to investigate host responses to FCV infection and now that it has been proven that post-genomic technologies can be applied to a feline host it may be worth investigating this option again in the near future.

The work completed within this thesis has proven that proteomic and transcriptomic techniques can be used to investigate host changes in response to viral challenge even within a non-model host organism. The results have shown that during infection with FCV, the host cytoskeletal proteins are modulated and these effects have been followed successfully for two cytoskeletal proteins using confocal microscopy with immunofluorescent staining. As for the other proteins and genes

found to be differentially expressed, their significance to viral replication can only be speculated upon. The global nature of the experiments conducted gives a good preliminary examination of the mechanisms of viral modulation of the host but it cannot give a definitive answer as to whether these modulations are essential for viral replication. However, the genes and proteins highlighted within this study can act as a good starting point for further investigations such as providing a list of candidate proteins for absolute quantification and live cell imaging analysis.

There is also scope for repeating this kind of post-genomic analysis with either a different *in vitro* model or even through use of an *in vivo* model. The discovery of murine norovirus (MNV) and its ability to grow in cell culture (Karst *et al.*, 2003) means it would be a good candidate to use these post-genomic techniques upon especially as the host genome is sequenced and annotated to a high standard. Using a mouse virus within a murine cell line would also offer the advantage of readily available mouse-specific reagents and laboratory mice for *in vivo* experimentation.

In conclusion, we have demonstrated the utility of modern "omic" technologies to the study of viral pathogenesis. Study of both the proteome and transcriptome of cells infected with FCV has identified new pathways that are modulated during infection and helped to confirm others. Our studies also suggest that such technologies may provide a new, sequence independent way of determining the sequence of variable viruses such as FCV.

Abd-Eldaim, M., Potgieter, L. & Kennedy, M. (2005). Genetic analysis of feline caliciviruses associated with a hemorrhagic-like disease. *J Vet Diagn Invest* **17**, 420-429.

Abente, E. J., Sosnovtsev, S. V., Bok, K. & Green, K. Y. (2010). Visualization of feline calicivirus replication in real-time with recombinant viruses engineered to express fluorescent reporter proteins. *Virology* **400**, 18-31.

Abramoff, M. D., Magelhaes, P. J. & Ram, S. J. (2004). Image Processing with ImageJ. *Biophotonics International* **11**, 36-42.

Addie, D., Poulet, H., Golder, M. C., McDonald, M., Brunet, S., Thibault, J. C. & Hosie, M. J. (2008). Ability of antibodies to two new caliciviral vaccine strains to neutralise feline calicivirus isolates from the UK. *The Veterinary record* **163**, 355-357.

Adler, J. L. & Zickl, R. (1969). Winter vomiting disease. *J Infect Dis* **119**, 668-673.

Al-Molawi, N., Beardmore, V. A., Carter, M. J., Kass, G. E. & Roberts, L. O. (2003). Caspase-mediated cleavage of the feline calicivirus capsid protein. *The Journal of general virology* **84**, 1237-1244.

Alonso, C., Oviedo, J. M., Martin-Alonso, J. M., Diaz, E., Boga, J. A. & Parra, F. (1998). Programmed cell death in the pathogenesis of rabbit hemorrhagic disease. *Archives of virology* **143**, 321-332.

Anders (2010). differential expression analysis for sequence count data. *Nature Precedings*.

Arcangeletti, M. C., De Conto, F., Ferraglia, F., Pinardi, F., Gatti, R., Orlandini, G., Covan, S., Motta, F., Rodighiero, I., Dettori, G. & Chezzi, C. (2008). Host-cell-dependent role of actin cytoskeleton during the replication of a human strain of influenza A virus. *Archives of virology* **153**, 1209-1221.

Armer, H., Moffat, K., Wileman, T., Belsham, G. J., Jackson, T., Duprex, W. P., Ryan, M. & Monaghan, P. (2008). Foot-and-mouth disease virus, but not bovine enterovirus, targets the host cell cytoskeleton via the nonstructural protein 3Cpro. *Journal of virology* **82**, 10556-10566.

Ayodeji, M., Kulka, M., Jackson, S. A., Patel, I., Mammel, M., Cebula, T. A. & Goswami, B. B. (2009). A microarray based approach for the identification of common foodborne viruses. *Open Virol J* **3**, 7-20.

Backes, P., Quinkert, D., Reiss, S., Binder, M., Zayas, M., Rescher, U., Gerke, V., Bartenschlager, R. & Lohmann, V. (2010). Role of annexin A2 in the production of infectious hepatitis C virus particles. *Journal of virology* **84**, 5775-5789.

Bailey, D., Kaiser, W. J., Hollinshead, M., Moffat, K., Chaudhry, Y., Wileman, T., Sosnovtsev, S. V. & Goodfellow, I. G. (2010). Feline calicivirus p32, p39 and p30 proteins localize to the endoplasmic reticulum to initiate replication complex formation. *The Journal of general virology* **91**, 739-749.

Baltimore, D. (1971). Expression of animal virus genomes. *Bacteriol Rev* **35**, 235-241.

Bannasch, M. J. & Foley, J. E. (2005). Epidemiologic evaluation of multiple respiratory pathogens in cats in animal shelters. *Journal of feline medicine and surgery* **7**, 109-119.

Barros, E., Lezar, S., Anttonen, M. J., van Dijk, J. P., Rohlig, R. M., Kok, E. J. & Engel, K. H. (2010). Comparison of two GM maize varieties with a near-isogenic non-GM variety using transcriptomics, proteomics and metabolomics. *Plant Biotechnol J* **8**, 436-451.

Benjamini, Y. & Hochberg, Y. (1995). Controlling the false discovery rate: a practical and powerful approach to multiple testing.. *J Roy Stat Soc* **57**, 289-300.

Bentley, D. R., Balasubramanian, S., Swerdlow, H. P., Smith, G. P., Milton, J., Brown, C. G., Hall, K. P., Evers, D. J., Barnes, C. L., Bignell, H. R., Boutell, J. M., Bryant, J., Carter, R. J., Keira Cheetham, R., Cox, A. J., Ellis, D. J., Flatbush, M. R., Gormley, N. A., Humphray, S. J., Irving, L. J., Karbelashvili, M. S., Kirk, S. M., Li, H., Liu, X., Maisinger, K. S., Murray, L. J., Obradovic, B., Ost, T., Parkinson, M. L., Pratt, M. R., Rasolonjatovo, I. M., Reed, M. T., Rigatti, R., Rodighiero, C., Ross, M. T., Sabot, A., Sankar, S. V., Scally, A., Schroth, G. P., Smith, M. E., Smith, V. P., Spiridou, A., Torrance, P. E., Tzonev, S. S., Vermaas, E. H., Walter, K., Wu, X., Zhang, L., Alam, M. D., Anastasi, C., Aniebo, I. C., Bailey, D. M., Bancarz, I. R., Banerjee, S., Barbour, S. G., Baybayan, P. A., Benoit, V. A., Benson, K. F., Bevis, C., Black, P. J., Boodhun, A., Brennan, J. S., Bridgham, J. A., Brown, R. C., Brown, A. A., Buermann, D. H., Bundu, A. A., Burrows, J. C., Carter, N. P., Castillo, N., Chiara, E. C. M., Chang, S., Neil Cooley, R., Crake, N. R., Dada, O. O., Diakoumakos, K. D., Dominguez-Fernandez, B., Earnshaw, D. J., Egbujor, U. C., Elmore, D. W., Etchin, S. S., Ewan, M. R., Fedurco, M., Fraser, L. J., Fuentes Fajardo, K. V., Scott Furey, W., George, D., Gietzen, K. J., Goddard, C. P., Golda, G. S., Granieri, P. A., Green, D. E., Gustafson, D. L., Hansen, N. F., Harnish, K., Haudenschild, C. D., Heyer, N. I., Hims, M. M., Ho, J. T., Horgan, A. M., Hoschler, K., Hurwitz, S., Ivanov, D. V., Johnson, M. Q., James, T., Huw Jones, T. A., Kang, G. D., Kerelska, T. H., Kersey, A. D., Khrebtukova, I., Kindwall, A. P., Kingsbury, Z., Kokko-Gonzales, P. I., Kumar, A., Laurent, M. A., Lawley, C. T., Lee, S. E., Lee, X., Liao, A. K., Loch, J. A., Lok, M., Luo, S., Mammen, R. M., Martin, J. W., McCauley, P. G., McNitt, P., Mehta, P., Moon, K. W., Mullens, J. W., Newington, T., Ning, Z., Ling Ng, B., Novo, S. M., O'Neill, M. J., Osborne, M. A., Osnowski, A., Ostadan, O., Paraschos, L. L., Pickering, L., Pike, A. C., Chris Pinkard, D., Pliskin, D. P., Podhasky, J., Quijano, V. J., Raczy, C., Rae, V. H., Rawlings, S. R., Chiva Rodriguez, A., Roe, P. M., Rogers, J., Rogert Bacigalupo, M. C., Romanov, N., Romieu, A., Roth, R. K., Rourke, N. J., Ruediger, S. T., Rusman, E., Sanches-Kuiper, R. M., Schenker, M. R., Seoane, J. M., Shaw, R. J., Shiver, M. K., Short, S. W., Sizto, N. L., Sluis, J. P., Smith, M. A., Ernest Sohna Sohna, J., Spence, E. J., Stevens, K., Sutton, N., Szajkowski, L., Tregidgo, C. L., Turcatti, G., Vandevondele, S., Verhovsky, Y., Virk, S. M., Wakelin, S., Walcott, G. C., Wang, J., Worsley, G. J., Yan, J., Yau, L., Zuerlein, M., Mullikin, J. C., Hurles, M. E., McCooke, N. J., West, J. S., Oaks, F. L., Lundberg, P. L., Klenerman, D., Durbin, R. & Smith, A. J. (2008). Accurate whole human genome sequencing using reversible terminator chemistry. *Nature* **456**, 53-59.

Bhattacharya, B., Noad, R. J. & Roy, P. (2007). Interaction between Bluetongue virus outer capsid protein VP2 and vimentin is necessary for virus egress. *Virology journal* **4**, 7.

Bhella, D., Gatherer, D., Chaudhry, Y., Pink, R. & Goodfellow, I. G. (2008). Structural insights into calicivirus attachment and uncoating. *Journal of virology* **82**, 8051-8058.

Bidawid, S., Malik, N., Adegbunrin, O., Sattar, S. A. & Farber, J. M. (2003). A feline kidney cell line-based plaque assay for feline calicivirus, a surrogate for Norwalk virus. *Journal of virological methods* **107**, 163-167.

Binns, S. H., Dawson, S., Speakman, A. J., Cuevas, L. E., Hart, C. A., Gaskell, C. J., Morgan, K. L. & Gaskell, R. M. (2000). A study of feline upper respiratory tract disease with reference to prevalence and risk factors for infection with feline calicivirus and feline herpesvirus. *Journal of feline medicine and surgery* **2**, 123-133.

Bittle, J. L. & Rubic, W. J. (1976). Immunization against feline calicivirus infection. *Am J Vet Res* **37**, 275-278.

Bittle, Y. C., Newberne JW & Martin M (1960). Serological relationships of new feline cytoplathic viruses. *American Journal of Veterinary Research* **21**, 547-550.

Black, D. N., Burroughs, J. N., Harris, T. J. & Brown, F. (1978). The structure and replication of calicivirus RNA. *Nature* **274**, 614-615.

Bok, K., Prikhodko, V. G., Green, K. Y. & Sosnovtsev, S. V. (2009). Apoptosis in murine norovirus-infected RAW264.7 cells is associated with downregulation of survivin. *Journal of virology* **83**, 3647-3656.

Bovellan, M., Fritzsche, M., Stevens, C. & Charras, G. (2010). Death-associated protein kinase (DAPK) and signal transduction: blebbing in programmed cell death. *The FEBS journal* **277**, 58-65.

Bridger, J. C. (1980). Detection by electron microscopy of caliciviruses, astroviruses and rotavirus-like particles in the faeces of piglets with diarrhoea. *The Veterinary record* **107**, 532-533.

Bridger, J. C., Hall, G. A. & Brown, J. F. (1984). Characterization of a calici-like virus (Newbury agent) found in association with astrovirus in bovine diarrhea. *Infection and immunity* **43**, 133-138.

Brinkman, N. E. & Fout, G. S. (2009). Development and evaluation of a generic tag array to detect and genotype noroviruses in water. *Journal of virological methods* **156**, 8-18.

Bruce, S. R., Atkins, C. L., Colasurdo, G. N. & Alcorn, J. L. (2009). Respiratory syncytial virus infection alters surfactant protein A expression in human pulmonary epithelial cells by reducing translation efficiency. *Am J Physiol Lung Cell Mol Physiol* **297**, L559-567.

Burki, F. (1965). Picornaviruses of cats. *Archiv fur die gesamte Virusforschung* **15**, 690-696.

Burroughs, J. N. & Brown, F. (1974). Physico-chemical evidence for the re-classification of the caliciviruses. *The Journal of general virology* **22**, 281-286.

Burroughs, J. N., Doel, T. R., Smale, C. J. & Brown, F. (1978). A model for vesicular exanthema virus, the prototype of the calicivirus group. *The Journal of general virology* **40**, 161-174.

Cai, Y., Fukushi, H., Koyasu, S., Kuroda, E., Yamaguchi, T. & Hirai, K. (2002). An etiological investigation of domestic cats with conjunctivitis and upper respiratory tract disease in Japan. *J Vet Med Sci* **64**, 215-219.

Capucci, L., Fusi, P., Lavazza, A., Pacciarini, M. L. & Rossi, C. (1996). Detection and preliminary characterization of a new rabbit calicivirus related to rabbit hemorrhagic disease virus but nonpathogenic. *Journal of virology* **70**, 8614-8623.

Carstens, E. B. & Ball, L. A. (2009). Ratification vote on taxonomic proposals to the International Committee on Taxonomy of Viruses (2008). *Archives of virology* **154**, 1181-1188.

Carter, G. C., Rodger, G., Murphy, B. J., Law, M., Krauss, O., Hollinshead, M. & Smith, G. L. (2003). Vaccinia virus cores are transported on microtubules. *The Journal of general virology* **84**, 2443-2458.

Carter, M. J. (1989). Feline calicivirus protein synthesis investigated by western blotting. *Archives of virology* **108**, 69-79.

Carter, M. J., Milton, I. D., Meanger, J., Bennett, M., Gaskell, R. M. & Turner, P. C. (1992). The complete nucleotide sequence of a feline calicivirus. *Virology* **190**, 443-448.

Carter, M. J., Routledge, E. G. & Toms, G. L. (1989). Monoclonal antibodies to feline calicivirus. *The Journal of general virology* **70 (Pt 8)**, 2197-2200.

Chang, K. O. (2009). Role of cholesterol pathways in norovirus replication. *Journal of virology* **83**, 8587-8595.

Chang, K. O., Sosnovtsev, S. V., Belliot, G., Kim, Y., Saif, L. J. & Green, K. Y. (2004). Bile acids are essential for porcine enteric calicivirus replication in association with down-regulation of signal transducer and activator of transcription 1. *Proceedings of the National Academy of Sciences of the United States of America* **101**, 8733-8738.

Charras, G. T. (2008). A short history of blebbing. *J Microsc* **231**, 466-478.

Chasey, D., Lucas, M., Westcott, D. & Williams, M. (1992). European brown hare syndrome in the U.K.; a calicivirus related to but distinct from that of viral haemorrhagic disease in rabbits. *Archives of virology* **124**, 363-370.

Chaudhry, Y., Nayak, A., Bordeleau, M. E., Tanaka, J., Pelletier, J., Belsham, G. J., Roberts, L. O. & Goodfellow, I. G. (2006). Caliciviruses differ in their functional requirements for eIF4F components. *The Journal of biological chemistry* **281**, 25315-25325.

Chen, R., Neill, J. D., Estes, M. K. & Prasad, B. V. (2006). X-ray structure of a native calicivirus: structural insights into antigenic diversity and host specificity. *Proceedings of the National Academy of Sciences of the United States of America* **103**, 8048-8053.

Chen, W., Gao, N., Wang, J. L., Tian, Y. P., Chen, Z. T. & An, J. (2008). Vimentin is required for dengue virus serotype 2 infection but microtubules are not necessary for this process. *Archives of virology* **153**, 1777-1781.

Chiba, S., Sakuma, Y., Kogasaka, R., Akihara, M., Terashima, H., Horino, K. & Nakao, T. (1980). Fecal shedding of virus in relation to the days of illness in infantile gastroenteritis due to calicivirus. *J Infect Dis* **142**, 247-249.

Clay, S., Maherchandani, S., Malik, Y. S. & Goyal, S. M. (2006). Survival on uncommon fomites of feline calicivirus, a surrogate of noroviruses. *Am J Infect Control* **34**, 41-43.

Cloonan, N., Forrest, A. R., Kolle, G., Gardiner, B. B., Faulkner, G. J., Brown, M. K., Taylor, D. F., Steptoe, A. L., Wani, S., Bethel, G., Robertson, A.

J., Perkins, A. C., Bruce, S. J., Lee, C. C., Ranade, S. S., Peckham, H. E., Manning, J. M., McKernan, K. J. & Grimmond, S. M. (2008). Stem cell transcriptome profiling via massive-scale mRNA sequencing. *Nat Methods* **5**, 613-619.

Coulombe, P. A. & Wong, P. (2004). Cytoplasmic intermediate filaments revealed as dynamic and multipurpose scaffolds. *Nat Cell Biol* **6**, 699-706.

Coyne, K. P. (2005). Epidemiology and evolution of feline calicivirus in naturally infected groups of domestic cats. *Thesis*.

Coyne, K. P., Dawson, S., Radford, A. D., Cripps, P. J., Porter, C. J., McCracken, C. M. & Gaskell, R. M. (2006a). Long-term analysis of feline calicivirus prevalence and viral shedding patterns in naturally infected colonies of domestic cats. *Veterinary microbiology* **118**, 12-25.

Coyne, K. P., Gaskell, R. M., Dawson, S., Porter, C. J. & Radford, A. D. (2007). Evolutionary mechanisms of persistence and diversification of a calicivirus within endemically infected natural host populations. *Journal of virology* **81**, 1961-1971.

Coyne, K. P., Jones, B. R., Kipar, A., Chantrey, J., Porter, C. J., Barber, P. J., Dawson, S., Gaskell, R. M. & Radford, A. D. (2006b). Lethal outbreak of disease associated with feline calicivirus infection in cats. *The Veterinary record* **158**, 544-550.

Coyne, K. P., Reed, F. C., Porter, C. J., Dawson, S., Gaskell, R. M. & Radford, A. D. (2006c). Recombination of Feline calicivirus within an endemically infected cat colony. *The Journal of general virology* **87**, 921-926.

Cudmore, S., Cossart, P., Griffiths, G. & Way, M. (1995). Actin-based motility of vaccinia virus. *Nature* **378**, 636-638.

Cureton, D. K., Massol, R. H., Whelan, S. P. & Kirchhausen, T. (2010). The length of vesicular stomatitis virus particles dictates a need for actin assembly during clathrin-dependent endocytosis. *PLoS pathogens* **6**.

Dawson, S., Bennett, D., Carter, S. D., Bennett, M., Meanger, J., Turner, P. C., Carter, M. J., Milton, I. & Gaskell, R. M. (1994). Acute arthritis of cats associated with feline calicivirus infection. *Res Vet Sci* **56**, 133-143.

Dawson, S., McArdle, F., Bennett, D., Carter, S. D., Bennett, M., Ryvar, R. & Gaskell, R. M. (1993a). Investigation of vaccine reactions and breakdowns after feline calicivirus vaccination. *The Veterinary record* **132**, 346-350.

Dawson, S., McArdle, F., Bennett, M., Carter, M., Milton, I. P., Turner, P., Meanger, J. & Gaskell, R. M. (1993b). Typing of feline calicivirus isolates from different clinical groups by virus neutralisation tests. *The Veterinary record* **133**, 13-17.

Dawson, S., Smyth, N. R., Bennett, M., Gaskell, R. M., McCracken, C. M., Brown, A. & Gaskell, C. J. (1991). Effect of primary-stage feline immunodeficiency virus infection on subsequent feline calicivirus vaccination and challenge in cats. *Aids* **5**, 747-750.

Di Martino, B. & Marsilio, F. (2010). Feline calicivirus VP2 is involved in the self-assembly of the capsid protein into virus-like particles. *Res Vet Sci* **89**, 279-281.

Domingo, E., Menendez-Arias, L. & Holland, J. J. (1997). RNA virus fitness. *Reviews in medical virology* **7**, 87-96.

Doultree, J. C., Druce, J. D., Birch, C. J., Bowden, D. S. & Marshall, J. A. (1999). Inactivation of feline calicivirus, a Norwalk virus surrogate. *J Hosp Infect* **41**, 51-57.

Drake, J. W. (1993). Rates of spontaneous mutation among RNA viruses. *Proceedings of the National Academy of Sciences of the United States of America* **90**, 4171-4175.

Drake, J. W. (1999). The distribution of rates of spontaneous mutation over viruses, prokaryotes, and eukaryotes. *Ann N Y Acad Sci* **870**, 100-107.

Drake, J. W. & Holland, J. J. (1999). Mutation rates among RNA viruses. *Proceedings of the National Academy of Sciences of the United States of America* **96**, 13910-13913.

Duizer, E., Schwab, K. J., Neill, F. H., Atmar, R. L., Koopmans, M. P. & Estes, M. K. (2004). Laboratory efforts to cultivate noroviruses. *The Journal of general virology* **85**, 79-87.

Dumontet, C. & Jordan, M. A. (2010). Microtubule-binding agents: a dynamic field of cancer therapeutics. *Nat Rev Drug Discov* **9**, 790-803.

Durinck, S., Moreau, Y., Kasprzyk, A., Davis, S., De Moor, B., Brazma, A. & Huber, W. (2005). BioMart and Bioconductor: a powerful link between biological databases and microarray data analysis. *Bioinformatics* **21**, 3439-3440.

Ehresmann, D. W. & Schaffer, F. L. (1977). RNA synthesized in calicivirus-infected cells is atypical of picornaviruses. *Journal of virology* **22**, 572-576.

Fastier, L. B. (1957). A new feline virus isolated in tissue culture. *Am J Vet Res* **18**, 382-389.

Faulstich, H., Zobeley, S., Rinnerthaler, G. & Small, J. V. (1988). Fluorescent phallotoxins as probes for filamentous actin. *J Muscle Res Cell Motil* **9**, 370-383.

Favoreel, H. W., Van Minnebruggen, G., Adriaensen, D. & Nauwynck, H. J. (2005). Cytoskeletal rearrangements and cell extensions induced by the US3 kinase of an alphaherpesvirus are associated with enhanced spread. *Proceedings of the National Academy of Sciences of the United States of America* **102**, 8990-8995.

Fenner, F. (1976). The classification and nomenclature of viruses. Summary of results of meetings of the International Committee on Taxonomy of Viruses in Madrid, September 1975. *The Journal of general virology* **31**, 463-470.

Flynn, W. T. & Saif, L. J. (1988). Serial propagation of porcine enteric calicivirus-like virus in primary porcine kidney cell cultures. *Journal of clinical microbiology* **26**, 206-212.

Foley, J., Hurley, K., Pesavento, P. A., Poland, A. & Pedersen, N. C. (2006). Virulent systemic feline calicivirus infection: local cytokine modulation and contribution of viral mutants. *Journal of feline medicine and surgery* **8**, 55-61.

Franke, E. K., Yuan, H. E. & Luban, J. (1994). Specific incorporation of cyclophilin A into HIV-1 virions. *Nature* **372**, 359-362.

Furman, L. M., Maaty, W. S., Petersen, L. K., Ettayebi, K., Hardy, M. E. & Bothner, B. (2009). Cysteine protease activation and apoptosis in Murine norovirus infection. *Virology journal* **6**, 139.

Gao, Y. & Sztul, E. (2001). A novel interaction of the Golgi complex with the vimentin intermediate filament cytoskeleton. *J Cell Biol* **152**, 877-894.

Gaskell, C. J., Gaskell, R. M., Dennis, P. E. & Wooldridge, M. J. (1982). Efficacy of an inactivated feline calicivirus (FCV) vaccine against challenge with United Kingdom field strains and its interaction with the FCV carrier state. *Res Vet Sci* **32**, 23-26.

Gavier-Widen, D. & Morner, T. (1993). Descriptive epizootiological study of European brown hare syndrome in Sweden. *J Wildl Dis* **29**, 15-20.

Geissler, K., Schneider, K., Platzer, G., Truyen, B., Kaaden, O. R. & Truyen, U. (1997). Genetic and antigenic heterogeneity among feline calicivirus isolates from distinct disease manifestations. *Virus research* **48**, 193-206.

Gill, M. B., Edgar, R., May, J. S. & Stevenson, P. G. (2008). A gamma-herpesvirus glycoprotein complex manipulates actin to promote viral spread. *PLoS ONE* **3**, e1808.

Glenn, M., Radford, A. D., Turner, P. C., Carter, M., Lowery, D., DeSilver, D. A., Meanger, J., Baulch-Brown, C., Bennett, M. & Gaskell, R. M. (1999). Nucleotide sequence of UK and Australian isolates of feline calicivirus (FCV) and phylogenetic analysis of FCVs. *Veterinary microbiology* **67**, 175-193.

Gonzalez-Reyes, S., Garcia-Manso, A., del Barrio, G., Dalton, K. P., Gonzalez-Molleda, L., Arrojo-Fernandez, J., Nicieza, I. & Parra, F. (2009). Role of annexin A2 in cellular entry of rabbit vesivirus. *The Journal of general virology* **90**, 2724-2730.

Goodfellow, I., Chaudhry, Y., Gioldasi, I., Gerondopoulos, A., Natoni, A., Labrie, L., Laliberte, J. F. & Roberts, L. (2005). Calicivirus translation initiation requires an interaction between VPg and eIF 4 E. *EMBO Rep* **6**, 968-972.

Green, K. Y., Ando, T., Balayan, M. S., Berke, T., Clarke, I. N., Estes, M. K., Matson, D. O., Nakata, S., Neill, J. D., Studdert, M. J. & Thiel, H. J. (2000). Taxonomy of the caliciviruses. *J Infect Dis* **181 Suppl 2**, S322-330.

Gruenbaum, L. M., Gilligan, D. M., Picciotto, M. R., Marinesco, S. & Carew, T. J. (2003). Identification and characterization of Aplysia adducin, an Aplysia cytoskeletal protein homologous to mammalian adducins: increased phosphorylation at a protein kinase C consensus site during long-term synaptic facilitation. *J Neurosci* **23**, 2675-2685.

Harbour, D. A., Howard, P. E. & Gaskell, R. M. (1991). Isolation of feline calicivirus and feline herpesvirus from domestic cats 1980 to 1989. *The Veterinary record* **128**, 77-80.

Harris, T. D., Buzby, P. R., Babcock, H., Beer, E., Bowers, J., Braslavsky, I., Causey, M., Colonell, J., Dimeo, J., Efcavitch, J. W., Giladi, E., Gill, J., Healy, J., Jarosz, M., Lapen, D., Moulton, K., Quake, S. R., Steinmann, K., Thayer, E., Tyurina, A., Ward, R., Weiss, H. & Xie, Z. (2008). Single-molecule DNA sequencing of a viral genome. *Science (New York, NY* **320**, 106-109.

Hashimoto, M., Roerink, F., Tohya, Y. & Mochizuki, M. (1999). Genetic analysis of the RNA polymerase gene of caliciviruses from dogs and cats. *J Vet Med Sci* **61**, 603-608.

Healey, K. A., Dawson, S., Burrow, R., Cripps, P., Gaskell, C. J., Hart, C. A., Pinchbeck, G. L., Radford, A. D. & Gaskell, R. M. (2007). Prevalence of feline chronic gingivo-stomatitis in first opinion veterinary practice. *Journal of feline medicine and surgery* **9**, 373-381.

Herbert, T. P., Brierley, I. & Brown, T. D. (1996). Detection of the ORF3 polypeptide of feline calicivirus in infected cells and evidence for its expression from a single, functionally bicistronic, subgenomic mRNA. *The Journal of general virology* **77 (Pt 1)**, 123-127.

Herbert, T. P., Brierley, I. & Brown, T. D. (1997). Identification of a protein linked to the genomic and subgenomic mRNAs of feline calicivirus and its role in translation. *The Journal of general virology* **78 (Pt 5)**, 1033-1040.

Holland, J., Spindler, K., Horodyski, F., Grabau, E., Nichol, S. & VandePol, S. (1982). Rapid evolution of RNA genomes. *Science (New York, NY* **215**, 1577-1585.

Howard, J. & Hyman, A. A. (2003). Dynamics and mechanics of the microtubule plus end. *Nature* **422**, 753-758.

Huang, C., Hess, J., Gill, M. & Hustead, D. (2010). A dual-strain feline calicivirus vaccine stimulates broader cross-neutralization antibodies than a single-strain vaccine and lessens clinical signs in vaccinated cats when challenged with a homologous feline calicivirus strain associated with virulent systemic disease. *Journal of feline medicine and surgery* **12**, 129-137.

Hurley, K. E., Pesavento, P. A., Pedersen, N. C., Poland, A. M., Wilson, E. & Foley, J. E. (2004). An outbreak of virulent systemic feline calicivirus disease. *Journal of the American Veterinary Medical Association* **224**, 241-249.

Jarrett, O., Laird, H. M., Hay, D. & Crighton, G. W. (1968). Replication of cat leukemia virus in cell cultures. *Nature* **219**, 521-522.

Jung, J. Y., Lee, B. J., Tai, J. H., Park, J. H. & Lee, Y. S. (2000). Apoptosis in rabbit haemorrhagic disease. *J Comp Pathol* **123**, 135-140.

Kaiser, W. J., Chaudhry, Y., Sosnovtsev, S. V. & Goodfellow, I. G. (2006). Analysis of protein-protein interactions in the feline calicivirus replication complex. *The Journal of general virology* **87**, 363-368.

Kanlaya, R., Pattanakitsakul, S. N., Sinchaikul, S., Chen, S. T. & Thongboonkerd, V. (2010). Vimentin interacts with heterogeneous nuclear ribonucleoproteins and dengue nonstructural protein 1 and is important for viral replication and release. *Molecular bioSystems* **6**, 795-806.

Kannan, H., Fan, S., Patel, D., Bossis, I. & Zhang, Y. J. (2009). The hepatitis E virus open reading frame 3 product interacts with microtubules and interferes with their dynamics. *Journal of virology* **83**, 6375-6382.

Karst, S. M., Wobus, C. E., Lay, M., Davidson, J. & Virgin, H. W. t. (2003). STAT1-dependent innate immunity to a Norwalk-like virus. *Science (New York, NY* **299**, 1575-1578.

Klauschies, F., Gutzkow, T., Hinkelmann, S., von Messling, V., Vaske, B., Herrler, G. & Haas, L. (2010). Viral infectivity and intracellular distribution of matrix (M) protein of canine distemper virus are affected by actin filaments. *Archives of virology*.

Knowles, J. O. (1988). Studies on feline calicivirus with particular reference to chronic stomatitis in the cat. *Thesis*.

Knowles, J. O., Gaskell, R. M., Gaskell, C. J., Harvey, C. E. & Lutz, H. (1989). Prevalence of feline calicivirus, feline leukaemia virus and antibodies to FIV in cats with chronic stomatitis. *The Veterinary record* **124**, 336-338.

Krausslich, H. G., Nicklin, M. J., Toyoda, H., Etchison, D. & Wimmer, E. (1987). Poliovirus proteinase 2A induces cleavage of eucaryotic initiation factor 4F polypeptide p220. *Journal of virology* **61**, 2711-2718.

Kreutz, L. C., Seal, B. S. & Mengeling, W. L. (1994). Early interaction of feline calicivirus with cells in culture. *Archives of virology* **136**, 19-34.

Kuhn, M., Desloges, N., Rahaus, M. & Wolff, M. H. (2005). Varicella-zoster virus infection influences expression and organization of actin and alpha-tubulin but does not affect lamin A and vimentin. *Intervirology* **48**, 312-320.

Le Gall-Recule, G., Zwingelstein, F., Fages, M. P., Bertagnoli, S., Gelfi, J., Aubineau, J., Roobrouck, A., Botti, G., Lavazza, A. & Marchandeau, S. (2011). Characterisation of a non-pathogenic and non-protective infectious rabbit lagovirus related to RHDV. *Virology* **410**, 395-402.

Leach, N. R. & Roller, R. J. (2010). Significance of host cell kinases in herpes simplex virus type 1 egress and lamin-associated protein disassembly from the nuclear lamina. *Virology* **406**, 127-137.

Legendre, M., Audic, S., Poirot, O., Hingamp, P., Seltzer, V., Byrne, D., Lartigue, A., Lescot, M., Bernadac, A., Poulain, J., Abergel, C. & Claverie, J. M. (2010). mRNA deep sequencing reveals 75 new genes and a complex transcriptional landscape in Mimivirus. *Genome Res* **20**, 664-674.

Li, S., Qu, H., Hao, J., Sun, J., Guo, H., Guo, C., Sun, B. & Tu, C. (2010). Proteomic analysis of primary porcine endothelial cells after infection by classical swine fever virus. *Biochim Biophys Acta* **1804**, 1882-1888.

Lin, Z., Xu, G., Deng, N., Taylor, C., Zhu, D. & Flemington, E. K. (2010). Quantitative and qualitative RNA-seq based evaluation of Epstein-Barr virus transcription in type I latency Burkitt's lymphoma cells. *Journal of virology*.

Liu, S., Xue, H., Pu, B. & Quian, N. (1984). A new viral disease in rabbits. *An Hus Vet Med* **16**, 253-255.

Liu, Y., Han, D., Han, Y., Yan, Z., Xie, B., Li, J., Qiao, N., Hu, H., Khaitovich, P., Gao, Y. & Han, J. D. (2010). Ab initio identification of transcription start sites in the Rhesus macaque genome by histone modification and RNA-Seq. *Nucleic Acids Res*.

Lole, K. S., Bollinger, R. C., Paranjape, R. S., Gadkari, D., Kulkarni, S. S., Novak, N. G., Ingersoll, R., Sheppard, H. W. & Ray, S. C. (1999). Full-length human immunodeficiency virus type 1 genomes from subtype C-infected seroconverters in India, with evidence of intersubtype recombination. *Journal of virology* **73**, 152-160.

Love, D. N. & Baker, K. D. (1972). Sudden death in kittens associated with a feline picornavirus. *Australian veterinary journal* **48**, 643.

Makino, A., Shimojima, M., Miyazawa, T., Kato, K., Tohya, Y. & Akashi, H. (2006). Junctional adhesion molecule 1 is a functional receptor for feline calicivirus. *Journal of virology* **80**, 4482-4490.

Mallardo, M., Schleich, S. & Krijnse Locker, J. (2001). Microtubule-dependent organization of vaccinia virus core-derived early mRNAs into distinct cytoplasmic structures. *Mol Biol Cell* **12**, 3875-3891.

Margulies, M., Egholm, M., Altman, W. E., Attiya, S., Bader, J. S., Bemben, L. A., Berka, J., Braverman, M. S., Chen, Y. J., Chen, Z., Dewell, S. B., Du, L., Fierro, J. M., Gomes, X. V., Godwin, B. C., He, W., Helgesen, S., Ho, C. H., Irzyk, G. P., Jando, S. C., Alenquer, M. L., Jarvie, T. P., Jirage, K. B., Kim, J. B., Knight, J. R., Lanza, J. R., Leamon, J. H., Lefkowitz, S. M., Lei, M., Li, J., Lohman, K. L., Lu, H., Makhijani, V. B., McDade, K. E., McKenna, M. P., Myers, E. W., Nickerson, E., Nobile, J. R., Plant, R., Puc, B. P., Ronan, M. T., Roth, G. T., Sarkis, G. J., Simons, J. F., Simpson, J. W., Srinivasan, M., Tartaro, K. R., Tomasz, A., Vogt, K. A., Volkmer, G. A., Wang, S. H., Wang, Y., Weiner, M. P., Yu, P., Begley, R. F. & Rothberg, J. M. (2005). Genome sequencing in microfabricated high-density picolitre reactors. *Nature* **437**, 376-380.

Marioni, J. C., Mason, C. E., Mane, S. M., Stephens, M. & Gilad, Y. (2008). RNA-seq: an assessment of technical reproducibility and comparison with gene expression arrays. *Genome Res* **18**, 1509-1517.

Martella, V., Campolo, M., Lorusso, E., Cavicchio, P., Camero, M., Bellacicco, A. L., Decaro, N., Elia, G., Greco, G., Corrente, M., Desario, C., Arista, S., Banyai, K., Koopmans, M. & Buonavoglia, C. (2007). Norovirus in captive lion cub (Panthera leo). *Emerging infectious diseases* **13**, 1071-1073.

Martella, V., Lorusso, E., Decaro, N., Elia, G., Radogna, A., D'Abramo, M., Desario, C., Cavalli, A., Corrente, M., Camero, M., Germinario, C. A., Banyai, K., Di Martino, B., Marsilio, F., Carmichael, L. E. & Buonavoglia, C. (2008). Detection and molecular characterization of a canine norovirus. *Emerging infectious diseases* **14**, 1306-1308.

Martella, V., Pratelli, A., Gentile, M., Buonavoglia, D., Decaro, N., Fiorente, P. & Buonavoglia, C. (2002). Analysis of the capsid protein gene of a feline-like calicivirus isolated from a dog. *Veterinary microbiology* **85**, 315-322.

Masubuchi, K., Wakatsuki, A., Iwamoto, K., Takahashi, T., Kokubu, T. & Shimizu, M. (2010). Immunological and genetic characterization of feline caliciviruses used in the development of a new trivalent inactivated vaccine in Japan. *J Vet Med Sci* **72**, 1189-1194.

McArdle, F., Dawson, S., Carter, M. J., Milton, I. D., Turner, P. C., Meanger, J., Bennett, M. & Gaskell, R. M. (1996). Feline calicivirus strain differentiation using monoclonal antibody analysis in an enzyme-linked immuno-flow-assay. *Veterinary microbiology* **51**, 197-206.

McDonald, D., Vodicka, M. A., Lucero, G., Svitkina, T. M., Borisy, G. G., Emerman, M. & Hope, T. J. (2002). Visualization of the intracellular behavior of HIV in living cells. *J Cell Biol* **159**, 441-452.

Mead, P. S., Slutsker, L., Dietz, V., McCaig, L. F., Bresee, J. S., Shapiro, C., Griffin, P. M. & Tauxe, R. V. (1999). Food-related illness and death in the United States. *Emerging infectious diseases* **5**, 607-625.

Mercer, J. & Helenius, A. (2008). Vaccinia virus uses macropinocytosis and apoptotic mimicry to enter host cells. *Science (New York, NY* **320**, 531-535.

Mortazavi, A., Williams, B. A., McCue, K., Schaeffer, L. & Wold, B. (2008). Mapping and quantifying mammalian transcriptomes by RNA-Seq. *Nat Methods* **5**, 621-628.

Moss, S. R., Turner, S. L., Trout, R. C., White, P. J., Hudson, P. J., Desai, A., Armesto, M., Forrester, N. L. & Gould, E. A. (2002). Molecular epidemiology of Rabbit haemorrhagic disease virus. *The Journal of general virology* **83**, 2461-2467.

Natoni, A., Kass, G. E., Carter, M. J. & Roberts, L. O. (2006). The mitochondrial pathway of apoptosis is triggered during feline calicivirus infection. *The Journal of general virology* **87**, 357-361.

Neill, J. D. (1992). Nucleotide sequence of the capsid protein gene of two serotypes of San Miguel sea lion virus: identification of conserved and non-conserved amino acid sequences among calicivirus capsid proteins. *Virus research* **24**, 211-222.

Neill, J. D. & Mengeling, W. L. (1988). Further characterization of the virus-specific RNAs in feline calicivirus infected cells. *Virus research* **11**, 59-72.

Neill, J. D., Meyer, R. F. & Seal, B. S. (1995). Genetic relatedness of the caliciviruses: San Miguel sea lion and vesicular exanthema of swine viruses constitute a single genotype within the Caliciviridae. *Journal of virology* **69**, 4484-4488.

Neill, J. D., Reardon, I. M. & Heinrikson, R. L. (1991). Nucleotide sequence and expression of the capsid protein gene of feline calicivirus. *Journal of virology* **65**, 5440-5447.

Nelson, M. M., Jones, A. R., Carmen, J. C., Sinai, A. P., Burchmore, R. & Wastling, J. M. (2008). Modulation of the host cell proteome by the intracellular apicomplexan parasite Toxoplasma gondii. *Infection and immunity* **76**, 828-844.

Ng, K. K., Cherney, M. M., Vazquez, A. L., Machin, A., Alonso, J. M., Parra, F. & James, M. N. (2002). Crystal structures of active and inactive conformations of a caliciviral RNA-dependent RNA polymerase. *The Journal of biological chemistry* **277**, 1381-1387.

Nikitin, A., Egorov, S., Daraselia, N. & Mazo, I. (2003). Pathway studio--the analysis and navigation of molecular networks. *Bioinformatics* **19**, 2155-2157.

O'Reilly, E. K. & Kao, C. C. (1998). Analysis of RNA-dependent RNA polymerase structure and function as guided by known polymerase structures and computer predictions of secondary structure. *Virology* **252**, 287-303.

Ohlinger, V. F., Haas, B., Meyers, G., Weiland, F. & Thiel, H. J. (1990). Identification and characterization of the virus causing rabbit hemorrhagic disease. *Journal of virology* **64**, 3331-3336.

Oliver, S. L., Asobayire, E., Dastjerdi, A. M. & Bridger, J. C. (2006). Genomic characterization of the unclassified bovine enteric virus Newbury agent-1 (Newbury1) endorses a new genus in the family Caliciviridae. *Virology* **350**, 240-250.

Ong, S. E., Blagoev, B., Kratchmarova, I., Kristensen, D. B., Steen, H., Pandey, A. & Mann, M. (2002). Stable isotope labeling by amino acids in cell culture, SILAC, as a simple and accurate approach to expression proteomics. *Mol Cell Proteomics* **1**, 376-386.

Oshikamo, R., Tohya, Y., Kawaguchi, K., Tomonaga, K., Maeda, K., Takeda, N., Utagawa, E., Kai, C. & Mikami, T. (1994). The molecular cloning andsequencing of an open reading frame encoding non-structural proteins of feline calicivirus F4 strain isolated in Japan.. *J Vet Med Sci* **56**, 1093-1099.

Ossiboff, R. J. & Parker, J. S. (2007). Identification of regions and residues in feline junctional adhesion molecule required for feline calicivirus binding and infection. *Journal of virology* **81**, 13608-13621.

Ossiboff, R. J., Sheh, A., Shotton, J., Pesavento, P. A. & Parker, J. S. (2007). Feline caliciviruses (FCVs) isolated from cats with virulent systemic disease possess in vitro phenotypes distinct from those of other FCV isolates. *The Journal of general virology* **88**, 506-527.

Ossiboff, R. J., Zhou, Y., Lightfoot, P. J., Prasad, B. V. & Parker, J. S. (2010). Conformational changes in the capsid of a calicivirus upon interaction with its functional receptor. *Journal of virology* **84**, 5550-5564.

Pang, X. L., Lee, B. E., Tyrrell, G. J. & Preiksaitis, J. K. (2009). Epidemiology and genotype analysis of sapovirus associated with gastroenteritis outbreaks in Alberta, Canada: 2004-2007. *J Infect Dis* **199**, 547-551.

Patterson, K. I., Brummer, T., O'Brien, P. M. & Daly, R. J. (2009). Dual-specificity phosphatases: critical regulators with diverse cellular targets. *Biochem J* **418**, 475-489.

Payne, L. G. & Kristensson, K. (1982). The effect of cytochalasin D and monensin on enveloped vaccinia virus release. *Archives of virology* **74**, 11-20.

Pedersen, N. C., Elliott, J. B., Glasgow, A., Poland, A. & Keel, K. (2000). An isolated epizootic of hemorrhagic-like fever in cats caused by a novel and highly virulent strain of feline calicivirus. *Veterinary microbiology* **73**, 281-300.

Pesavento, P. A., Stokol, T., Liu, H., van der List, D. A., Gaffney, P. M. & Parker, J. S. (2010). Distribution of the Feline Calicivirus Receptor Junctional Adhesion Molecule A in Feline Tissues. *Vet Pathol*.

Petrak, J., Ivanek, R., Toman, O., Cmejla, R., Cmejlova, J., Vyoral, D., Zivny, J. & Vulpe, C. D. (2008). Deja vu in proteomics. A hit parade of repeatedly identified differentially expressed proteins. *Proteomics* **8**, 1744-1749.

Pollard, T. D. & Cooper, J. A. (2009). Actin, a central player in cell shape and movement. *Science (New York, NY* **326**, 1208-1212.

Pontius, J. U., Mullikin, J. C., Smith, D. R., Lindblad-Toh, K., Gnerre, S., Clamp, M., Chang, J., Stephens, R., Neelam, B., Volfovsky, N., Schaffer, A. A., Agarwala, R., Narfstrom, K., Murphy, W. J., Giger, U., Roca, A. L., Antunes, A., Menotti-Raymond, M., Yuhki, N., Pecon-Slattery, J., Johnson, W. E., Bourque, G., Tesler, G. & O'Brien, S. J. (2007). Initial sequence and comparative analysis of the cat genome. *Genome Res* **17**, 1675-1689.

Porter, C. J. (2004). Studies on the molecular biology of feline calicivirus replication. *Thesis*.

Porter, C. J., Radford, A. D., Gaskell, R. M., Ryvar, R., Coyne, K. P., Pinchbeck, G. L. & Dawson, S. (2008). Comparison of the ability of feline calicivirus (FCV) vaccines to neutralise a panel of current UK FCV isolates. *Journal of feline medicine and surgery* **10**, 32-40.

Poulet, H., Brunet, S., Leroy, V. & Chappuis, G. (2005). Immunisation with a combination of two complementary feline calicivirus strains induces a broad cross-protection against heterologous challenges. *Veterinary microbiology* **106**, 17-31.

Poulet, H., Brunet, S., Soulier, M., Leroy, V., Goutebroze, S. & Chappuis, G. (2000). Comparison between acute oral/respiratory and chronic stomatitis/gingivitis isolates of feline calicivirus: pathogenicity, antigenic profile and cross-neutralisation studies. *Archives of virology* **145**, 243-261.

Povey, R. C. (1974). Serological relationships among feline caliciviruses. *Infection and immunity* **10**, 1307-1314.

Prasad, B. V., Hardy, M. E., Dokland, T., Bella, J., Rossmann, M. G. & Estes, M. K. (1999). X-ray crystallographic structure of the Norwalk virus capsid. *Science (New York, NY* **286**, 287-290.

Pratt, J. M., Simpson, D. M., Doherty, M. K., Rivers, J., Gaskell, S. J. & Beynon, R. J. (2006). Multiplexed absolute quantification for proteomics using concatenated signature peptides encoded by QconCAT genes. *Nat Protoc* **1**, 1029-1043.

Radford, A. D., Addie, D., Belak, S., Boucraut-Baralon, C., Egberink, H., Frymus, T., Gruffydd-Jones, T., Hartmann, K., Hosie, M. J., Lloret, A., Lutz, H., Marsilio, F., Pennisi, M. G., Thiry, E., Truyen, U. & Horzinek, M. C. (2009). Feline calicivirus infection. ABCD guidelines on prevention and management. *Journal of feline medicine and surgery* **11**, 556-564.

Radford, A. D., Coyne, K. P., Dawson, S., Porter, C. J. & Gaskell, R. M. (2007). Feline calicivirus. *Vet Res* **38**, 319-335.

Radford, A. D., Dawson, S., Ryvar, R., Coyne, K., Johnson, D. R., Cox, M. B., Acke, E. F., Addie, D. D. & Gaskell, R. M. (2003). High genetic diversity of the immunodominant region of the feline calicivirus capsid gene in endemically infected cat colonies. *Virus Genes* **27**, 145-155.

Radford, A. D., Sommerville, L. M., Dawson, S., Kerins, A. M., Ryvar, R. & Gaskell, R. M. (2001). Molecular analysis of isolates of feline calicivirus from a population of cats in a rescue shelter. *The Veterinary record* **149**, 477-481.

Radford, A. D., Willoughby, K., Dawson, S., McCracken, C. & Gaskell, R. M. (1999). The capsid gene of feline calicivirus contains linear B-cell epitopes in both variable and conserved regions. *Journal of virology* **73**, 8496-8502.

Ramanathan, H. N. & Jonsson, C. B. (2008). New and Old World hantaviruses differentially utilize host cytoskeletal components during their life cycles. *Virology* **374**, 138-150.

Ramsay, G. (1998). DNA chips: state-of-the art. *Nature biotechnology* **16**, 40-44.

Reed, L. a. M., H (1938). A simple method for estimating fifty percent endpoints. *The American Journal of Hygiene* **27**, 5.

Reid, S. M., King, D. P., Shaw, A. E., Knowles, N. J., Hutchings, G. H., Cooper, E. J., Smith, A. W. & Ferris, N. P. (2007). Development of a real-time reverse transcription polymerase chain reaction assay for detection of marine caliciviruses (genus Vesivirus). *Journal of virological methods* **140**, 166-173.

Reynolds, B. S., Poulet, H., Pingret, J. L., Jas, D., Brunet, S., Lemeter, C., Etievant, M. & Boucraut-Baralon, C. (2009). A nosocomial outbreak of feline calicivirus associated virulent systemic disease in France. *Journal of feline medicine and surgery*.

Roberts, L. O., Al-Molawi, N., Carter, M. J. & Kass, G. E. (2003). Apoptosis in cultured cells infected with feline calicivirus. *Ann N Y Acad Sci* **1010**, 587-590.

Roerink, F., Hashimoto, M., Tohya, Y. & Mochizuki, M. (1999). Genetic analysis of a canine calicivirus: evidence for a new clade of animal caliciviruses. *Veterinary microbiology* **69**, 69-72.

Rogers, S., Girolami, M., Kolch, W., Waters, K. M., Liu, T., Thrall, B. & Wiley, H. S. (2008). Investigating the correspondence between transcriptomic and proteomic expression profiles using coupled cluster models. *Bioinformatics* **24**, 2894-2900.

Roohvand, F., Maillard, P., Lavergne, J. P., Boulant, S., Walic, M., Andreo, U., Goueslain, L., Helle, F., Mallet, A., McLauchlan, J. & Budkowska, A. (2009). Initiation of hepatitis C virus infection requires the dynamic microtubule network: role of the viral nucleocapsid protein. *The Journal of biological chemistry* **284**, 13778-13791.

Saif, L. J., Bohl, E. H., Theil, K. W., Cross, R. F. & House, J. A. (1980). Rotavirus-like, calicivirus-like, and 23-nm virus-like particles associated with diarrhea in young pigs. *Journal of clinical microbiology* **12**, 105-111.

Sanderson, C. M., Way, M. & Smith, G. L. (1998). Virus-induced cell motility. *Journal of virology* **72**, 1235-1243.

Sanger, F., Nicklen, S. & Coulson, A. R. (1977). DNA sequencing with chain-terminating inhibitors. *Proceedings of the National Academy of Sciences of the United States of America* **74**, 5463-5467.

Saphire, A. C., Bobardt, M. D. & Gallay, P. A. (2000). Human immunodeficiency virus type 1 hijacks host cyclophilin A for its attachment to target cells. *Immunol Res* **21**, 211-217.

Sato, Y., Ohe, K., Murakami, M., Fukuyama, M., Furuhata, K., Kishikawa, S., Suzuki, Y., Kiuchi, A., Hara, M., Ishikawa, Y. & Taneno, A. (2002). Phylogenetic analysis of field isolates of feline calcivirus (FCV) in Japan by sequencing part of its capsid gene. *Vet Res Commun* **26**, 205-219.

Schena, M., Shalon, D., Davis, R. W. & Brown, P. O. (1995). Quantitative monitoring of gene expression patterns with a complementary DNA microarray. *Science (New York, NY* **270**, 467-470.

Schepis, A., Schramm, B., de Haan, C. A. & Locker, J. K. (2006). Vaccinia virus-induced microtubule-dependent cellular rearrangements. *Traffic (Copenhagen, Denmark)* **7**, 308-323.

Schorr-Evans, E. M., Poland, A., Johnson, W. E. & Pedersen, N. C. (2003). An epizootic of highly virulent feline calicivirus disease in a hospital setting in New England. *Journal of feline medicine and surgery* **5**, 217-226.

Seal, B. S. (1994). Analysis of capsid protein gene variation among divergent isolates of feline calicivirus. *Virus research* **33**, 39-53.

Seal, B. S. & Neill, J. D. (1995). Capsid protein gene sequence of feline calicivirus isolates 255 and LLK: further evidence for capsid protein configuration among feline caliciviruses. *Virus Genes* **9**, 183-187.

Seal, B. S., Ridpath, J. F. & Mengeling, W. L. (1993). Analysis of feline calicivirus capsid protein genes: identification of variable antigenic determinant regions of the protein. *The Journal of general virology* **74 (Pt 11)**, 2519-2524.

Smith, A. W., Akers, T. G., Madin, S. H. & Vedros, N. A. (1973). San Miguel sea lion virus isolation, preliminary characterization and relationship to vesicular exanthema of swine virus. *Nature* **244**, 108-110.

Smith, A. W., Skilling, D. E., Dardiri, A. H. & Latham, A. B. (1980). Calicivirus pathogenic for swine: a new serotype isolated from opaleye Girella nigricans, an ocean fish. *Science (New York, NY* **209**, 940-941.

Sodeik, B. (2000). Mechanisms of viral transport in the cytoplasm. *Trends Microbiol* **8**, 465-472.

Sosnovtsev, S. & Green, K. Y. (1995). RNA transcripts derived from a cloned full-length copy of the feline calicivirus genome do not require VpG for infectivity. *Virology* **210**, 383-390.

Sosnovtsev, S. V., Belliot, G., Chang, K. O., Onwudiwe, O. & Green, K. Y. (2005). Feline calicivirus VP2 is essential for the production of infectious virions. *Journal of virology* **79**, 4012-4024.

Sosnovtsev, S. V., Garfield, M. & Green, K. Y. (2002). Processing map and essential cleavage sites of the nonstructural polyprotein encoded by ORF1 of the feline calicivirus genome. *Journal of virology* **76**, 7060-7072.

Sosnovtsev, S. V. & Green, K. Y. (2000). Identification and genomic mapping of the ORF3 and VPg proteins in feline calicivirus virions. *Virology* **277**, 193-203.

Sosnovtsev, S. V., Prikhod'ko, E. A., Belliot, G., Cohen, J. I. & Green, K. Y. (2003). Feline calicivirus replication induces apoptosis in cultured cells. *Virus research* **94**, 1-10.

Sosnovtsev, S. V., Sosnovtseva, S. A. & Green, K. Y. (1998). Cleavage of the feline calicivirus capsid precursor is mediated by a virus-encoded proteinase. *Journal of virology* **72**, 3051-3059.

Sosnovtseva, S. A., Sosnovtsev, S. V. & Green, K. Y. (1999). Mapping of the feline calicivirus proteinase responsible for autocatalytic processing of the nonstructural polyprotein and identification of a stable proteinase-polymerase precursor protein. *Journal of virology* **73**, 6626-6633.

Steinhauer, D. A., Domingo, E. & Holland, J. J. (1992). Lack of evidence for proofreading mechanisms associated with an RNA virus polymerase. *Gene* **122**, 281-288.

Stuart, A. D. & Brown, T. D. (2007). Alpha2,6-linked sialic acid acts as a receptor for Feline calicivirus. *The Journal of general virology* **88**, 177-186.

Styers, M. L., Salazar, G., Love, R., Peden, A. A., Kowalczyk, A. P. & Faundez, V. (2004). The endo-lysosomal sorting machinery interacts with the intermediate filament cytoskeleton. *Mol Biol Cell* **15**, 5369-5382.

Tamura, K., Dudley, J., Nei, M. & Kumar, S. (2007). MEGA4: Molecular Evolutionary Genetics Analysis (MEGA) software version 4.0. *Molecular biology and evolution* **24**, 1596-1599.

Taneja, S., Sen, S., Gupta, V. K., Aggarwal, R. & Jameel, S. (2009). Plasma and urine biomarkers in acute viral hepatitis E. *Proteome Sci* **7**, 39.

Tassin, A. M. & Bornens, M. (1999). Centrosome structure and microtubule nucleation in animal cells. *Biol Cell* **91**, 343-354.

TerWee, J., Lauritzen, A. Y., Sabara, M., Dreier, K. J. & Kokjohn, K. (1997). Comparison of the primary signs induced by experimental exposure to either a pneumotrophic or a 'limping' strain of feline calicivirus. *Veterinary microbiology* **56**, 33-45.

Thumfart, J. O. & Meyers, G. (2002). Feline calicivirus: recovery of wild-type and recombinant viruses after transfection of cRNA or cDNA constructs. *Journal of virology* **76**, 6398-6407.

Tohya, Y., Taniguchi, Y., Takahashi, E., Utagawa, E., Takeda, N., Miyamura, K., Yamazaki, S. & Mikami, T. (1991). Sequence analysis of the 3'-end of feline calicivirus genome. *Virology* **183**, 810-814.

Turowska, A., Pajak, B., Godlewski, M. M., Dzieciatkowski, T., Chmielewska, A., Tucholska, A. & Banbura, M. (2010). Opposite effects of two different strains of equine herpesvirus 1 infection on cytoskeleton composition in equine dermal ED and African green monkey kidney Vero cell lines: application of scanning cytometry and confocal-microscopy-based image analysis in a quantitative study. *Archives of virology* **155**, 733-743.

Unlu, M., Morgan, M. E. & Minden, J. S. (1997). Difference gel electrophoresis: a single gel method for detecting changes in protein extracts. *Electrophoresis* **18**, 2071-2077.

Velculescu, V. E., Zhang, L., Vogelstein, B. & Kinzler, K. W. (1995). Serial analysis of gene expression. *Science (New York, NY* **270**, 484-487.

Vester, D., Rapp, E., Gade, D., Genzel, Y. & Reichl, U. (2009). Quantitative analysis of cellular proteome alterations in human influenza A virus-infected mammalian cell lines. *Proteomics* **9**, 3316-3327.

Wang, H., Wang, Q., Pape, U. J., Shen, B., Huang, J., Wu, B. & Li, X. (2010). Systematic investigation of global coordination among mRNA and protein in cellular society. *BMC Genomics* **11**, 364.

Wang, Z., Gerstein, M. & Snyder, M. (2009). RNA-Seq: a revolutionary tool for transcriptomics. *Nat Rev Genet* **10**, 57-63.

Wardley, R. C., Gaskell, R. M. & Povey, R. C. (1974). Feline respiratory viruses--their prevalence in clinically healthy cats. *J Small Anim Pract* **15**, 579-586.

Waters, L., Hopper, C. D., Gruffydd-Jones, T. J. & Harbour, D. A. (1993). Chronic gingivitis in a colony of cats infected with feline immunodeficiency virus and feline calicivirus. *The Veterinary record* **132**, 340-342.

Wegner, A. (1976). Head to tail polymerization of actin. *J Mol Biol* **108**, 139-150.

Wei, L., Huhn, J. S., Mory, A., Pathak, H. B., Sosnovtsev, S. V., Green, K. Y. & Cameron, C. E. (2001). Proteinase-polymerase precursor as the active form of feline calicivirus RNA-dependent RNA polymerase. *Journal of virology* **75**, 1211-1219.

White, P. J., Trout, R. C., Moss, S. R., Desai, A., Armesto, M., Forrester, N. L., Gould, E. A. & Hudson, P. J. (2004). Epidemiology of rabbit haemorrhagic disease virus in the United Kingdom: evidence for seasonal transmission by both virulent and avirulent modes of infection. *Epidemiol Infect* **132**, 555-567.

Willcocks, M. M., Carter, M. J. & Roberts, L. O. (2004). Cleavage of eukaryotic initiation factor eIF4G and inhibition of host-cell protein synthesis during feline calicivirus infection. *The Journal of general virology* **85**, 1125-1130.

Woode, G. N. & Bridger, J. C. (1978). Isolation of small viruses resembling astroviruses and caliciviruses from acute enteritis of calves. *J Med Microbiol* **11**, 441-452.

Woodhouse, S. D., Narayan, R., Latham, S., Lee, S., Antrobus, R., Gangadharan, B., Luo, S., Schroth, G. P., Klenerman, P. & Zitzmann, N. (2010). Transcriptome sequencing, microarray, and proteomic analyses reveal cellular and metabolic impact of hepatitis C virus infection in vitro. *Hepatology* **52**, 443-453.

Xia, D., Sanderson, S. J., Jones, A. R., Prieto, J. H., Yates, J. R., Bromley, E., Tomley, F. M., Lal, K., Sinden, R. E., Brunk, B. P., Roos, D. S. & Wastling, J. M. (2008). The proteome of Toxoplasma gondii: integration with the genome provides novel insights into gene expression and annotation. *Genome Biol* **9**, R116.

Xiao, S., Wang, Q., Jia, J., Cong, P., Mo, D., Yu, X., Qin, L., Li, A., Niu, Y., Zhu, K., Wang, X., Liu, X. & Chen, Y. (2010). Proteome changes of lungs artificially infected with H-PRRSV and N-PRRSV by two-dimensional fluorescence difference gel electrophoresis. *Virology journal* **7**, 107.

Zwillenberg, L. O. & Burki, F. (1966). On the cpsid structure of some small feline and bovine RNA viruses. *Archiv fur die gesamte Virusforschung* **19**, 373-384.

Appendices

Appendix I - Mascot identifications of differentially expressed FEA cell proteins from 2D-DIGE analysis of FCV-F9 infection

Appendix II - Mascot identifications of differentially expressed FEA cell proteins from 2D-DIGE analysis of FCV-F9, LS015, R591 and UKOS-A infection

Appendix III - Average greyscale values of FCV capsid stain and tubulin stain in infected and mock infected FEA cells

Appendix IV - Average greyscale values of FCV capsid stain and vimentin stain in infected and mock infected FEA cells

Appendix V - Mann Whitney U test results comparing tubulin and vimentin expression between infected and uninfected FEA cells

Appendix VI - Results of DeSeq analysis of all genes comparing all datasets

Appendix VII - Genes found to be significantly differentially transcribed ($p \leq 0.01$) by DeSeq analysis

Appendix VIII - Pathway analysis of differentially transcribed genes in FEA cells in response to FCV-F9 infection including full gene identification key

All appendices can be found on the enclosed CD.

Appendices I - VI and VIII are also attached on the following pages.

Appendix I - Mascot identifications of differentially expressed FEA cell proteins from 2D-DIGE analysis of FCV-F9 infection

Protein Spot No	Ensembl ID hit (Cat database)	Mascot Score	No of peptide hits	Identification	Gene ID	MSDB ID hit	Mascot Score	No of peptide hits	Identification
5074	ENSFCAP00000004426	84	2	Thioredoxin	TXN	ACT_YARLI	129	6	Actin
	scaffold_8235_2912_3415_-1	53	7	Beta-actin	ACTB	COF1_BOVIN	120	4	Cofilin-1
	GeneScaffold_2764_3025_217086_-1	58	6	family with sequence similarity 171, member A1	FAM171A1	THIO_BOVIN	110	2	Thioredoxin
4924	-	-	-	-	-	Q53YJ2_HUMAN	103	2	Proteolysis inducing factor
						Q1KMR5_RHIFE	85	3	Beta-actin
4797	ENSFCAP00000012591	125	7	Transgelin	TAGLN	TAGL_BOVIN	270	6	Transgelin
	ENSFCAP00000006138	105	3	protein disulfide isomerase family A, member 3	PDIA3	JC5704	168	3	Cyclophilin A
	GeneScaffold_2389_274827_323289_-1	85	10	fumarylacetoacetate hydrolase	FAH	O35248_CRISP	119	3	Beta actin
	GeneScaffold_2764_3025_217086_-1	74	2	family with sequence similarity 171, member A1	FAM171A1	Q6ZYE7_RAT	85	2	Plectin
	ENSFCAP00000007128	52	3	Tubulin beta chain	TUBB	Q5DT20_HUMAN	77	3	Hornerin
	GeneScaffold_3763_4924_53472_-1	47	2	non imprinted in Prader-Willi/Angelman syndrome 1	NIPA1	Q9UVS5_9FUNG	76	2	Beta tubulin
	GeneScaffold_2798_18850_78140_1	43	3	Novel gene	x	ANXA2_BOVIN	60	2	Annexin A2
4777	ENSFCAP00000008491	45	4	Cyclophilin A	PPIA_FELCA	Q53YJ2_HUMAN	128	3	Proteolysis Inducing Factor
						CSBOAB	100	3	Cyclophilin A

4376	scaffold_101245_108936_112032_-1	170	5	beta-actin	ACTB	ACTB_CAMDR	288	5	Actin
	GeneScaffold_2764_3025_217086_-1	87	3	family with sequence similarity 171, member A1	FAM171A1	PPIA_FELCA	149	4	Cyclophilin A
	ENSFCAP00000008491	67	5	Cyclophilin A	PPIA_FELCA				
4370	scaffold_101245_108936_112032_-1	849	27	beta-actin	ACTB	ACTB_CAMDR	619	26	Actin
	scaffold_181185_2388_3518_-1	305	12	actin, beta-like 2	ACTBL2	Q258K2_CANFA	342	6	Myosin
	ENSFCAP00000006138	95	6	Protein disulphide-isomerase A3 precursor	PDIA3	JC5704	192	4	protein disulfide-isomerase
	ENSFCAP00000004098	82	7	Annexin A5	ANXA5	AQHUP	150	3	annexin V
4293	GeneScaffold_2798_18850_78140_1	151	12	solute carrier family 22	x	LMNA_RAT	533	14	Lamin A
	ENSFCAP00000012591	123	8	Transgelin	TAGLN	Q5JQ13_HUMAN	254	5	Vinculin
	scaffold_101245_108936_112032_-1	88	3	beta-actin	ACTB	FAHUAA	148	6	alpha-actinin 1
	GeneScaffold_4125_187395_227637_-1	38	3	p21 protein (Cdc42/Rac)-activated kinase 1	PAK1	Q1KMR5_RHIFE	133	3	Beta-actin
4290	scaffold_101245_108936_112032_-1	334	8	beta-actin	ACTB	ACTB_CAMDR	437	8	Actin
3999	-	-	-	-	-	-	-	-	-
3991	-	-	-	-	-	-	-	-	-
3881	-	-	-	-	-	-	-	-	-
3795	-	-	-	-	-	-	-	-	-
3645	-	-	-	-	-	-	-	-	-
3595	-	-	-	-	-	-	-	-	-
3538	scaffold_101245_108936_112032_-1	1447	64	beta-actin	ACTB	Q9QZ83_MOUSE	745	58	Actin
	GeneScaffold_3749_426274_507033_-1	764	42	roundabout, axon guidance receptor, homolog 1	ROBO1				
	GeneScaffold_2764_3025_217086_-1	650	32	family with sequence similarity 171, member A1	FAM171A1				
	ENSFCAP00000000438	132	7	Peroxiredoxin-2	PRDX2				

3516	scaffold_101245_108936_112032_-1	959	34	beta-actin	ACTB	ACTB_CAMDR	787	33	Actin
	GeneScaffold_2764_3025_217086_-1	262	15	family with sequence similarity 171, member A1	FAM171A1	Q17QM7_BOVIN	534	17	Vimentin
	GeneScaffold_3175_2520_86852_-1	93	2	NEDD8 activating enzyme E1 subunit 1	NAE1				
	ENSFCAP00000007281	87	3	annexin A2	ANXA2				
	scaffold_124947_7729_58479_-1	58	2	Peroxiredoxin-1	PRDX1				
	GeneScaffold_2254_325966_333780_1	48	4	thrombospondin, type I, domain containing 4	THSD4				
3503	-	-	-	-	-	-	-	-	-
3357	GeneScaffold_2254_325966_333780_1	100	5	thrombospondin, type I, domain containing 4	THSD4	VIME_HUMAN	902	31	Vimentin
	GeneScaffold_2428_5475_79246_1	43	4	Novel gene	x	Q7SYF4_ACIBE	108	4	Desmin
3351	scaffold_101245_108936_112032_-1	110	4	beta-actin	ACTB	ACTB_CAMDR	224	5	Actin
3177	-	-	-	-	-	-	-	-	-
3174	-	-	-	-	-	-	-	-	-
3129	scaffold_101245_108936_112032_-1	62	4	Beta-actin	ACTB	ACTB_CAMDR	156	4	Actin
	ENSFCAP00000001042	61	2	myosin, heavy chain 9	MYH9	Q3KQJ4_MOUSE	93	3	Hspa8 protein
						MYH9_HUMAN	86	2	Myosin-9
						Q7T275_CYPCA	83	2	HSP70
						S11456	63	3	dnaK-type molecular chaperone hsc70
3032	scaffold_101245_108936_112032_-1	92	6	beta-actin	ACTB	ACTB_CAMDR	239	6	Actin
						A39638	76	2	Plectin
2775	-	-	-	-	-	-	-	-	-
2661	-	-	-	-	-	Q76II5_9ZYGO	125	4	Elongation factor 1 alpha
2319	ENSFCAP00000010586	41	2	Filamin-A	FLNA	-	-	-	-

1843	-	-	-	-	-	-	-	-	-
1354	-	-	-	-	-	-	-	-	-
1084	-	-	-	-	-	-	-	-	-
1073	-	-	-	-	-	-	-	-	-

Appendix II - Mascot identifications of differentially expressed FEA cell proteins from 2D-DIGE analysis of FCV-F9, LS015, R591 and UKOS-A infection

Protein Spot No	Ensembl ID hit (Cat database)	Mascot Score	No of peptide hits	Identification	Gene ID	MSDB ID hit	Mascot Score	No of peptide hits	Identification
2390	GeneScaffold_3760_7502_298316_1	53	2	activated leukocyte cell adhesion molecule	ALCAM	-	-	-	-
2551	scaffold_59989_186_324_-1	41	2	hypothetical protein	-	CAF01065	66	4	ubiquitin-conjugating enzyme E2O
	GeneScaffold_2406_52531_181244_-1	38	2	elongation factor Tu GTP-binding domain-containing protein 1	EFTUD1				
2700	scaffold_101097_76774_76917_1	54	4	phospholipase C, gamma 2	Plcg2	Q4CE28_CLOTM	59	2	Fe-S type hydro-lyases tartrate/fumarate alpha region
2758	GeneScaffold_4664_2439_137299_1	79	2	protein kinase C substrate 80K-H	Prkcsh	AAQ14482	56	2	protein kinase C substrate 80K-H
2945	GeneScaffold_1627_9781_709188_1	86	3	FK506 binding protein 9	Fkbp9	LMNA_RAT	214	5	Lamin-A
						HHRTGB	189	4	dnaK-type molecular chaperone precursor
						Q2VA67_9APIC	102	4	Putative heat shock protein 70
						AAI05408	68	3	FK506 binding protein 9 precursor

2954	GeneScaffold_3211_19329_79211_1	127	2	lamin a/c	Lmna	VEHULC	280	5	lamin C
	GeneScaffold_2827_365420_480146_1	126	7	dihydrolipoamide S-acetyltransferase	Dlat	Q3B7V7_RAT	118	4	Dihydrolipoamide S-acetyltransferase
	GeneScaffold_3126_74284_369431_1	40	2	calsyntenin 2	Clstn2	Q2VA67_9APIC	65	3	Putative heat schock protein 70
3012	GeneScaffold_1158_811146_814937_-1	342	11	heat shock 70kDa protein 8	Q670L1_FELCA	Q3TH56_MOUSE	787	24	heat shock protein 8
	GeneScaffold_1158_811146_973521_-1	224	9	heat shock 70kDa protein 8	Q670L1_FELCA	Q2KJF1_BOVIN	129	5	Alpha-1-B glycoprotein
	GeneScaffold_762_340398_342317_1	183	5	heat shock 70kDa protein 2	HSPA2				
	scaffold_176644_45903_47090_-1	163	5	heat shock 70kDa protein 8	Q670L1_FELCA				
	GeneScaffold_3635_490733_694556_-1	37	2	Eukaryotic translation initiation factor 2C	Eif2c2				
3087	GeneScaffold_1955_712509_729649_-1	126	4	heat shock 70kDa protein 9	HSPA9	Q3TW93_MOUSE	174	4	heat shock protein, A
	GeneScaffold_3211_19329_79211_1	111	3	lamin a/c	Lmna	VEHULA	162	3	lamin A
	scaffold_136947_1406_3132_-1	37	2	RNA pseudouridylate synthase domain-containing protein 4	C15orf19				
3100	scaffold_92712_2520_4533_-1	112	2	histone cluster 1, H2b	Hist1h2ba	VEHULA	234	3	lamin A
	scaffold_124187_37582_71984_-1	97	2	enolase 1	Eno1	ENOA_MOUSE	186	2	Alpha-enolase
	GeneScaffold_3211_68494_792	78	2	lamin a/c	Lmna	VEHY	130	2	Vimentin

	11_1								
	GeneScaffold_762_340398_342317_1	74	2	heat shock 70kDa protein 2	HSPA7	Q4U3C7_9TREM	107	3	Actin
	GeneScaffold_3528_1141909_1206005_1	69	4	vimentin	Vim	1KAZ	102	2	70kd heat shock cognate protein
	scaffold_181185_2388_3518_-1	58	3	actin	Actb				
3133	GeneScaffold_762_340398_342317_1	92	3	heat shock 70kDa protein 2	HSPA2	1ATR	180	4	heat shock cognate protein 70 kD
	GeneScaffold_1158_811146_973521_-1	67	3	heat shock 70kDa protein 8	HSPA8	ABBOS	150	3	serum albumin precursor
						KABOSB	121	3	alpha-s1-casein precursor
3150	scaffold_101245_108936_112032_-1	102	4	beta-actin	Actb	ACTB_CAMDR	304	6	Actin
	GeneScaffold_2556_264487_337382_1	92	3	actin	Actb	AAH06551	125	2	lamin B2
	scaffold_8235_2912_3415_-1	82	2	actin	Actb	Q8MJ76_PIG	71	2	Alpha-fetoprotein
	GeneScaffold_3168_3407_254369_-1	74	2	actin	Actb	Q2WG65_PLUXY	60	2	Heat shock cognate 70
	GeneScaffold_1158_811146_973521_-1	55	2	heat shock 70kDa protein 8	HSPA8				
	GeneScaffold_4790_320911_361683_-1	55	2	G7c	G7c				
	GeneScaffold_3341_245_47680_1	54	3	albumin	ALB				
3160	GeneScaffold_4038_1699_9138_-1	52	2	lamin b2	Lmna	AAH06551	185	3	lamin B2
	GeneScaffold_3341_245_47680_1	40	3	albumin	ALB	Q8MJ76_PIG	69	3	Alpha-fetoprotein

3162	GeneScaffold_3341_245_47680_1	53	2	albumin	ALB	LMNA_RAT	151	2	Lamin-A
3167	scaffold_217191_43844_49826_1	40	4	G-protein coupled receptor-associated sorting protein 2	GPRASP2	-	-	-	-
	GeneScaffold_1083_156145_277749_-1	39	6	acetyl-Coenzyme A carboxylase alpha	Acaca				
	GeneScaffold_1788_133919_216524_-1	39	4	transmembrane protein 120A	Tmem120a				
	GeneScaffold_2406_52531_181244_-1	39	2	elongation factor Tu GTP-binding domain-containing protein 1	EFTUD1				
3235	GeneScaffold_805_95206_371996_-1	73	9	laminin alpha 1	Lama1	-	-	-	-
	GeneScaffold_4991_901280_969073_-1	65	8	hypothetical protein	-				
3292	GeneScaffold_4226_44961_169647_1	39	4	obscurin	OBSCN	CAA23753	63	3	albumin
	GeneScaffold_805_95206_426426_-1	40	2	laminin alpha 1	Lama1				
3256	GeneScaffold_4226_44961_169647_1	38	3	obscurin	OBSCN	Q1RU50_MEDTR	67	2	AAA ATPase
3289	GeneScaffold_3211_19329_79211_1	101	2	lamin a/c	Lmna	VEHULA	361	6	lamin A
3389	GeneScaffold_3211_19329_79211_1	89	2	lamin a/c	Lmna	VEHULC	407	6	lamin C
						KABOSB	223	7	alpha-s1-casein precursor
						LGBO	149	3	beta-lactoglobulin precursor
3491	GeneScaffold_4107_135960_25	77	2	calmodulin-like 3	Calml3	MCHUNB	56	2	calmodulin-

	5019_1								related protein NB-1
	GeneScaffold_3375_32777_178692_1	39	3	PDZ domain containing 6 isoform 4	-				
3494	GeneScaffold_3474_76305_343178_1	106	3	chaperonin	HSPD1	Q38L19_HUMAN	1214	20	Heat shock protein 60
	GeneScaffold_3946_188733_189698_1	103	3	chaperonin	HSPD1	Q803B0_BRARE	735	12	Hspd1 protein
	scaffold_162142_6364_35406_-1	100	4	chaperonin	Hspd1				
3497	GeneScaffold_3474_76305_343178_1	212	11	chaperonin	HSPD1	A32800	1995	41	chaperonin GroEL precursor
	scaffold_162142_6364_35406_-1	122	6	chaperonin	HSPD1	CAI29638	1787	38	60 kDa heat shock protein
	GeneScaffold_3093_3883_124517_-1	105	4	cell division cycle protein 27	Cdc27				
	GeneScaffold_3946_188733_189698_1	58	3	chaperonin	HSPD1				
3498	GeneScaffold_2462_28221_79423_-1	125	3	JUP protein	Jup	Q3KQP2_MOUSE	581	10	Hspd1 protein
	GeneScaffold_3474_76305_343178_1	97	2	chaperonin	HSPD1	Q38L19_HUMAN	581	11	Heat shock protein 60
	GeneScaffold_3093_3883_124517_-1	73	2	cell division cycle protein 27	Cdc27	Q7L3S5_HUMAN	184	3	JUP protein
	GeneScaffold_2556_264487_337382_1	60	2	actin	Actb				
3499	GeneScaffold_3609_122715_163311_1	119	5	protein disulphide isomerase	PRDX2	Q4VIT4_CERAE	322	6	protein disulfide isomerase family A
	GeneScaffold_385_5798_123714_-1	52	2	procollagen-proline	P4ha1	Q3KQP2_MOUSE	61	2	Hspd1 protein

						CAG31521	61	2	60 kDa heat shock protein,
3514	GeneScaffold_4226_44961_169647_1	38	3	obscurin	OBSCN	Q56SZ8_9AVES	76	2	Recombination activating protein 1
3516	GeneScaffold_4321_1497121_1527549_1	46	3	zinc finger, DHHC-type containing 18	Zdhhc18	Q1DCD7_MYXXA	63	2	Response regulator receiver domain/DnaJ domain protein
						H97196	56	2	glycosyltransferase
3559	GeneScaffold_3548_151228_166150_-1	44	2	pyruvate kinase	KPYM_FELCA	-	-	-	-
3612	GeneScaffold_3474_76305_343178_1	135	3	chaperonin	HSPD1	Q38L19_HUMAN	1034	19	Heat shock protein 60
	GeneScaffold_3528_1141909_1206005_1	88	6	vimentin	Vim	Q3KQP2_MOUSE	908	14	Hspd1 protein
	GeneScaffold_3528_1196033_1199831_1	85	4	vimentin	Vim	VIME_HUMAN	293	7	Vimentin
	GeneScaffold_3946_188733_189698_1	76	2	chaperonin	HSPD1				
	scaffold_162142_6364_35406_-1	47	3	chaperonin	HSPD2				
	GeneScaffold_4213_849006_928448_1	38	2	protein tyrosine phosphatase	Ptp4a1				
3690	GeneScaffold_3609_122715_163311_1	76	2	protein disulphide isomerase	PDIA3	Q3TEI9_MOUSE	64	3	glucose regulated protein
						Q53YJ2_HUMAN	59	2	Proteolysis inducing factor
3698	GeneScaffold_3528_1196033_1199831_1	429	24	vimentin	Vim	VIME_HUMAN	1044	44	Vimentin

	GeneScaffold_3528_1141909_1206005_1	373	31	vimentin	Vim	Q6IP60_XENLA	246	8	Hspd1 protein
	GeneScaffold_3973_532871_574596_-1	142	4	alpha-tubulin	Tuba1a	Q5YLV6_BRARE	184	7	Glial fibrillary acidic protein
	GeneScaffold_2584_191620_211797_1	114	3	alpha-tubulin	Tuba1a	Q6P869_XENTR	164	7	Desmin
						S43425	144	13	tubulin alpha chain
						AQHUP	88	4	annexin V
3777	GeneScaffold_4223_531307_550048_-1	436	17	mitochondrial ATP synthase	Q0QEN3_FELCA	VIME_HUMAN	342	23	Vimentin
	GeneScaffold_3528_1141909_1206005_1	177	26	vimentin	Vim	Q3TFD7_MOUSE	506	20	ATP synthase
	GeneScaffold_3528_1196033_1199831_1	177	11	vimentin	Vim	Q5YLV6_BRARE	178	6	Glial fibrillary acidic protein
	GeneScaffold_1393_514148_544856_-1	119	5	protein disulfide isomerase associated 6	PDIA6	PDIA6_MOUSE	76	3	Protein disulfide-isomerase A6 precursor
	GeneScaffold_2584_328853_336667_1	71	5	desmin	Des				
	GeneScaffold_4554_9087_530021_-1	70	2	cathepsin d precursor	Ctsd				
	GeneScaffold_3168_3407_254369_-1	53	4	actin	Actb				
	scaffold_166313_3103_9882_-1	49	2	alpha-N-acetylgalactosaminidase	NAGA				
	GeneScaffold_2028_484482_507249_1	40	2	dihydrolipoamide S-succinyltransferase	Dlst				
	GeneScaffold_4556_244215_427858_-1	39	2	retinoblastoma binding protein 7	Rbbp7				

	GeneScaffold_2777_5475_79246_1	38	2	alpha-internexin	INA				
3808	GeneScaffold_630_86315_204372_1	131	2	lysozyme	LYZ	AAA30032	144	4	actin 2
	scaffold_8235_2912_3415_-1	69	3	actin	Actb	LZHU	124	4	lysozyme
	GeneScaffold_3168_3407_254369_-1	60	3	actin	Actb				
	scaffold_132537_6120_47775_-1	60	3	actin	Actb				
	GeneScaffold_1554_151383_200166_-1	54	4	low density lipoprotein receptor-related protein 11	Ldlr				
	scaffold_101701_7494_37474_1	40	2	A-kinase anchor protein 2	AKAP2				
3839	GeneScaffold_4226_3314_169647_1	38	2	obscurin	OBSCN	Q9G986_VESGE	68	13	Cytochrome b
						Q9M699_CATRO	63	2	Putative glycine-rich RNA-binding protein 2
						Q4UH60_THEAN	54	2	Myosin a tail domain interacting protein mtip
3892	GeneScaffold_3168_3407_254369_-1	49	2	actin	Actb	Q3U8X1_MOUSE	110	4	eukaryotic translation initiation factor 3
						Q8I861_GLORO	63	2	Actin 2
						Q9G986_VESGE	54	12	Cytochrome b
3936	GeneScaffold_5179_297902_30	45	6	calreticulin	Calr	JH0819	131	6	calreticulin

	1190_1								precursor
4098	GeneScaffold_4554_9087_53021_-1	90	4	cathepsin d precursor	Ctsd	LMNA_RAT	135	3	Lamin-A
4104	GeneScaffold_4554_9087_53021_-1	83	4	cathepsin d precursor	Ctsd	LMNA_RAT	62	2	Lamin-A
	scaffold_171890_524_612_1	35	2	sulfate ABC transporter	-				
4105	GeneScaffold_4554_9087_53021_-1	116	5	cathepsin d precursor	Ctsd	AQHUP	128	4	annexin V
	GeneScaffold_3382_25337_117455_-1	74	3	annexin A5	Anxa5				
4256	GeneScaffold_3211_68494_79211_1	100	4	lamin a/c	Lmna	-	-	-	-
4270	GeneScaffold_3211_68494_79211_1	127	6	lamin a/c	Lmna	Q3SZI2_BOVIN	477	14	LMNA protein
4271	scaffold_156020_24876_33658_-1	58	4	peptidase	Pepb	LGBUI	412	19	beta-lactoglobulin
	GeneScaffold_2241_72789_295895_1	50	2	sortilin-related receptor preproprotein	SORL1	Q3SZI2_BOVIN	264	5	LMNA protein
	GeneScaffold_3211_68494_79211_1	39	2	lamin a/c	Lmna	KABOSB	172	12	alpha-s1-casein precursor
	scaffold_9462_8927_14629_1	39	2	envelope glycoprotein syncytin-B	-				
	GeneScaffold_2664_17707_78345_1	37	2	pleckstrin and Sec7 domain containing 2	Psd2				
4397	GeneScaffold_2404_187013_255811_1	38	2	Loricrin	Lor	Q66J53_XENLA	261	9	acyl-coenzyme A dehydrogenase
4810	GeneScaffold_4261_38206_96580_-1	111	3	annexin A2	Anxa2	ANXA2_BOVIN	121	3	Annexin A2

	GeneScaffold_4261_4924_53732_-1	83	4	annexin A2	Anxa2				
	GeneScaffold_2878_80075_110256_1	36	2	piccolo	PCLO				
4852	GeneScaffold_2096_57622_76474_1	164	6	annexin A1	Anxa1	Q6BCI9_FELCA	136	4	Lipocortin-1 (annexin II)
	GeneScaffold_4261_4924_53732_-1	78	3	annexin A2	Anxa2	LUHU	80	3	annexin I
4859	GeneScaffold_4261_38206_96580_-1	132	8	annexin A2	Anxa2	Q6N0B3_HUMAN	221	7	annexin A2 isoform 1
	GeneScaffold_2096_57622_76474_1	76	3	annexin A1	Anxa1	Q6BCI9_FELCA	104	3	Lipocortin-1
	GeneScaffold_616_113865_116741_-1	39	2	acidic ribosomal phosphoprotein P0	-				
4869	GeneScaffold_2582_288979_514454_-1	74	2	ATPase, Ca++ transporting, plasma membrane 2	Atp2b2	Q6BCI9_FELCA	58	2	Lipocortin-1
	GeneScaffold_2096_33194_105616_-1	72	2	Annexin A1	Anxa1				
4985	GeneScaffold_4261_38206_96580_-1	460	18	annexin A2	Anxa2	Q8TBV2_HUMAN	534	18	ANXA2 protein
	GeneScaffold_4261_4924_53732_-1	207	10	annexin A2	Anxa2	Q6JVS7_9PAST	54	2	ATP synthase beta subunit
5020	scaffold_156020_24876_33658_-1	38	2	peptidase	Pepb	LGBUI	78	4	beta-lactoglobulin
5105	GeneScaffold_2096_57622_76474_1	173	10	annexin A1	Anxa1	Q6BCI9_FELCA	235	7	Lipocortin-1
	GeneScaffold_668_2874_109658_-1	36	2	Sodium channel protein type XI alpha	SCN11A	Q659U4_HALGR	189	6	Annexin 1
5106	scaffold_149331_31069_70108_1	74	3	voltage-dependent anion channel 2	-	Q5VWK3_HUMAN	236	6	Voltage-dependent anion

	GeneScaffold_4261_4924_53732_-1	65	3	annexin A2	Anxa2				channel 2
	GeneScaffold_4546_152267_270655_-1	36	3	intestinal cell kinase	ICK				
5456	GeneScaffold_4226_44961_169647_1	39	2	obscurin	OBSCN	-	-	-	-
	GeneScaffold_2000_280932_399261_-1	37	2	multiple C2 and transmembrane domain-containing protein 1	MCTP1				
5558	GeneScaffold_2975_39350_96163_1	42	2	MYB DNA-binding domain protein	Mybbp1a	-	-	-	-
5666	GeneScaffold_3612_312285_320583_-1	234	16	prohibitin	Phb	Q4R5M5_MACFA	581	25	similar to human prohibitin
	scaffold_101245_108936_112032_-1	81	5	beta-actin	Actb	ACTB_CAMDR	112	4	Actin
	GeneScaffold_2905_96136_153267_-1	42	3	ARMET-like protein 1 precursor	-	Q6JVS7_9PAST	55	3	ATP synthase beta subunit
5676	GeneScaffold_4226_3314_169647_1	50	5	obscurin	OBSCN	Q3B3F0_PELLD	52	2	Fe-S type hydro-lyases tartrate/fumarate alpha and beta region
5806	GeneScaffold_2000_280932_399261_-1	37	4	multiple C2 domains, transmembrane 1	Mctp1	Q6JVS7_9PAST	58	3	ATP synthase beta subunit
6113	GeneScaffold_2000_280932_399261_-1	47	2	multiple C2 domains, transmembrane 1	Mctp1	-	-	-	-
6440	scaffold_156020_24876_33658_-1	47	2	peptidase	Pepb	LGBUI	192	5	beta-lactoglobulin
						S52094	74	2	sorcin
6970	GeneScaffold_5226_230166_23	47	2	60S ribosomal	RPL12	Q8I9M1_9BI	61	3	Ribosomal

	4031_-1			protein L12		VA			protein L12
7246	scaffold_184291_104232_151340_-1	104	3	40S ribosomal protein S14	RPS14	Q1HR24_AEDAE	101	3	40S ribosomal protein S141
7401	GeneScaffold_4224_169830_172759_1	139	7	myosin, light polypeptide 6, alkali, smooth muscle and non-muscle	MYH1	MOHU6E	196	7	myosin alkali light chain 6
	GeneScaffold_4213_139484_160246_-1	40	4	Myosin light polypeptide 3	MYH1				
7732	GeneScaffold_3577_286209_330946_-1	49	2	alpha 2 macroglobulin	A2m	-	-	-	-

Appendix III - Average greyscale values of FCV capsid stain and tubulin stain in infected and mock infected FEA cells

Distance (µm)	FCV-F9				LS015				UKOS-A				R591				Mock infected			
	7 h p.i.		13h p.i.		7 h p.i.		13h p.i.		7 h p.i.		13h p.i.		7 h p.i.		13h p.i.		7 h p.i.		13h p.i.	
	FCV	Tubulin	FCV	Tubulin	FCV	Tubulin	FCV	Tubulin	FCV	Tubulin	FCV	Tubulin	FCV	Tubulin	FCV	Tubulin	FCV	Tubulin	FCV	Tubulin
0.0	86.0	35.3	114.3	65.2	108.3	154.3	65.2	152.0	97.9	86.1	210.1	114.7	172.4	161.7	199.0	142.3	0.0	35.3	3.7	55.9
0.2	90.7	54.2	109.7	66.1	118.5	151.3	69.9	152.1	96.9	87.8	202.0	108.5	176.3	147.7	199.2	149.2	0.9	50.8	0.9	41.1
0.4	92.2	38.8	118.6	78.6	121.5	141.9	74.2	154.6	114.0	93.8	185.9	107.2	171.1	144.4	196.8	144.0	1.3	49.9	0.3	37.9
0.7	94.0	39.2	124.3	70.8	122.1	127.9	61.8	154.0	113.1	107.2	184.5	118.4	168.7	150.1	200.2	144.6	0.8	46.3	1.3	40.2
0.9	93.5	42.2	128.4	76.0	121.6	128.5	66.6	162.1	114.0	106.4	189.7	110.8	160.2	139.4	201.6	147.6	0.9	38.2	0.4	41.5
1.1	98.2	40.4	128.8	99.9	106.9	139.3	75.5	168.5	121.7	99.3	195.2	102.6	158.1	142.1	202.3	135.0	0.2	49.9	0.2	35.7
1.3	117.3	40.9	134.8	92.3	98.6	128.2	78.5	171.0	122.0	105.7	193.0	102.4	158.6	146.5	194.5	142.1	0.7	43.7	1.3	36.3
1.6	120.9	42.9	132.7	96.9	98.3	120.9	69.0	163.7	116.7	123.1	187.5	132.9	159.3	139.7	189.5	143.1	0.3	52.1	1.2	59.3
1.8	119.9	48.4	141.2	92.7	102.9	133.4	69.7	167.1	119.6	126.6	183.8	143.3	157.5	136.0	179.9	129.8	0.0	58.1	0.3	45.5
2.0	121.4	52.5	135.8	86.7	102.5	141.3	58.9	164.2	113.0	136.7	180.6	136.3	154.1	144.4	185.8	128.6	0.0	37.5	0.1	55.5
2.2	113.1	64.3	129.0	94.8	108.6	147.9	69.7	153.5	121.4	133.1	183.0	143.1	156.3	154.6	193.9	129.1	0.0	40.8	0.5	67.8
2.5	119.6	64.8	137.3	102.7	93.2	154.9	73.7	164.6	117.2	135.0	178.7	132.7	150.1	152.4	183.4	129.6	0.0	45.9	0.0	38.4
2.7	125.4	66.8	127.9	115.1	94.9	147.2	81.1	162.6	108.6	131.8	180.2	136.9	147.3	155.7	185.4	151.0	0.0	51.4	0.0	43.6
2.9	127.4	75.5	139.5	113.8	92.7	155.2	89.0	173.3	119.2	132.9	195.4	135.1	141.1	157.6	190.9	152.4	0.0	49.8	0.0	37.1
3.1	144.2	68.0	138.7	113.0	92.6	144.3	77.6	171.2	114.8	139.9	192.6	128.7	143.3	173.5	179.8	144.6	0.0	66.3	0.0	53.2
3.4	143.6	61.0	154.0	116.7	96.9	156.2	79.0	171.5	106.6	132.3	194.0	144.2	153.4	169.7	172.6	135.1	2.3	54.6	0.0	57.2
3.6	140.8	65.7	157.8	123.3	92.3	146.1	77.0	166.5	102.4	121.1	202.5	147.8	158.1	181.8	178.0	151.2	0.2	45.7	0.6	48.7
3.8	141.0	73.1	160.9	119.8	98.4	142.7	82.6	154.2	97.4	123.5	194.5	130.8	166.2	170.8	176.7	162.3	0.0	48.0	0.4	57.3
4.0	148.9	86.3	148.8	113.1	94.9	158.4	80.6	160.9	95.4	124.9	197.6	139.8	166.1	175.5	171.3	145.8	0.4	39.5	0.1	65.0
4.3	137.3	76.0	148.8	123.9	93.3	146.5	76.1	169.3	102.8	121.0	197.0	156.7	165.6	186.6	160.8	162.3	0.5	51.7	0.6	66.5
4.5	130.6	86.7	149.2	131.9	97.5	147.6	81.5	168.1	95.7	136.1	184.0	155.9	166.2	188.8	156.0	156.2	0.1	60.6	2.0	66.5
4.7	129.7	83.6	129.7	131.5	94.3	162.3	76.0	174.0	91.3	115.2	190.6	138.6	173.3	182.2	160.6	142.2	0.0	60.0	1.9	53.5
4.9	131.1	92.9	108.4	126.3	94.9	157.6	72.7	156.6	87.1	102.9	187.4	141.3	179.5	191.6	162.2	143.7	0.0	83.2	0.8	63.8
5.2	135.1	96.2	106.7	136.8	97.9	158.8	68.0	165.5	85.1	117.5	189.7	158.3	182.2	183.4	151.4	141.9	0.1	97.4	0.3	94.0
5.4	126.7	105.4	91.8	145.2	98.6	160.4	69.1	153.5	76.8	107.1	187.8	159.0	180.9	195.4	150.4	150.0	0.5	76.9	0.2	87.4

5.6	123.6	102.0	83.6	144.2	99.0	167.4	61.3	164.6	81.7	110.1	174.6	161.4	175.8	189.2	152.6	126.1	0.2	84.8	0.1	95.3
5.8	135.9	126.6	76.9	138.7	95.3	162.6	54.1	150.7	85.8	109.3	177.5	158.9	172.4	197.6	154.1	134.9	0.4	90.5	0.3	95.7
6.1	129.3	121.9	64.1	126.4	95.3	160.3	44.3	146.2	73.4	93.2	169.6	156.6	161.3	190.4	152.8	139.6	0.3	74.7	0.1	82.0
6.3	130.6	132.6	61.2	124.2	86.2	155.6	41.8	146.7	78.2	90.8	153.3	168.8	152.9	178.7	150.0	143.8	0.3	78.2	0.4	71.9
6.5	128.8	129.8	54.9	126.9	90.2	161.8	32.0	135.0	71.7	92.5	151.8	156.2	144.4	179.4	144.5	140.8	0.1	76.2	0.6	65.0
6.7	107.0	113.5	46.7	112.4	90.0	141.1	32.1	130.0	72.9	84.3	144.7	151.6	127.8	180.3	139.7	139.5	0.0	97.9	0.4	77.9
7.0	112.1	116.3	37.6	104.9	91.1	145.3	32.2	130.3	79.7	90.2	136.3	148.6	119.3	170.8	133.1	141.7	1.2	100.2	2.0	80.5
7.2	113.7	121.1	27.3	100.1	81.7	138.5	25.5	111.9	84.0	96.9	125.0	132.7	111.3	181.7	115.8	137.1	0.3	89.7	0.2	76.3
7.4	107.6	132.8	30.6	107.0	83.8	141.7	21.7	106.3	85.8	98.2	124.9	144.0	100.8	173.2	118.2	139.6	0.2	102.1	0.2	77.6
7.6	105.2	125.9	39.2	119.8	74.7	141.1	14.7	119.4	83.2	94.2	113.5	139.3	91.2	171.5	119.3	136.8	0.4	105.2	0.5	84.5
7.9	95.8	109.9	39.3	122.1	74.0	137.8	19.6	116.1	80.5	93.3	101.9	128.6	83.0	163.4	111.2	126.4	0.4	102.0	0.3	80.5
8.1	78.5	109.1	36.6	114.8	74.6	116.9	14.9	121.9	81.9	90.9	83.9	152.7	80.6	150.5	96.4	123.6	0.3	107.6	0.6	82.2
8.3	83.3	122.1	30.6	109.8	64.5	122.4	11.6	114.2	91.0	95.8	73.6	139.5	70.5	165.8	94.9	121.1	1.7	113.1	0.9	75.7
8.5	83.4	112.6	28.0	107.8	57.0	129.4	11.2	115.1	74.3	98.9	80.8	148.6	62.1	154.1	92.3	135.9	0.4	110.3	0.8	75.2
8.8	74.8	106.7	23.2	123.8	49.9	121.4	8.3	118.1	62.7	100.0	82.7	150.0	59.7	165.8	79.4	114.8	0.4	100.5	1.6	81.3
9.0	55.6	106.3	19.7	113.2	42.0	124.2	8.0	114.1	46.1	76.6	81.4	163.5	49.1	159.7	80.3	128.3	0.2	113.9	0.6	99.7
9.2	57.9	120.5	21.9	108.5	35.5	113.2	6.0	109.0	36.7	58.2	74.1	159.2	41.1	157.1	84.7	120.0	0.4	115.2	0.2	81.5
9.4	53.8	97.4	18.0	96.5	32.6	113.5	6.1	94.0	38.4	57.4	68.4	168.8	35.0	146.3	89.0	113.0	0.1	120.2	0.3	86.5
9.7	46.7	91.5	10.8	89.6	22.6	112.0	5.0	90.9	38.4	68.6	55.2	161.5	32.2	155.8	82.3	122.5	0.0	128.0	0.4	81.8
9.9	53.9	94.8	6.8	85.6	18.1	106.6	6.8	101.3	38.5	80.0	55.8	156.4	30.7	163.9	67.7	109.7	0.1	122.8	2.3	97.6
10.1	46.1	90.7	7.4	82.2	17.7	108.4	4.7	83.5	39.5	76.6	59.5	152.1	26.1	156.6	68.1	104.7	0.3	125.4	0.7	97.2
10.3	46.5	99.2	10.0	78.5	15.3	105.5	3.3	84.1	33.0	87.4	57.6	158.1	25.9	145.3	69.4	108.7	0.0	150.6	0.3	107.2
10.6	39.9	80.4	9.8	83.4	8.7	88.2	3.9	92.3	31.5	80.9	63.4	165.0	26.8	142.5	57.6	113.0	1.7	119.7	0.0	112.2
10.8	43.6	94.2	7.3	77.1	7.6	85.0	3.7	92.4	27.0	72.9	62.4	178.3	26.7	154.9	51.0	124.5	0.0	122.4	0.1	130.0
11.0	39.7	87.6	6.2	80.7	8.1	93.0	4.1	89.6	25.9	75.1	56.2	163.7	25.7	142.6	45.8	114.1	0.0	134.0	0.1	113.0
11.2	38.8	89.4	5.3	91.1	10.5	81.2	4.0	82.5	26.1	75.5	54.6	166.2	21.2	147.0	48.1	109.8	0.0	120.0	0.2	106.7
11.5	29.0	85.9	4.2	91.9	5.6	75.3	2.7	92.8	20.6	69.6	62.2	136.3	18.4	145.1	56.2	115.6	0.3	127.3	0.5	101.3
11.7	24.4	83.5	4.1	81.5	5.0	87.8	3.7	86.6	28.7	55.2	71.3	131.2	17.3	150.2	57.2	113.1	0.7	115.8	0.7	105.7
11.9	26.4	81.9	6.8	92.2	5.4	82.6	6.9	81.6	20.6	70.4	66.9	131.0	11.2	154.7	45.3	108.2	0.1	106.6	0.2	89.4
12.1	32.1	82.0	3.1	89.6	4.1	85.6	5.2	73.1	13.0	84.9	51.1	119.3	13.4	134.1	50.9	117.8	0.9	115.2	0.3	90.5
12.4	29.0	96.4	3.4	84.6	4.7	81.3	3.8	79.5	12.1	96.7	41.5	128.1	12.5	135.1	47.3	120.1	0.3	105.8	1.1	96.9
12.6	26.0	94.7	6.4	95.7	6.0	77.2	3.8	78.8	14.0	90.0	48.4	134.9	9.9	148.6	52.0	127.6	0.4	90.7	0.2	87.7

12.8	22.7	69.5	10.1	100.3	3.5	73.7	3.6	92.5	10.7	82.0	47.0	123.5	9.6	149.4	50.3	136.5	0.3	92.9	0.3	97.0
13.0	22.0	77.3	5.5	99.9	3.4	87.9	3.2	87.8	9.4	79.8	41.0	114.1	8.4	131.1	53.7	128.5	0.2	88.9	0.2	84.3
13.3	22.9	83.7	1.6	93.6	1.3	70.9	1.9	71.8	10.5	83.3	49.8	113.4	6.0	135.3	50.4	119.0	0.3	84.3	0.3	80.8
13.5	25.9	68.4	1.0	94.8	4.5	90.5	3.9	70.5	12.7	79.3	51.8	120.2	5.8	128.3	35.6	123.8	0.0	83.1	0.0	70.2
13.7	24.1	68.0	3.0	91.9	3.5	91.0	6.1	76.4	6.8	91.4	40.7	111.4	5.3	126.8	32.5	138.8	0.1	106.7	0.2	84.5
13.9	22.4	78.9	3.7	86.4	1.0	90.3	1.2	84.2	8.4	90.1	38.5	109.1	4.9	122.0	25.1	144.7	0.8	87.9	0.0	86.1
14.2	24.8	88.3	2.1	84.1	4.4	89.5	2.0	85.7	8.9	89.6	42.7	107.7	6.3	119.4	27.1	132.7	0.4	81.3	0.2	78.7
14.4	19.9	81.6	3.1	83.9	6.1	98.7	1.4	63.2	11.7	80.3	38.1	105.6	5.8	112.4	29.5	113.6	0.9	70.2	0.1	82.6
14.6	13.4	72.9	4.6	67.8	5.8	105.3	0.7	85.8	10.5	91.2	34.0	116.0	4.6	109.0	30.2	118.9	1.1	63.5	0.2	88.0
14.8	10.8	79.3	7.2	70.9	5.8	90.1	0.5	92.0	10.0	88.8	46.6	113.8	5.6	112.2	32.5	141.4	0.9	70.9	0.8	96.3
15.1	17.3	89.0	8.3	88.5	6.0	93.4	0.9	90.8	7.5	82.4	47.6	112.2	5.3	112.5	25.6	126.7	0.0	68.2	1.1	76.6
15.3	23.0	82.2	3.5	82.4	7.0	97.1	3.0	83.5	11.6	89.8	54.9	97.2	7.9	112.3	22.6	109.5	0.1	71.2	0.2	65.5
15.5	28.1	72.7	6.5	71.1	6.3	91.6	1.8	80.7	8.1	98.1	45.6	112.6	4.5	118.8	20.0	112.0	0.2	75.3	0.2	81.7
15.7	31.7	64.7	2.6	63.1	4.5	99.5	0.9	83.7	7.8	99.7	47.6	94.0	3.6	89.8	19.6	130.2	0.8	62.4	0.1	87.8
16.0	21.9	65.5	2.9	74.8	5.5	89.8	1.4	78.0	11.5	100.7	48.1	85.5	4.2	89.2	20.2	122.2	0.9	71.3	0.3	70.3
16.2	20.5	57.6	5.3	66.8	5.0	82.0	1.8	76.4	10.0	90.4	33.8	85.1	4.0	105.9	23.8	102.0	0.3	59.5	0.3	69.3
16.4	20.1	51.2	11.9	71.3	6.1	80.2	2.6	75.9	7.2	97.2	29.1	70.4	4.0	98.6	14.7	105.3	0.7	47.4	1.1	76.0
16.6	17.0	46.9	8.8	65.8	5.0	89.9	1.0	68.3	7.1	89.8	31.8	71.6	2.0	76.9	17.2	103.9	0.6	45.8	0.3	76.6
16.9	16.2	35.0	3.9	57.1	4.1	98.8	1.0	63.4	8.2	90.3	33.9	69.1	1.1	82.8	20.1	102.6	0.1	50.8	0.1	63.1
17.1	18.7	37.2	2.7	63.0	3.9	74.5	1.5	61.4	6.4	88.1	29.4	62.1	0.2	68.2	23.7	94.3	0.1	47.0	0.3	76.2
17.3	16.0	36.6	4.6	75.2	3.1	78.7	1.8	62.7	8.0	81.1	22.8	70.4	0.3	71.9	23.4	81.0	0.8	62.2	0.2	72.0
17.5	18.2	34.5	4.4	62.7	3.2	66.4	0.7	52.4	4.8	76.2	25.4	74.5	1.1	81.2	22.6	81.1	1.1	52.0	1.6	70.2
17.8	16.4	42.2	4.4	66.5	4.0	58.0	1.5	65.7	5.8	69.2	26.4	76.4	2.1	81.0	34.0	80.1	1.3	42.2	0.5	58.2
18.0	10.6	28.7	3.3	68.8	3.4	59.7	0.5	60.3	11.6	60.4	36.4	62.9	1.6	66.9	31.2	81.4	0.7	45.4	0.1	65.4
18.2	13.8	23.4	2.5	71.8	2.1	66.4	0.9	64.7	10.4	56.1	37.0	69.4	1.1	67.6	25.8	83.7	0.0	51.5	0.3	63.5
18.4	30.3	29.0	4.2	68.8	2.8	73.3	0.3	63.9	4.5	48.0	29.1	65.6	0.5	56.6	29.8	67.3	0.0	66.1	0.0	59.3
18.7	29.0	23.5	4.3	56.0	3.8	64.7	0.5	67.7	5.5	47.7	28.4	63.4	0.8	52.4	27.3	65.4	0.1	49.8	0.1	47.8
18.9	21.5	28.9	2.4	65.6	3.9	62.3	1.1	71.4	4.1	43.8	19.9	59.5	2.0	55.8	22.1	66.3	0.2	49.4	1.0	46.7
19.1	22.2	24.8	4.3	62.2	4.5	63.5	0.8	67.7	6.8	46.0	31.0	62.9	2.0	71.3	24.3	76.5	0.3	43.1	0.2	58.7
19.3	18.3	27.8	6.4	62.4	6.0	52.9	1.1	69.2	11.0	37.4	30.1	68.9	0.8	53.7	29.7	70.7	0.3	52.9	0.2	67.0
19.6	22.3	25.6	6.9	55.9	5.0	59.9	0.8	67.9	5.8	38.3	27.5	59.5	1.7	49.7	22.0	71.0	1.1	61.8	0.2	57.0
19.8	15.7	19.8	2.7	54.0	4.3	51.8	1.7	71.3	5.4	47.8	34.5	54.7	0.3	59.4	25.2	70.1	0.1	65.8	0.1	51.0

Appendix IV - Average greyscale values of FCV capsid stain and vimentin stain in infected and mock infected FEA cells

Distance (µm)	FCV-F9				LS015				UKOS-A				R591				Mock infected			
	7 h p.i.		13h p.i.		7 h p.i.		13h p.i.		7 h p.i.		13h p.i.		7 h p.i.		13h p.i.		7 h p.i.		13h p.i.	
	FCV	Vimentin	FCV	Vimentin	FCV	Vimentin	FCV	Vimentin	FCV	Vimentin	FCV	Vimentin	FCV	Vimentin	FCV	Vimentin	FCV	Vimentin	FCV	Vimentin
0.0	189.7	218.7	182.0	99.8	57.4	168.5	28.2	162.0	62.5	172.6	85.1	144.5	169.2	243.4	134.3	70.6	10.0	90.4	9.1	83.3
0.2	193.7	219.2	183.2	103.4	62.0	164.7	27.5	163.5	66.7	175.5	77.6	146.9	171.7	244.6	135.0	67.6	6.6	89.4	7.8	74.9
0.4	197.1	215.0	189.6	99.4	65.4	162.6	28.9	166.9	67.7	176.2	81.8	142.8	172.7	243.7	128.7	62.7	6.7	92.1	8.0	80.0
0.7	194.8	218.5	186.8	102.2	60.4	160.3	31.1	170.1	69.2	171.9	81.0	147.2	175.2	240.2	132.2	66.8	6.8	91.8	5.6	81.7
0.9	197.0	217.1	186.7	105.9	60.3	164.8	42.4	168.2	69.4	172.2	79.7	147.1	177.8	239.1	129.6	66.9	6.3	84.3	5.6	80.2
1.1	188.5	221.6	186.7	107.3	55.1	163.1	37.3	166.5	68.8	167.8	84.0	143.0	179.0	240.9	132.7	64.9	6.2	78.5	8.9	77.5
1.3	190.2	223.2	190.1	106.9	64.3	159.1	43.0	168.5	65.9	176.4	81.9	149.5	174.9	240.1	139.0	67.7	9.3	77.3	9.8	82.3
1.6	189.2	223.0	192.6	111.8	67.0	160.9	45.4	171.2	67.7	182.6	85.5	147.4	171.0	241.1	141.2	69.9	9.6	77.9	8.0	83.7
1.8	189.1	221.8	194.4	112.9	62.8	156.4	41.7	175.3	69.3	175.9	79.4	149.7	165.6	241.0	137.9	72.0	11.4	73.8	5.5	83.2
2.0	198.2	221.9	191.4	112.7	49.7	153.7	43.8	171.3	69.2	175.2	85.5	154.2	167.8	239.9	136.7	73.0	9.6	77.9	7.4	87.3
2.2	197.8	222.7	195.6	114.5	52.1	154.4	41.8	168.0	66.5	175.4	87.0	155.7	160.1	239.2	131.7	74.2	9.8	73.2	8.3	84.0
2.5	200.4	224.4	195.2	114.7	56.1	154.5	52.8	169.4	68.6	179.9	85.0	155.9	161.6	241.7	136.1	70.4	8.1	72.3	7.5	88.3
2.7	199.4	223.0	199.7	117.6	49.1	151.1	52.2	169.6	64.9	172.5	95.3	158.2	157.7	239.8	136.0	70.4	7.9	68.7	6.2	89.3
2.9	198.9	226.7	199.3	119.5	52.9	152.4	57.2	166.5	66.2	163.3	91.0	158.1	165.0	241.3	140.6	71.6	9.8	68.1	5.1	92.6
3.1	204.3	224.3	201.8	123.0	52.2	148.5	58.8	171.3	61.3	173.9	92.2	164.6	154.3	238.7	138.4	72.2	7.7	71.7	7.3	91.7
3.4	204.6	224.8	207.1	122.9	47.5	140.9	52.8	166.0	66.5	171.0	94.3	168.6	143.9	237.7	143.0	68.0	6.1	71.6	8.0	92.5
3.6	210.0	224.1	207.7	124.2	49.0	142.0	55.9	161.4	59.7	165.3	91.9	169.7	147.9	237.0	144.3	72.8	6.7	70.1	6.6	99.0
3.8	207.7	221.6	212.3	125.9	51.0	142.8	58.3	165.0	59.3	163.7	98.6	168.4	144.0	236.8	145.7	69.7	6.2	72.5	6.2	98.0
4.0	200.9	220.9	211.0	126.2	50.8	147.5	59.9	154.8	59.1	157.6	93.5	174.7	150.7	233.2	146.3	74.4	8.1	74.6	5.6	100.2
4.3	206.1	219.9	215.6	128.3	51.1	141.1	55.1	160.9	57.6	157.8	92.6	171.3	144.0	232.4	151.6	72.9	6.4	74.2	7.0	100.7
4.5	198.5	220.6	213.5	127.1	47.4	140.2	54.7	162.5	56.8	157.2	87.1	172.2	133.0	233.9	149.1	71.3	7.9	72.2	8.2	98.2
4.7	194.7	217.9	213.2	132.3	47.5	138.1	50.6	156.0	56.3	154.7	93.3	173.5	127.6	228.0	146.1	72.8	6.7	72.1	7.8	99.6
4.9	186.3	212.1	211.3	133.1	47.0	144.9	50.3	148.9	55.7	158.7	88.0	167.9	125.9	224.1	141.5	69.6	7.7	73.6	6.8	99.0
5.2	181.0	204.6	211.6	131.7	45.9	147.4	46.1	144.0	56.8	152.7	92.3	166.4	112.6	221.5	147.0	69.8	9.6	73.6	6.9	99.9
5.4	178.1	201.3	212.0	131.7	48.0	146.3	49.3	139.7	58.4	152.3	83.5	164.6	114.0	218.6	142.8	67.3	9.0	78.6	6.8	95.8
5.6	170.6	195.1	207.4	129.7	46.4	145.3	52.2	133.0	54.7	150.2	83.8	166.2	111.8	212.0	143.4	70.2	5.4	80.2	8.7	92.8

5.8	163.4	189.6	208.8	130.2	43.9	146.1	50.3	127.6	53.2	150.9	81.2	164.4	107.5	205.3	144.0	73.9	5.6	80.8	8.3	93.7
6.1	159.8	187.1	202.4	127.7	47.9	141.0	57.2	120.0	51.3	147.0	83.0	161.6	103.8	201.7	143.9	71.5	4.7	75.9	7.7	94.7
6.3	155.1	180.1	197.0	127.4	44.6	142.5	60.1	122.6	51.9	144.5	87.1	156.9	107.1	203.1	142.6	72.7	7.1	76.6	7.7	95.0
6.5	153.0	182.3	199.2	124.4	43.4	142.7	57.3	120.9	47.9	143.9	92.9	157.0	103.1	196.6	140.2	66.2	7.4	81.0	6.8	98.6
6.7	151.1	179.4	202.1	119.8	41.1	143.2	57.5	114.9	50.8	140.8	95.9	147.1	98.3	196.8	130.3	62.4	6.5	81.1	9.7	92.3
7.0	148.1	176.1	203.4	120.2	38.2	142.5	56.2	115.3	53.6	132.8	91.0	147.2	91.5	194.7	127.4	68.3	4.8	83.6	9.2	88.8
7.2	142.2	170.4	201.2	118.3	35.6	133.7	54.0	112.1	50.8	134.3	92.8	137.1	94.7	190.8	123.1	62.0	5.4	89.6	8.9	86.0
7.4	135.0	165.8	207.8	114.5	35.6	134.0	49.0	106.9	45.6	125.3	90.0	138.0	84.0	186.9	120.1	65.1	5.8	89.7	6.8	95.2
7.6	126.5	161.2	208.5	111.9	30.3	129.9	43.4	105.5	48.2	123.9	97.7	135.3	88.4	186.1	116.6	64.8	4.9	95.5	6.9	91.8
7.9	119.2	159.1	209.6	111.8	29.2	125.0	37.6	110.0	48.0	116.2	85.8	131.4	80.9	185.9	115.4	67.6	5.1	98.0	10.7	90.8
8.1	113.8	155.6	205.1	108.3	29.9	119.2	30.2	110.3	45.1	116.1	78.7	125.3	83.1	183.4	112.0	60.0	5.8	98.9	12.9	91.7
8.3	109.8	151.7	208.1	104.3	28.1	117.4	22.9	110.0	43.3	113.0	78.5	121.6	83.8	180.7	107.4	62.0	4.5	99.1	11.6	92.0
8.5	106.5	147.5	210.4	101.3	30.5	109.8	15.0	102.8	44.0	109.5	69.2	121.0	80.9	179.0	101.8	62.4	6.1	105.3	9.3	88.3
8.8	108.2	146.3	207.7	101.3	28.1	108.5	12.1	98.9	40.9	111.7	59.6	114.7	81.1	167.8	98.6	63.0	5.9	103.7	7.1	90.1
9.0	104.3	144.9	202.5	97.7	27.0	105.2	9.4	95.1	35.9	107.7	58.2	112.2	87.6	168.2	96.2	55.9	4.6	109.7	8.9	92.5
9.2	95.9	141.0	198.7	92.7	25.3	104.7	11.7	95.2	32.4	109.3	52.5	109.5	85.2	165.2	88.6	55.3	4.1	109.9	9.3	99.2
9.4	91.5	138.1	191.0	90.9	24.6	106.3	13.5	89.9	31.9	106.5	47.3	112.0	80.9	160.4	84.2	54.5	4.9	105.0	7.7	94.6
9.7	87.3	136.8	181.8	90.7	25.0	103.9	11.8	93.3	37.3	102.5	45.8	106.4	79.7	159.6	80.7	51.0	4.5	108.6	4.7	96.6
9.9	83.5	136.2	182.7	86.8	27.4	96.2	9.8	82.7	34.9	103.2	40.3	105.9	73.8	147.8	77.7	51.6	6.3	105.3	6.1	97.1
10.1	78.2	133.2	177.1	85.0	28.3	95.3	11.4	80.2	29.8	101.0	37.7	103.5	70.6	136.8	71.2	48.5	6.9	105.4	6.2	97.1
10.3	74.2	131.9	174.3	83.8	27.4	95.2	11.9	85.7	30.5	100.2	43.6	98.6	69.3	134.9	68.4	47.5	6.9	103.2	5.0	100.5
10.6	69.8	131.9	167.1	78.6	28.9	94.8	11.2	87.6	36.3	98.9	38.8	94.2	61.6	136.0	63.9	50.6	6.3	100.9	6.7	100.2
10.8	68.1	133.1	161.3	77.3	28.2	91.2	10.8	90.3	32.1	93.6	43.4	94.7	51.8	130.4	55.7	46.4	6.3	97.3	6.4	101.4
11.0	66.1	132.2	154.4	78.7	27.3	89.2	12.8	83.0	28.1	97.0	39.8	92.0	48.9	133.0	52.6	44.0	9.6	95.5	7.2	102.4
11.2	65.5	132.9	146.6	76.4	25.0	92.4	13.5	85.7	35.4	96.4	33.0	89.7	45.4	131.5	42.8	40.7	6.7	97.7	6.8	98.9
11.5	62.6	133.9	145.4	77.0	22.0	87.6	15.3	87.3	32.3	96.1	33.1	85.8	41.0	133.1	39.2	38.9	6.7	96.8	10.8	98.5
11.7	62.0	131.4	136.2	75.2	21.4	85.4	9.4	90.4	24.4	102.5	29.0	80.6	39.2	136.4	35.9	38.2	5.9	97.9	10.4	97.2
11.9	61.8	129.8	130.2	71.1	20.2	85.1	8.2	84.1	25.8	100.3	27.2	76.2	37.4	130.3	35.6	40.6	4.9	97.8	10.0	92.1
12.1	61.0	125.4	119.2	70.0	18.4	84.1	10.6	90.4	23.6	94.6	30.5	70.0	33.8	133.1	32.0	38.3	5.3	101.2	6.7	97.5
12.4	58.5	125.6	108.3	67.7	23.0	82.8	11.4	94.8	20.4	91.4	31.4	71.9	29.3	136.6	29.6	37.8	5.0	99.8	5.9	95.9
12.6	54.2	124.6	100.2	65.7	19.9	84.8	10.7	95.9	21.2	92.5	28.6	68.4	28.8	136.3	29.7	37.8	7.9	97.5	5.2	92.8
12.8	51.7	122.8	91.2	64.7	20.4	83.3	11.6	89.3	21.3	96.2	26.4	64.4	30.7	135.9	32.9	39.6	7.3	97.6	6.8	92.0

13.0	48.9	124.3	89.6	61.0	17.5	82.0	10.0	92.9	21.5	92.1	29.7	66.5	30.6	130.0	31.7	39.0	8.6	95.7	5.4	92.2
13.3	44.8	118.4	80.7	63.1	17.8	78.3	11.5	97.9	17.1	93.3	28.9	62.1	28.3	126.3	27.3	37.2	6.6	97.8	4.5	95.8
13.5	43.0	118.4	72.4	61.1	17.2	82.4	10.3	98.0	18.7	96.5	27.7	60.7	29.6	132.1	29.7	37.7	4.1	101.4	4.4	94.3
13.7	41.0	113.7	67.7	59.5	15.0	80.3	10.8	104.7	17.7	97.9	26.0	61.1	23.7	135.2	29.9	38.2	5.6	111.0	5.3	94.3
13.9	40.5	119.0	65.7	58.7	12.1	79.0	9.5	102.5	15.3	91.6	23.7	62.1	22.1	136.7	28.1	36.9	6.0	112.3	6.1	94.5
14.2	41.9	115.2	63.8	58.6	10.7	79.7	10.6	98.0	13.8	96.1	24.6	54.1	22.1	130.4	27.6	37.3	7.2	111.0	8.1	97.2
14.4	36.3	117.4	60.5	58.4	11.6	73.3	13.3	100.3	13.2	94.1	22.3	55.2	14.2	126.2	25.3	36.1	10.2	107.8	9.5	94.6
14.6	35.7	114.5	63.4	59.9	11.2	68.4	11.8	94.4	13.5	96.2	24.9	58.1	14.8	130.4	25.2	37.1	5.5	111.5	9.0	97.6
14.8	33.4	118.1	59.8	60.3	9.8	70.6	13.4	93.0	16.6	95.4	26.4	53.8	11.8	134.5	24.5	35.3	7.1	108.0	6.6	101.0
15.1	33.8	114.7	57.3	58.6	9.0	71.2	11.5	92.7	16.3	88.0	28.1	52.9	13.2	138.8	20.2	35.2	6.6	108.5	8.0	103.0
15.3	32.4	112.4	57.1	59.6	8.7	69.2	10.0	94.7	12.3	91.6	28.4	57.1	9.8	140.4	22.7	39.7	6.4	100.6	8.6	105.5
15.5	29.4	113.6	54.1	59.9	9.3	70.4	11.7	96.2	10.7	85.7	25.6	58.6	9.8	139.6	18.6	35.1	4.9	98.2	9.7	99.2
15.7	24.3	113.9	51.5	58.0	10.6	70.4	11.1	97.2	10.6	89.2	27.6	60.0	9.3	139.0	13.7	35.2	3.9	96.6	7.1	92.8
16.0	24.0	114.4	47.0	58.2	10.3	66.5	11.0	97.3	9.2	83.8	26.6	60.3	8.9	140.2	13.7	36.6	6.6	92.4	7.0	92.4
16.2	24.0	116.1	49.1	63.3	9.5	70.9	8.8	92.7	7.8	82.2	28.2	57.4	10.0	139.2	13.1	34.9	9.1	96.7	4.1	93.3
16.4	22.5	119.1	47.8	62.7	12.9	68.4	6.8	88.7	8.4	76.2	25.2	59.5	9.1	141.9	12.0	34.4	6.1	89.2	4.2	96.4
16.6	22.6	115.6	46.3	63.2	7.7	71.5	5.5	93.2	9.1	73.3	25.1	62.3	7.2	135.3	11.7	34.7	6.7	89.1	4.4	88.9
16.9	23.2	114.7	44.0	66.5	6.3	73.4	6.1	103.0	10.1	74.9	23.6	61.8	5.0	130.3	8.2	33.1	7.6	87.9	4.5	93.0
17.1	21.4	115.6	44.2	68.0	7.1	71.1	6.1	106.1	8.1	73.0	31.8	63.9	4.7	127.9	10.7	33.4	8.8	91.8	4.4	87.8
17.3	20.7	113.1	39.1	71.4	7.4	72.1	4.9	98.2	8.7	70.6	30.3	66.3	3.9	128.3	10.1	34.7	7.0	98.1	5.3	92.8
17.5	20.6	118.0	33.8	70.2	8.4	70.7	4.8	102.1	8.3	80.5	34.2	71.6	5.2	132.2	8.5	34.4	6.6	97.1	5.2	90.8
17.8	19.5	122.8	37.0	71.9	8.5	70.1	4.7	98.8	8.9	82.7	30.7	69.7	7.2	133.7	9.2	34.5	6.0	102.2	4.8	92.6
18.0	21.0	125.5	34.9	73.3	7.3	66.2	6.7	97.1	10.2	82.5	28.1	67.3	6.8	130.1	6.7	36.3	4.6	99.9	6.2	92.7
18.2	23.6	131.5	31.2	73.4	7.7	68.6	5.8	96.4	9.0	87.3	29.8	69.9	6.7	129.1	6.2	37.6	4.6	99.7	9.2	94.0
18.4	20.5	130.2	36.3	73.9	5.4	66.7	5.6	91.9	8.3	89.2	29.3	72.0	7.3	125.2	6.1	36.6	4.7	110.5	7.0	84.2
18.7	19.2	129.9	34.9	71.6	5.2	71.2	6.6	90.8	13.3	88.0	32.3	72.8	7.2	120.4	5.2	31.0	4.9	113.2	7.2	90.2
18.9	15.5	133.2	35.6	70.2	6.5	75.4	6.5	92.0	13.1	92.0	30.0	74.0	7.4	121.4	7.5	33.6	5.3	114.7	7.2	94.5
19.1	12.0	128.5	34.6	68.3	5.1	74.1	3.9	94.6	10.5	95.0	30.8	77.4	8.9	125.0	7.0	36.5	4.7	112.3	8.9	94.2
19.3	9.5	121.9	31.4	71.3	4.4	75.2	4.6	89.3	9.3	99.5	31.5	80.5	5.7	123.8	7.1	34.9	5.6	114.7	7.2	93.9
19.6	9.1	124.7	32.3	73.6	6.0	68.2	4.3	88.2	9.3	97.2	28.2	76.6	6.3	122.4	8.1	33.6	7.2	112.7	7.9	86.8
19.8	8.7	126.6	33.0	75.3	4.7	67.1	4.6	89.7	8.8	95.0	26.5	82.3	6.3	125.7	8.0	37.3	8.3	115.9	8.0	89.5

Appendix V - Mann Whitney U test results comparing tubulin and vimentin expression between infected and uninfected FEA cells

FCV-F9 Tubulin

Mann-Whitney Test and CI: Average Tubulin 7pi I, Average Tubulin 7pi UI

	N	Median
Average Tubulin 7pi I	45	91.46
Average Tubulin 7pi UI	44	71.09

Point estimate for ETA1-ETA2 is 24.35
95.1 Percent CI for ETA1-ETA2 is (11.86,36.46)
W = 2456.0
Test of ETA1 = ETA2 vs. ETA1 > ETA2 is significant at 0.0002

Mann-Whitney Test and CI: Average Tubulin 13pi I, Average Tubulin 13pi UI

	N	Median
Average Tubulin 13pi I	45	113.03
Average Tubulin 13pi UI	44	76.13

Point estimate for ETA1-ETA2 is 33.34
95.1 Percent CI for ETA1-ETA2 is (26.13,41.26)
W = 2825.0
Test of ETA1 = ETA2 vs. ETA1 > ETA2 is significant at 0.0000

UKOS-A Tubulin

Mann-Whitney Test and CI: Average Tubulin 7pi I, Average Tubulin 7pi UI

	N	Median
Average Tubulin 7pi I	45	102.90
Average Tubulin 7pi UI	44	81.01

Point estimate for ETA1-ETA2 is 27.31
95.1 Percent CI for ETA1-ETA2 is (17.77,37.21)
W = 2745.0
Test of ETA1 = ETA2 vs. ETA1 > ETA2 is significant at 0.0000

Mann-Whitney Test and CI: Average Tubulin 13pi I, Average Tubulin 13pi UI

	N	Median
Average Tubulin 13pi I	45	143.30
Average Tubulin 13pi UI	44	108.38

Point estimate for ETA1-ETA2 is 39.66
95.1 Percent CI for ETA1-ETA2 is (27.71,52.23)
W = 2655.0
Test of ETA1 = ETA2 vs. ETA1 > ETA2 is significant at 0.0000

R591 Tubulin

Mann-Whitney Test and CI: Average Tubulin 7pi I, Average Tubulin 7pi UI

	N	Median
Average Tubulin 7pi I	45	165.75
Average Tubulin 7pi UI	44	112.35

Point estimate for ETA1-ETA2 is 55.65
95.1 Percent CI for ETA1-ETA2 is (41.46,71.50)
W = 2915.0
Test of ETA1 = ETA2 vs. ETA1 > ETA2 is significant at 0.0000

Mann-Whitney Test and CI: Average Tubulin 13pi I, Average Tubulin 13pi UI

	N	Median
Average Tubulin 13pi I	45	139.64
Average Tubulin 13pi UI	44	110.88

Point estimate for ETA1-ETA2 is 28.88
95.1 Percent CI for ETA1-ETA2 is (21.44,36.93)
W = 2817.0
Test of ETA1 = ETA2 vs. ETA1 > ETA2 is significant at 0.0000

LS015 Tubulin

Mann-Whitney Test and CI: Average Tubulin 7pi I, Average Tubulin 7pi UI

	N	Median
Average Tubulin 7pi I	133	128.53
Average Tubulin 7pi UI	44	83.79

Point estimate for ETA1-ETA2 is 46.15
95.0 Percent CI for ETA1-ETA2 is (33.94,54.57)
W = 13793.0
Test of ETA1 = ETA2 vs. ETA1 > ETA2 is significant at 0.0000

Mann-Whitney Test and CI: Average Tubulin 13pi I, Average Tubulin 13pi UI

	N	Median
Average Tubulin 13pi I	45	153.51
Average Tubulin 13pi UI	44	77.22

Point estimate for ETA1-ETA2 is 74.32
95.1 Percent CI for ETA1-ETA2 is (63.68,81.57)
W = 3010.0
Test of ETA1 = ETA2 vs. ETA1 > ETA2 is significant at 0.0000

Mock Infected Tubulin

Mann-Whitney Test and CI: Average Tubulin 7pi I, Average Tubulin 7pi UI

	N	Median
Average Tubulin 7pi I	45	74.68
Average Tubulin 7pi UI	44	71.02

Point estimate for ETA1-ETA2 is -5.02
95.1 Percent CI for ETA1-ETA2 is (-16.08,6.72)
W = 1920.0
Test of ETA1 = ETA2 vs. ETA1 not = ETA2 is NOT significant at 0.3911

Mann-Whitney Test and CI: Average Tubulin MI 13pi I, Average Tubulin MI 13pi UI

	N	Median
Average Tubulin 13pi I	45	66.55
Average Tubulin 13pi UI	44	79.72

Point estimate for ETA1-ETA2 is -12.99
95.1 Percent CI for ETA1-ETA2 is (-21.99,-4.64)
W = 1654.0
Test of ETA1 = ETA2 vs. ETA1 < ETA2 is significant at 0.0012

FCV-F9 Vimentin

Mann-Whitney Test and CI: Average vimentin 7 pi I, Average vimentin 7 pi UI

	N	Median
Average vimentin 7 pi I	64	173.27
Average vimentin 7 pi UI	63	125.49

Point estimate for ETA1-ETA2 is 48.59
95.0 Percent CI for ETA1-ETA2 is (25.18,71.42)
W = 5630.0
Test of ETA1 = ETA2 vs. ETA1 > ETA2 is significant at 0.0000

Mann-Whitney Test and CI: Average vimentin 13pi I, Average vimentin 13pi UI

	N	Median
Average vimentin 13pi I	64	106.45
Average vimentin 13pi UI	63	83.20

Point estimate for ETA1-ETA2 is 26.21
95.0 Percent CI for ETA1-ETA2 is (18.20,33.22)
W = 5212.0
Test of ETA1 = ETA2 vs. ETA1 > ETA2 is significant at 0.0000

R591 Vimentin

Mann-Whitney Test and CI: Average vimentin 7pi I, Average vimentin 7pi UI

	N	Median
Average vimentin 7pi I	64	192.73
Average vimentin 7pi UI	63	123.56

Point estimate for ETA1-ETA2 is 70.54
95.0 Percent CI for ETA1-ETA2 is (52.81,90.09)
W = 5925.0
Test of ETA1 = ETA2 vs. ETA1 > ETA2 is significant at 0.0000

Mann-Whitney Test and CI: Average vimentin 13pi I, Average vimentin 13pi UI

	N	Median
Average vimentin 13pi I	64	64.837
Average vimentin 13pi UI	63	37.437

Point estimate for ETA1-ETA2 is 26.553
95.0 Percent CI for ETA1-ETA2 is (22.065,29.347)
W = 5769.0
Test of ETA1 = ETA2 vs. ETA1 > ETA2 is significant at 0.0000

UKOS-A Vimentin

Mann-Whitney Test and CI: Average vimentin 7pi I, Average vimentin 7pi UI

	N	Median
Average vimentin 7pi I	64	133.59
Average vimentin 7pi UI	63	85.71

Point estimate for ETA1-ETA2 is 45.84
95.0 Percent CI for ETA1-ETA2 is (26.87,62.62)
W = 5934.0
Test of ETA1 = ETA2 vs. ETA1 > ETA2 is significant at 0.0000

Mann-Whitney Test and CI: Average vimentin 13pi I, Average vimentin 13pi UI

	N	Median
Average vimentin 13pi I	64	140.38
Average vimentin 13pi UI	63	69.46

Point estimate for ETA1-ETA2 is 68.12
95.0 Percent CI for ETA1-ETA2 is (51.59,78.10)
W = 5676.0
Test of ETA1 = ETA2 vs. ETA1 > ETA2 is significant at 0.0000

LS015 Vimentin

Mann-Whitney Test and CI: Average vimentin 7pi I, Average vimentin 7pi UI

	N	Median
Average vimentin 7pi I	64	136.05
Average vimentin 7pi UI	63	70.67

Point estimate for ETA1-ETA2 is 59.60
95.0 Percent CI for ETA1-ETA2 is (40.35,69.98)
W = 6005.0
Test of ETA1 = ETA2 vs. ETA1 > ETA2 is significant at 0.0000

Mann-Whitney Test and CI: Average vimentin 13pi I, Average vimentin 13pi UI

	N	Median
Average vimentin 13pi I	64	113.53
Average vimentin 13pi UI	63	89.94

Point estimate for ETA1-ETA2 is 28.25
95.0 Percent CI for ETA1-ETA2 is (18.68,46.92)
W = 5498.0
Test of ETA1 = ETA2 vs. ETA1 > ETA2 is significant at 0.0000

Mock Infected Vimentin

Mann-Whitney Test and CI: Average vimentin, Average vimentin

	N	Median
Average vimentin mock 7pi I	64	91.068
Average vimentin mock 7pi UI	63	92.389

Point estimate for ETA1-ETA2 is -2.575
95.0 Percent CI for ETA1-ETA2 is (-7.381,1.871)
W = 3855.0
Test of ETA1 = ETA2 vs. ETA1 > ETA2
P>0.05 NOT SIGNIFICANT

Mann-Whitney Test and CI: Average vimentin, Average vimentin

	N	Median
Average vimentin mock I 13pi	64	93.979
Average vimentin mock UI 13pi	63	92.827

Point estimate for ETA1-ETA2 is 0.615
95.0 Percent CI for ETA1-ETA2 is (-0.989,2.394)
W = 4230.0
Test of ETA1 = ETA2 vs. ETA1 > ETA2 is NOT significant at 0.2599

Appendix VIII - Pathway analysis of differentially transcribed genes in FEA cells in response to FCV-F9 infection

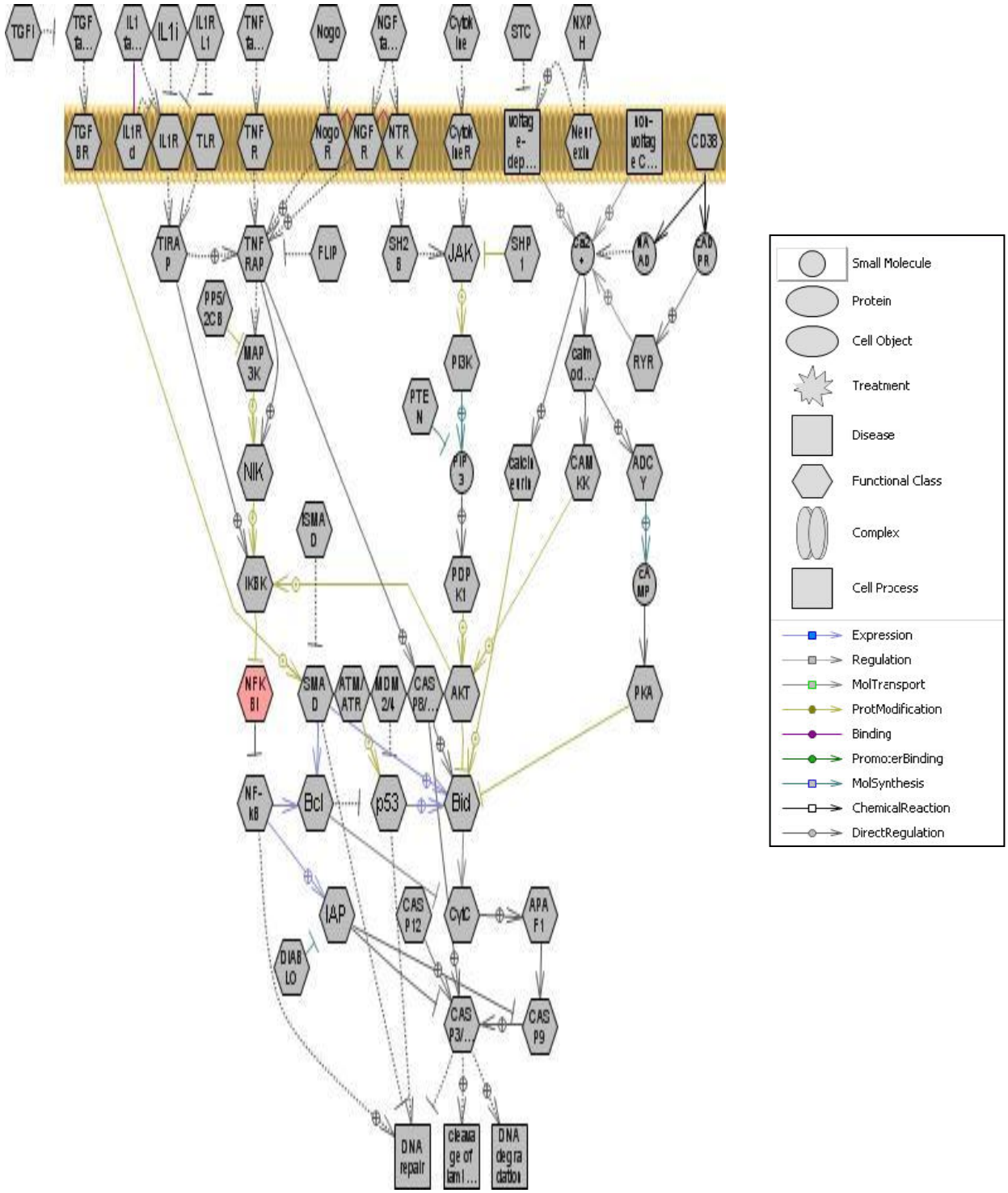

Figure A8.1. Apoptosis regulation pathway. Pathway is the comparison of mock infected and infected FEA cells at 4 h p.i.. Those genes highlighted in red are up-regulated in the infected samples, the brighter the colouration, the greater the up-regulation in transcription. A full key of gene identification can be found in the appendix (Table A8.1).

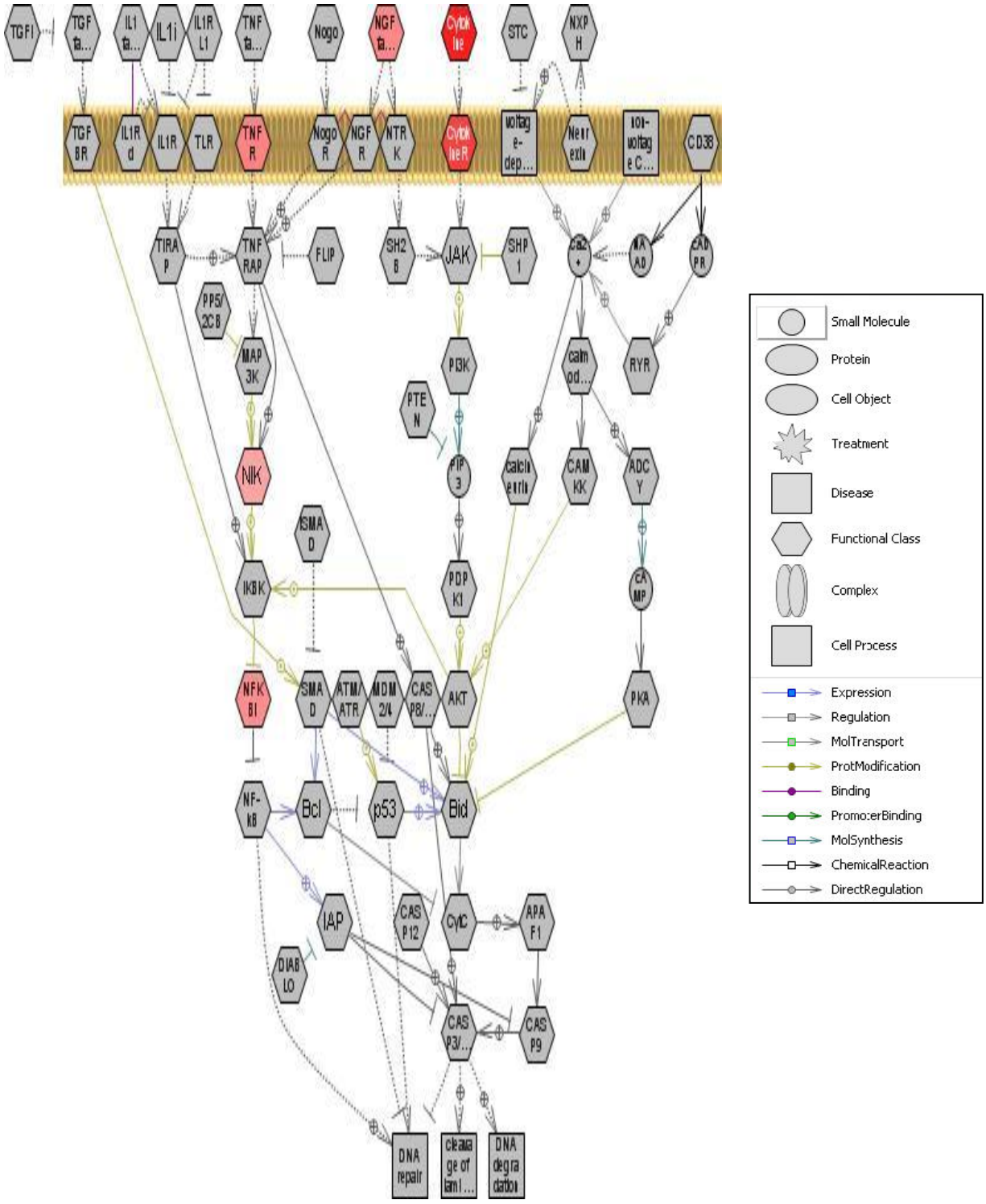

Figure A8.2. Apoptosis regulation pathway. Pathway is the comparison of mock infected and infected FEA cells at 7 h p.i.. Those genes highlighted in red are up-regulated in the infected samples, the brighter the colouration, the greater the up-regulation in transcription. A full key of gene identification can be found in the appendix (Table A8.1).

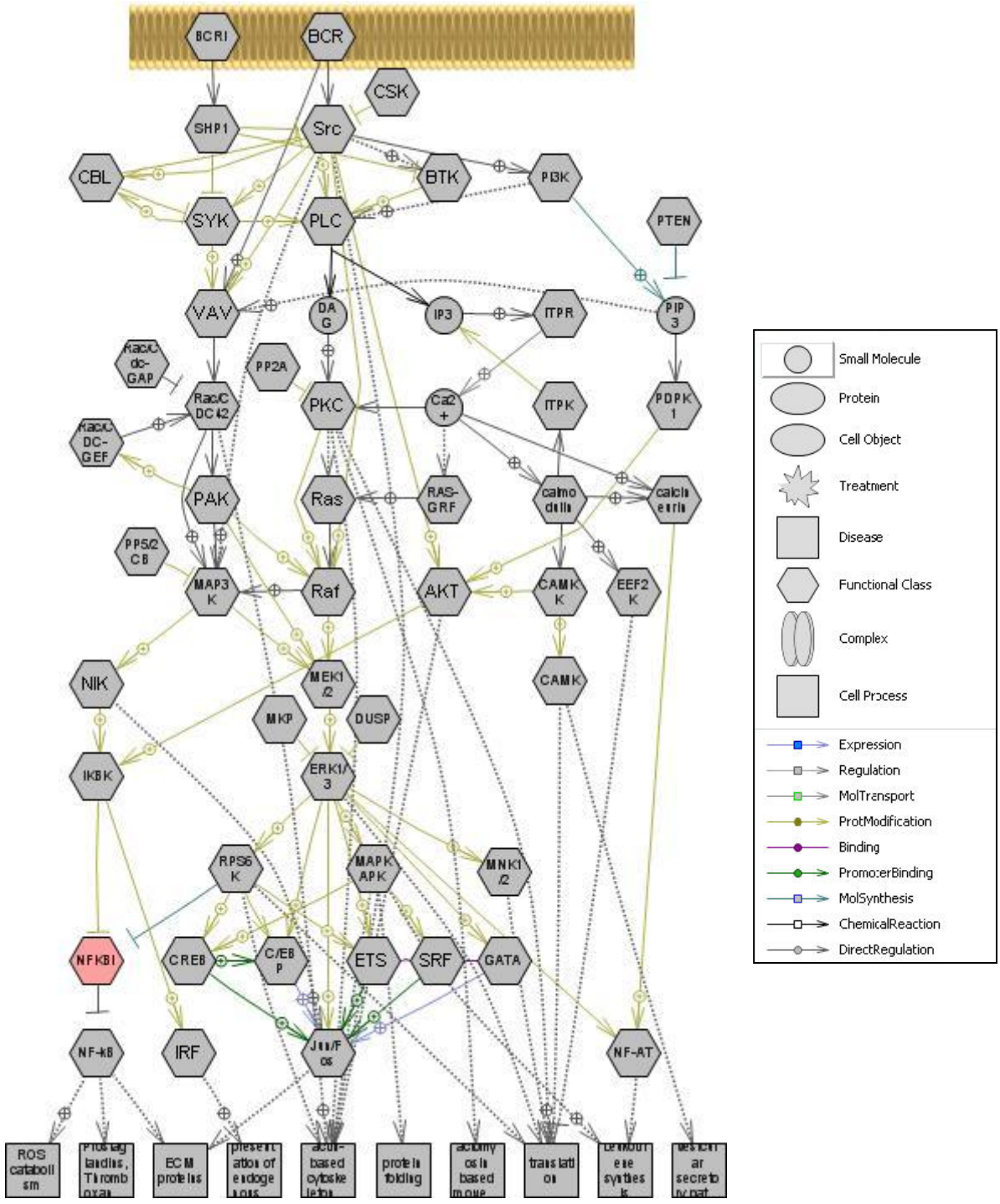

Figure A8.3. B cell activation pathway. Pathway is the comparison of mock infected and infected FEA cells at 4 h p.i.. Those genes highlighted in red are up-regulated in the infected samples, the brighter the colouration, the greater the up-regulation in transcription. A full key of gene identification can be found in the appendix (Table A8.1).

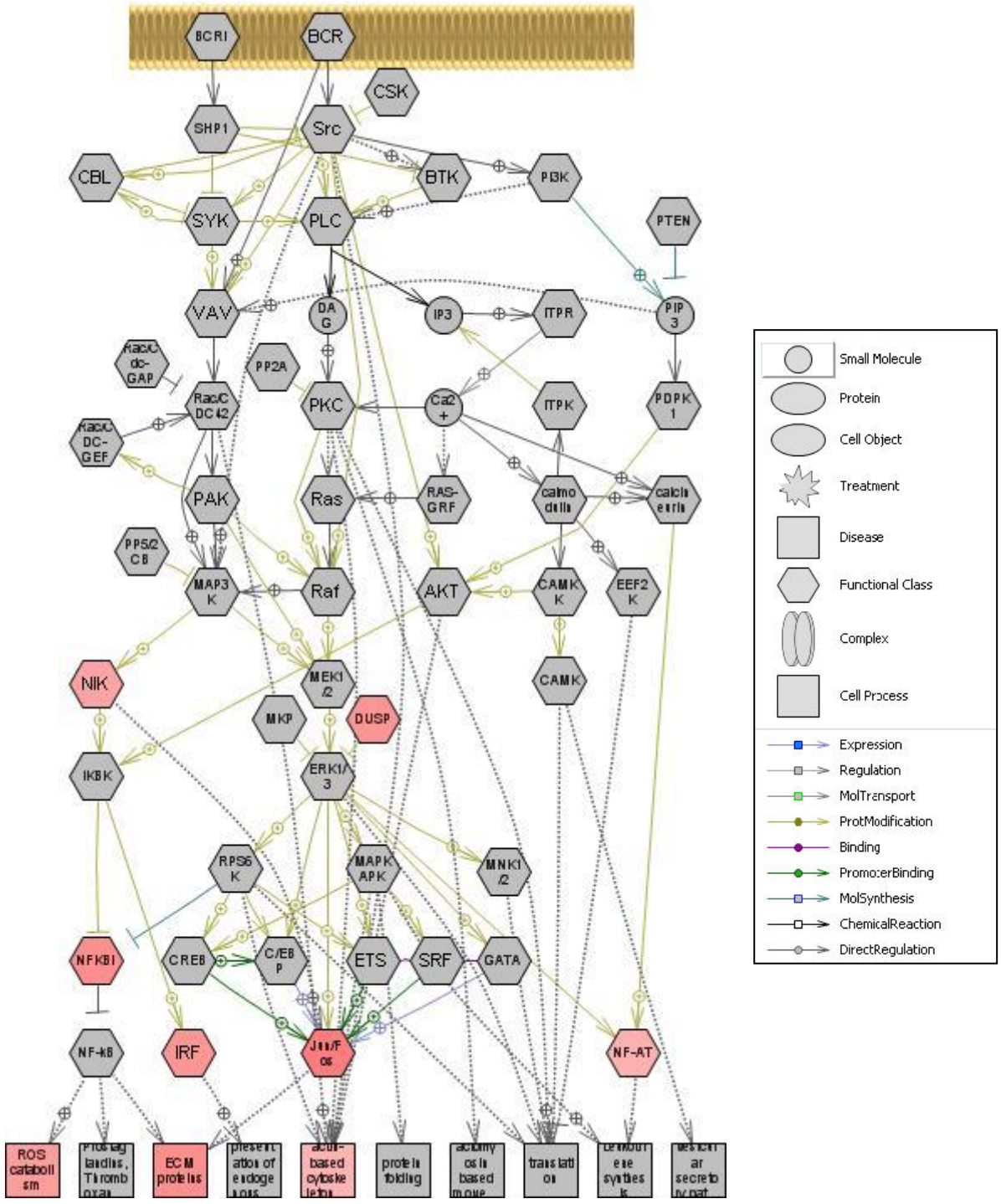

Figure A8.4. B cell activation pathway. Pathway is the comparison of mock infected and infected FEA cells at 7 h p.i.. Those genes highlighted in red are up-regulated in the infected samples, the brighter the colouration, the greater the up-regulation in transcription. A full key of gene identification can be found in the appendix (Table A8.1).

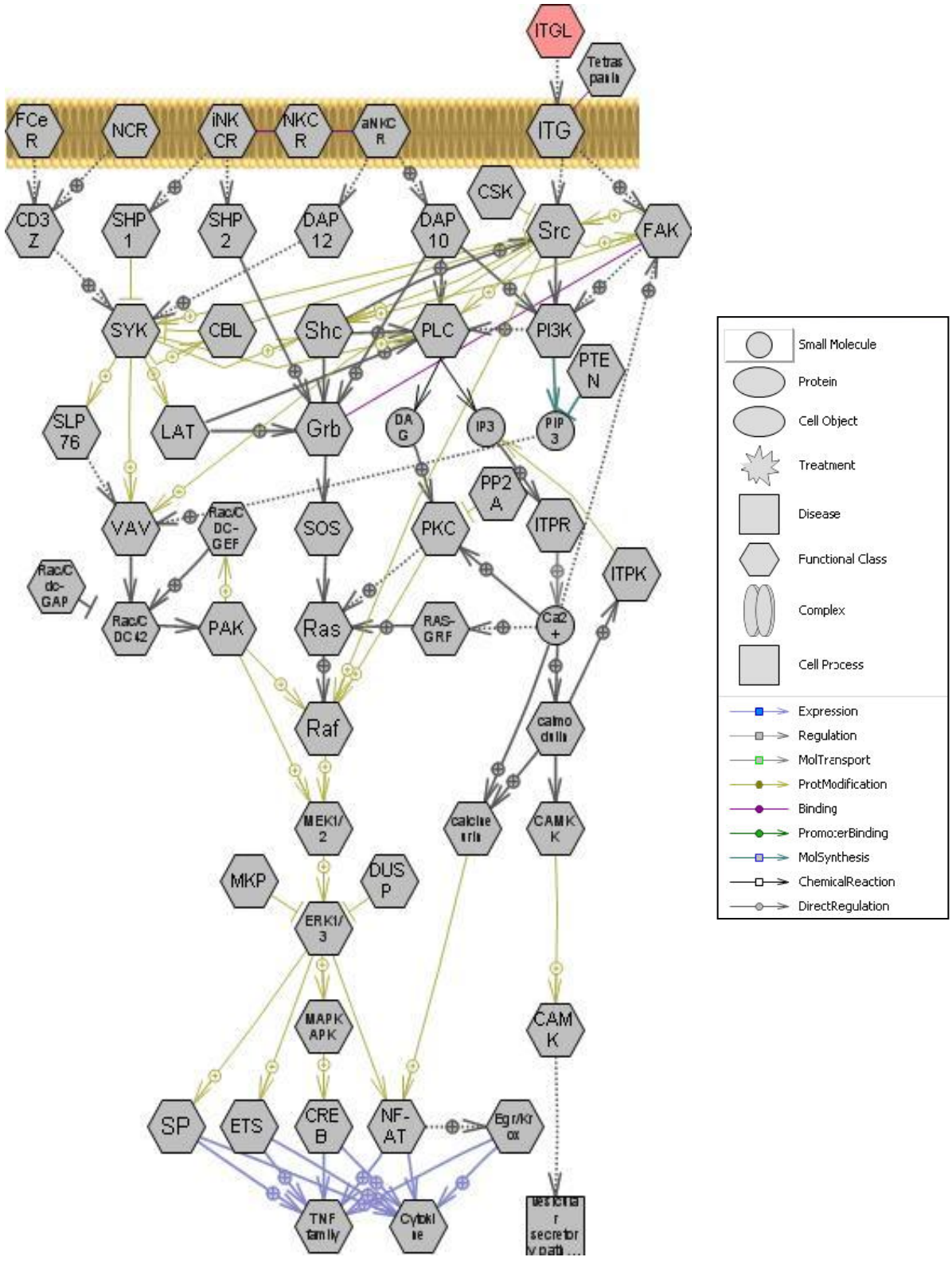

Figure A8.5. Natural killer cell activation pathway. Pathway is the comparison of mock infected and infected FEA cells at 4 h p.i.. Those genes highlighted in red are up-regulated in the infected samples, the brighter the colouration, the greater the up-regulation in transcription. A full key of gene identification can be found in the appendix (Table A8.1).

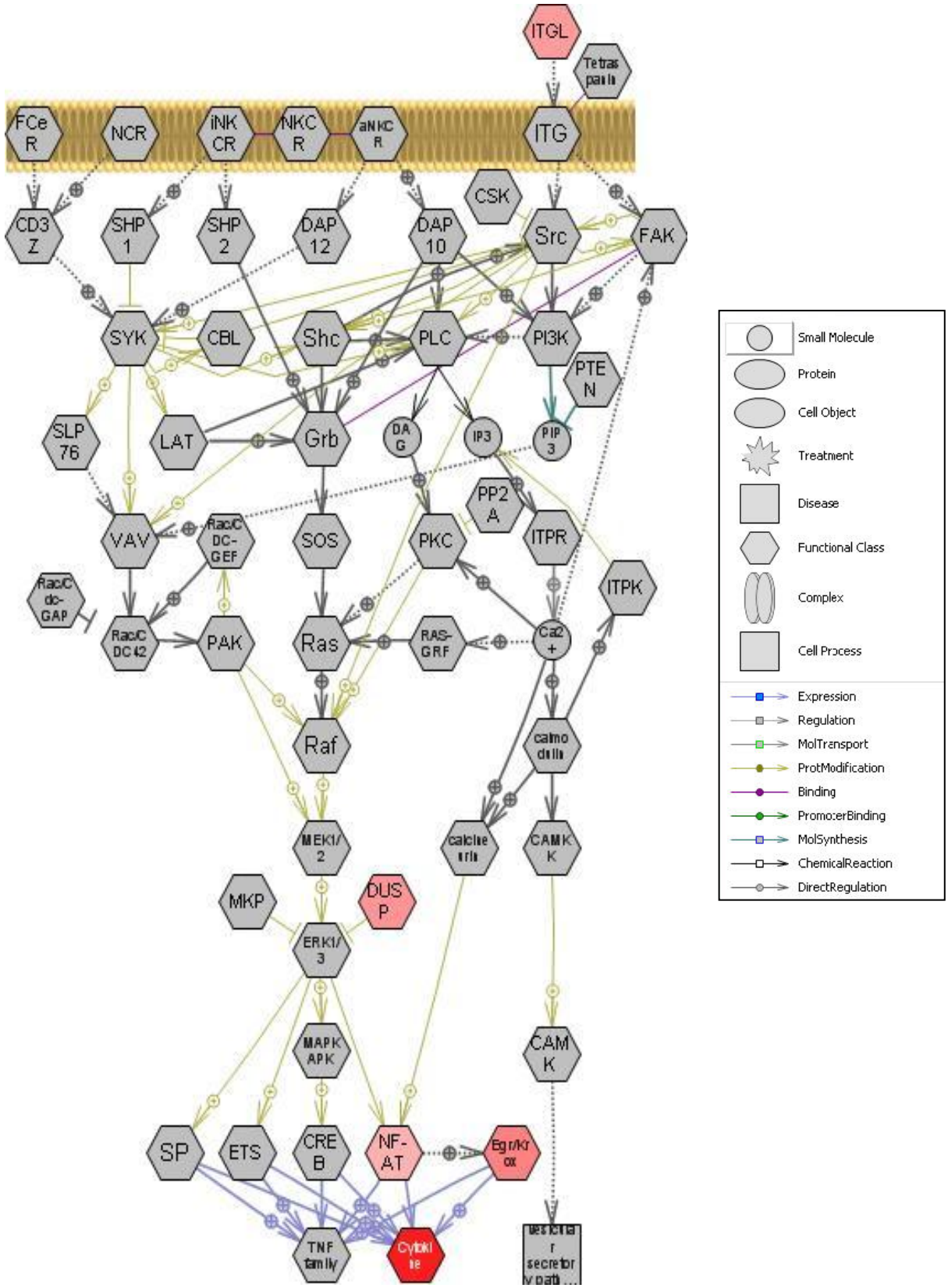

Figure A8.6. Natural killer cell activation pathway. Pathway is the comparison of mock infected and infected FEA cells at 7 h p.i.. Those genes highlighted in red are up-regulated in the infected samples, the brighter the colouration, the greater the up-regulation in transcription. A full key of gene identification can be found in the appendix (Table A8.1).

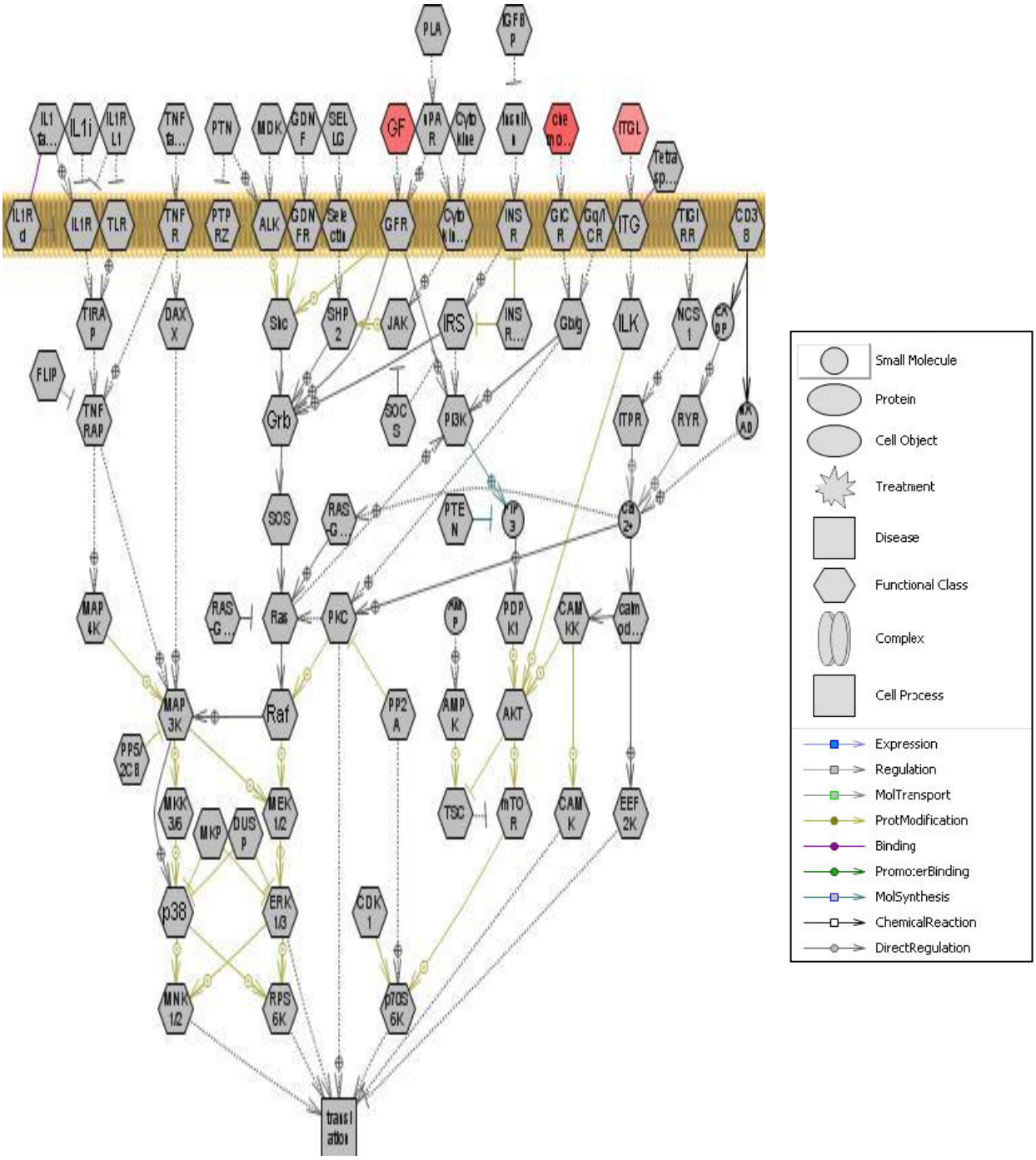

Figure A8.7. Translation control pathway. Pathway is the comparison of mock infected and infected FEA cells at 4 h p.i.. Those genes highlighted in red are up-regulated in the infected samples, the brighter the colouration, the greater the up-regulation in transcription. A full key of gene identification can be found in the appendix (Table A8.1).

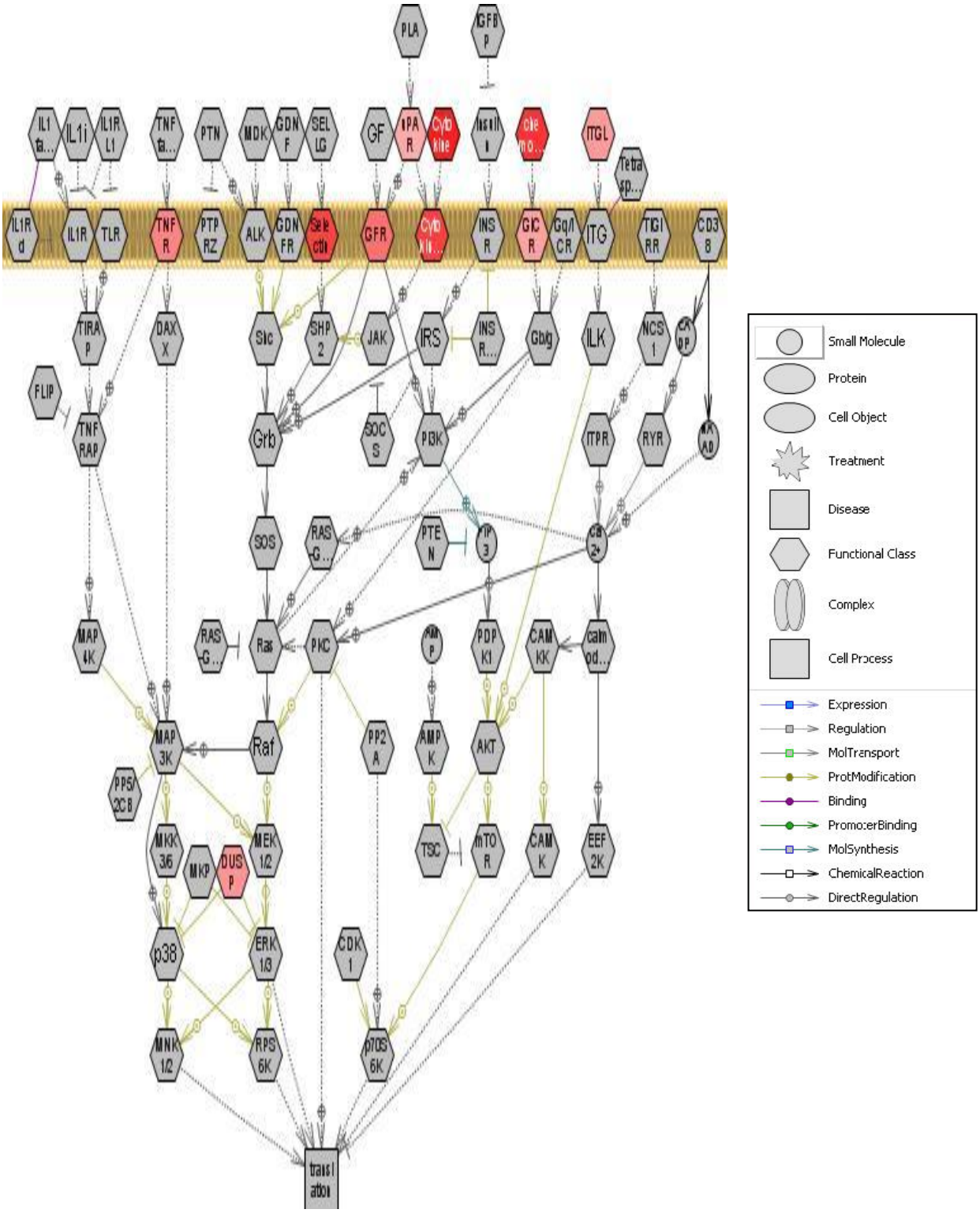

Figure A8.8. Translation control pathway. Pathway is the comparison of mock infected and infected FEA cells at 4 h p.i.. Those genes highlighted in red are up-regulated in the infected samples, the brighter the colouration, the greater the up-regulation in transcription. A full key of gene identification can be found in the appendix (Table A8.1).

Table A8.1. Pathway studio gene identification key

Gene ID	Gene name	Gene ID	Gene name
ADCY	Adenylate cyclase	**MAP4K**	Mitogen-activated protein kinase 4
AKT	v-akt murine thymoma viral oncogene homolog	**MAPKAPK**	MAP kinase-activated protein kinase
ALK	Anaplastic lymphoma kinase	**mDia**	Diaphanous homolog
AMP	Adenosine monophosphate	**MDK**	Midkine
AMPK	AMP-dependent protein kinase	**MDM2/4**	p53-binding protein
aNKCR	Activatory natural killer cell receptor	**MEK1/2**	Mitogen-activated protein kinase 1/2
APAF1	Apoptotic peptidase activating factor 1	**MKK3/6**	Mitogen-activated protein kinase kinase 3/6
ATM/ATR	ATM/ATR protein kinase	**MKP**	MAP kinase phosphatase
Bcl	Bcl2-like anti-apoptotic regulator	**MLCP**	Myosin light chain phosphatase
BCR	Breakpoint cluster region	**MNK1/2**	MAP kinase interacting serine/threonine kinase
Bid	BCL2-antagonist	**mTOR**	FK506 binding protein 12-rapamycin associated protein 1
BTK	Bruton agammaglobulinemia tyrosine kinase	**NAAD**	Nicotinate-nucleotide adenylyltransferase
C/EBP	C/EBP	**NAADP**	Nicotinic acid adenine dinucleotide phosphate
Ca2+	Calcium	**NCR**	Natural Cytotoxicity Triggering receptor
CADP	Cadherin 3	**NCS1**	Neuronal calcium sensor 1
cADPR	Cyclic ADP-ribose	**Neurexin**	Neurexin
calcineurin	Protein phosphatase 3	**NF-AT**	Nuclear factor of activated T-cells
calmodulin	Calmodulin	**NF-Kb**	Nuclear factor of kappa light polypeptide gene enhancer in B-cells 1
CAMK	CaM kinase	**NFKBI**	NF kappa B inhibitor
CAMKK	CaM kinase kinase	**NGF family**	Nerve growth factor family
cAMP	Adenosine 3',5'-cyclic monophosphate	**NGFR**	Nerve growth factor receptor
CASP12	Caspase 12	**NIK**	Mitogen-activated protein kinase 14
CASP3/6/7	Caspase 3/6/7	**NKCR**	Natural killer cell receptor
CASP8/10	Caspase 8/10	**Nogo**	Nogo ligand
CASP9	Caspase 9	**NogoR**	Nogo receptor
CBL	Ubiquitin-ligase of receptor protein-tyrosine kinases	**NTRK**	Neurotrophic tyrosine kinase
CD38	NAD+ nucleosidase	**NXPH**	Neurexophilin
CD3Z	T-cell receptor zeta chain	**P130CAS**	Breast cancer anti-estrogen resistance 1
CDK1	Cyclin-dependent kinase 1	**P13K**	Phosphatidylinositol 3-kinase
Chemokine	Chemokine	**P38**	Mitogen-activated protein kinase 11/12/13/14
CREB	CREB	**p53**	p53 kinase
Crk	v-crk sarcoma virus CT10 oncogene homolog (avian)	**p70S6K**	p70 ribosomal S6 kinase
CSK	c-src tyrosine kinase	**PAK**	p21/Cdc42/Rac-activated kinase
CytC	Cytochrome c	**PDPK1**	3-phosphoinositide dependent protein kinase-1
Cytokine	Cytokine	**PI3K**	Phosphatidylinositol 3-kinase
CytokineR	Cytokine receptor	**PIP3**	Phosphatidylinositol 3,4,5-triphosphate
DAG	Diacylglycerol	**PKA**	Protein kinase A
DAP10	Hematopoietic cell signal transducer	**PKC**	Protein kinase C
DAP12	Killer activating receptor associated protein	**PLA**	Outer membrane protease
DAXX	Fas death domain-associated protein	**PLC**	Phospholipase C
DIABLO	Diablo homolog	**PP2A**	Protein phosphatase 2
DOCK	Dedicator of cytokinesis	**PP5/2CB**	Protein phosphatase 5/1B
DUSP	Dual specificity phosphatase	**PTEN**	Phosphatase and tensin homolog
EEF2K	Eukaryotic elongation factor-2 kinase	**PTN**	Pleiotrophin
Egr/Krox	Egr transcription factor	**PTPRZ**	Protein tyrosine phosphatase, receptor type, zeta polypeptide
ERK1/3	Mitogen-activated protein kinase	**Rac/CDC42**	Rho family small GTP-binding protein

	1/3		
ETS	ETS-domain containing	**Rac/Cdc-GAP**	SLIT-ROBO Rho GTPase activating protein
FAK	Focal adhesion kinase	**Rac/CDC-GEF**	Rac/Cdc42 guanine nucleotide exchange factor
FCeR	Fc IgE receptor	**Raf**	Raf proto-oncogene serine/threonine protein kinase
FIP3	Fungus-Induced Protein	**RAP**	Ras family small GTP binding protein
FLIP	CASP8 and FADD-like apoptosis regulator	**RAP-GAP**	RAP1 GTPase activating protein
G12CR	G12/13-coupled receptor	**RAP-GEF**	Rap guanine nucleotide exchange factor
Ga12/13	G protein alpha 12/13	**Ras**	Ras oncogene homolog
GATA	Glutamyl-tRNA amidotransferase subunit A	**RAS-GAP**	RAS GTPase activating protein
Gb/g	G protein beta/gamma	**RAS-GRF**	Ras-specific guanine nucleotide-releasing factor
GDNF	Glial cell line derived neurotrophic factor	**Rho**	Rho GTPase
GDNFR	Glial cell line derived neurotrophic factor receptor	**Rho-GAP**	Rho GTPase activating protein
GF	Growth Factor	**Rho-GEF**	RhoA-specific guanine nucleotide exchange factor
GFR	Growth factor receptor	**ROCK1/2**	Rho-associated, coiled-coil containing protein kinase
GiCR	Gi-coupled receptor	**RPS6K**	Ribosomal protein S6 kinase
Gq/12CR	Gq/12/13-coupled receptor	**RYR**	Ryanodine receptor
Gq/iCR	Gq/i-coupled receptor	**Selectin**	Selectin
Grb	Growth factor receptor-bound protein	**SELLG**	Selectin L
Gs/12CR	Gs/12/13-coupled receptor	**SH2B**	SH2B adaptor protein
IAP	Apoptosis inhibitor	**Shc**	Src homology 2 domain containing
IGFBP	Insulin-like growth factor binding protein	**SHP1**	Protein tyrosine phosphatase, non-receptor type 6
IKBK	IkappaB kinase	**SHP2**	Protein tyrosine phosphatase
IL1 family	Interleukin 1 complex	**SLP76**	Lymphocyte cytosolic protein 2
IL1i	Inhibit the activities of IL1 family	**SMAD**	Pathway-specific SMAD proteins
IL1R	IL1/18 receptor	**SOCS**	Suppressor of cytokine signaling
IL1Rd	IL1R decoy	**SOS**	Son of sevenless homolog
IL1RL1	IL1R-like	**SP**	Transcription factor Sp
ILK	Integrin-linked kinase	**Src**	Src family
iNKCR	Inhibitory natural killer cell receptor	**SRF**	Serum response factor
INSR	Insulin receptor	**STC**	Stanniocalcin
Insulin	Insulin	**SYK**	Spleen tyrosine kinase
IP3	Inositol 1,4,5-triphosphate	**Tetraspanin**	Tetraspanin
iPAR	virB transcriptional activator	**TGF family**	Transforming growth factors
Irf	Iron regulatory protein	**TGFBR**	TGF-beta receptor
IRS	Insulin receptor substrate	**TGFi**	TGF-beta inhibitor
iSMAD	Inhibitory SMADs	**TIGIRR**	Three immunoglobulin domain-containing IL-1 receptor-related
ITG	Integrin	**TIRAP**	Toll-interleukin 1 receptor adaptor protein
ITGL	Novel Integrin Ligand	**TLR**	Toll receptor
ITPK	Inositol 1,4,5-triphosphate kinase	**TNF family**	Tumor necrosis factors
ITPR	Inositol 1,4,5-triphosphate receptor	**TNFR**	Tumor necrosis factor receptor
JAK	Janus kinase	**TNFRAP**	Tumor necrosis factor receptor associated factor
LAT	Linker for activation of T cells	**TSC**	Tuberous sclerosis
LIMK	LIM domain kinase	**VAV**	Rac/Cdc42 guanine nucleotide exchange factor
MAP3K	Mitogen activated protein kinase 3		